Single frequency Vertical External Cavity Surface Emitting Lasers

By

Kyle Scot Gardner

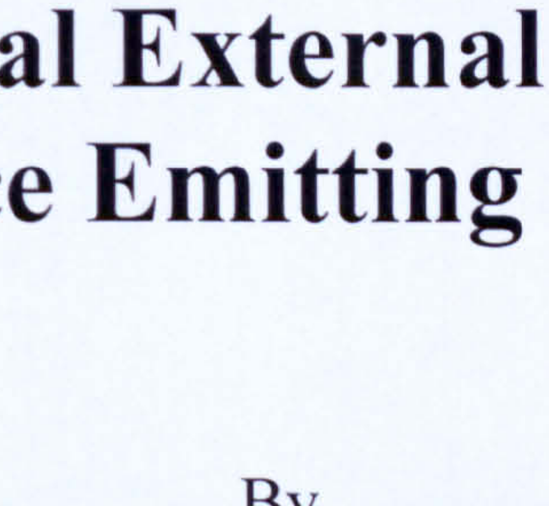

UNIVERSITY OF STRATHCLYDE

A thesis presented in fulfilment
of the requirements for the degree of
Doctor of Philosophy

Department of Physics, University of Strathclyde

2007

For their love, support and encouragement
I dedicate this work to my parents
Robin and Lynda

Acknowledgements

Throughout the course of this work I would first and foremost like to thank my supervisor professor Erling Riis for his friendship, guidance and wisdom. For sharing his massive knowledge and intuitive ideas on all aspects of physics I am eternally grateful.

A special thanks must also be given to the photonics academic team both past and present for their useful helps and hints in guiding me throughout my PhD, namely Prof Allister Ferguson, Dr Marc Schmid, Dr Thorsten Ackeman, Dr Nigel Langford, Dr Richard Abram. Additional thanks goes to Dr Alan Kemp for instructing me on the basics of Femlab and helping me through the thermal modelling of several VECSEL scenarios.

In most of my complex cavity designs the need for intricate mounts was essential. Without the technical expertise and design assistance of both Mr Robert Wylie and Mr Ewan MacLagan this would not have been possible.

A big thanks to Stephen McGinily for his friendship, king-dongs, and caramel short cake expertise. As one of fife creamery's biggest fans he has never failed to create a fun atmosphere in the office nor missed to spot a pinger, even round corners.

Fion, Seve, Wei, Ian (chuck) Norris and Hawk for the numerous PPC nights throughout my PhD. Including Fions amazing recepie for chicken satay, awesome!

Finally my parents Robin and Lynda for there love, support and financial assistance, for this I am eternally grateful.

ABSTRACT

The thesis presents the development and implementation of single frequency vertical external cavity surface emitting lasers (VECSELs). Numerous cavity designs are reported, exploiting some unique features for single frequency operation.

A small VECSEL cavity configuration is reported utilising a positive curvature mirror in reverse to create a 6mm cavity where the air gap between the mirror surface and VECSEL wafer act as an etalon, which induces single frequency operation. A 7nm tuning range has been shown with maximum output of 19.4mW. Thermal modelling was undertaken to analyse how the removal of the VECSEL's substrate could increase the thermal efficiency for high power operation.

Another small cavity design of length 50mm was created, producing a high power, compact single frequency VECSEL. Using a birefringent filter and solid etalon single frequency operation was achieved. A tuning range of 10nm was achieved with output powers of 271mW. Extensive mapping of the pump profile and eventual manipulation of this resulted in the M^2 of the laser of 1.1 being reduced to 1.02. In addition an air etalon system was constructed to eliminate walk-off losses experienced by the solid etalon. This resulted in a 20nm tuning range.

Frequency doubling of an 850nm VECSEL using $KNbO_3$ is reported with 1.3mW of 425nm being achieved, corresponding to an efficiency of 3.2%/W. This system also incorporates a polarisation coupled pump system delivering 3W at 670nm from a 100μm fibre. The relationship between the VECSEL's gain and frequency conversion efficiency is also analysed in detail.

THESIS OUTLINE

Chapter one gives a brief introduction in to the development of the VECSEL. The design of the VECSEL is discussed with a detailed overview of the characteristic layers incorporated in its structure and how this is manufactured.

Chapter two discusses the analysis of a VECSEL wafer so that an efficient sample can be selected for use in a laser. It also discusses procedures to appropriately mount the VECSEL chip, including detailed steps on how to cleave and capillary bond a wafer to an optical heat spreader.

Chapter three gives an overview of a single frequency laser. Detailed analyses of intra cavity elements for single frequency selection are discussed with reference to previous work carried out [1].

Chapter four investigates thermal management of VECSELs. Conventional methods of efficiently extracting heat from the VECSEL are shown. In addition, computer modelling and experimental techniques are performed to show the thermal implications of removing the VECSEL's rear GaAs substrate in an attempt to create an alternative solution to using a diamond heat spreader.

Chapter five introduces the first ever-reported ring-cavity VECSEL. As a new configuration for a VECSEL cavity, the laser was analysed in detail with investigation into common features of a ring cavity, which included unidirectional operation and a high tolerance to feedback. This work has since been presented at the Europhoton Conference [2] and is in the initial stages of publication.

Chapter six discusses a unique cavity design, which utilises a small micron sized air gap as an intra-cavity etalon. This novel design is an attempt to create a small robust single frequency laser.

Chapter seven is motivated from the previous chapter in designing a small single frequency VECSEL. This incorporates a slightly larger design with intra-cavity elements for single frequency operation. One of these elements, the etalon, is discussed further, with the eventual creation of a purpose built air-etalon to maximise the VECSELs tuning capability.

Chapter eight demonstrates the frequency doubling of an 850nm VESCEL. Detailed analysis of the conversion efficiency of the $KNbO_3$ crystal was carried out with respect to the laser gain and internal losses [3]. Using a $KNbO_3$ crystal an effective cavity design is created with the addition of a bright optical pumping source.

Chapter nine gives an overall conclusion of the entire work carried out in this thesis, summing up and discussing the relevant findings.

REFERENCES

1. K. S. Gardner, R. H. Abram and E. Riis, "A birefringent etalon as single-mode selector in a laser cavity", Optics express, **12**, no.12, (2004)
2. K. S. Gardner "VECSEL ring laser" oral presentation, 2nd EPS-QEOD Europhoton Conference, Polo G. Carmignani, Pisa, Italy.
3. Stephen J. McGinily, Richard H. Abram, Kyle S. Gardner, Erling Riis, *Member, IEEE*, Allister I. Ferguson, *Fellow, IEEE*, and John S. Roberts, "Novel gain medium design for short-wavlength vertical-external-cavity surface-emitting laser", Optics Express, **43**, no.6, (2007)

CONTENTS

5- RING-CAVITY VECSEL PAGE NO.

6- MICRO-CAVITY VECSEL

7- SMALL-CAVITY VECSEL

8- FREQUENCY DOUBLED VECSEL

9- OVERALL CONCLUSION

CHAPTER ONE

INTRODUCTION AND BACKGROUND

Vertical External Cavity Surface Emitting Lasers (VECSELs) are a unique blend of both solid state and semiconductor lasers. The semiconductor material is designed to emit and absorb desirable wavelengths. The unique external cavity gives this laser the ability to define the laser mode and utilise intra-cavity elements for several applications, like that of a traditional solid-state laser. This flexibility gives VECSELs a large wavelength coverage, similar to diode lasers and output powers >1W, making it a very versatile tool.

This chapter gives an insight into the development of the VECSEL and the main aspects behind its design.

1.1 INTRODUCTION

Semiconductor lasers are at the forefront of the modern world. Since their introduction in 1962 [1], they have been developed into one of man's most powerful tools. Semiconductor lasers are now part of every day use, featuring in many devices that are used on a daily basis, for example CD players, DVD players, telecoms networks and laser printers.

1.2 DEVELOPMENT OF LASER DIODES

Since the first proposal of laser amplification in 1958 [2], laser diodes have been developed to produce a wide range of wavelengths and high power emission. The creation of the laser diode in 1962 by Hall and colleagues [1], was the first step in the semiconductor laser development. This small device is formed by doping a piece of semiconductor wafer in two regions, creating two areas in close proximity, p-type and n-type. The p-type semiconductor area has a preponderance of vacancies for

donor electrons, simply called holes that are positively charged. The n-type area has a preponderance of electrons that are negatively charged hence the names n/p-type. When these two materials are in close proximity their band structures intermix. This is called the depletion layer (active region). When current is passed through this device electron and hole recombination occurs and light emission is generated. This process is very efficient due to the direct bandgap in the semiconductor. The maximum of the valence band is directly below the minimum of the conduction band in momentum space, this allows for optical emission through efficient recombination of electron-hole pairs while conserving momentum. This can be seen below in figure (1.2.1)

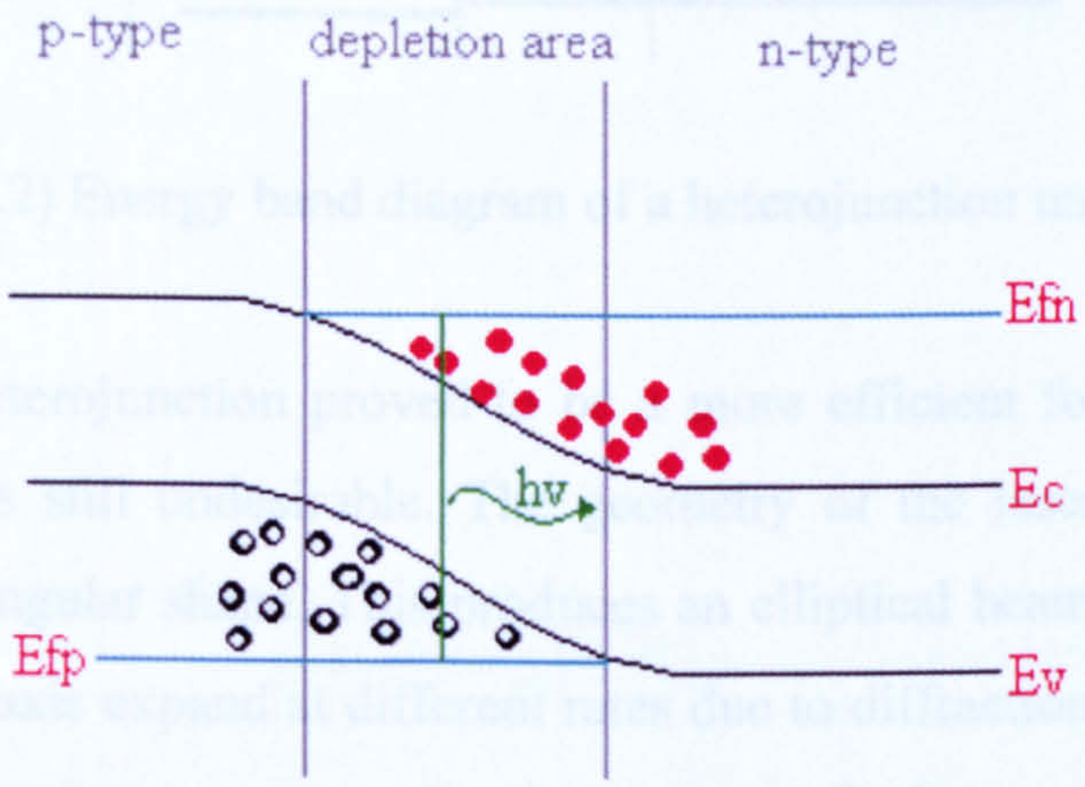

Figure (1.2.1): Degenerately doped pn junction under forward bias with photon emission

In the above diagram the depletion layer shows where the recombination of the electron and hole pairs occur. This is an uncontrolled area formed by the overlapping of the two semiconductor doped regions. Only electrons and holes in this region will recombine and photon emission occurs. A further step in 1969 by Izuo Hayashi and colleagues [3], was to alter the band structures of the semiconductor material to create an optical waveguide. It consists of three doped regions of semiconductor material forming a heterojunction. The requirement for this type of waveguide is that the central material has a lower bandgap than the other two materials. This confines the carriers in an energy well in the centre of the semiconductor. Radiative

recombination is then confined and this enhances the process of light amplification. The depletion area is no longer an uncontrollable parameter thus it can be designed for maximum carrier confinement and efficiency. The diagram (figure 1.2.2) shows the energy band structure and typical material layout.

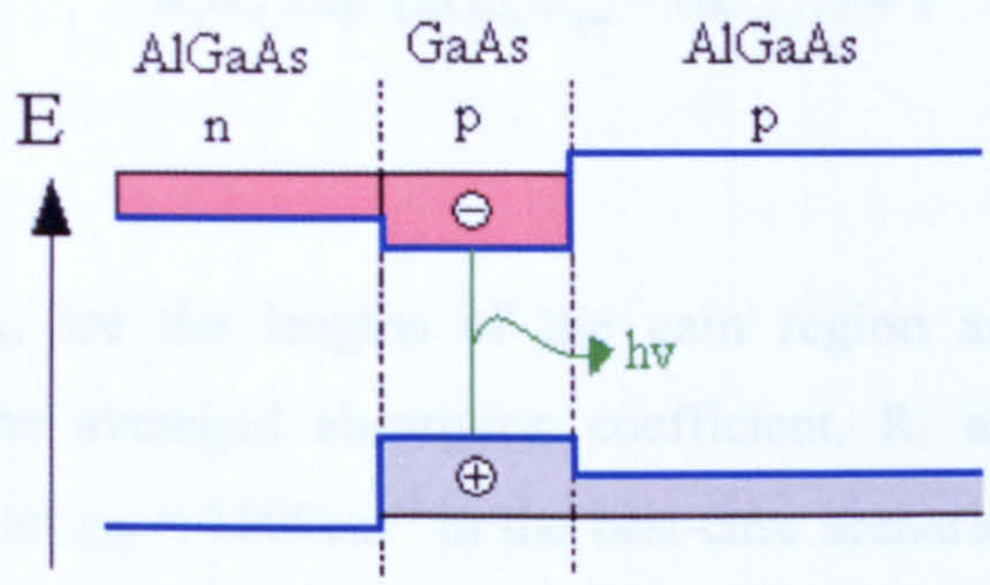

Figure (1.2.2) Energy band diagram of a heterojunction under forward bias.

Although the heterojunction proved to be a more efficient form of laser diode the beam shape was still undesirable. The geometry of the laser diode produces end facets of a rectangular shape. This produces an elliptical beam from the laser as the light from both axis expand at different rates due to diffraction. The elliptical shape is undesirable as it causes complications to use further optics or launching into optical fibres. This beam shape can be adjusted using lenses or anamorphic prism pairs, which can be time consuming, costly and lossy. The next major development in semiconductor lasers was the production of a circular output beam, this would make coupling the laser light in to optical fibre much easier and would be more desired in the optical industry. The first reported Vertical Cavity Surface Emitting Laser (VCSEL) was in 1965 by Melingailis [4]. It consisted of an npp junction of InSb. The material was cooled to 10K and magnetic fields were used to confine the carriers, this emitted coherent radiation around 5.2μm. This was then developed further in the late 1970's where Kenichi Iga and associates used the novel idea of Bragg stacks in conjunction with semiconductor gain mediums to create a surface emitting semiconductor laser which consisted of two semiconductor Bragg stack

mirrors with a semiconductor gain medium between them forming a micro laser cavity [5].

The threshold gain of the laser occurs when the optical gain equals that of the optical losses in the cavity. This can be expressed in the following equation,

$$R_1 R_2 \exp\{2(g_{th} L_{qw} - \alpha L_{cav})\} = 1 \qquad \text{equ:(1.2.1)}$$

where L_{qw} and L_{cav} are the lengths of the gain region and the quantum well respectively, α is the averaged absorption coefficient, R_1 and R_2 are the mirror reflectivities. If we let $g_{th} = 1000\text{cm}^{-1}$ in the best-case scenario for the gain then the Bragg mirror has to be as much as 99.95% reflective.

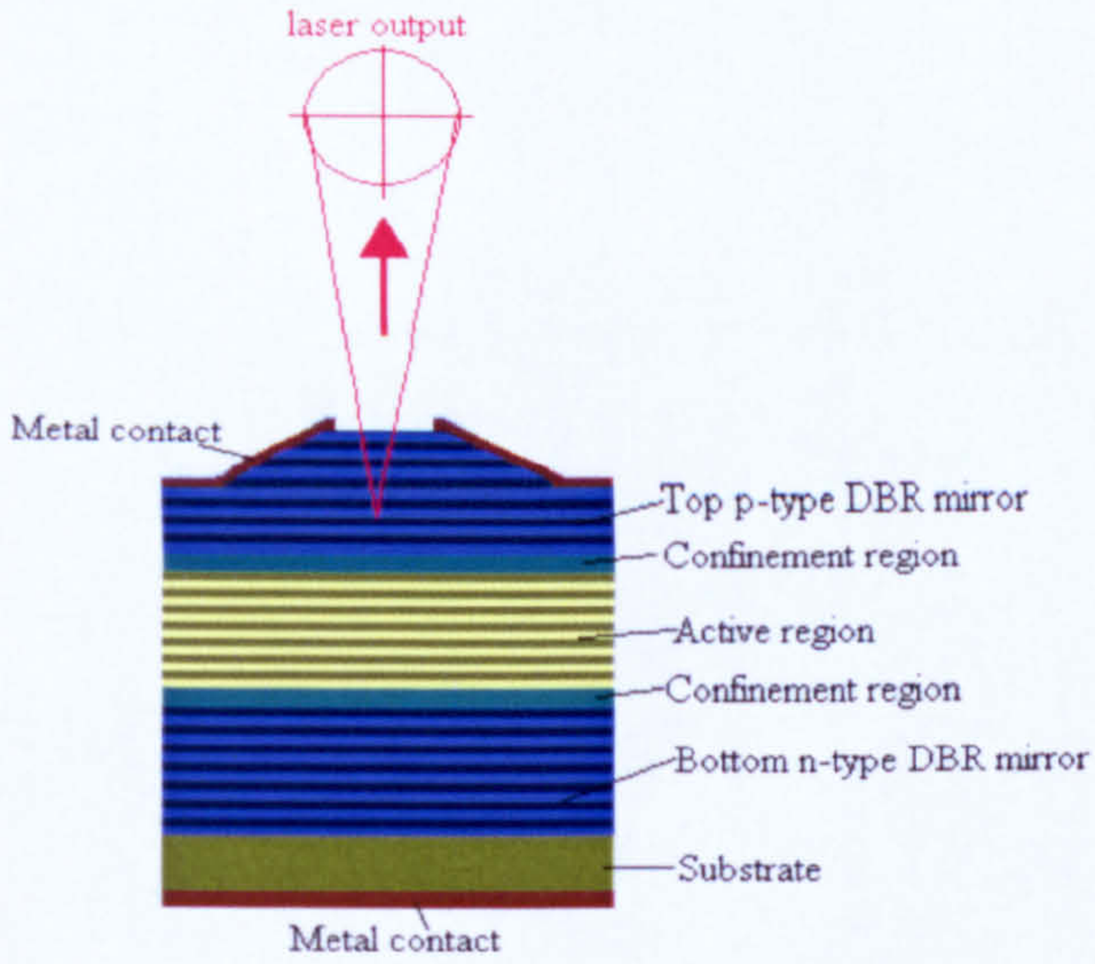

Figure (1.2.3): VCSEL design showing all major regions.

The main disadvantage of the VCSEL is the large amount of current that is needed for electrical pumping and with low output powers it was a very inefficient laser. Due to inhomogeneties in electrical pumping, namely a limited size of pumping region, VCSELs cannot emit high powers in the fundamental mode. Currently this is limited to 6mW [6,7]. This inherent power scalability problem of the VCSEL was a major contributing factor that drove the development of semiconductor lasers to the VECSEL.

The first VECSEL was reported in 1991 by the Jiang group [8], from an InGaAs based material. The design of the VECSEL is taken from the VCSEL. The removal of the top distributed Bragg Reflector (DBR) from the VCSEL gives the laser the ability to have an external mirror to complete the cavity. This allows a wide variety of intra-cavity components to be used. The addition of birefringent filters and etalons into the cavity can turn this broadband device into single frequency operation with large tunability [9]. Frequency doubling crystals can be utilised intra-cavity to produce efficient second harmonic generation of the fundamental wavelength. [10]. In addition to adding intra-cavity elements the VECSEL also has the advantage of being able to be optically pumped. This also makes it possible to increase the gain volume as no electrical complexities apply, therefore VECSELs can achieve larger output powers.

1.3 THE VECSEL

The vertical external cavity surface emitting laser is a robust laser. With careful design of the distributed Bragg reflector and quantum wells it can be a very comprehensive laser. Currently the VECSEL's wavelengths span covers 391nm-2.3μm, (Table 1.3.1). With good beam quality TEM_{00} mode, high power, narrow line width(<1MHz), compact and very efficient, the VECSEL is a formidable replacement for the Ti:Sapphire.

Emission wavelength	**Quantum well material**	**DBR material**	**REFERENCE**
391nm	$In_{0.1}Ga_{0.9}N/GaN$	$In_{0.1}Ga_{0.9}N/GaN$	[11]
660nm	InGaP	AlGaInP	[12]
850-870nm	$GaAs/Al_{0.2}Ga_{0.8}As$	AlAs/A $l_{0.2}Ga_{0.8}As$	[13]
960-1030nm	$InAs/Al_{0.2}Ga_{0.8}As$	$AlAs/Al_{0.2}Ga_{0.8}As$	[14]
1300nm	$Ga_{0.63}In_{0.37}N_{0.012}As/GaAs$	AlAs/GaAs	[15]
1500nm	InGaAs/InGaAsP	InAlAs/GaInAlAs	[16]
2300nm	$Ga_{0.71}In_{0.29}As_{0.03}Sb_{0.97}$	GaSb/AlAsSb	[17]

Table (1.3.1): Wavelength range of VECSELs

The design of the VECSEL is critical to its efficiency. There are 3 main areas to consider, the distributed Bragg reflector (DBR), the quantum well region and the capping layer. These sections can be seen below in the schematic drawing of a typical VECSEL, figure (1.3.1).

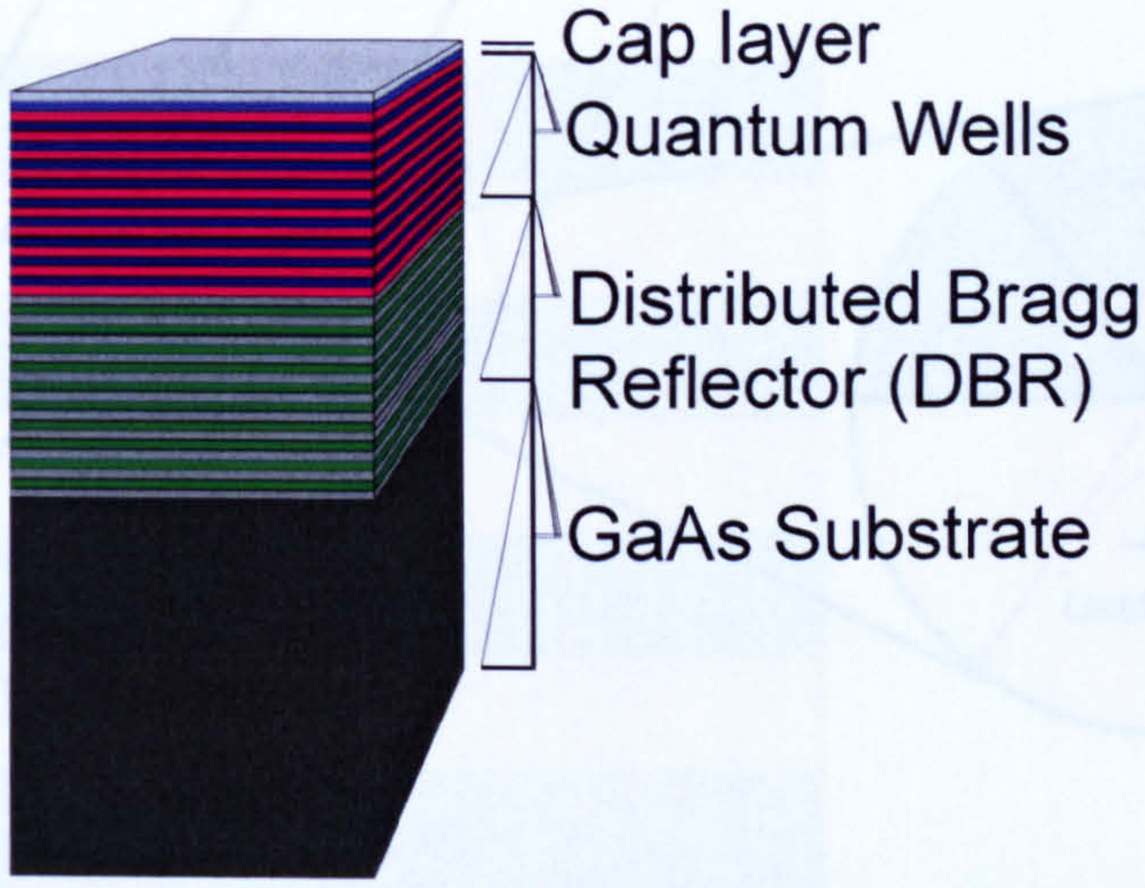

Figure (1.3.1): Basic VECSEL structure

1.4 Distributed Bragg Reflector

The VECSEL mirror is made from a distributed Bragg reflector (DBR). This consists of alternating layers of semiconductor material with different refractive index. Each layer is one-quarter wavelength of optical thickness. When light is incident on the Bragg stack it experiences a 180^0 phase shift when passing through a single layer, this phase allows the reflected beam to constructively interfere which results in a strong refection. As each layer is partially reflective, multiple layers of refractive index pairs are used to increase the reflectivity of the stack until a maximum reflection is achieved, typically 30 layer pairs are used. This maximum is achieved

when all the possible light is reflected by the Bragg stack, although some proportion will be absorbed by the mirror substrate. Reflectance's of 99.9% can be achieved with this method. The mirrors bandwidth is determined by the contrast in refractive index of the two materials. Figure (1.4.1) below shows how an off axis beam being reflected by this method.

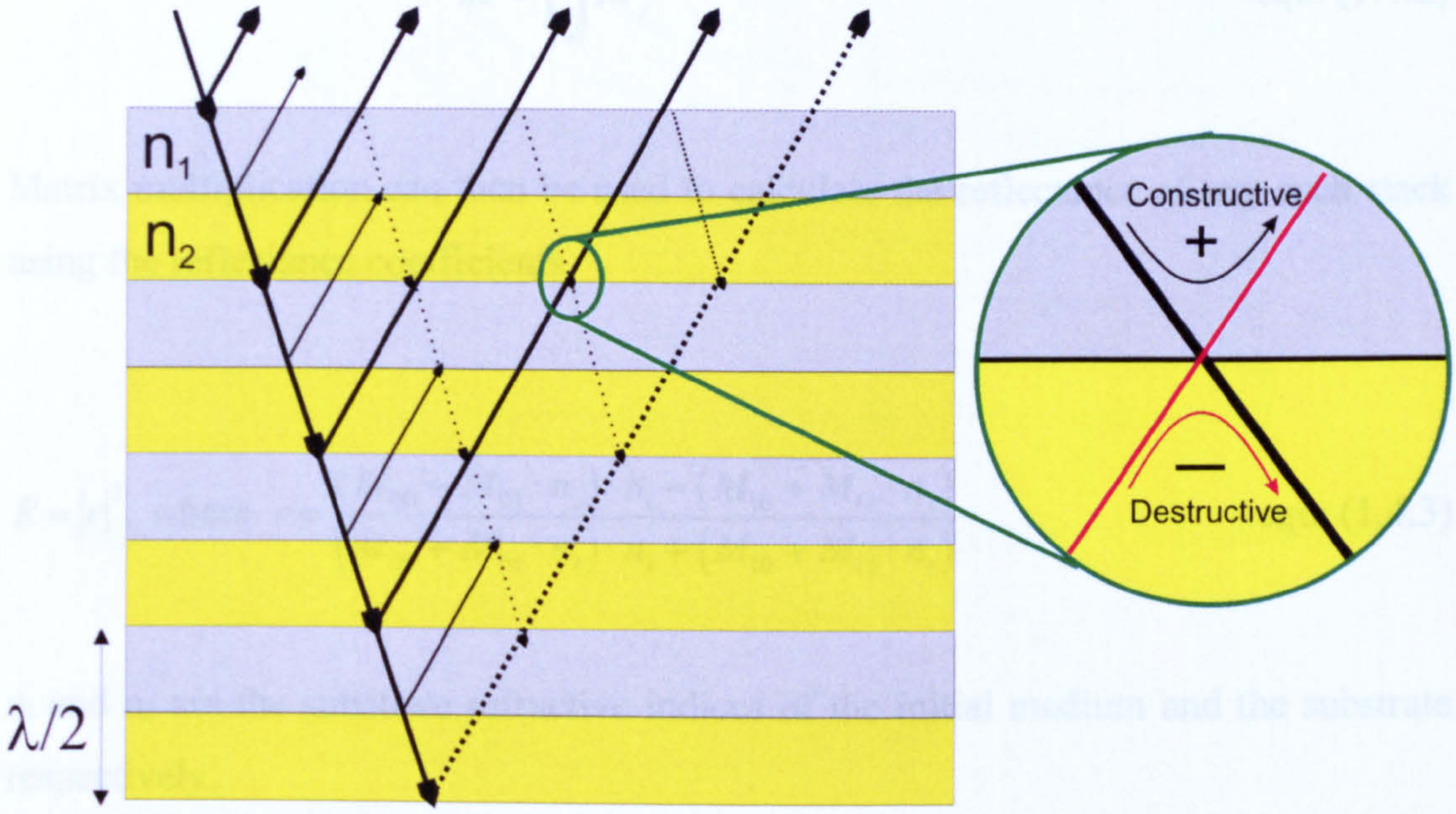

Figure (1.4.1): Distributed Bragg Reflector with off axis beam reflection. Light propagating from a low to high refractive index experiences a 180 degrees phase shift that adds constructively to form a high reflector.

Maxwell's equations of thin films of electro magnetism can be used to describe the theory if DBR thin films [18]. Matrices are used to describe the characteristics.

$$M(z)=\begin{bmatrix} \cos(k_0 nz\cos\theta) & -\dfrac{i}{n\cos\theta}\sin(k_0 nz\cos\theta) \\ -i(n\cos\theta)\sin(k_0 nz\cos\theta) & \cos(k_0 nz\cos\theta) \end{bmatrix}=\begin{bmatrix} M_{00} & M_{01} \\ M_{10} & M_{11} \end{bmatrix} \quad \text{equ:(1.4.1)}$$

Where $k_0=\dfrac{2\pi}{\lambda}$ = Wave vector

n = Refractive index of the film

z = film thickness

θ= Angle of electromagnetic wave to normal incidence

A series of such films is then given by the expression,

$$M = \prod_{j=1}^{N} M_j \qquad \text{equ: (1.4.2)}$$

Matrix multiplication can then be used to calculate the reflectance of any such stack using the reflectance coefficients,

$$R = |r|^2, \text{ where } r = \frac{(M_{00} + M_{01} \cdot n_s) \cdot n_i - (M_{10} + M_{11} \cdot n_s)}{(M_{00} + M_{01} \cdot n_s) \cdot n_i + (M_{10} + M_{11} \cdot n_s)} \qquad \text{equ: (1.4.3)}$$

n_i and n_s are the substrate refractive indices of the initial medium and the substrate respectively.

GaAs based VECSELs use AlGaAs DBRs as lattice matching between the layers is acceptable, this reduces the risk of stresses and cracks caused by lattice mismatch. The materials refractive index can be tailored by increasing or decreasing the amount of aluminium content present. This gives a simple way to engineer the DBR to the desired reflectance at the desired wavelength. Figure (1.4.2) shows how the change in refractive index with wavelength for varying concentrations of the Al mole fraction.

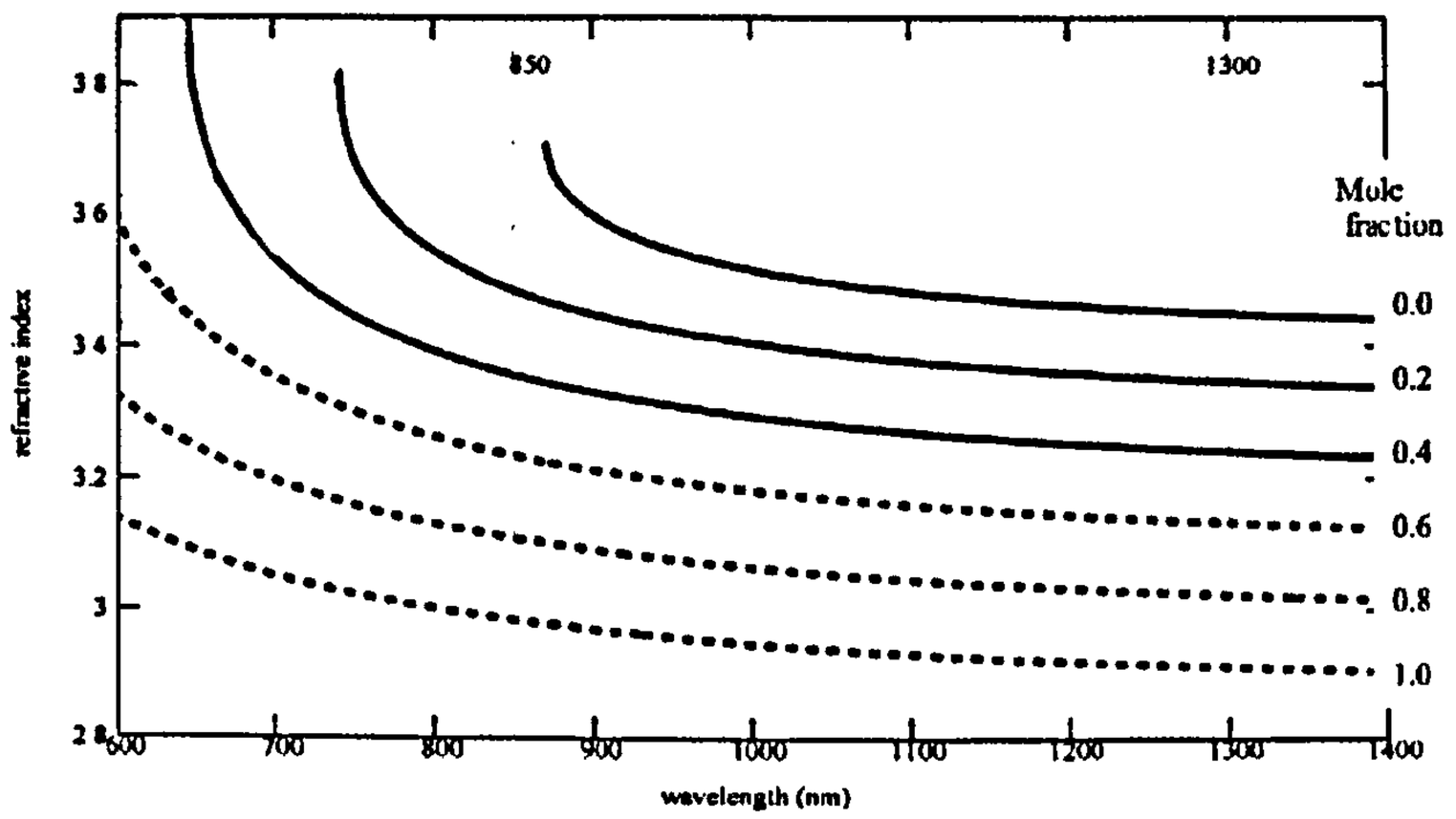

Figure (1.4.2): Refractive index of $Al_xGa_{1-x}As$ as a function of wavelength for different Al mole fractions [19].

In the above graph it is clear as you increase the aluminium mole fraction (0.0 at the top) the refractive index is reduced (1.0 mole fraction, bottom line). A large change in refractive index (Δn) between the two layers is desirable as this allows for a stronger reflection and wide bandwidth. The reflectivity of the mirror increases as the number of layer pairs is increased. Typically around 25 or more layers are needed for a reflectivity of 99.9% for a large Δn.

Computer simulations can be used to model Bragg stacks [20], as seen in figure (1.4.3)

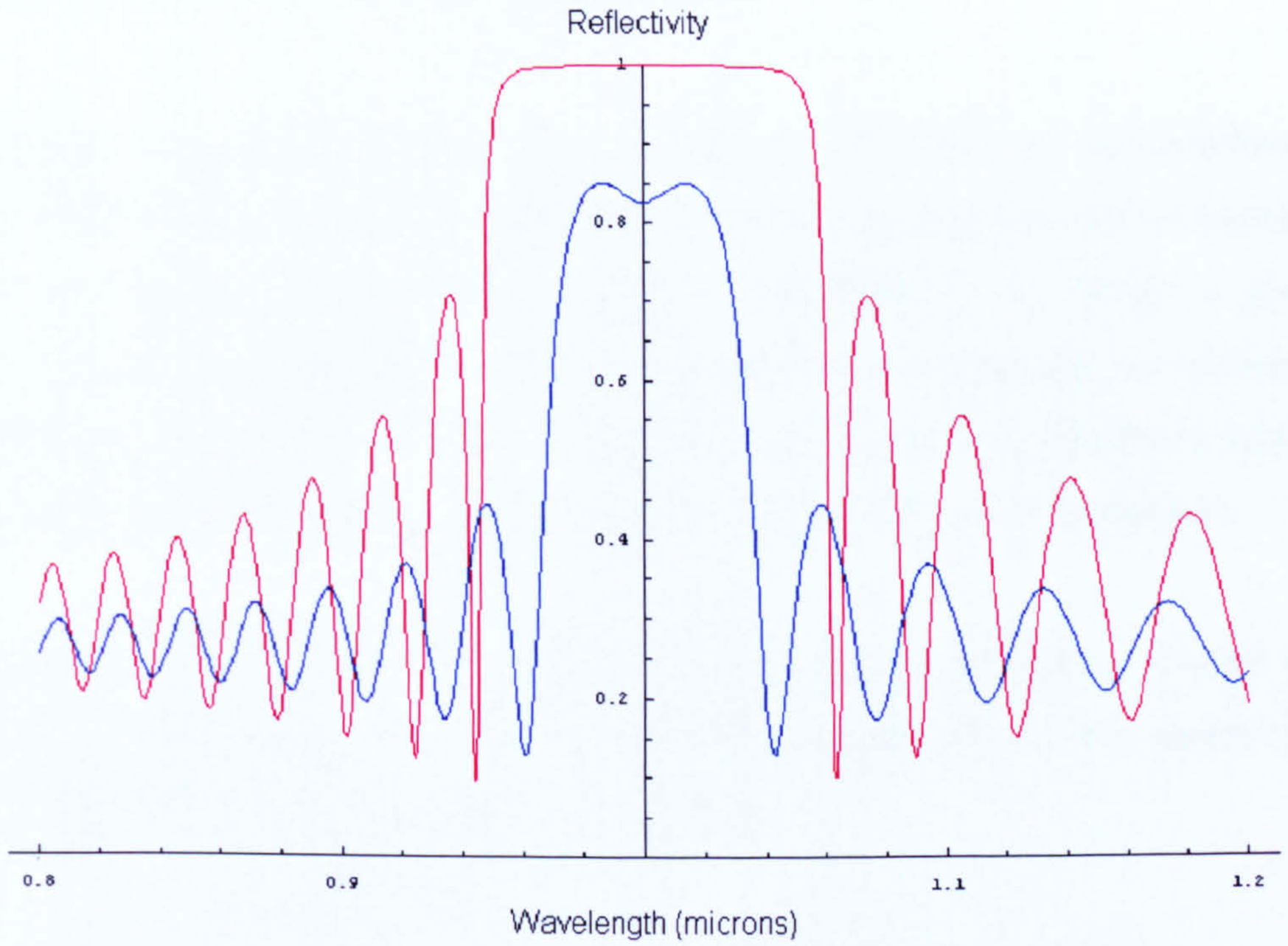

Figure (1.4.3): Mathematica simulation of a AlGaAs DBR. The red line indicates the reflectivity of 30 layer pairs showing a 99.99% reflectivity over a 60nm range. The blue line shows 20 layer pairs showing a reduced reflectivity of 85% and a reduced bandwidth around 40nm.

Figure (1.4.3) above shows a computer simulation of a 980nm-centred DBR. The red line indicates a 30 pair combination of $Al_xGa_{1-x}As$ layers with n=3.2 and n=2.86 due to an Al mole fraction of x=0.6 and x=1.0 respectively. 30 pairs give a strong reflection approximately 99.99% @ 980nm. The large difference in refractive index between the layers (Δn=0.34) gives a broad reflection band. In contrast, the blue line indicates a poor DBR. Here $\Delta n = 0.2$ therefore the reflection maxima is decreased and width of DBR profile is also reduced. Using this software it is possible to design a desirable DBR for use in a VECSEL wafer. The next stage is to design the quantum well region, which is grown directly on top of the DBR.

1.5 QUANTUM WELL REGION

The quantum well region is made up of a sequence of layers of semiconductor material. These materials can be manipulated to allow the emission and absorption bands of the quantum wells to be designed to specification. To design a good quantum well one must take into account the desired pump wavelength, the emission wavelength and the gain. These three features are the underlining attributes which must remain constant in the design when adjusting the quantum well parameters.

The absorption and emission wavelengths of a quantum well can be chosen by altering the semiconductor composition and thickness. Figure (1.5.1), shows the quantum well structure and the relevant energy bands.

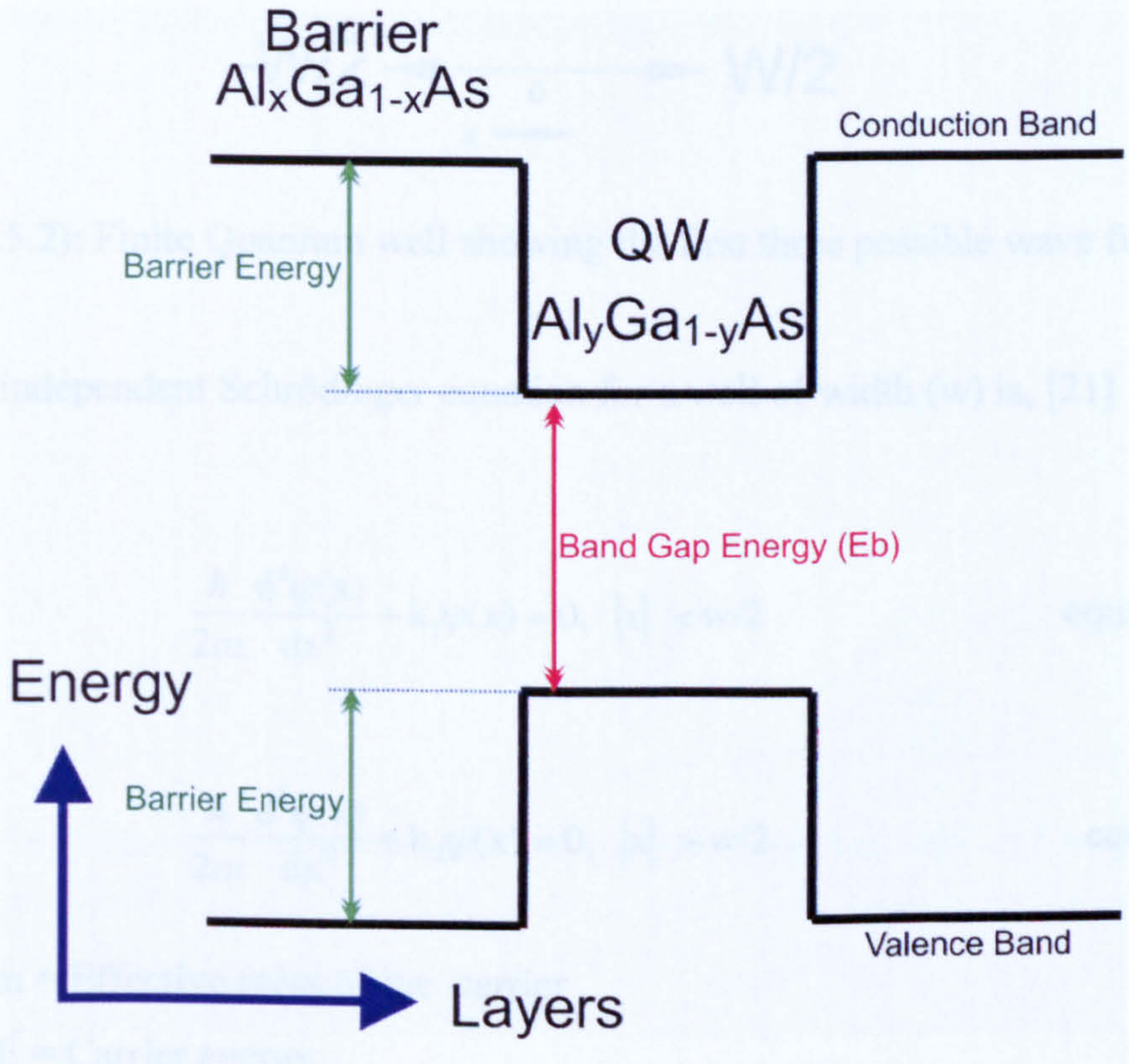

Figure (1.5.1): Energy bands in quantum well region.

To calculate the exact wavelength, which the quantum well will absorb and emit, Schrödinger's equation must be used to determine the transition energies present in a finite quantum well.

Consider a finite quantum well with width (w) and finite barriers (V_0) as shown in figure (1.5.2) below.

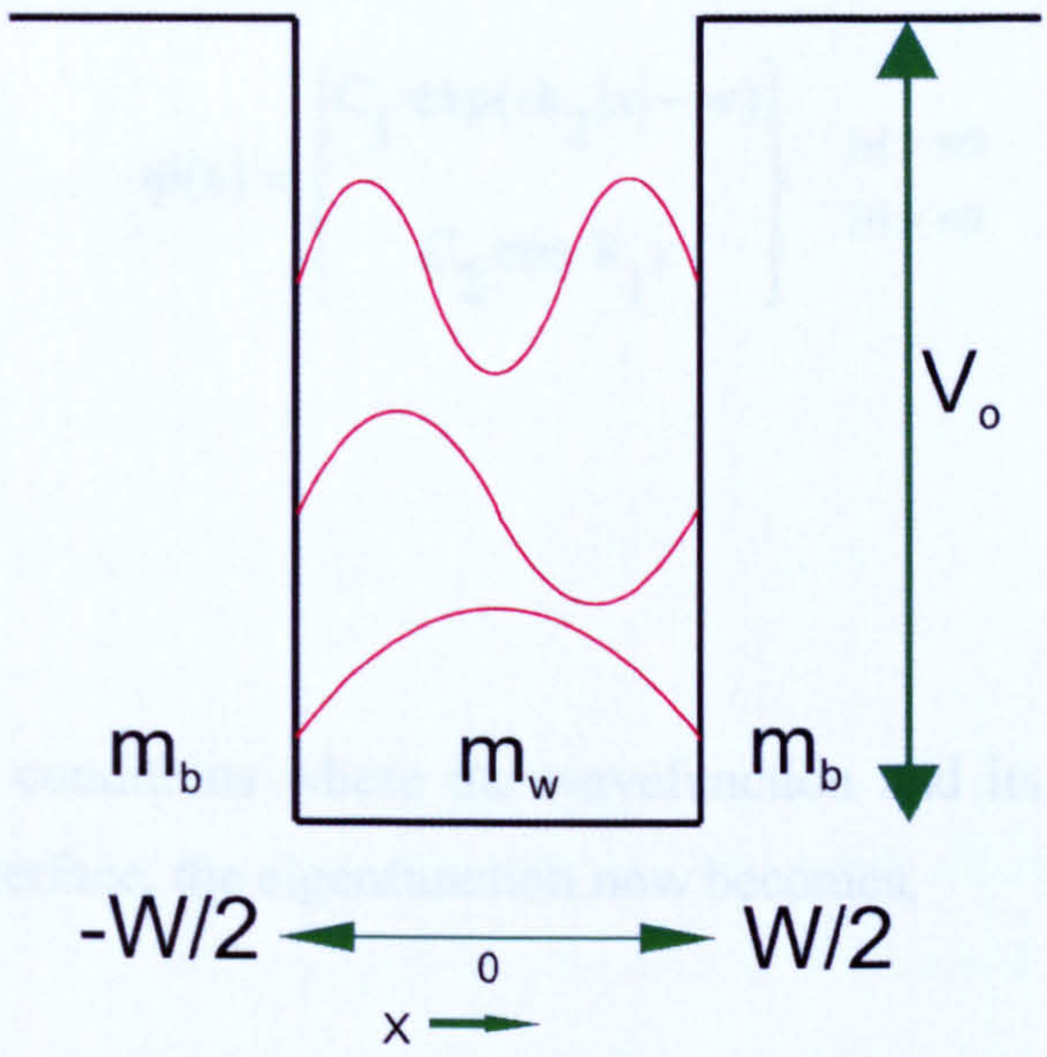

Figure (1.5.2): Finite Quantum well showing the first three possible wave functions

The time independent Schrödinger equation for a well of width (w) is, [21]

$$\frac{\hbar}{2m}\frac{d^2\psi(x)}{dx^2} + k_1\psi(x) = 0, \quad |x| < w/2 \qquad \text{equ:(1.5.1)}$$

$$\frac{\hbar}{2m}\frac{d^2\psi(x)}{dx^2} + k_2\psi(x) = 0, \quad |x| > w/2 \qquad \text{equ:(1.5.2)}$$

Where, m = Effective mass of the carrier

E = Carrier energy

$$k_1 = \sqrt{\frac{2mE}{\hbar^2}}$$

$$k_2 = \sqrt{\frac{2m(V_0 - E)}{\hbar^2}}$$

For an even wavefunction the solution now becomes.

$$\psi(x) = \begin{cases} C_1 \exp(-k_2|x| - w) & |x| > w/2 \\ C_2 \cos k_1 x & |x| < w/2 \end{cases} \qquad \text{equ:(1.5.3)}$$

Applying boundary conditions where the wavefunction and its derivative must be continuous at the interface, the eigenfunction now becomes,

$$C_1 = C_2 \cos k_1 \frac{w}{2} \qquad \text{equ:(1.5.4)}$$

$$\frac{k_2}{m_b} C_1 = \frac{k_1}{m_w} C_2 \sin k_1 \frac{w}{2} \qquad \text{equ:(1.5.5)}$$

Where m_w and m_b is the effective mass of the carrier in the well and in the barrier respectively.

Substitution of C1 and C2 gives,

$$k_2 = \frac{m_b}{k_w} \tan k_1 \frac{w}{2} \qquad \text{equ:(1.5.6)}$$

Where $k_1 = \sqrt{\frac{2mE}{\hbar^2}}$ and $k_2 = \sqrt{\frac{2m(V_0 - E)}{\hbar^2}}$

Substituting values for k_1 and k_2 gives

$$E - V_0 + \frac{m_b}{m_w} E\left[\tan\left(\sqrt{\frac{2m_w E}{\hbar^2}}\frac{w}{2}\right)^2\right] = 0 \qquad \text{equ:(1.5.7)}$$

This equation can now be used to solve for the transition energies of any possible quantum well design. This information can be used to indicate the correct aluminium mole fraction needed for efficient pump absorption into the barrier regions and also indicate the quantum well thickness needed for the desired emission wavelength.

Once the design of a single quantum well has been complete the number of quantum wells has to be taken into account. The quantum well can produce a certain amount of gain. Multiple quantum wells are used to increase the available gain of the laser so that it is larger than the losses experienced in the material and hence laser action can take place. The quantum wells in the structure have to be kept to an optimum number as an increase in well number also increases the lasing threshold, due to an increase in absorption from the barriers material. These affects can be seen in figures (1.5.3, 1.5.4), [22]

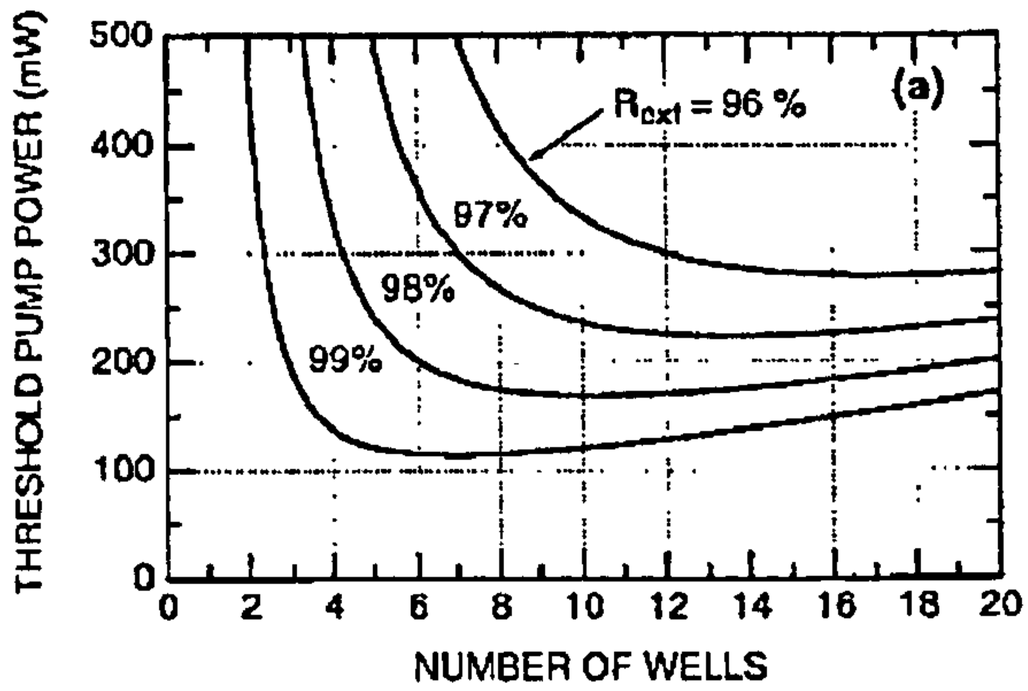

Figure:(1.5.3) Threshold power as a function of QW number for a varied output coupling of 96%-99%.

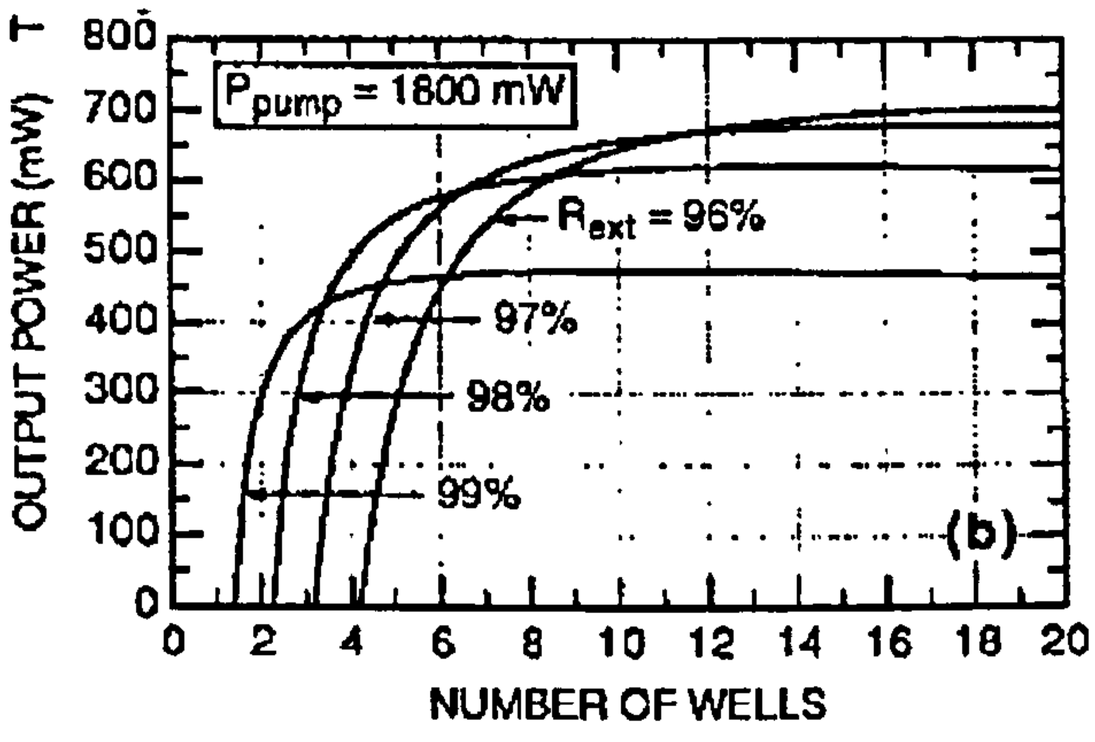

Figure:(1.5.4) Maximum output power for a fixed input power as a function of QW number for a varied output coupling of 96-99% [22].

As seen in figure (1.5.3), the increasing number of Quantum wells increases the lasing threshold. Figure (1.5.4) shows with increasing number of quantum wells the maximum output power is increased as more gain is provided. Figure (1.5.3) provides 4 plots of increased internal losses by using varied output coupling 96%-4% loss, to 99%-1% loss. From these graphs it is clear that an optimum number of quantum wells must be used to give a low lasing threshold however enough for gain to exceed the losses and lasing to occur.

1.6 WINDOW LAYER

The final layer in the design of the VECSEL is the capping layer. Its role is to prevent carrier diffusion from the quantum wells and also reduce oxidation of the VECSEL's surface. The capping layer is made from semiconductor material which has a higher energy gap than that of the barrier region. This acts as a barrier for those electrons with high energies, which can escape the well confinement.

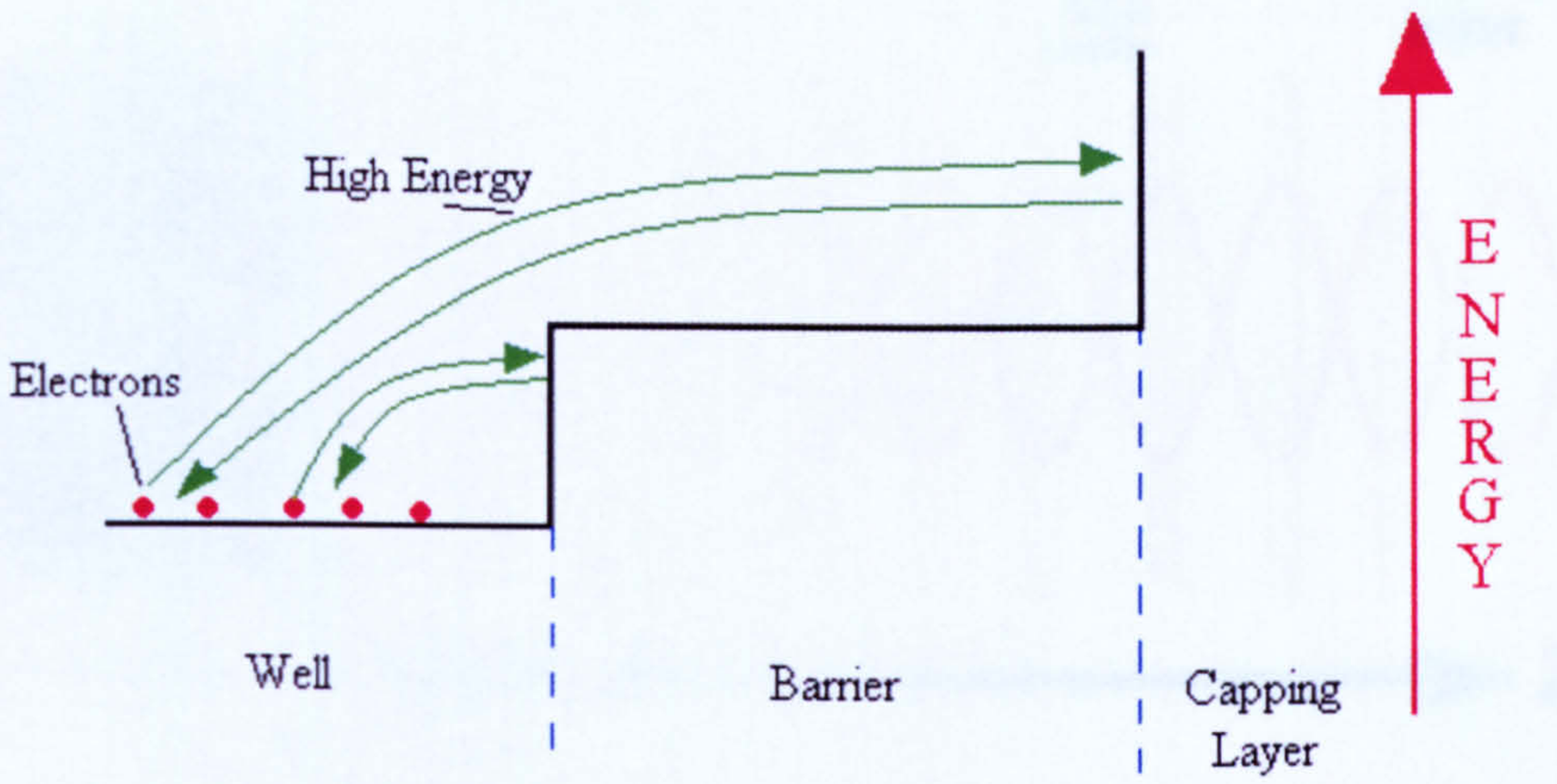

Figure (1.6.1): Capping layer energy diagram

The additional benefit from this layer is that it can be grown to desired thicknesses. This can enhance the available gain from the laser by forming a resonant structure in the small micro-cavity between the DBR and air surface.

1.7 Resonant periodic gain

The VECSEL optical length can be configured to produce a micro-cavity between the Distributed Bragg Reflector (DBR) and the capping layer. This cavity can be designed to be of suitable length to form a resonant waveform inside the gain region. The quantum wells are placed at the antinodes of the resonant wave. The electric field being the strongest at these points, means the maximum amount of gain can be extracted from the quantum wells. An additional benefit of the resonant effect is strong wavelength selectability and removal of spatial hole burning. The diagram below, figure (1.7.1) shows this effect.

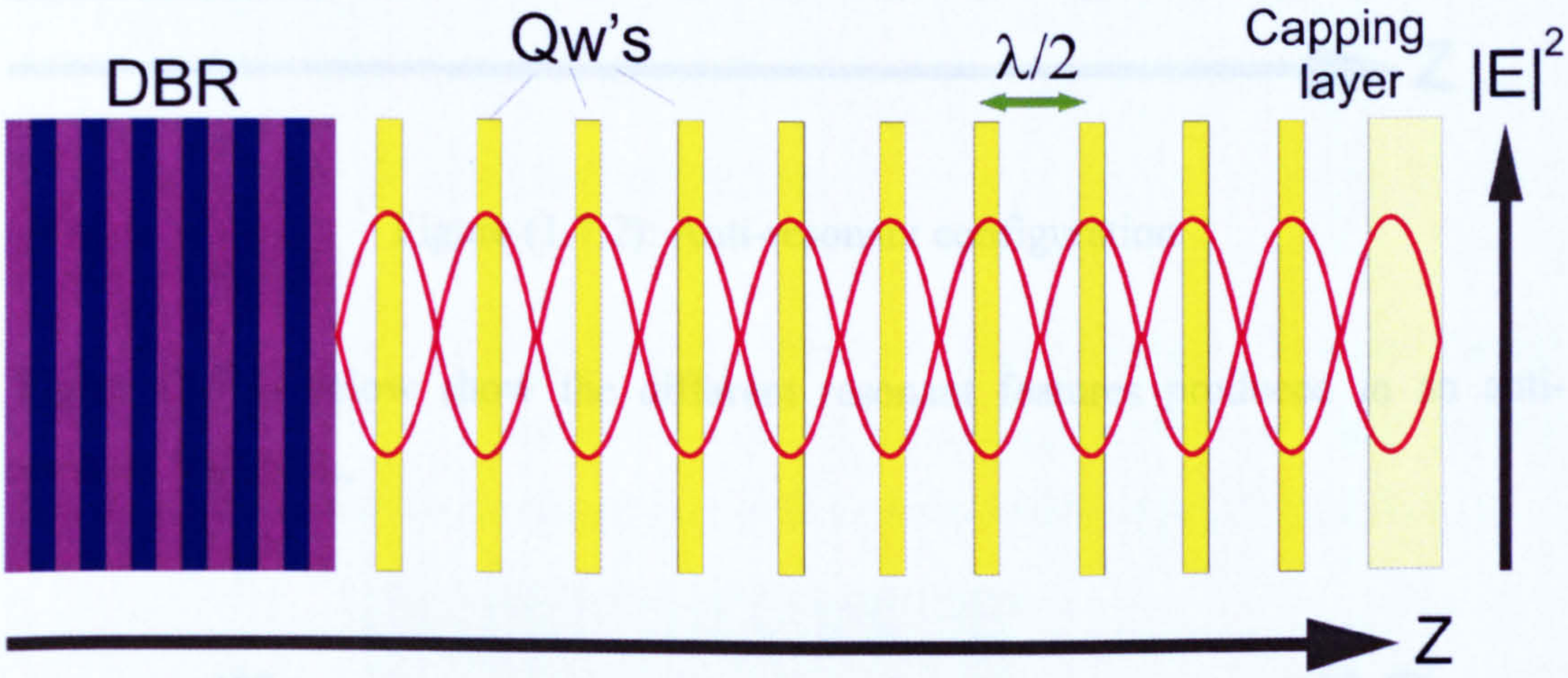

Figure (1.7.1): Resonant periodic gain structure design

The effective gain from the quantum wells can be increased using this technique, as much as double the gain can be achieved to that of a non-resonant structure [23]. However if the quantum wells are misplaced with respect to the quantum wells the effective gain will be lowered significantly.

Anti-resonant VECSELs can be produced by designing the cavity length so that no resonant features are present. This produces a lower gain extraction compared with a resonant VECSEL, however it has the compensating benefit of being a more stable laser due to the flexibility in the DBR-capping layer cavity length, which can be

influenced by temperature build up in the gain region. Figure (1.7.2) below show an anti-resonant VECSEL design.

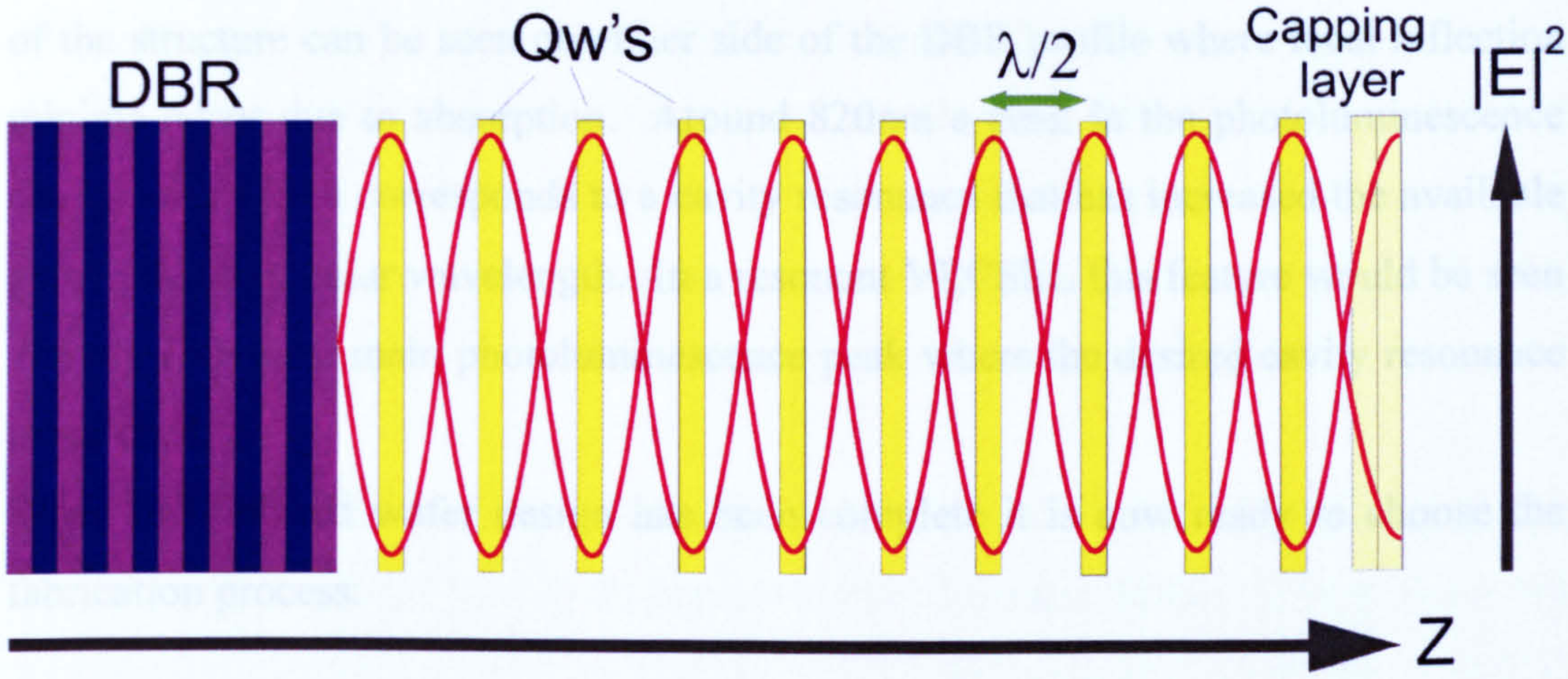

Figure (1.7.2): Anti-resonant configuration

Figure (1.7.3) below show the different resonant features produced in an anti-resonant VECSEL.

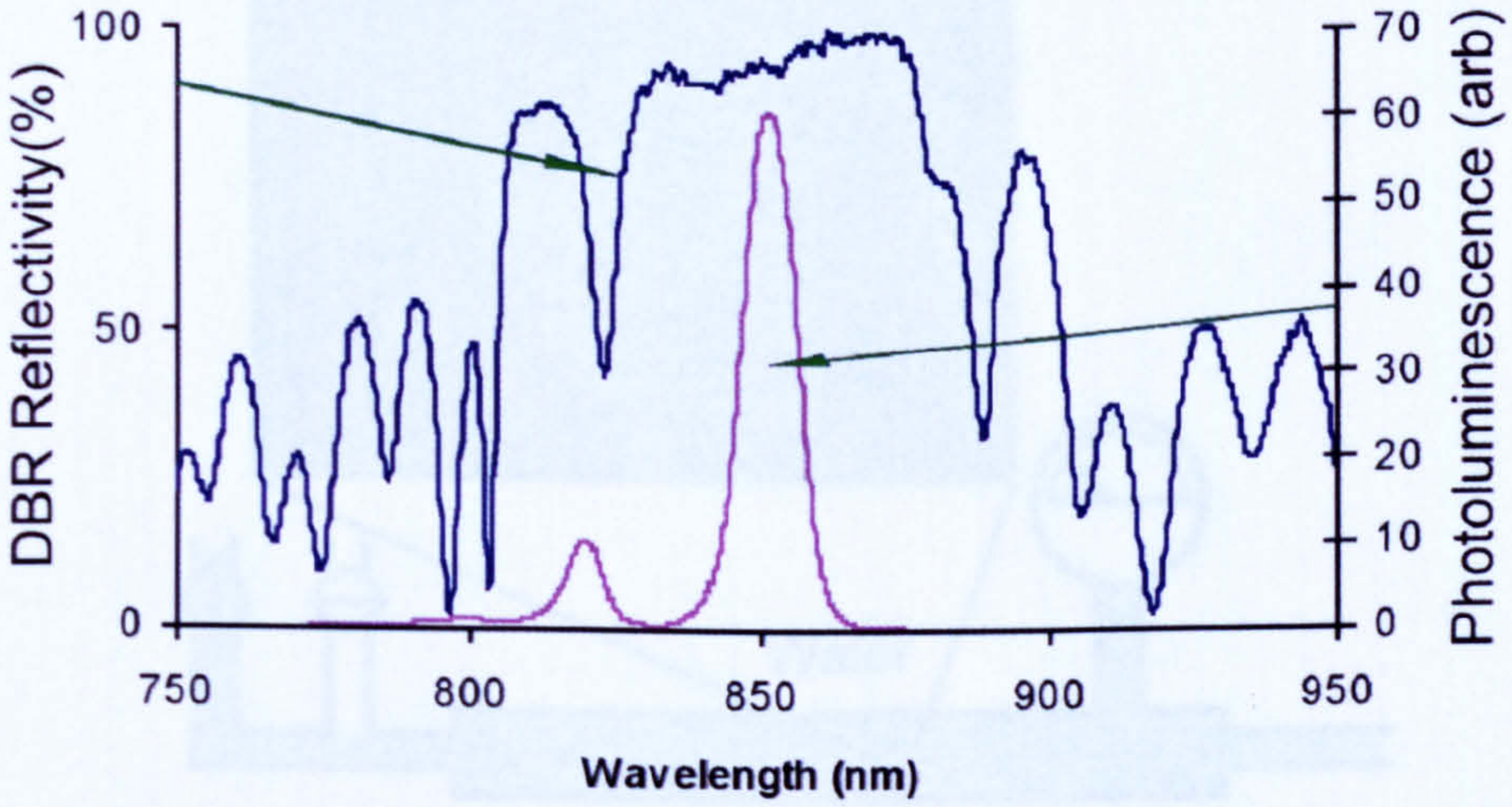

Figure (1.7.3): 850nm Anti-resonant VECSEL's
DBR & photoluminescence profile.

As seen in figure (1.7.3) the main photoluminescence (red trace) is directly under the centre of the DBR. No absorption of the DBR profile above the main photoluminescence peak indicates the sample is anti-resonant. The resonant features of the structure can be seen on either side of the DBR profile where local reflection minima occur due to absorption. Around 820nm a peak in the photoluminescence can be seen which corresponds to a cavity resonance that has increased the available gain at this particular wavelength. In a resonant VECSEL this feature would be seen directly above the main photoluminescence peak where the desired cavity resonance is matched.

When the finished wafer design has been complete it is now ready to choose the fabrication process.

1.8 Wafer Fabrication

The main process of fabricating these structures is Metal-Organic Chemical Vapour Deposition (MOCVD) or similarly known as Metal-Organic Vapour Phase Epitaxy (MOVPE). A schematic representation of this can be seen below in figure (1.8.1).

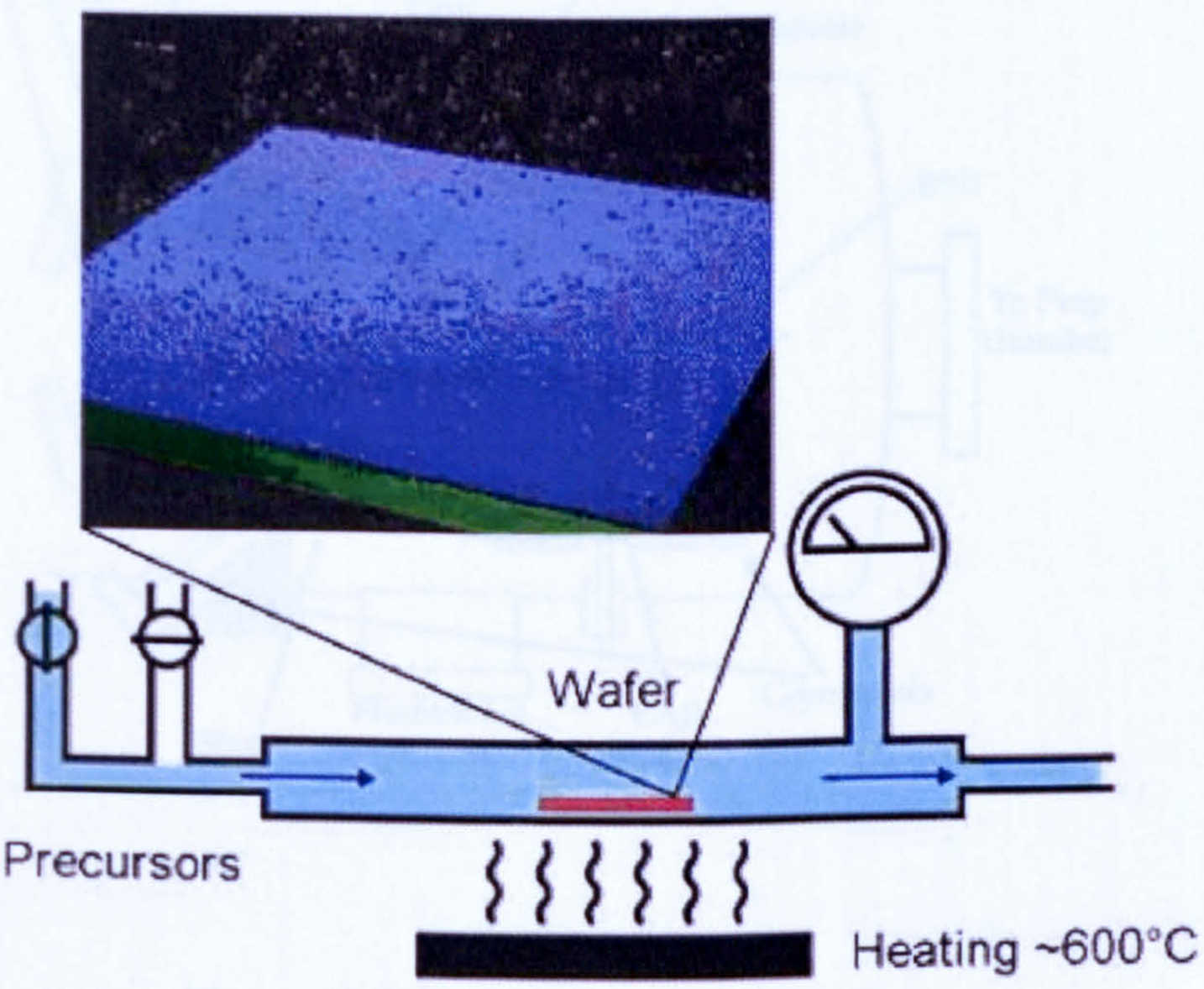

Figure (1.8.1): Schematic drawing of a MOCVD growth chamber with a magnified image of a GaAs wafer being processed. [24]

A suitable substrate is placed inside the reactor, e.g GaAs. This is then exposed to metal-organic gases (precursors) like that of arsenide, trimethyl gallium and triemthly aluminium, which pass over the substrate forming AlGaAs. The precursors are delivered into the chamber, which is heated (~600 ^{0}C) and maintained at a suitable pressure. The precursors then break up allowing desired atoms to adhere to the substrate surface. This process allows fine layers of atoms to build up over the substrate and precise layer thicknesses and compositions can be achieved. This process may take several hours for a layer of a few microns to be formed.

An additional process, which is a less favoured method for fabricating wafers due to its high vacuum tolerance, is Molecular Beam Epitaxy (MBE). This process can involve solid substrates such as arsenic, indium and gallium, which are heated in separate effusion cells. This heating causes a cloud of atoms that evaporate from the substrates surface. This can then be directed onto the acceptor substrate. This process can be seen in figure (1.8.2).

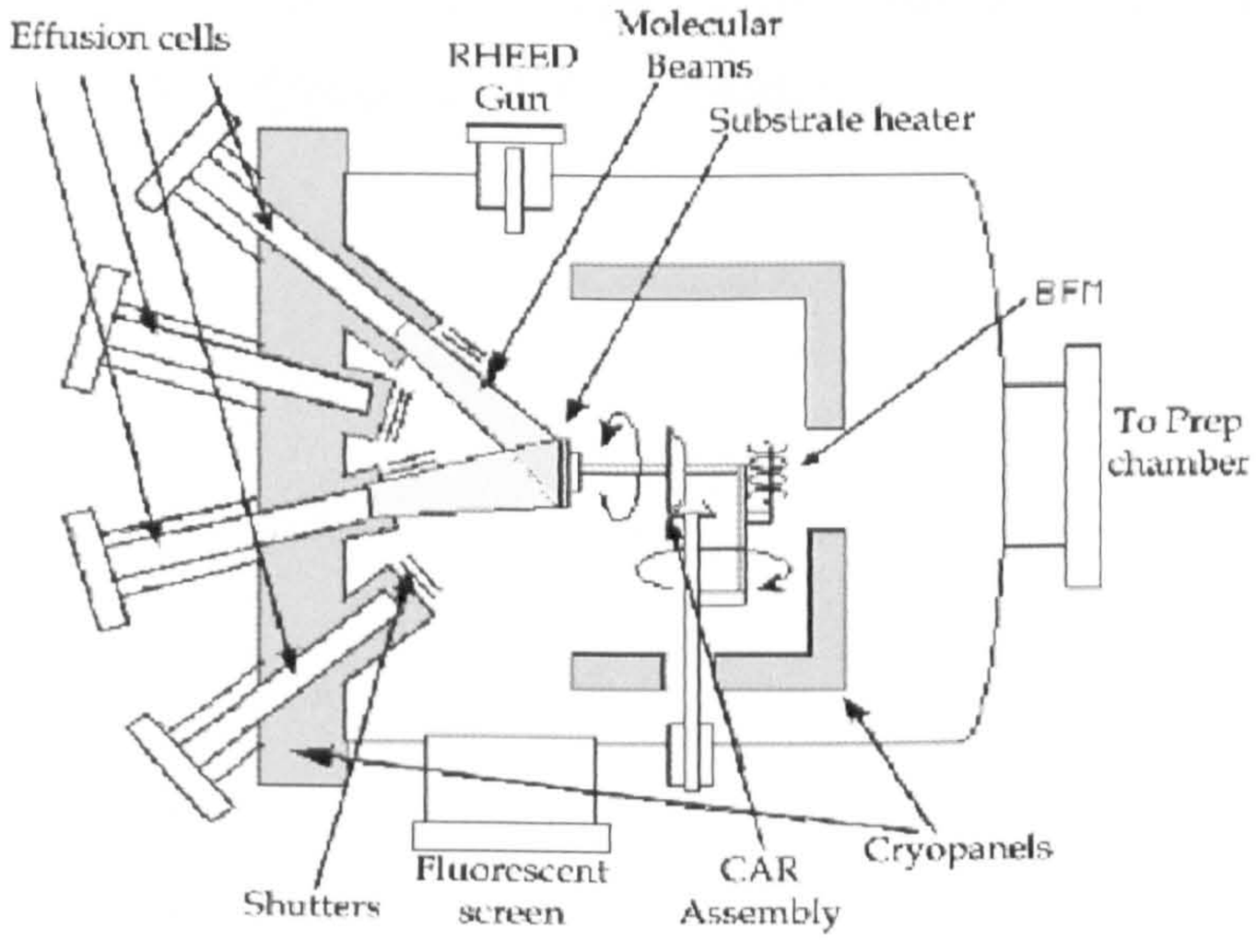

Figure (1.8.2): MBE schematic [25]

Once the desired elements have condensed on the substrate surface they interact and can form compounds. In the case of VECSEL fabrication gallium and arsenic interact on the substrate surface to form single crystal gallium arsenide. During this process careful monitoring of the thickness of the material is carried out using a process called Reflection High Energy Electron Diffraction (RHEED). RHEED involves an electron gun projected at a very wide glancing angle (>85^0). The high energy electrons (5-100keV) are recorded on a fluorescent screen or photo emission sensor. This allows precise measurement of the step edge density, which is a calibration of surface roughness. The RHEED produces an oscillating signal when deflected off the substrate that is directly proportional to the rate of increasing atom layer thickness. This makes it a perfect tool to detect surface roughness and layer growth, allowing fine adjustments and corrections to be made in real time.

Both these processes can adopt a spinning substrate sample for a more homogenous deposition. A non-rotating substrate can show slight differences over its whole area, which gives a variety of areas where the structures will be slightly different. This can be very desirable if the wafer design is new and gives an insight through experimental testing which structure is most suitable.

1.9 Conclusion

This chapter has given an introduction into how VECSELs have evolved from the semiconductor diode laser. The VECSELs design characteristics including the DBR, the quantum well and the capping layer have been outlined. This gives the basic ideas behind designing a VECSEL structure. The following chapter demonstrates how to select and package a VECSEL chip for integration into a laser cavity.

1.10 References

1. R.N. Hall, G.E. Fenner, J.D. Kingsley, T.J. Soltys, and R.O. Carlson, "Coherent light emission from GaAs junctions", Physics Review Letters, **9**, p366, (1962)

2. A.L. Schawlow and C.H. Townes, Physics Review Letters, **112**, p1940, (1958)

3. I. Hayashi, M. B. Panish and P. W. Foy, "A technique for the preparation of low-threshold room temperature GaAs laser diode structures", IEEE Journal of Quantum Electronics, **5**, no.4, p210 (1969).

4. I. Melngailis, "Longitudinal injection-plasma laser of InSb", Applied Physics Letters, **6** , no.3, p59, (1965).

5. H. Soda, K. Iga, C. Kitahara and Y. Seematsu, "GaInAsP/InP Surface Emitting Semiconductor lasers", Applied Physics Letters, **18**, p2329, (1979)

6. H.j. Unold, S.W.Z. Mahmoud, R. Jager, M. Kichere, M.C. Riedl, and K.J. Ebeling, " Improved Single Mode VCSEL Performance by Introducing a

Long Monolithic Cavity", IEEE Photonics Technology Letters, **12**, no. 8, p939, (2000)

7. A.J. Fischer, K.D. Choquette, W. W. Chow, A.A. Allermnn, and K.M. Geib, "5.2mW single-mode power from a coupled resonator vertical cavity laser", IEEE, LEOS 2000 Lasers and Electro-Optics Society, 13th Annual Meeting, Rio Grande, Puerto Rico, ThN2, p802, (2000).

8. W. B Jiang, S. R. Friberg, H Iwamura, and Y. Yamamoto, "High powers and sub picosecond pulses from an external cavity surface emitting InGaAs/InP multiple quantum well laser," Applied Physics Letters, **58**, no. 8, p807, (1991).

9. Richard H. Abram, Kyle S. Gardner, Erling Riis, Allister I. Ferguson "Narrow linewidth operation of a tunable optically pumped semiconductor laser" Optics Express, **12,** no. 22, p5434, (2004).

10 Rafailov and W. Sibbett, "Efficient frequency doubling of a vertical-extended-cavity surface-emitting laser diode by use of a periodically poled KTP crystal" Optics Letters, **28**, no.21, (2003)

11 S.H. Park, J. Kim, H. Jeon, T. Sakong, S. N. Lee, S. Chae, Y. Park, C. H. Jeong, G.Y. Yeom and H. Y. Cho, Applied Physics Letters, **83,** p2121, (2003)

12 M. Mueller, N. Linder, C. Karnutsch, W. Schmid, W.P. Streubel, J. Luft, S. Beyertt, A. Geisen and G.H. Doehier, Proc. SPIE, **4649**, p265, (2002)

13 M.A. Holm, D. Burns, P. Cusumano, A.I. Ferguson and M.D. Dawson, Applied Optics, **38**, p5781, (1999)

14 M. Kuznetsov, F. Hakimi, R. Sprague, and A. Mooradian, "High-power (>0.5-W CW) diode-pumped vertical-external-cavity surface-emitting semiconductor lasers with circular TEM_{00} beams," IEEE Photonics Technology Letters, **9**, no. 8, p1063, (1997).

15 S.Calvez, D Burns and M.D. Dawson, IEEE Photonics Technology Letters. **14**, p131, (2002)

16 A. Garnache, W.Y. Hwang, S. Hoogland, W. Martin, S. Koulikov, D. Permogorov, A.C Tropper, B. Paldus and A.A. Kanchanov, IEEE 14th Indium Phosphide and relative materials conf. Post deadline paper 3,(2002).

17 L. Cerutti, A. Garnache, A. Ouvard, F. Genty," High temperature continuous wave operation of Sb-based vertical external cavity surface emitting laser near 2.3 μm", Journal of Crystal Growth, **268**, p128, (2004)

18 Born, M., Wolf, E. "Principles of optics", Pergamon Oxford, (1970)

19 A. M. Afromowitz, "Refractive index of $Ga_{1-x}Al_xAs$" Solid State Communications, **15**, no.1, p59, (1974).

20 Wolfram, Mathematica version 4.2

21 L.S. Chuang, "Basic Quantum Mechanics", Physics of Optoelectronic Devices© John Wiley and Son Inc., p82, (1995).

22 M. Kuznetsov, F. Hakimi, R. Sprague, and A. Mooradian, "Design and characteristics of high-power (>0.5-W CW) diode-pumped vertical-external-cavity surface-emitting semiconductor lasers with circular TEM_{00} beams," IEEE Journal of Selected Topics in Quantum Electronics, **5**, no. 3, p561, (1999).

23 M. Y. A. Raya, S. R. J. Brueck, M. Osinsky, C. F. Schaus, J. G. McInery, T. M. Brennan and B. E. Hammons, "Resonant Periodic Gain Surface-Emitting Semiconductor Lasers", IEEE Journal of Quantum Electronics, **25**, no.6, p1500, (1989).

24 www.nanop.de

25 www.elettra.trieste.it

CHAPTER TWO

VECSEL WAFER ANALYSIS

This chapter demonstrates the characterisation of a VECSEL wafer and an appropriate way of mounting a VECSEL chip for implementation into a laser cavity.

2.1 THE VECSEL WAFER

Once manufactured it is important to characterise the VECSEL wafer. This ensures you are able to select a piece of wafer, which has the desirable qualities you are looking for. The three main characterisations performed on a wafer before selecting are to characterise the Distributed Bragg Reflector (DBR) and to measure the florescence levels and wavelength.

2.2 SCANNING THE DBR

A typical wafer is 2 inches in diameter. When undergoing the fabrication of these wafers small changes in uniformity can occur, creating an inhomogeneous wafer with different features throughout its area. By using a white light source it is possible to map out the wafer to show these variations. The experimental setup is shown in figure (2.2.1).

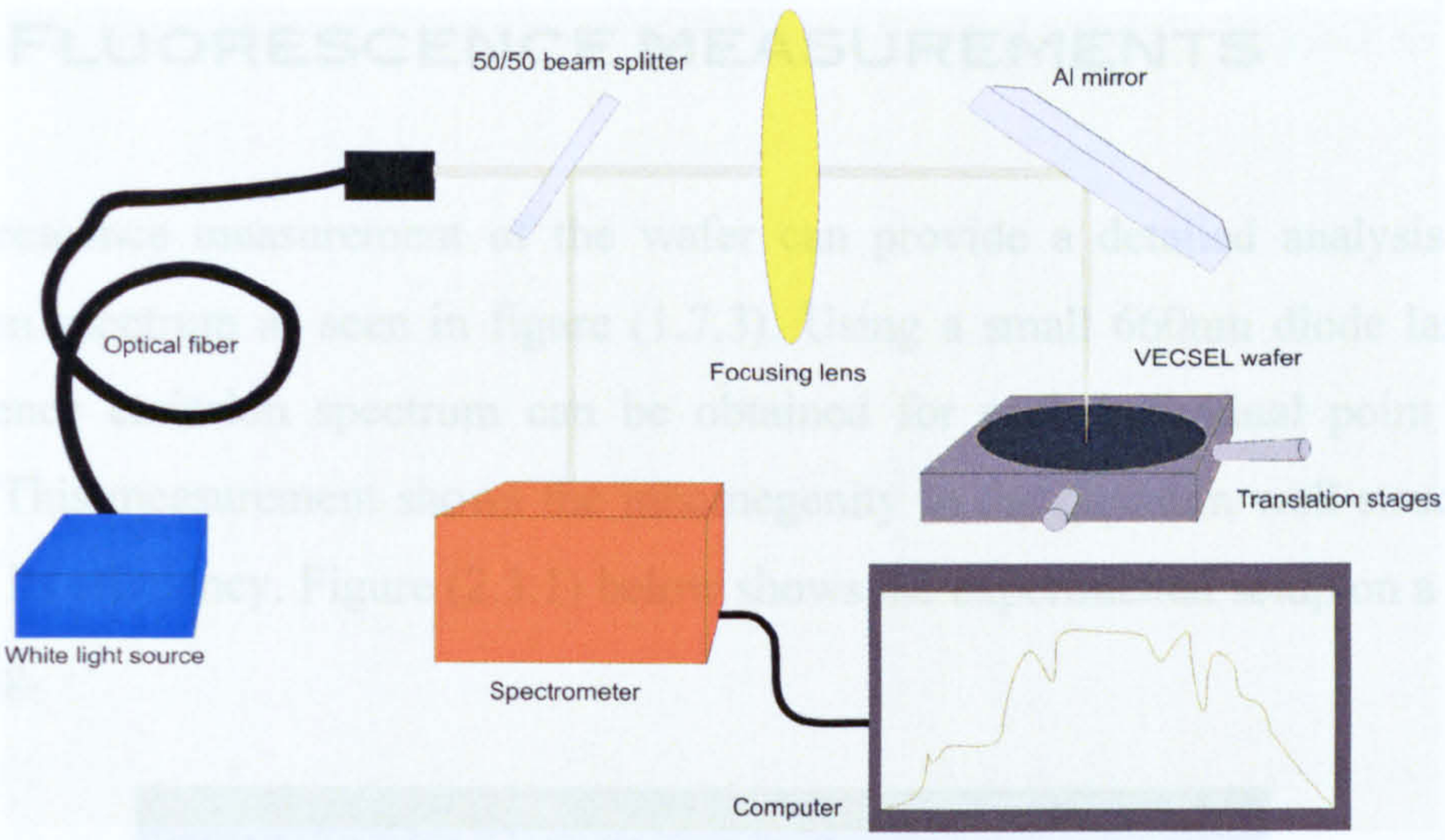

Figure (2.2.1): Mapping out the DBR profile of the wafer

The tungsten lamp emits a broad spectrum of light from 250nm-2500nm, which provides a perfect optical source to scan the wafer over its critical wavelengths. By illuminating a small part of the wafer, a profile of the DBR can be achieved. In addition this process also allows the sub-cavity resonances to be seen. By scanning the wafer in a 3mm x 3mm grid a map of the wafer's structure can be generated. From this map it is now possible to pick a piece of wafer with desired features. Figure (2.2.2) below shows a typical map of VECSEL wafer.

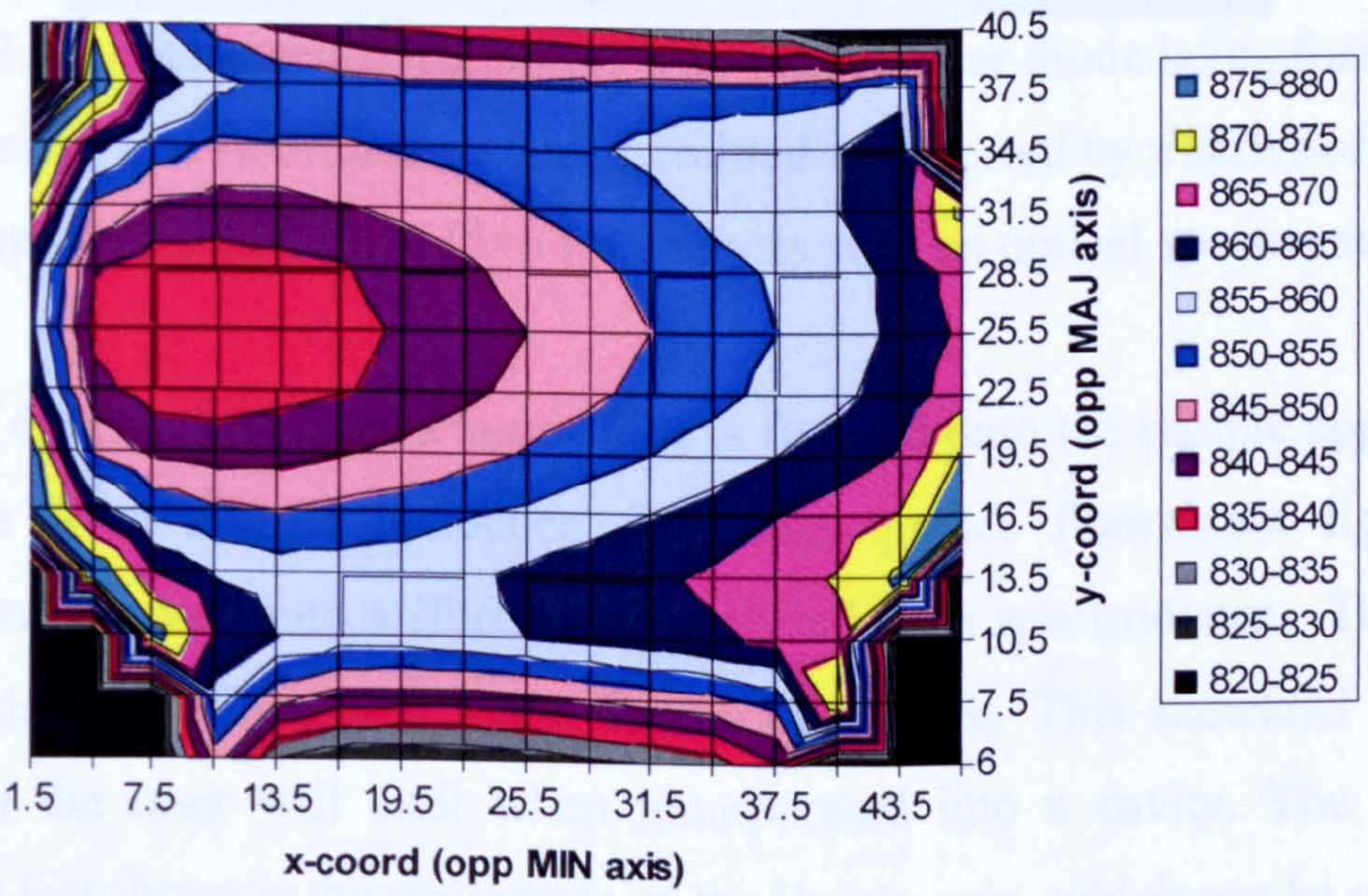

Figure (2.2.2): DBR scan of VECSEL wafer showing central wavelengths of DBR stop band

2.3 Fluorescence measurements

A fluorescence measurement of the wafer can provide a detailed analysis of the emission spectrum as seen in figure (1.7.3). Using a small 660nm diode laser, the florescence emission spectrum can be obtained for each individual point on the wafer. This measurement shows the inhomegenity in the quantum well structure as well as its efficiency. Figure (2.3.1) below shows the experimental setup on a custom made jig.

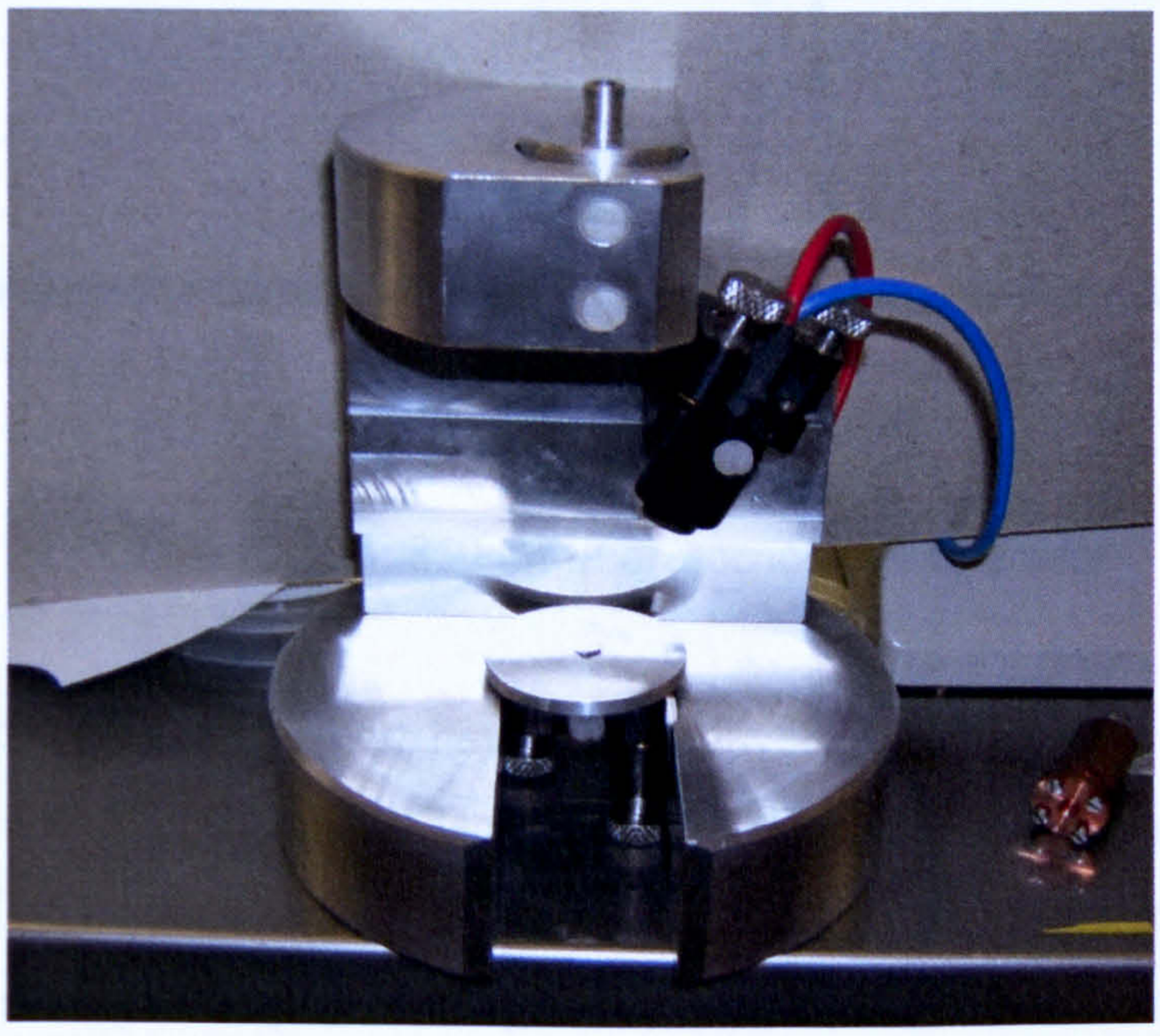

Figure (2.3.1): Fluorescence testing jig with 660nm laser diode being focused on the VECSEL chip. The fluorescence that is emitted is collected by a series of lenses and coupled into an optical fibre for analysis with an optical spectrometer.

A beam of 660nm light from a laser diode is focused onto the sample approximately 15 degrees from normal incidence. The subsequence fluorescent light is then collected and focused into a fibre to be analysed by a spectrometer. The resulting data provides the VECSEL's main fluorescence peak. This indicated the natural wavelength the laser will emit when incorporated into a cavity. The other main feature this test shows is the magnitude of the laser's gain, which can be compared to other samples that have been taken. If the alignment and composition of the quantum wells are correct then a large fluorescence is measured relative to the wafer. This can

be used to determine a satisfactory piece of wafer that can be utilised in a laser cavity.

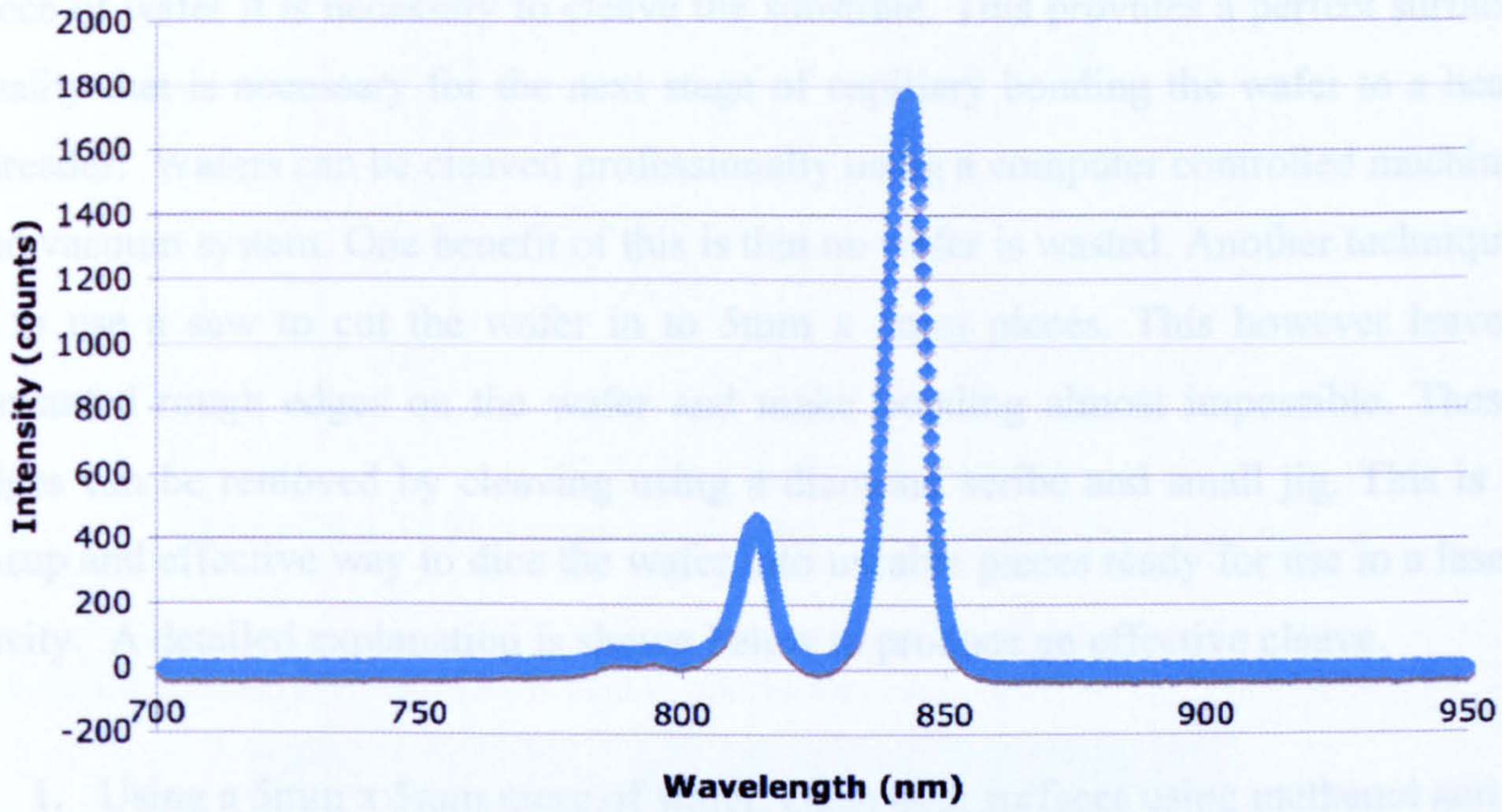

Graph (2.3.1): 850nm fluorescence measurement

A desirable piece of wafer will have a high level of fluorescence relative to the whole wafer and a high DBR reflectivity at the fluorescent maxima. In addition a resonant VECSEL will have a dip in DBR reflectivity above the main fluorescent peak due to absorption by the cavity enhancement, as shown in a the schematic figure (2.3.2) below.

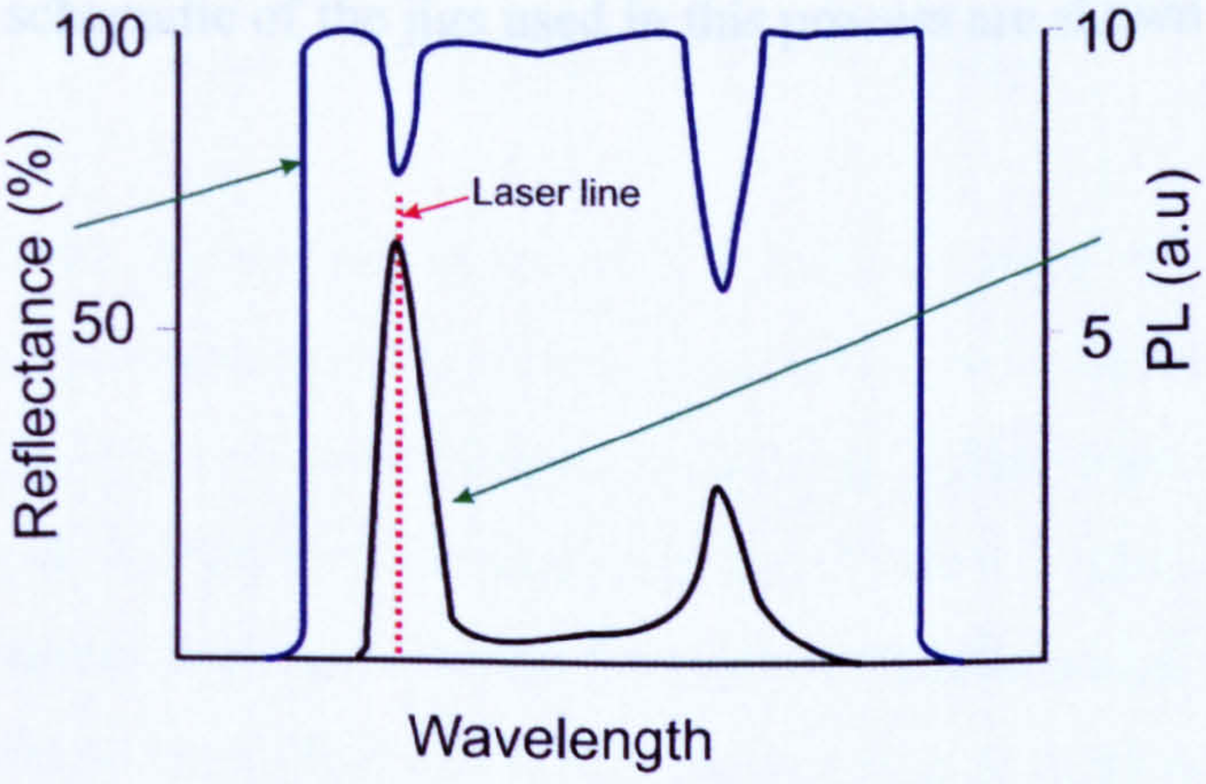

Figure (2.3.2): Resonant VECSEL showing DBR reflection minima aligned with main photoluminescence peak.

2.4 CLEAVING

Once a suitable piece of wafer has been selected from the above steps it is now ready to be cleaved and mounted into a VECSEL cooling block. To remove the desired piece of wafer it is necessary to cleave the substrate. This provides a perfect surface quality that is necessary for the next stage of capillary bonding the wafer to a heat spreader. Wafers can be cleaved professionally using a computer controlled machine and vacuum system. One benefit of this is that no wafer is wasted. Another technique is to use a saw to cut the wafer in to 5mm x 5mm pieces. This however leaves unwanted rough edges on the wafer and make bonding almost impossible. These edges can be removed by cleaving using a diamond scribe and small jig. This is a cheap and effective way to dice the wafer into useable pieces ready for use in a laser cavity. A detailed explanation is shown below to produce an effective cleave.

1. Using a 5mm x 5mm piece of wafer, clean both surfaces using methanol and place face down on lens tissue.
2. Scribe using a diamond tool across the back surface of the wafer in one clean motion. A jig can be used to guide the scribe.
3. Place this scribed piece into a small jig of correct depth and bend away from scribed surface.
4. Clean sample and repeat process for the remaining 3 sides.

These steps should leave a small piece of VECSEL chip left with four perfectly cleaved sides. A schematic of the jigs used in this process are shown in figure (2.4.1).

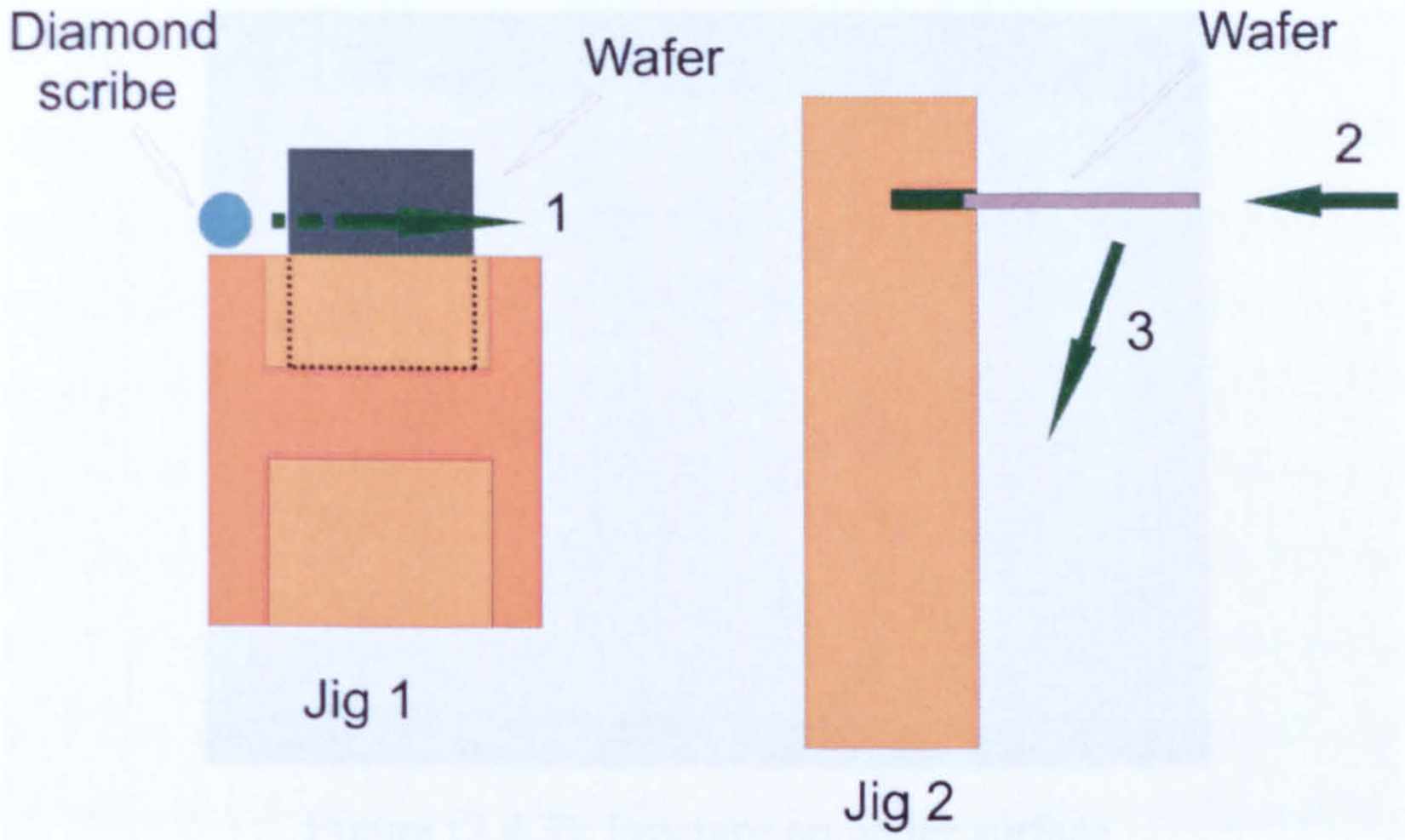

Figure (2.4.1) Schematic representation of wafer cleaving jigs

An example of a good cleaved wafer is shown below.

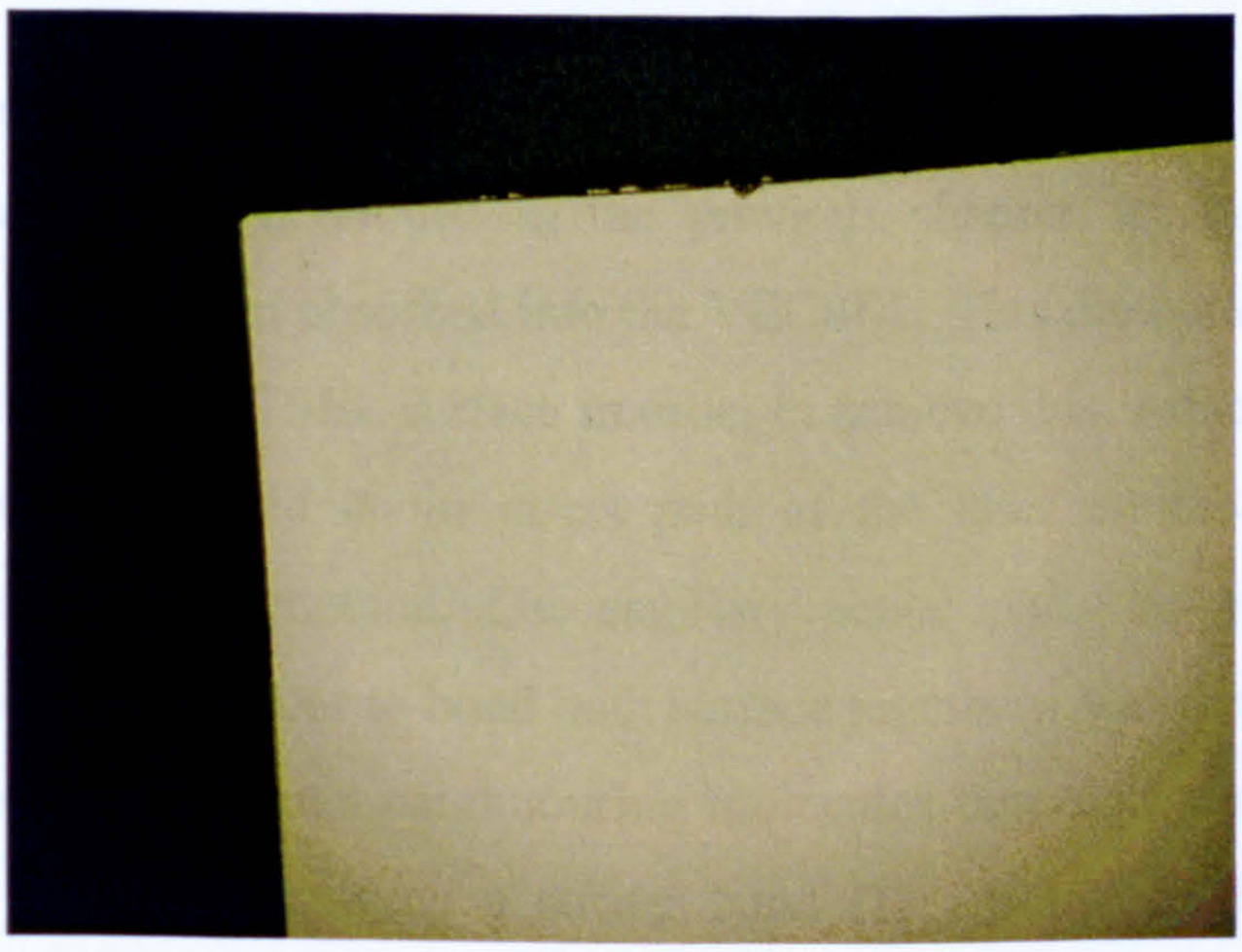

Figure (2.4.2): Cleaved VECSEL edge

Figure (2.4.2) above shows two sides of a VECSEL wafer that has undergone cleaving. Cleaving provides a clean perfect edge, which helps in the next process of capillary bonding. Although most cleaves produce a perfect edge, small chips can occur but will not hinder the bonding process. However poor cleaving of the VECSEL substrate can cause small stress fractures on the surface of the wafer, which causes raised layers to form. This can hinder the bonding process causing pockets of poorly bonded areas, which can perform ineffectively in a laser cavity. Figure (2.4.3) shows an optical microscope image of these fractures.

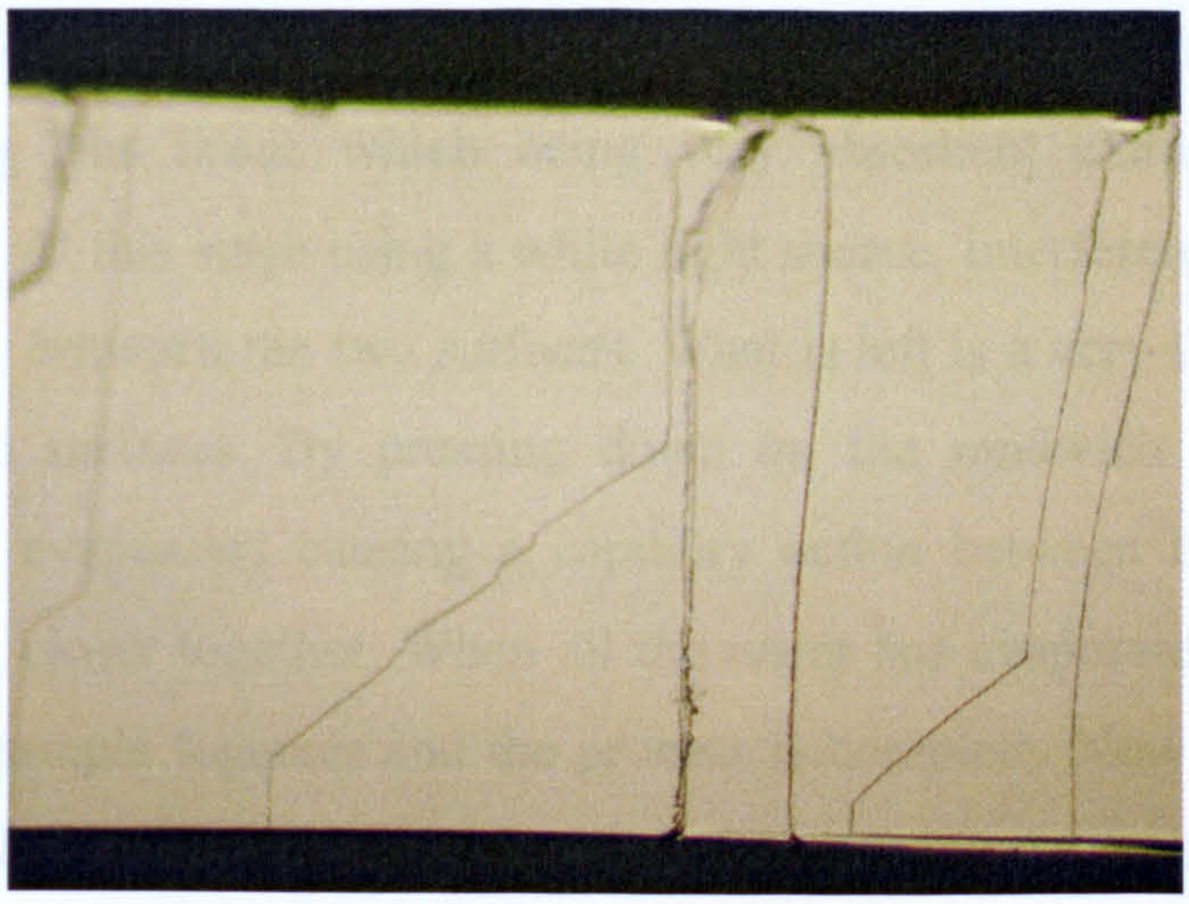

Figure (2.4.3): Fracture on wafer surface

2.5 CAPILLARY BONDING

The next and most critical step to packaging a VECSEL is the capillary bonding of the heat spreader. As mentioned in the previous chapter, diamond is used to effectively remove the heat absorbed into the VECSEL. This diamond needs to be in good contact with the VECSEL surface in order to achieve this. Adhesive provides a secondary layer and would be in direct path of the laser emission so capillary bonding is the preferred method. The capillary action pulls the surface together allowing van der Waals forces to bond both surface together. Van der Waals force is the dipole interaction between neighbouring molecules that electrically attract each other in close proximity creating a strong bond [1]. Below is the step-by-step process to achieving a good capillary bond.

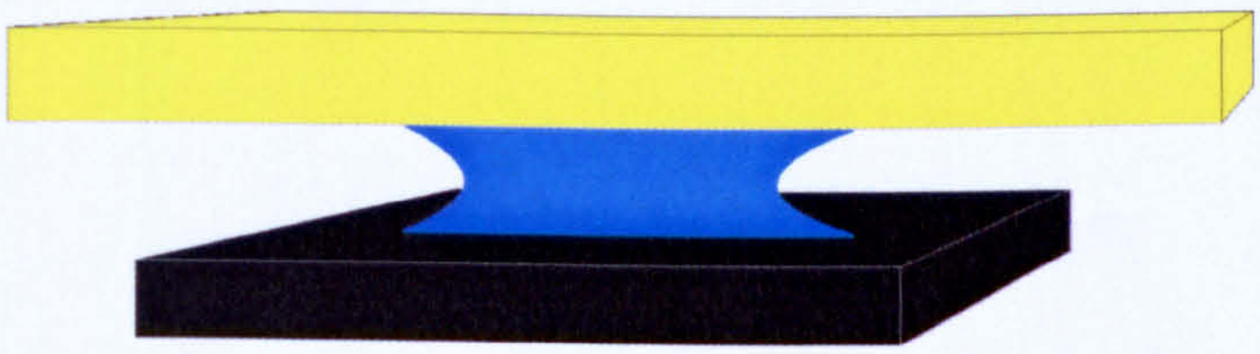

Figure (2.5.1): Diamond/VECSEL substrate with H_2O droplet

Both surfaces have to be immaculately clean for this process to work. Once clean a droplet of pure water is placed on the VECSEL surface. This diamond is then placed

on top of this and the water is squeezed out, figure (2.5.1). The remaining water is drawn out using lens tissue which being very absorbent extracts most of the remaining water. At this stage using a white light source, interference fringes can be seen quite clearly between the two surfaces. What is left is a very thin film of water between the two surfaces. By pressing down on the sandwich of materials the remaining water evaporates causing a capillary action between the two surfaces, which are drawn closer together. When all the water has evaporated, van der Walls forces bond the sample together and the process is complete. Now the pressure can be released and the bond can be inspected. A good bond is shown by all areas of the VECSEL being black. A bad bond shows grey areas on the edges and/or in other areas surrounding the bonded (black) areas. If bonding is not successful the process must be repeated from the start, after further cleaning of the two surfaces. Figure (2.5.2) shows a schematic representation of these bonding types.

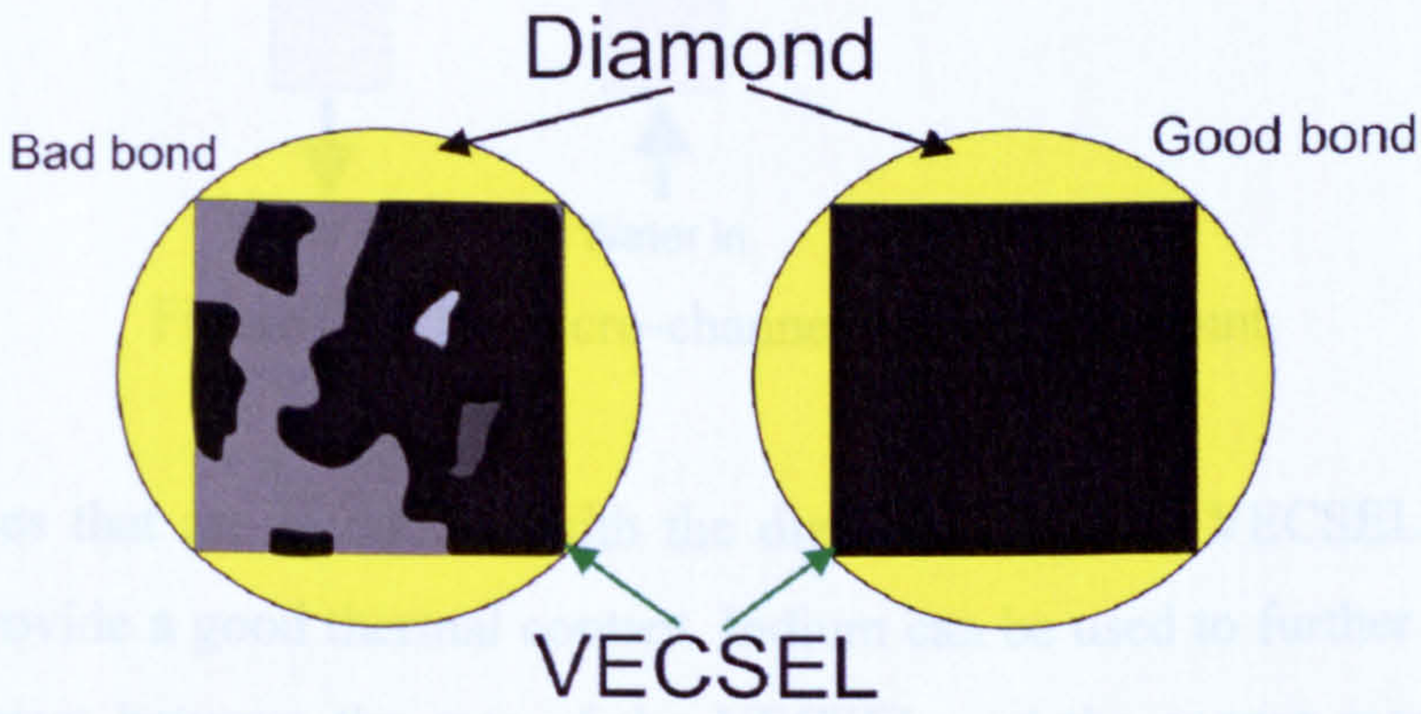

Figure (2.5.2): Capillary-bonding characteristics of good and bad bonds.

2.6 Mounting the wafer

The last step in preparing the VECSEL ready for use is to mount the wafer/diamond sandwich into a copper cooling block. This block acts as a heat sink for the diamond and rear surface of the VECSEL. Figure (2.6.1) shows a typical copper mount.

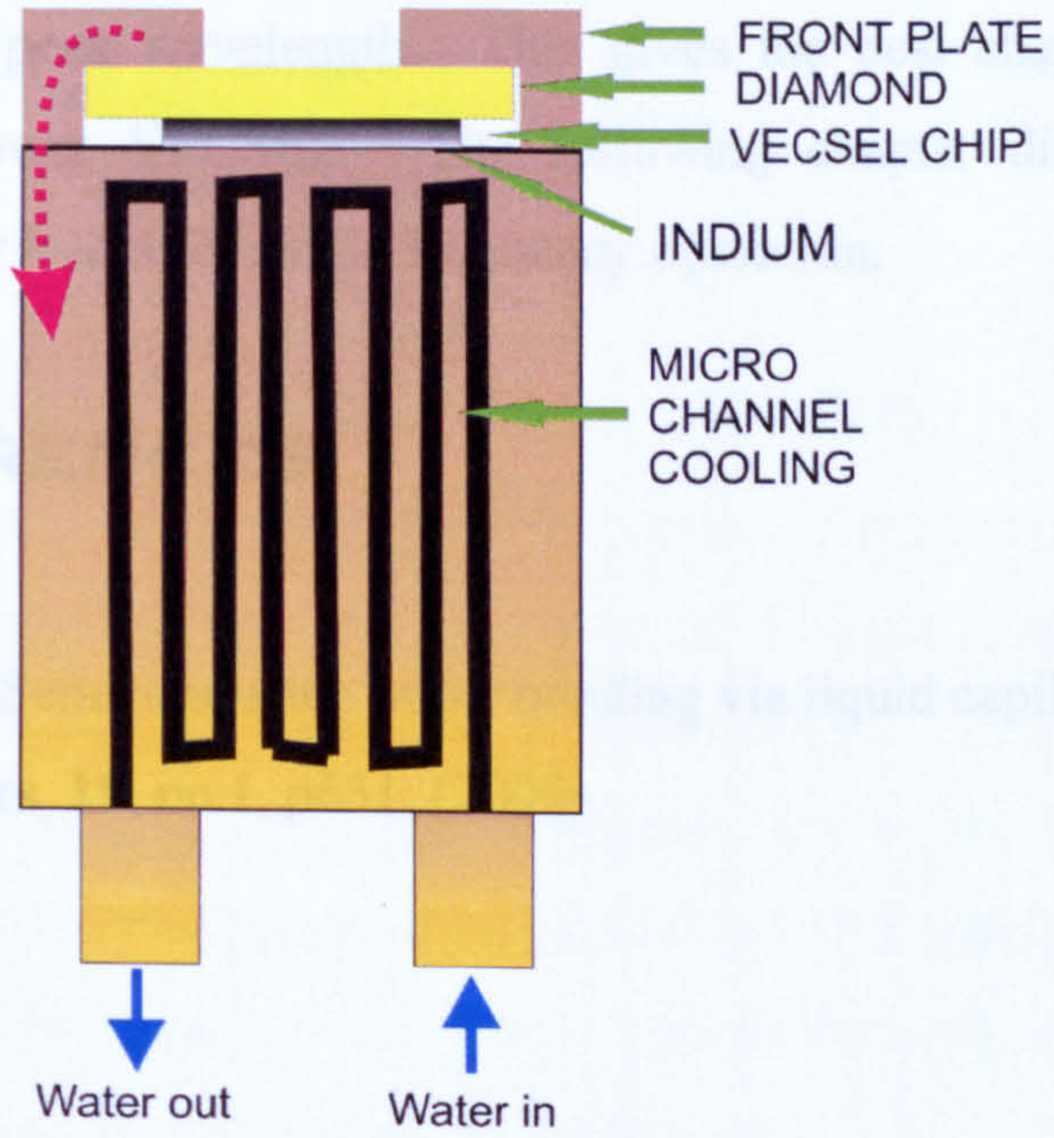

Figure (2.6.1): Micro-channelled cooling mount.

Both surfaces that are in contact with the diamond and rear VECSEL surface are lapped to provide a good thermal contact. Indium can be used to further increase the thermal contact between the rear of the VECSEL and the copper mount. Micro-channelled waterways are incorporated into the rear of the copper mount to provide efficient heat removal by water-cooling.

2.7 Conclusion

The process of picking the right sample of VECSEL has been discussed and how to correctly bond and mount for use in a laser cavity. It is essential to pick a correct piece of VECSEL wafer with high fluorescence levels, good DBR profile and an agreeable resonant peak wavelength. This gives the best chance to successfully creating a high power VECSEL. The following chapter discusses the use of VECSELs and other lasers for single frequency operation.

2.8 References

1. Z. L. Liau, "Semiconductor wafer bonding via liquid capillarity", Applied physics letters, **19**, no.1, p651, (2000).

CHAPTER THREE

SINGLE FREQUENCY OPERATION

This chapter introduces single frequency lasers and the motivation for a single frequency VECSEL.

3.1 SINGLE FREQUENCY LASERS

Single frequency lasers are a very desirable tool in several optical applications. A truly single frequency laser has the attributes of a single longitudinal and single transverse mode with narrow bandwidth, a single coherent state. This feature gives the laser only one true frequency present at one time in the laser cavity. These features allow it to be used as a very precise tool in many applications such as fibre optic sensing, atom trapping, precise distance measurements with interferometery, fibre optic communication and sensing to name a few.

Spectroscopy is perhaps the biggest application for single frequency laser. The narrow linewidths of single frequency lasers [1], make it possible to detect atomic transitions that enable the study of atoms and material composition. These studies have encouraged the growth of the single frequency laser from its introduction in 1981 by Arthur L. Schawlow [2]. Consisting of a dye laser that incorporated a Fabry Perot etalon and Echelle grating to initiate single frequency operation. Dye lasers offered a wide range of wavelength availability from the visible to near infrared. One main problem with the dye laser is that it requires constant maintenance of the dye solutions. The introduction of the Ti:sapphire laser in 1986 by Moulton [3] was the next major step in single frequency lasers. The wide tunability of the solid state crystal medium made it possible to create a single frequency laser with tuning ranges from ~650-1100nm with long stability and useful lifetime. The Ti:sapphire replaced its predecessor the dye laser and is to this date the most widely used single frequency laser for spectroscopy applications.

Many solid state lasers inherently produce a wide broadband emission spectrum like that of the Ti:sapphire and dye lasers. Using intra-cavity elements it is possible to force single frequency operation. Most commonly the use of a birefringent filter (BRF) and solid etalon are used as spectral filters to filter out any unwanted cavity modes and allow the frequency of the laser to be tuned to the desired wavelength with a reduced bandwidth depending on the spectral filtering of these elements.

3.2 Birefringent filters (BRF)

A BRF is made from a birefringent material, typically quartz. This is cut at Brewster's angle for low loss insertion in a laser cavity. The birefringent effect of this filter splits up the extraordinary and ordinary rays, as each ray experiences a difference in refractive index, producing two rays with different phase velocities. Only wavelengths with path length differences of integral multiple wavelengths will pass thought the BRF. Low losses occur for integral orders of full waves, producing a comb-like transmission. In addition this effect gives the element an incremental tuning ability of its transmission fringes. Typically the free spectral range of a BRF it 300GHz. A slight rotation of the BFR allows the laser to translate the wavelengths of the transmission peaks. This allows course tuning of the laser and lowers the bandwidth. This however is sometime not enough to force the laser into pure single frequency mode. An etalon is added with a smaller free spectral range, which reduces the bandwidth and suppresses additional modes.

3.3 Etalon

A standard soild etalon (Fabry-Perot etalon) uses multiple reflections to act as an optical interferometer. An etalon is made from a thin plate of non-birefringent material, whose surfaces are parallel. Dielectric coatings can be used to enhance the reflectivity of both surfaces to a desired value. Multiple reflection between its two surfaces results in constructive and destructive interference that produces a periodic wavelength transmission. Optical transmission is determined by the etalon thickness and the reflectivity of its surfaces.

Consider a solid etalon made from fused silica in an ambient medium of air. A light path (A_i) traverses the etalon of length (l), which is tilted by θ_0, shown below in figure (3.3.1)

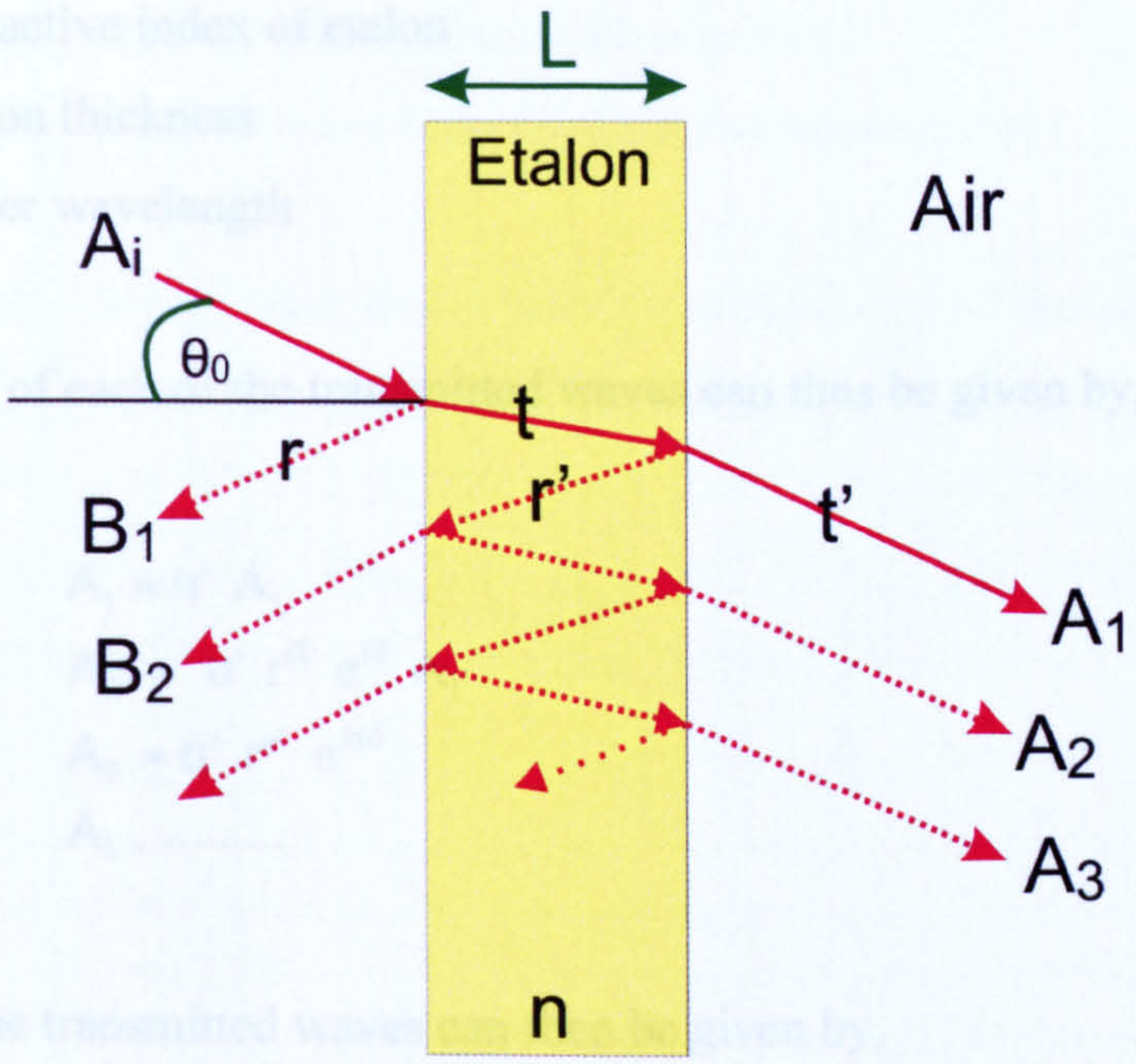

Figure (3.3.1): Fabry-Perot etalon, multiple reflection model. r and t are the coefficients of reflection and transmission respectively from air to silica. Likewise r' and t' are the coefficients of reflection and transmission respectively from silica to air. A_i, A1, A_2, A3, B1 and B_2 are the amplitude of the electric field at the various positions.

Starting with the amplitude of the incident electric field, A_t, the reflected amplitude from the first interface is given by B_1, in addition the partially transmitted amplitude from the second interface is given by A_1. The coefficients of amplitude reflection, r, and transmission, t, denote light travelling from air to silica and likewise the coefficients r' and t' denote the light travelling from silica to air. The multiple output beams differ in phase due to differences in path lengths traversed by each of the beams. The optical phase acquired by the light on one round trip through the etalon is given by, [4]

$$\delta = \frac{4\pi n l \cos\theta}{\lambda}$$

equ:(3.3.1)

Where n = Refractive index of etalon

l = Etalon thickness

λ = Laser wavelength

The amplitudes of each of the transmitted waves can thus be given by,

$A_1 = tt'\ A_i$ equ:(3.3.2)

$A_2 = tt'\ r'^2\ e^{i\delta}\ A_i$ equ:(3.3.3)

$A_3 = tt'\ r'^4\ e^{2i\delta}$ equ:(3.3.4)

A_i , ... equ:(3.3.5)

The sum of these transmitted waves can then be given by,

$$A_t = A_i tt'(1 + r'^2 e^{i\delta} + r'^4 e^{2i\delta} + ...) = \frac{tt'}{1 - rr'e^{i\delta}} A_i \quad \text{equ:(3.3.6)}$$

The fractional output intensity, or power transmission, $T=I_t/I_i$, from the ideal etalon is then given by,

$$T = \frac{I_t}{I_i} = \frac{A_t A^*_t}{A_i A_i^*} = \frac{(tt')^2}{(1 - rr')^2 + 4\sqrt{rr'}\sin^2(\delta/2)} \quad \text{equ:(3.3.7)}$$

In a perfect lossless system, with r = r' for identical surfaces, this above equation simplifies to the following equation

$$T = \frac{1}{1 + F\sin^2(\delta/2)} \quad \text{equ:(3.3.8)}$$

Where, $F = \frac{4R}{(1-R)^2}$, the etalon's finesse

$$\delta = \frac{2\pi}{\lambda} 2nd\cos\theta$$

R = reflectivity of each face = $|r|^2$

d = The physical separation of the etalon mirrors

θ= Internal angle between light rays and the etalon normal

This equation can now be used to see how the reflectivity of the etalon affects the width of the pass band and the attenuation of side modes.

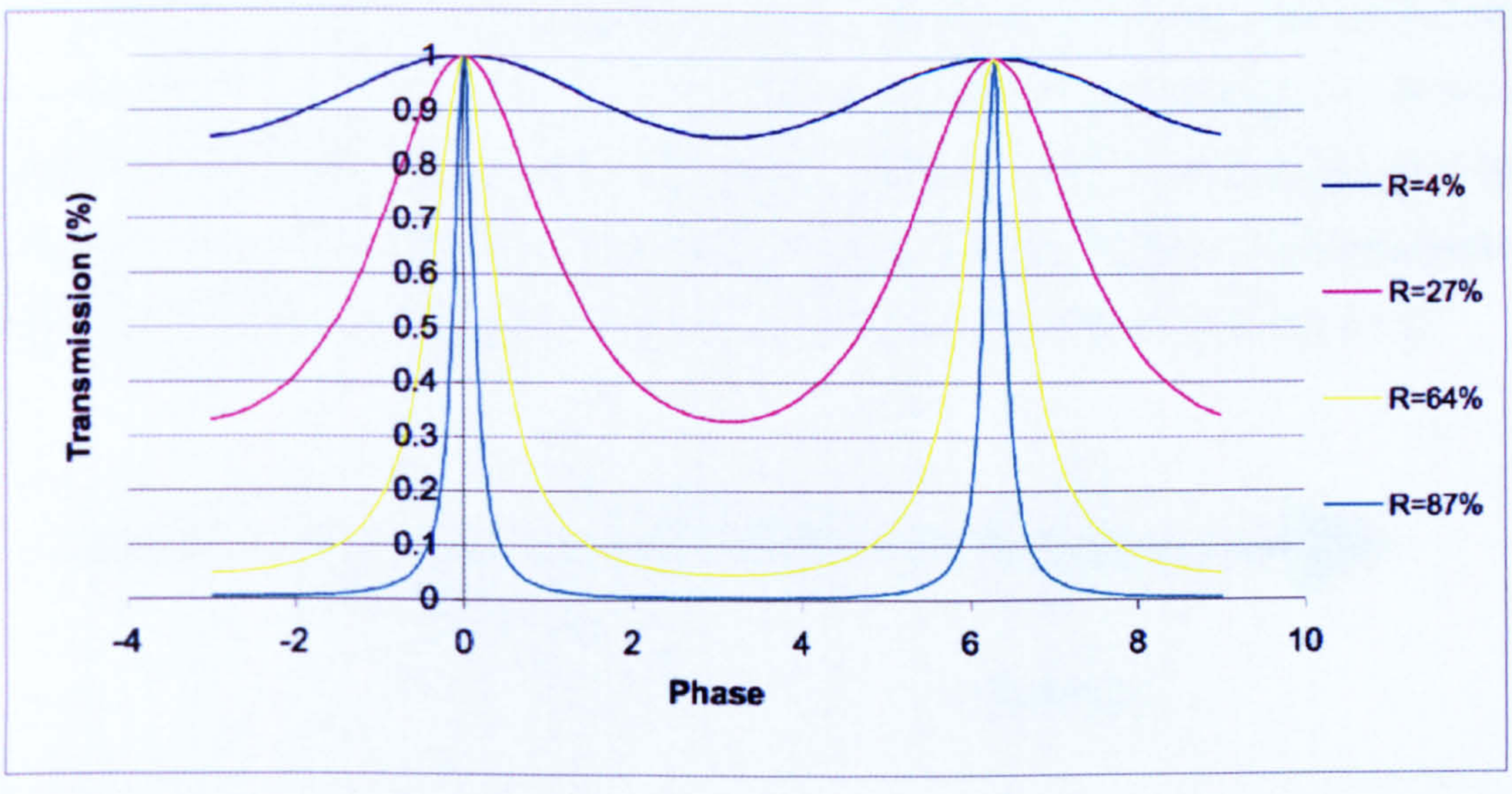

Figure (3.3.2): Etalon transmission for various surface reflectivities.

It can be seen that as the reflectivity of the etalon is increased the band pass of the etalon is greatly reduced. This however also increases the intra-cavity losses due to the etalon being more reflective which causes significant losses [5]. This can be balanced by using the lowest reflecting etalon, which will produce single mode operation.

In most applications it is necessary to select a single mode and maintain it for an extended period of time. The laser can jump modes with as little as one thousandth of a degrees rotation of the etalon therefore it must be controlled to prevent this. Currently there are two main methods to control this, a passive technique and an active technique. The passive technique involves the addition of another etalon with a reduced FSR. The active technique and the most commonly used method, is to use

feedback to control the rotation of the etalon. An electronically derived modulation signal is fed back to the etalon at a frequency of 80-90 kHz around the refection minimum. This stabilises the laser mode, however it also creates a loss at twice the modulation frequency in addition to acoustic vibrations, which produce undesirable modulations (amplitude noise).

A solution to this problem is to use a birefringent etalon [6]. A quarter wave plate with reflection coating on both sides can be used as an intra-cavity etalon. The etalon is inserted into the cavity as a slight angle to the laser beam. It is then rotated just off one of the optic axes with respect to the laser beams polarisation to create a reflection beam that is frequency dependent. This can then be used to generate an electronic signal to stabilise the etalon by feeding back a signal to a galvanometer that controls the etalon rotation. Figure (3.3.3) shows polarisation analysis setup.

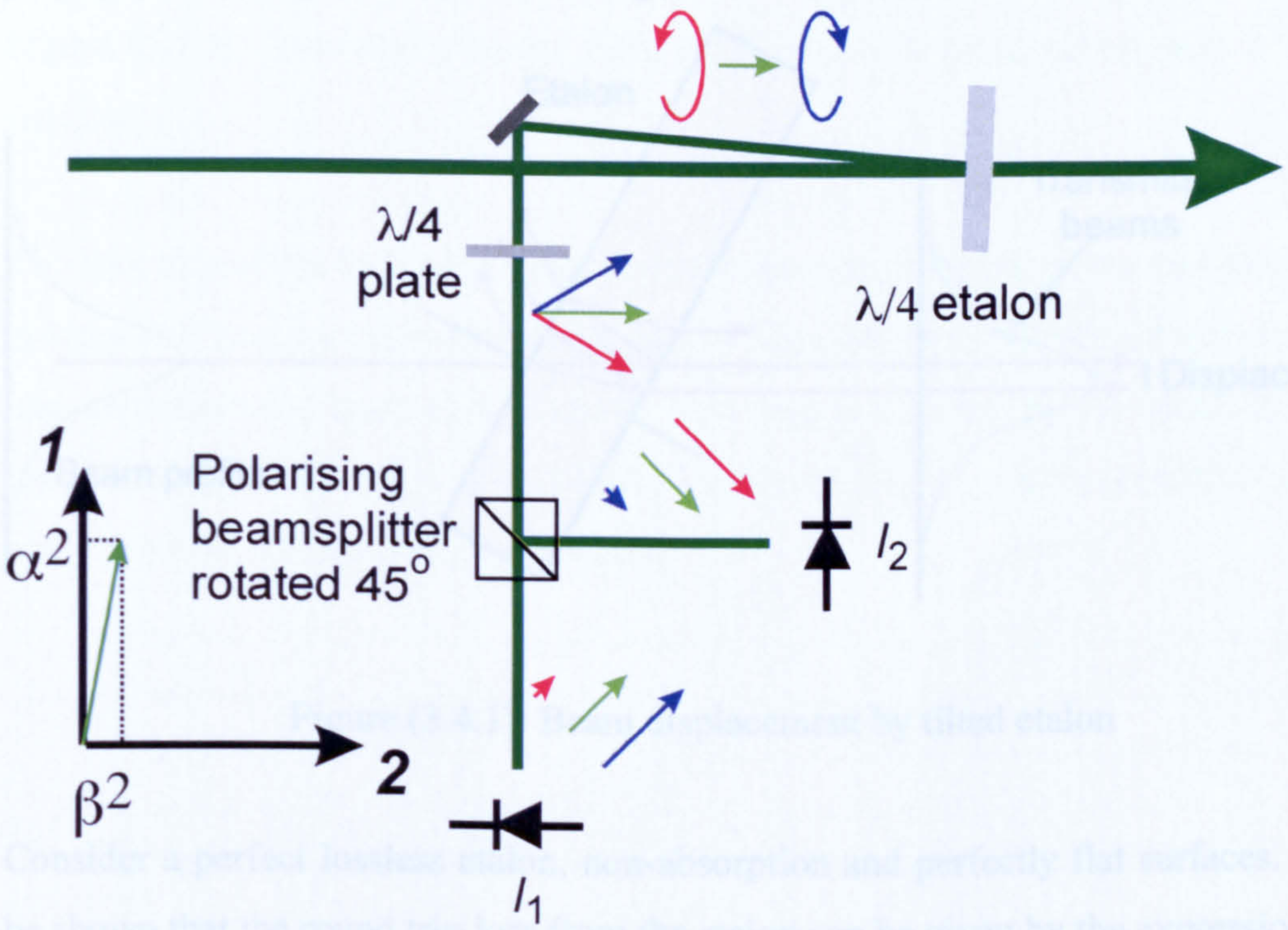

Figure (3.3.3): Birefringent etalon feedback analysis, using a combination of a quarter wave plate and a polarising beamsplitter cube. Blue and red arrows indicate the 1 and 2 axis polarisation magnitude respectively.

This technique obviates the need to modulate the etalon to achieve stable single mode operation, which has the added benefit of producing a low noise laser. Linewidths of 5kHz have been demonstrated [7].

3.4 Etalon losses

Although solid etalons give good selectivity of the available laser modes the process can generate considerable losses in the extremes of the tuning range. Simply by tilting the etalon in the cavity causes the cavity mode to "walk-off" causing a displacement of the laser beam. This displacement causes slight misalignment of the laser cavity, which causes significant losses in the laser to the extent of stopping lasing. Calculations can be made to determine the losses experienced in a laser cavity when the angle of the etalon is tilted. Figure (3.4.1) shows the beam propagation through an etalon at an angle θ.

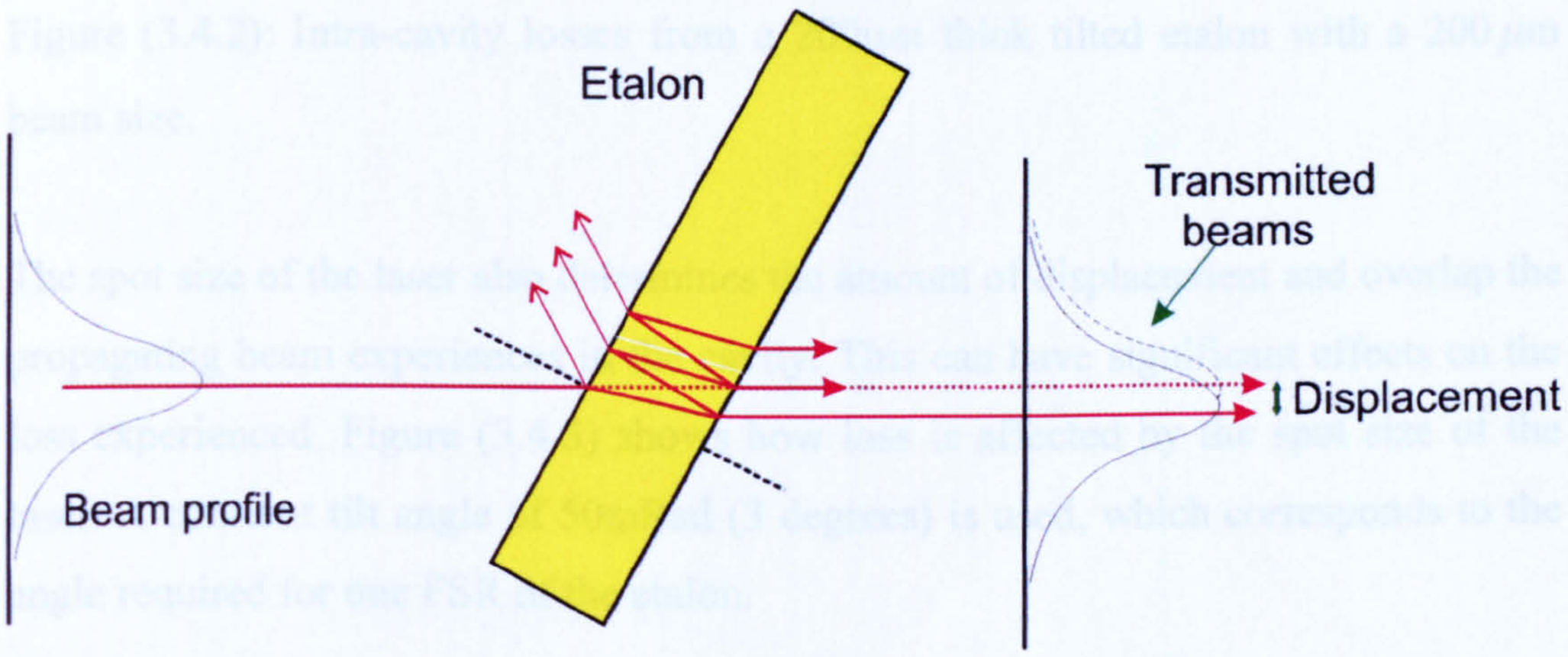

Figure (3.4.1): Beam displacement by tilted etalon

Consider a perfect lossless etalon, non-absorption and perfectly flat surfaces. It can be shown that the round trip loss from the etalon can be given by the expression [5],

$$l = 1 - (\gamma_m \varepsilon)^2 \qquad \text{equ:(3.4.1)}$$

$\gamma_m \varepsilon$ is the amplitude attenuation factor, which considers the angle of the etalon, displacement, beam size and reflectivity of the etalon's surfaces. Using this theory it

is possible to determine the losses induced in a laser cavity using a tilted etalon. Figure (3.4.2) shows how the intra-cavity losses depend on the angle θ for a fixed spot size of 200 microns.

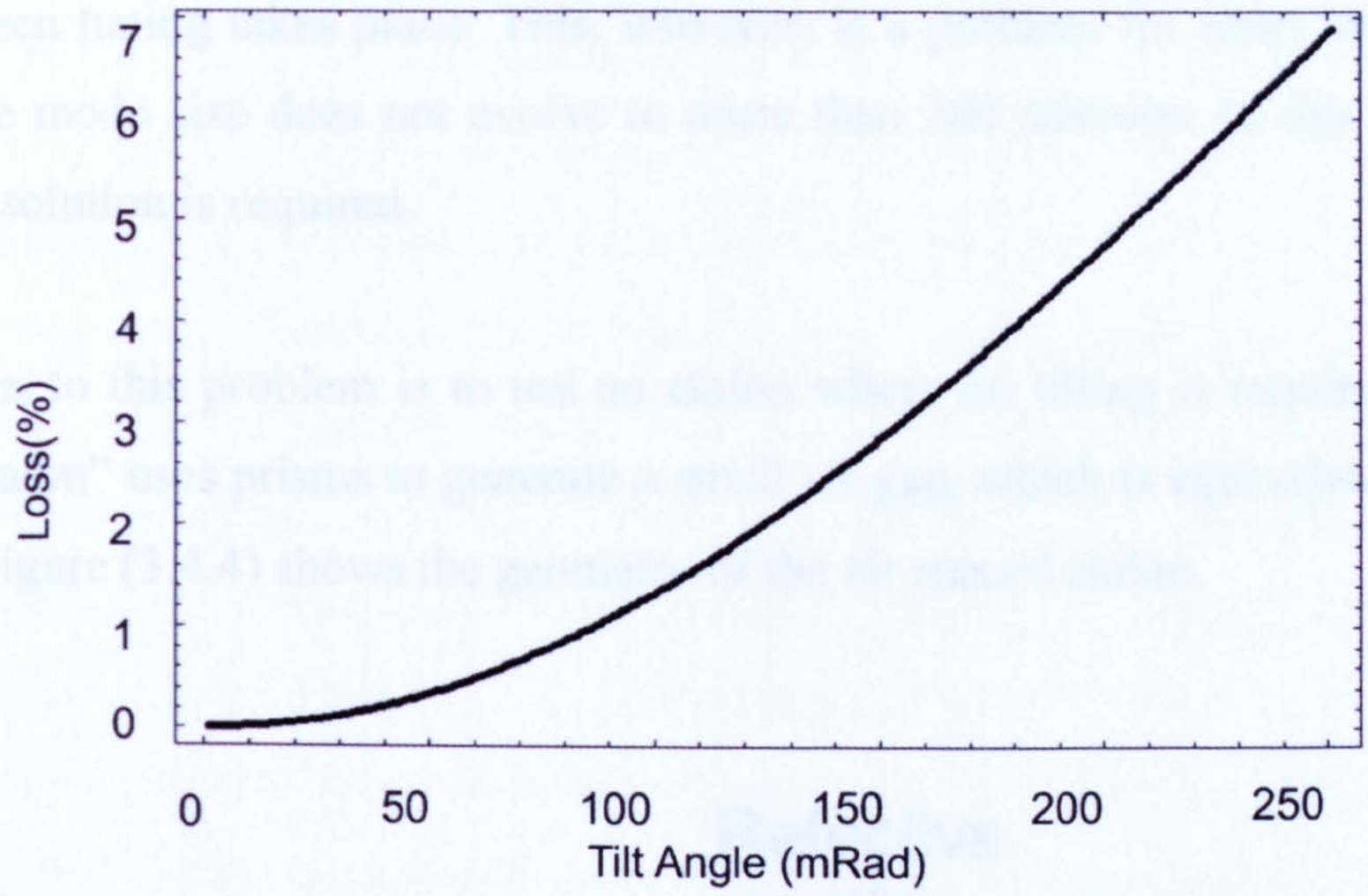

Figure (3.4.2): Intra-cavity losses from a 200μm thick tilted etalon with a 200 μm beam size.

The spot size of the laser also determines the amount of displacement and overlap the propagating beam experiences in the cavity. This can have significant effects on the loss experienced. Figure (3.4.3) shows how loss is affected by the spot size of the laser. A constant tilt angle of 50mRad (3 degrees) is used, which corresponds to the angle required for one FSR of the etalon.

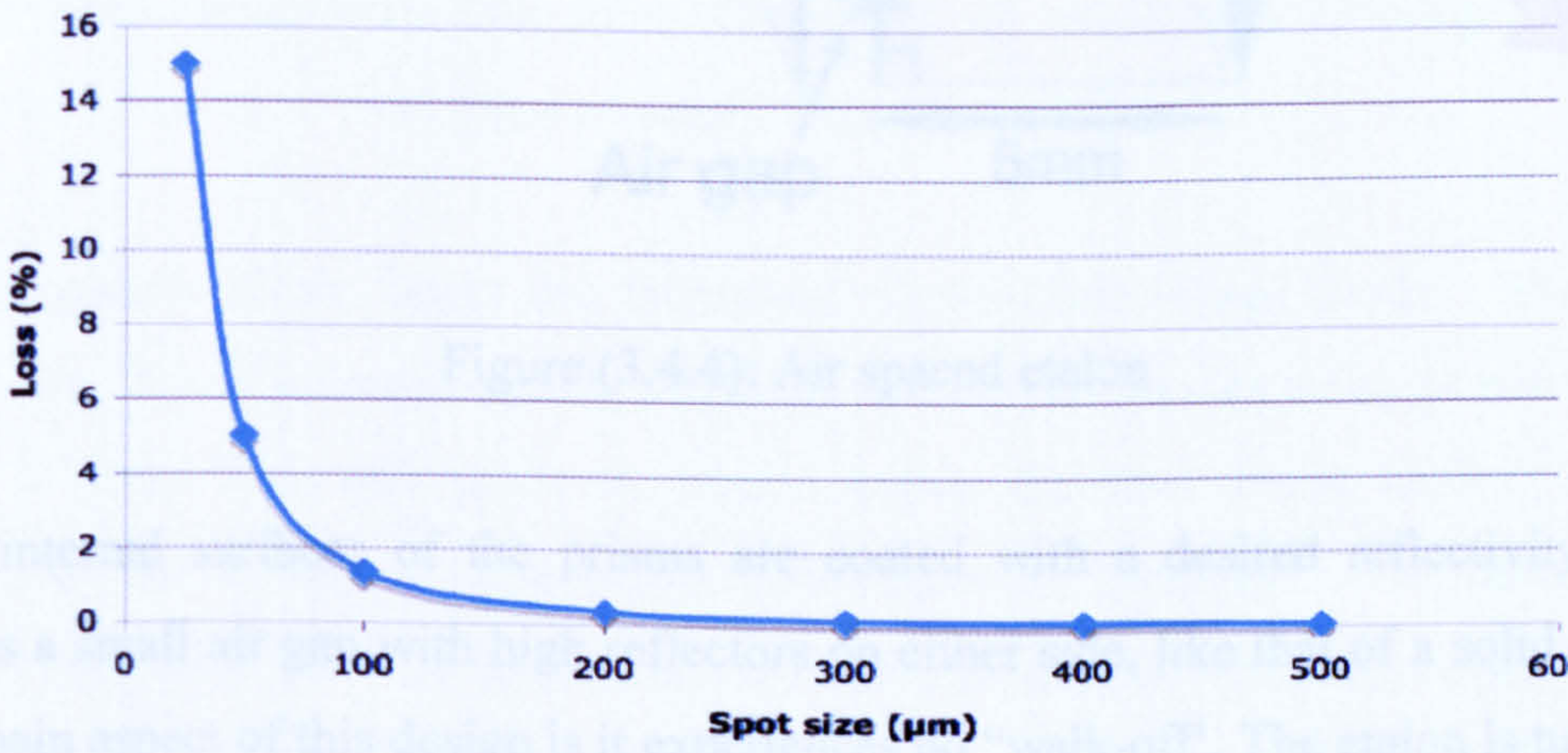

Figure (3.4.3): loss determined by an increase of laser spot size for a 200μm thick etalon at an angle of 50mRad.

As the spot size is decreased the losses dramatically increase, this means that optimum placement of the etalon in the cavity is crucial to minimise these losses. A position where the mode size is large is preferred where the laser will see the least losses when tuning takes place. This, however, is a problem for short laser cavities where the mode size does not evolve to more than 200 microns. In this situation a different solution is required.

A solution to this problem is to use an etalon where no tilting is required. An "air spaced etalon" uses prisms to generate a small air gap, which is equivalent to a solid etalon. Figure (3.4.4) shows the geometry of the air spaced etalon.

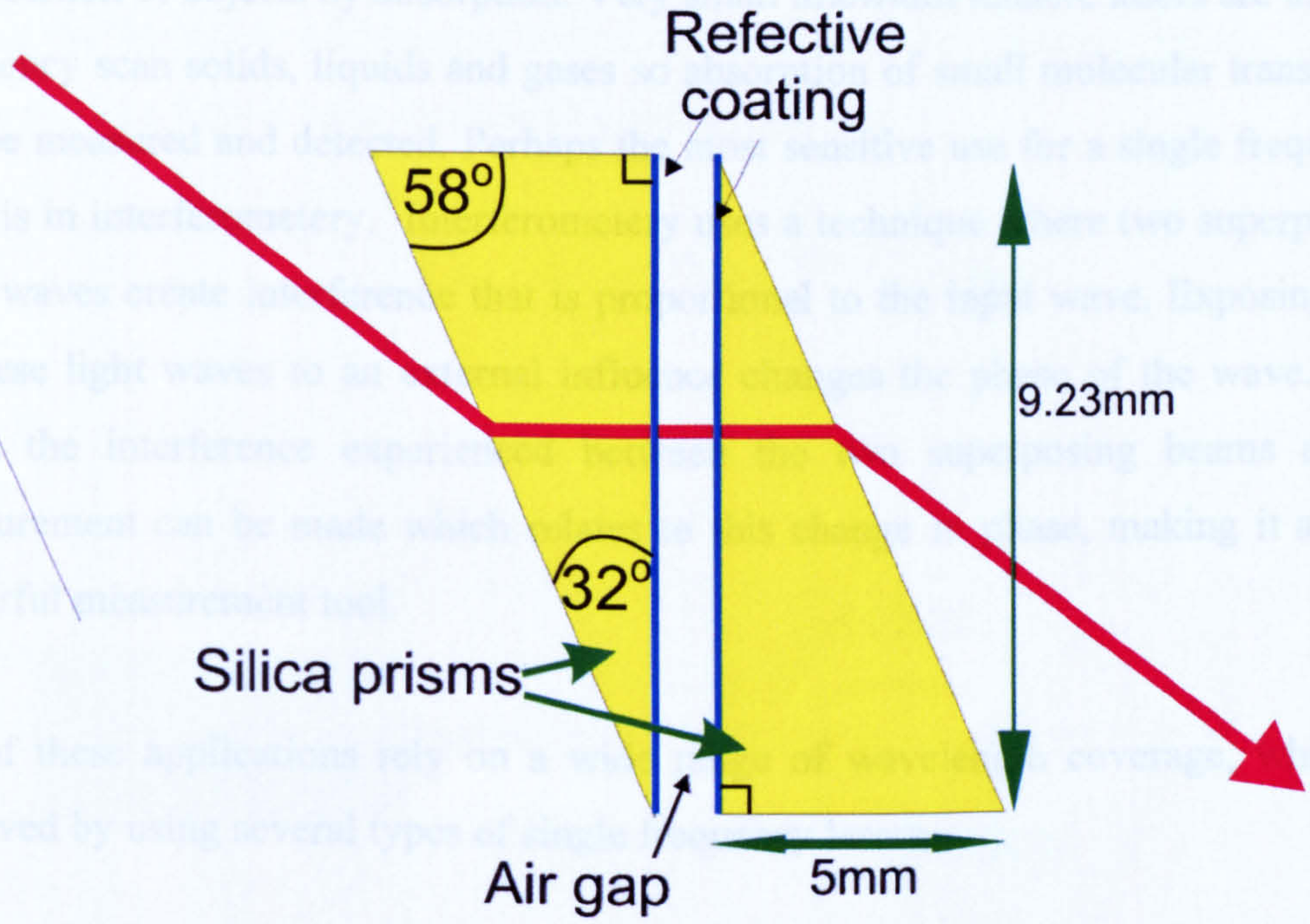

Figure (3.4.4): Air spaced etalon

Both internal surfaces of the prisms are coated with a desired reflectivity. This creates a small air gap with high reflectors on either side, like that of a solid etalon. The main aspect of this design is it experiences no "walk-off'. The etalon is tuned by increasing the air-gap between the reflective surfaces using piezo-controlled movements. This will be discussed further in chapter (7).

3.5 SINGLE FREQUENCY APPLICATIONS

The inherent properties of a single frequency laser; narrow linewidth, single cavity mode, high spectral purity and low intensity noise, make it an ideal tool for many applications. In laser cooling and trapping of atoms it is essential to have a narrow linewidth laser. The linewidth must be close to or below the atom's natural linewidth of its excited state. For rubidium 87, the transition used in laser cooling is 5.9MHz, so typically single frequency lasers with linewidths of 1MHz are used, [8]. In communications single frequency lasers are used, as the inherent low noise characteristic of a single mode laser makes it possible to transmit clear signals through many km of fibre [9]. In spectroscopy, lasers are used to determine the composition of objects by absorption. Very small linewidth tunable lasers are used to frequency scan solids, liquids and gases so absorption of small molecular transitions can be measured and detected. Perhaps the most sensitive use for a single frequency laser is in interferometery. Interferometery uses a technique where two superposing light waves create interference that is proportional to the input wave. Exposing one of these light waves to an external influence changes the phase of the wave. This alters the interference experienced between the two superposing beams and a measurement can be made which relates to this change in phase, making it a very powerful measurement tool.

All of these applications rely on a wide range of wavelength coverage, which is achieved by using several types of single frequency lasers.

Semiconductor diode lasers are inherently single longitudinal mode. The small cavity length and homogeneous broadening ensures few modes being present at one time. If more than one mode is present inside the laser diode cavity, external influences can be used to force single mode operation. External cavities can be used to feed light back into the laser diode to force a predominantly single mode. Figure (3.5.1) shows a typical laser diode with external mirror and internal etalon. The etalon filters the multimode beam emitted by the laser diode, which is then reflected

back into the diodes micro-cavity where the low loss mode dominates and single mode operation occurs.

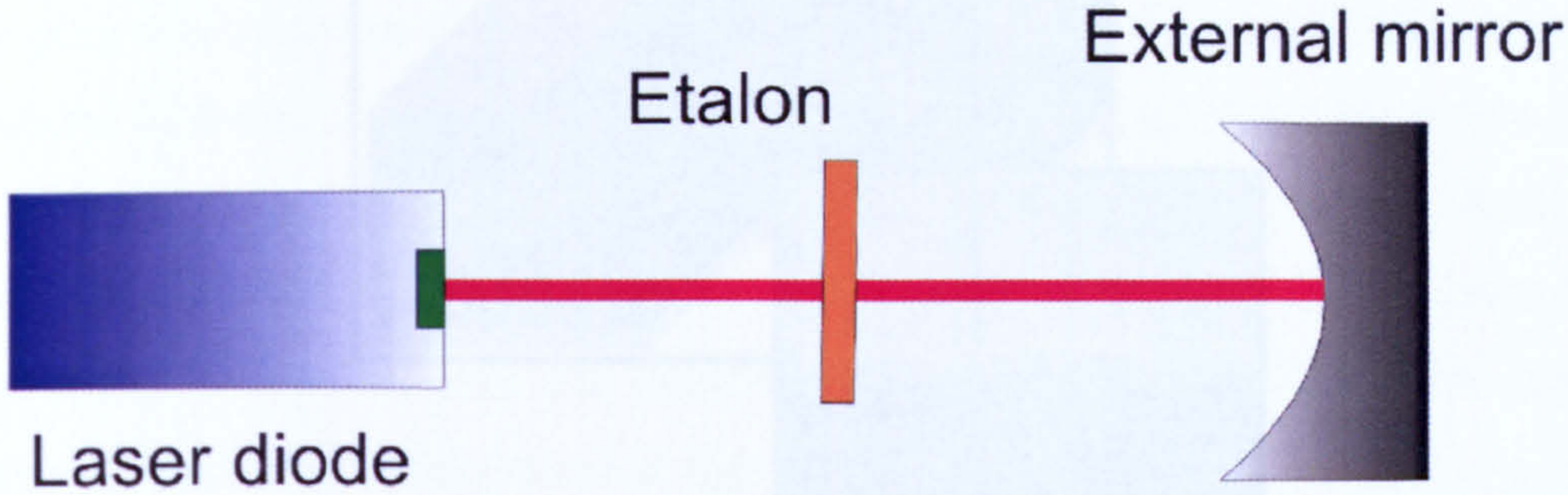

Figure (3.5.1): Single mode laser diode with selected spectral feedback.

An additional method for utilising feedback to initiate single mode operation is the use of an optical grating. The grating is used to feedback a single wavelength that defines the emission wavelength and single frequency is obtained. Figure (3.5.2) below shows a typical laser diode with grating feedback.

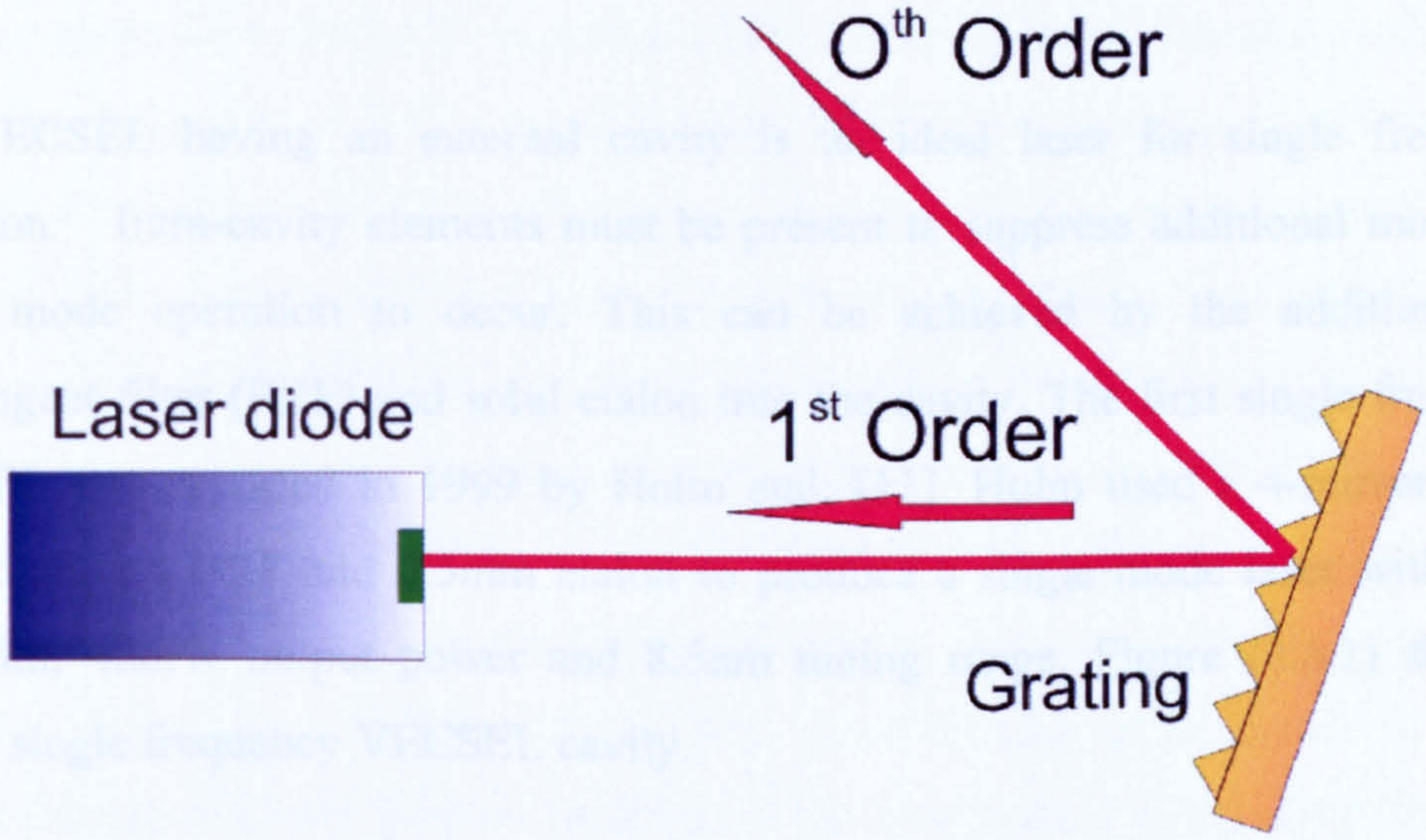

Figure (3.5.2) Grating feedback to induce single mode operation

Another type of semiconductor laser, which is inherently single frequency, is the Distributed Feedback Laser (DFB). The use of distributed reflectors constructs a periodic structure in the cavity. This structure is designed to suppress additional modes thus the least suppressed mode is favoured and single frequency operation is obtained. Figure (3.5.3) shows the typical structure of a (DFB) laser.

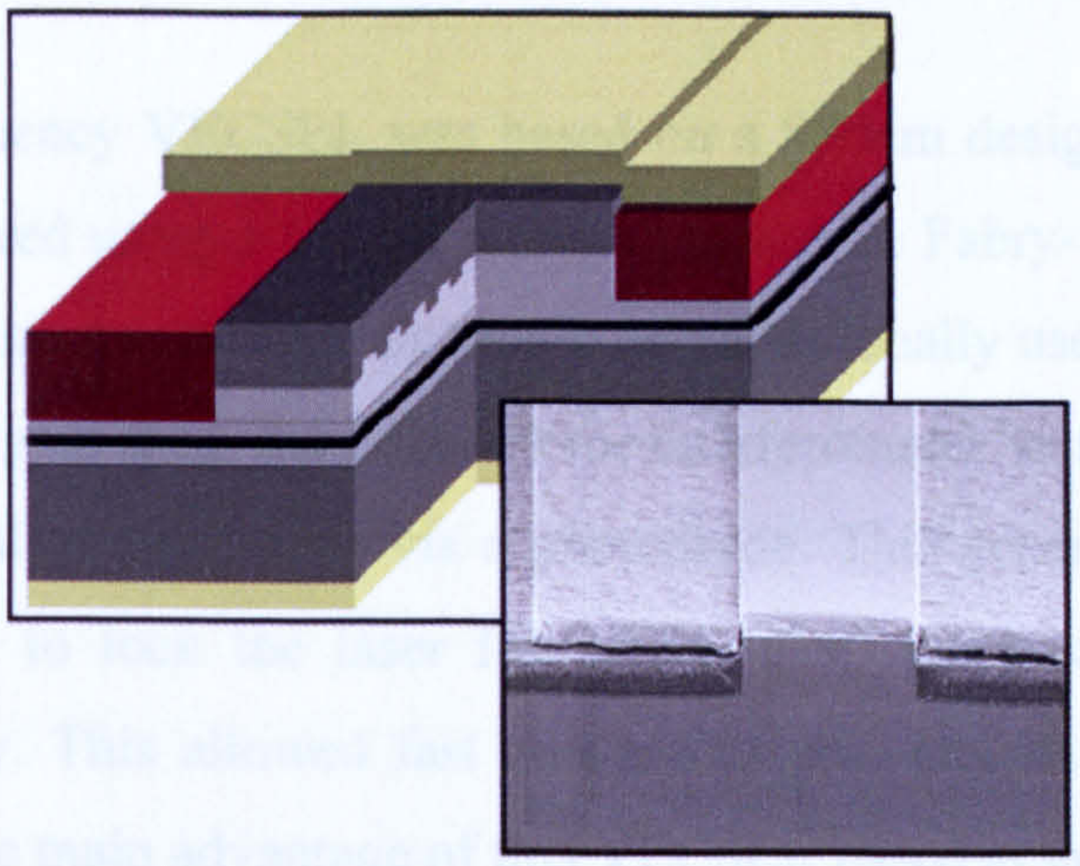

Figure (3.5.3) : DFB laser structure with electron microscope image of periodic grating structure,[10]

This technique can also be used in fibre lasers with a fibre Bragg grating.

3.6 SINGLE FREQUENCY VECSELS

The VECSEL having an external cavity is an ideal laser for single frequency operation. Intra-cavity elements must be present to suppress additional modes for single mode operation to occur. This can be achieved by the addition of a birefringent filter (BRF) and solid etalon into the cavity. The first single frequency VECSEL was reported in 1999 by Holm etal. [11]. Holm used a 4-mirror cavity incorporating a BRF and 0.5mm etalon to produce a single mode laser with 3kHz linewidth, 42mW output power and 8.5nm tuning range. Figure (3.6.1) shows a typical single frequency VECSEL cavity.

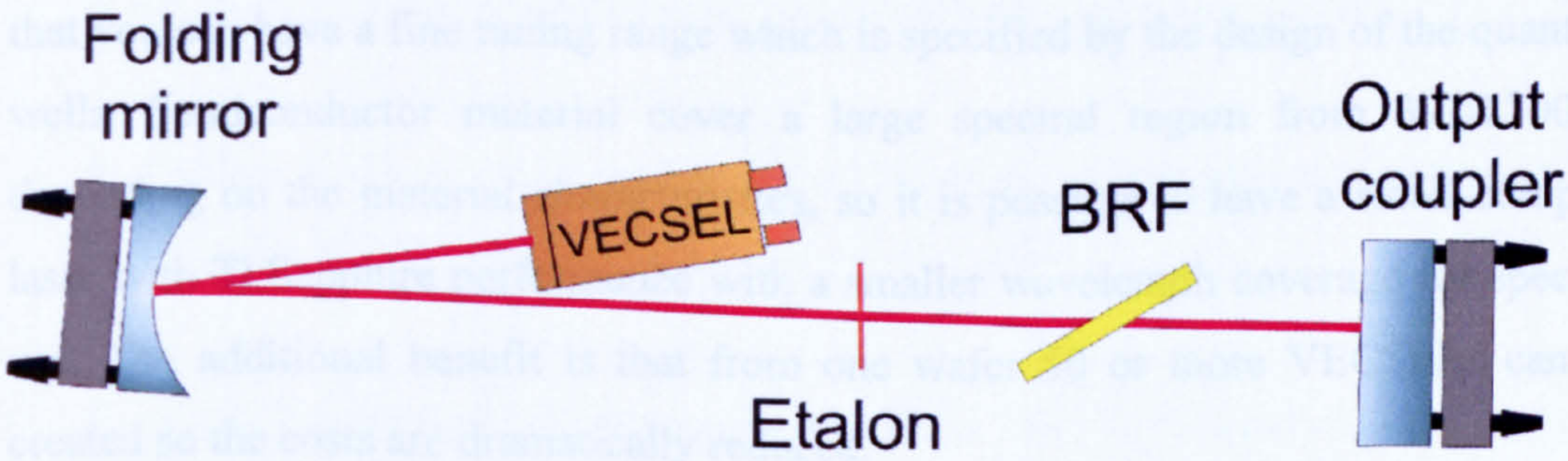

Figure (3.6.1): Single frequency VECSEL cavity

Holm's single frequency VECSEL was based on a 870nm designed wafer. Optical pumping was achieved using a 670nm diode. A reference Fabry-Perot interferometer was used to determine single mode operation and additionally used to lock the laser's wavelength. The signal from the Fabry-Perot interferometer was used to feedback a stable locking signal to electronics via a photodiode. This generated an error signal that could be used to lock the laser frequency using the piezo-electric mounted mirror in the cavity. This allowed fast and precise movements needed to lock the laser frequency. One main advantage of this VECSEL based system over other single frequency lasers was its high power potential. Typical narrow linewidth lasers such as the ones mentioned previously have very small output powers of a few milliwatts. With an output power of 42mW Holm set a new mark for single frequency semiconductor lasers. Further work in these semiconductors based VECSELs has been dramatic. With refined techniques in manufacturing including developing techniques in thermal management has taken the single frequency VECSEL into direct competition with the Ti:Sapphire laser. Using a diamond heat spreaders,[12] and thinner substrates [13] it is possible to get VECSELs with output powers of 30W cw. Single frequency VECSELs have been developed using these new techniques and now tuning ranges of 70nm with high output powers have been achieved [14]. Using wedged diamond heat spreaders and compact cavity designs it has been possible to achieve single frequency lasers with output powers 400mW and 5kHz linewidth [7]. The recent progress in single frequency VECSELs makes it more and more viable option to replace the Ti:Sapphire laser. With broad tuning over 70nm, compact design, narrow linewidths <MHz, good TEM_{00} mode and high output powers this type of laser is at the forefront of the laser world. VECSELs do not have the broad tuning range of a Ti:Sapphire (690-1050nm), however the advantage is that you can have a fine tuning range which is specified by the design of the quantum wells. Semiconductor material cover a large spectral region from 391-2300nm depending on the material characteristics, so it is possible to have a small compact laser with Ti:Sapphire performance with a smaller wavelength coverage for specific use. The additional benefit is that from one wafer 50 or more VECSELs can be created so the costs are dramatically reduced.

3.7 CONCLUSION

This chapter has given a general overview of single frequency laser such that a comparison can be made to the single frequency VECSEL. Previous experimentation in VECSELs have shown the good beam qualities, including TEM_{00} mode, narrow linewidths and high power levels. Detail analysis of the intra cavity elements used in single frequency VECSEL has been shown with special attention to walk off losses induced from intra cavity etalons. Mathematical predictions of walk off losses show a reduced tuning potential due to losses experienced at the extremes of the etalon tilt angle. The solution is to use an air etalon which induces no walk off losses and should increase the tuning range of the laser.

3.8 REFERENCES

1. T. Day, R. A. Marsland and R. L. Byer, "Optical generation of stable MM-wave radiation using diode pumped Nd:YAG lasers" Proceedings of the SPIE-International Society for Optical Engineering, **1839**, (1992)

2. A. L. Schawlow, "Spectroscopy in a new light", Nobel lecture, (1981)

3. P. F. Moulton, "Spectroscopic and laser characteristics of Ti:Al2O3" Optical Society of America, **3**, no.1, p125, (1986).

4. A. Yariv, "*Optical Electronics*, fourth edition", Saunders, (1991).

5. Walter R. Leeb, "Losses introduced by tilting intracavity etalons", Applied Physics, **6**, 267, (1975).

6. K. S. Gardner, R. H. Abram and E. Riis, "A birefringent etalon as single-mode selector in a laser cavity", Optics Express, **12**, no.12, (2004)

7. R.H. Abram, K.S. Gardner, E. Riis, and A.I. Ferguson, "Narrow linewidth of a tunable optically pumped semiconductor laser", Optics Express, **12**, 5434, (2004).

8. Ying-Cheng Chen ,Wen-Bin Lin , Hsuin-Chia Hsue , Long Hsu and Ite A. Yu, "Effect of the Trapping Laser Linewidth on the Atom Number in a Magneto-Optical Trap" Chinese Journal of Physics, **38**, no.5, (2000).

9. Lob, W.H. Laming, R.I. Ellis, A.D. Atkinson, D. "10 Gb/s transmission over 700 km of standard single-mode fibre with10-cm chirped fibre grating compensator and duobinary transmitter, Photonics Technology Letters, **8**, 1258, (1996)

10. http://www.myoops.org

11. Holm, M. A., Burns, D., Cusumano, P., Ferguson, A. I., and Dawson, M. D., "High-Power Diode-Pumped AlGaAs Surface-Emitting Laser", Applied Optics, **38**, 5781, (1999).

12. J. E. Hastie, J. M. Hopkins, S. Calvez, C. W. Jeon, D. Burns, R. Abram, E. Riis, A.I. Ferguson and M. D. Dawson. "0.5-W Single Transverse-Mode Operation of an 850nm Diode-Pumped Surface-Emitting Semiconductor Laser" IEEE Photonics Technology Letters, **15**, no.7, p894, (2003).

13. J. Chilla, S. Butterworth, A. Zeitschel, J. Charles, A. Caprara, M. Reed and L. Spinelli, "High power optically pumped semiconductor lasers", Solid sate lasers XIII, SPIE, **5332**, (2004).

14. J. M. Hopkins, A. J. Maclean, E. Riis, N. Schulz, M. Rattunde, C. Manz, K. Köhler, J. Wagner and D. Burns." Tunable, single frequency, diode pumped 2.3μm VECSEL" Optics Express, **15**, no.13, (2007).

CHAPTER FOUR

THERMAL MANAGEMENT

4.1 INTRODUCTION

In most semiconductor lasers the most significant limitation for high power operation is heat build-up within the quantum structures. Heat is generated inside the semi-conductor that causes trapped electron to escape from their quantum well confinement. The overall effect decreases the available gain by reducing the population inversion present in the quantum well areas, commonly called thermal rollover. The photoluminescence peak wavelength and resonant periodic gain (RPG) shift by different rates with temperature. Heat build-up inside the structure causes thermal expansion thus altering the resonant structure, which can reduce the lasers available gain. Similarly the gain spectrum shifts, but with a lesser effect, due to change in band gap energy. VECSELs are designed to operate at a specific temperature and beyond this point resonant features are no longer aligned. To limit this effect, heat has to be efficiently extracted. Optical heat spreaders are a very efficient way of achieving this, however they come at a cost and can produce unwanted etalon effects in the laser. This chapter investigates suitable alternatives to using an optical heat spreader. Computer modelling is used to give detailed analysis of efficient thermal extraction techniques.

4.2 THERMO-ELECTRIC COOLING

Initial experiments in VECSEL lasers required the VECSEL chip to be cooled to very low temperatures. Thermoelectric coolers (TECs) can been used to provide thermal extraction from the rear of the VECSEL through the DBR and substrate [1].

A thermoelectric cooler otherwise known as a Peltier effect cooler is a made from an array of bismuth telluride cubes that are sandwiched between two ceramic plates. When a current is applied heat is forced to one side of the plate creating an effective heat pump. Heat is then removed from the "hot side" by water-cooling or an additional TEC can be used in series. This makes it possible to cool VECSEL chips to a temperature as low as -40°C. This provides an effective heat sink to extract the heat generated from within the quantum well region. Figure 4.2.1 below shows a typical VECSEL/TEC mount in a water-cooled block.

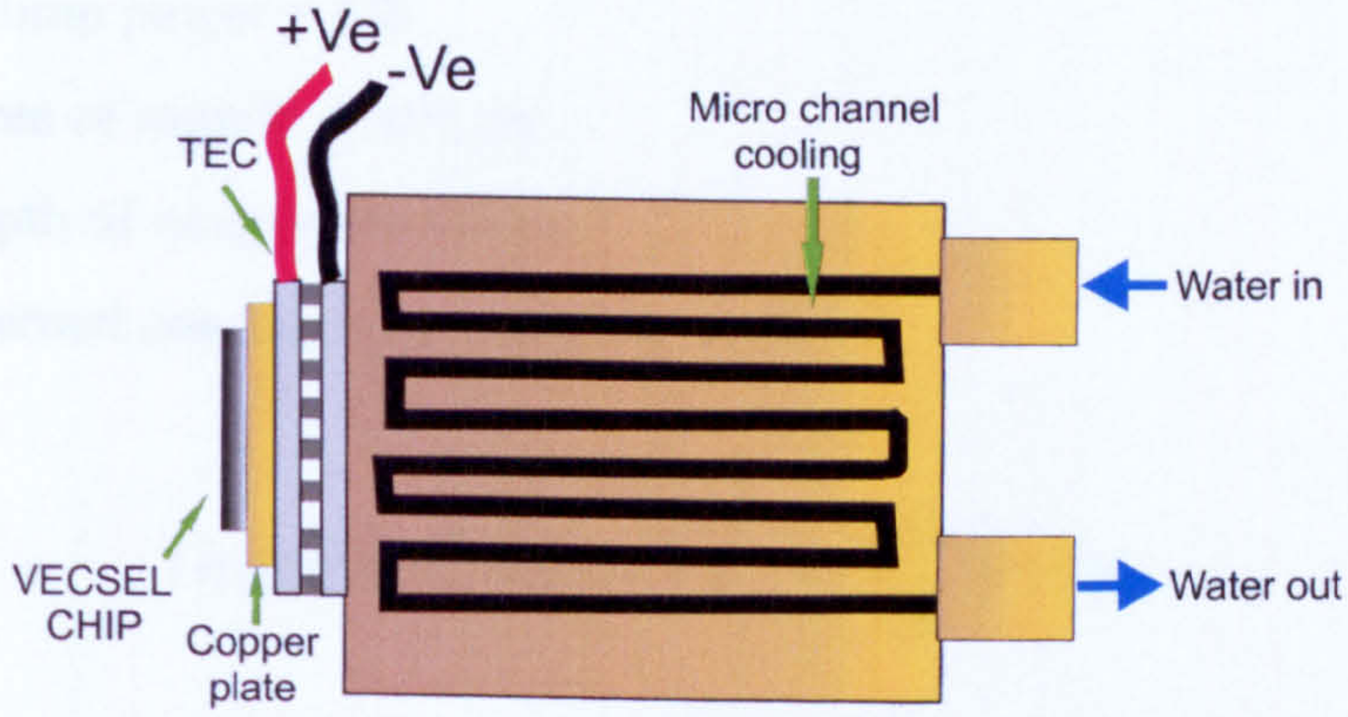

Figure (4.2.1): VECSEL TEC mount

Although this method is an effective way of cooling the VECSEL structure it relies on heat being drawn from the quantum well and barrier regions through the DBR and GaAs substrate. Comparing the thermal conductivity of these structures with more common elements it is clear that this process is inefficient. Table (4.2.1).

Material	**Thermal Conductivity (W/cmK)**
GaAs	0.46
Stainless Steel	~0.2
Sapphire	0.4
SiC	~5
Diamond	20
Ag	4.2

Table (4.2.1): Thermal conductivity comparison, [2], [3].

In a VECSEL structure the DBR and quantum wells are typically grown on top of a 400-500 micrometer thick GaAs substrate. This can lead to poor thermal extraction from the rear surface. Consider a typical VECSEL laser with a 5W pump and 500 micron thick GaAs substrate. The heat generated inside the gain region can be calculated as follows [4].

$$\Delta P = \zeta \frac{A}{d} \Delta T \qquad \text{equ:(4.2.1)}$$

Where ΔP = Pump power = 5W

A = Area of sample = 0.01cm

d = Depth of sample = 0.05cm

ζ = Thermal conductivity = 0.46 W/cmK

Therefore,

$$\text{Temperature change } (\Delta T) = \frac{\Delta P d}{\zeta A} = 53^{\circ}\text{C}$$

This gives a 53°C temperature increase inside the VECSEL wafer. Heat extraction from the rear of the VECSEL is hindered by the GaAs poor thermal conductivity. For \efficient thermal transfer the substrate should be thinned or completely removed. This will be explored further in section 4.5. Heat extraction is more efficient the closer you are to the gain region where the heat is present. One method that takes advantage of this close proximity is the use of an optically transparent heat spreader.

4.3 HEAT SPREADERS

To effectively extract heat from a VECSEL, cooling must be focused near to the source of heating. An optically transparent heat spreader can be used to extract heat. This acts as a thermal channel, which extracts the heat from the front surface of the VECSEL. The heat spreader is capillary bonded to the wafer and this is packaged into a copper heat sink where the heat rapidly removed with water-cooling as seen in chapter 2, section 2.6. Initial experiments involving sapphire and silicon carbide proved to be most effective. Figure (4.3.1) shows the comparison of an 850nm VECSEL with these heat spreaders.

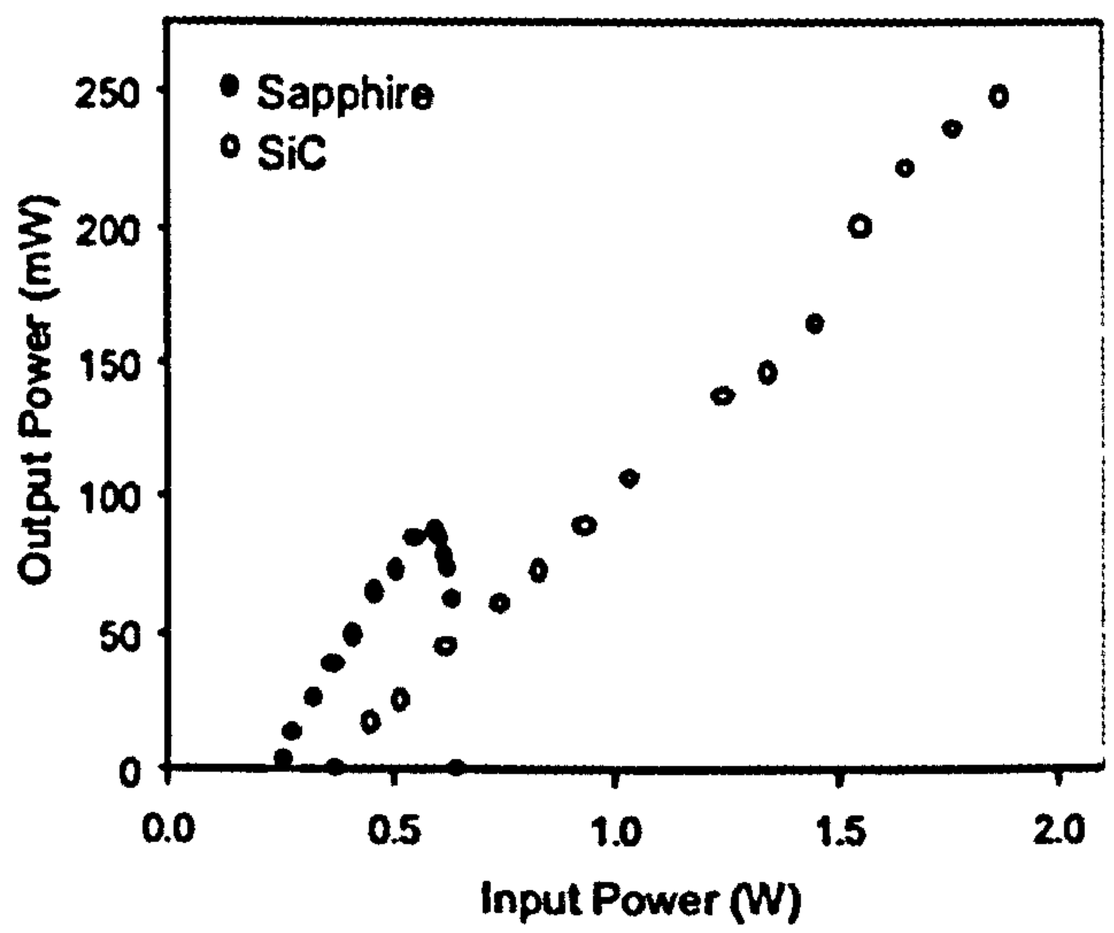

Figure (4.3.1): Silicon carbide and sapphire heat spreader comparison [5]

It can be seen from figure (4.3.1) that the use of silicon carbide as a heat spreader allows the VECSEL to achieve higher output powers to that of sapphire before thermal rollover occurs > 250mW. This advancement in heat management meant the VECSEL could be used for high power applications. The next stage was to use diamond as an optical heat spreader. Previous experiments with semiconductor lasers showed that diamond could be used to effectively remove the heat due to its high thermal conductivity. The diamond was pressure bonded to the semiconductor laser and bound in a copper heat sink [6]. Diamond being relativley non-birefringent, optically transparent at ultraviolet to far-infrared wavelengths and very good thermal conductivity (20W/cmK) makes it an ideal optical heat spreader. This has further

increased the power scalability of the VECSEL with current output powers of several watts achievable, [7].

4.4 THERMAL MODELLING

Although diamond is a very effective heat spreader, when utilised in a single frequency VECSEL it produces a problem. The thin layer of diamond acts as an intra-cavity etalon, which affects the lasers spectrum. Figure (4.4.0) shows the etalon modes produces by an intra-cavity diamond heat spreader.

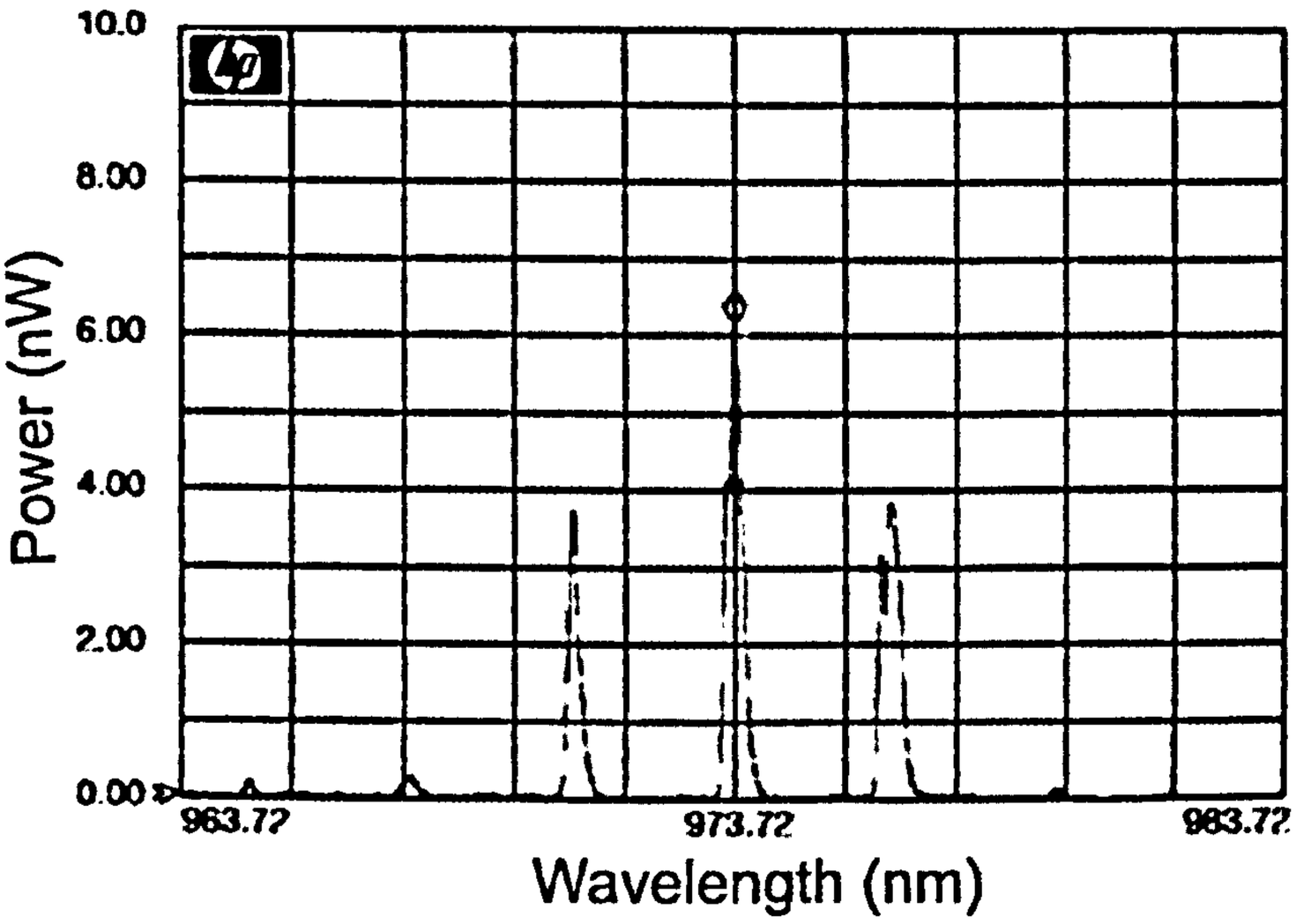

Figure (4.4.0): Spectral output from VECSEL with a plane diamond heat spreader

Thermal modelling was carried out to find out if another solution was feasible to cool the VECSEL to the performance that diamond has achieved. Using computer modelling (FEMLAB Comsol AB, Sweden) with guidance from Dr Alan Kemp several scenarios were modelled. With no heat spreader the only viable area to extract heat from the VECSEL is through its rear surface. At the rear of the VECSEL is a substrate layer of gallium arsenide (GaAs). This has the thermal conductivity of 0.46 W/cmK, so is a relatively poor conductor of heat. Computer

model was carried out using an 850nm VECSEL design. The 850nm VECSEL structure is shown in table (4.4.1).

Layer	Material	Mole fraction(x)	Thickness (microns)	Purpose
14	$GaAsP_{0.01}$	0.1	0.0200	Cap
13	Al_xGaAs	0.5	0.309	5 λ/4 window
12	Al_xGaAs	0.26	0.1123	λ/2 layer
11	$Al_{0.115}GaIn_{0.1}AsP_{0.18}$		0.0050	Strain comp
10 (x16)	$In_{0.1}Al_{0.115}GaAs$		0.1000	QW
9 (x16)	$Al_{0.115}GaIn_{0.1}AsP_{0.18}$		0.0050	Strain comp
8 (x16)	Al_xGaAs	0.26	0.1017	λ/2 layer
7 (x16)	$Al_{0.115}GaIn_{0.1}AsP_{0.18}$		0.0050	Stain comp
6	In0.1Al0.115GaAs		0.0100	QW
5	$Al_{0.115}GaIn_{0.1}AsP_{0.18}$		0.0050	Strain comp
4	Al_xGaAs	0.26	0.1123	λ/2 layer
3 (x30)	Al_xGaAs	1	0.0698	DBR
2 (x30)	Al_xGaAs	0.18	0.0599	DBR
1	GaAs	0	0.5	Buffer

Table (4.4.1): 850nm VECSEL structure [8]

Using the thermal conductivities of these layers "femlab" can predict the thermal flow of heat from the pump spot on the wafer to its extremities where cooling is applied. This give a detailed model of the temperature rise within the quantum wells and allows us to model different scenarios. As the temperature change will be symmetric around the symmetry axis, only one half is considered thus simplifying the model for computational purposes.

The layers of the VECSEL have to be broken down into it constituent parts. Figure (4.4.1) is a detail representation of the VECSEL regions.

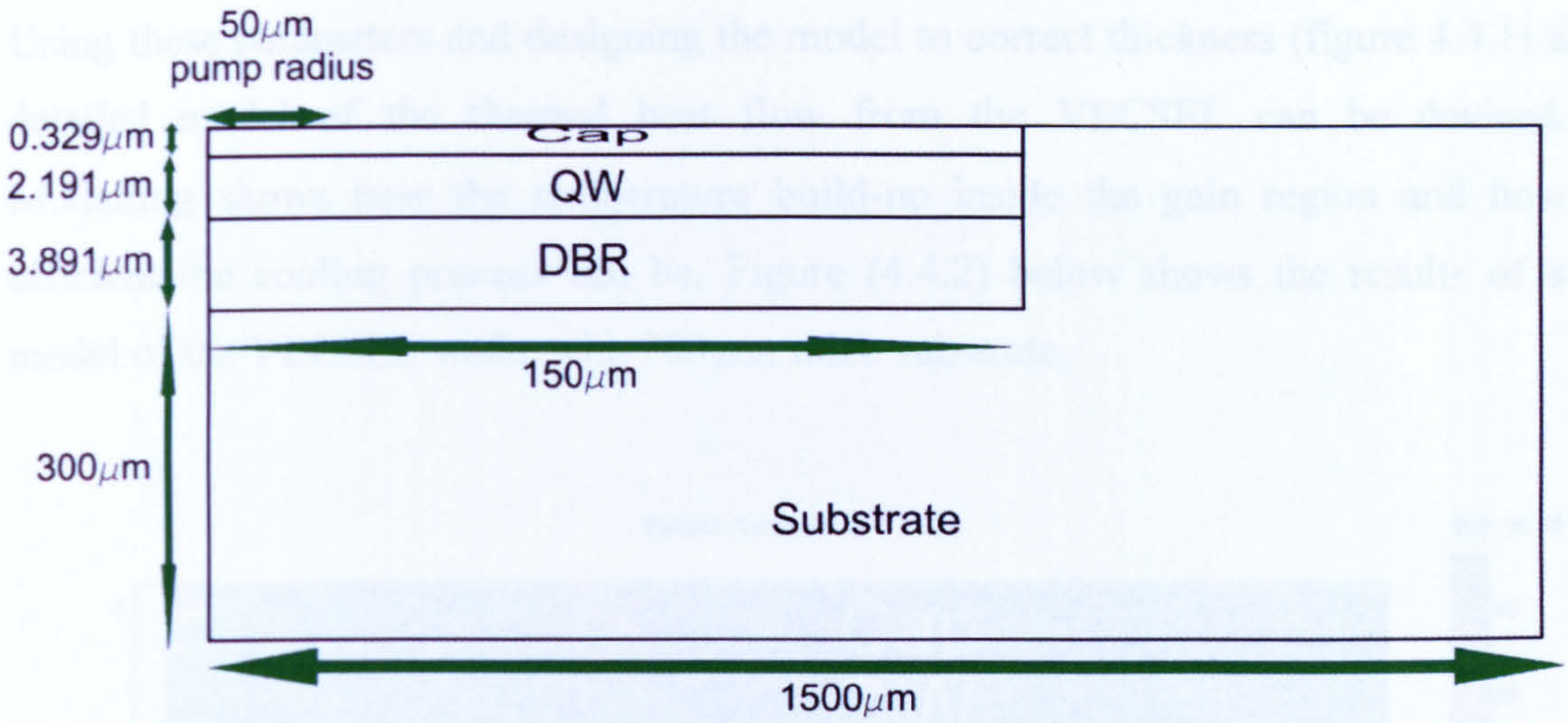

Figure (4.4.1): Femlab VECSEL representation

Heat flow in these layers is anisotropic therefore correct analysis must consider the thermal conductivity in all dimensions both parallel and perpendicular to the layers. Table:(4.4.2) Shows the parameters calculated using various resource papers [2,9,10]

Parameter	Value (W/mmK)
Cap layer ($GaAsP_{0.01}$) Thermal coefficient	0.025 W/mmK
5/4 λ window (Al_xGaAs) Thermal coefficient	0.011 W/mmK
λ/2 layer (Al_xGaAs) Thermal coefficient	0.017 W/mmK
Strain comp layer ($Al_{0.115}GaIn_{0.1}AsP_{0.18}$) Thermal coefficient	0.008 W/mmK
QW ($In_{0.1}Al_{0.115}GaAs$) Thermal coefficient	0.0011 Wmm/K
DBR 1 (Al_xGaAs) Thermal coefficient	0.017 W/mmK
DBR 2 (Al_xGaAs) Thermal coefficient	0.025 W/mmK
Substrate (GaAs) Thermal coefficient	0.047 W/mmK
Diamond Thermal coefficient	2 W/mmK
Incident pump power	10W
Pump spot radius	50 μm
Absorption coefficient of QW's	$1000mm^{-1}$
Absorption coefficient DBR	$547mm^{-1}$

Table (4.4.2): Wafer quantities for Femlab modelling

Using these parameters and designing the model to correct thickness (figure 4.4.1) a detailed model of the thermal heat flow from the VECSEL can be devised. Modelling shows how the temperature build-up inside the gain region and how efficient the cooling process can be. Figure (4.4.2) below shows the results of a model of the VECSEL wafer with 300 μm thick substrate.

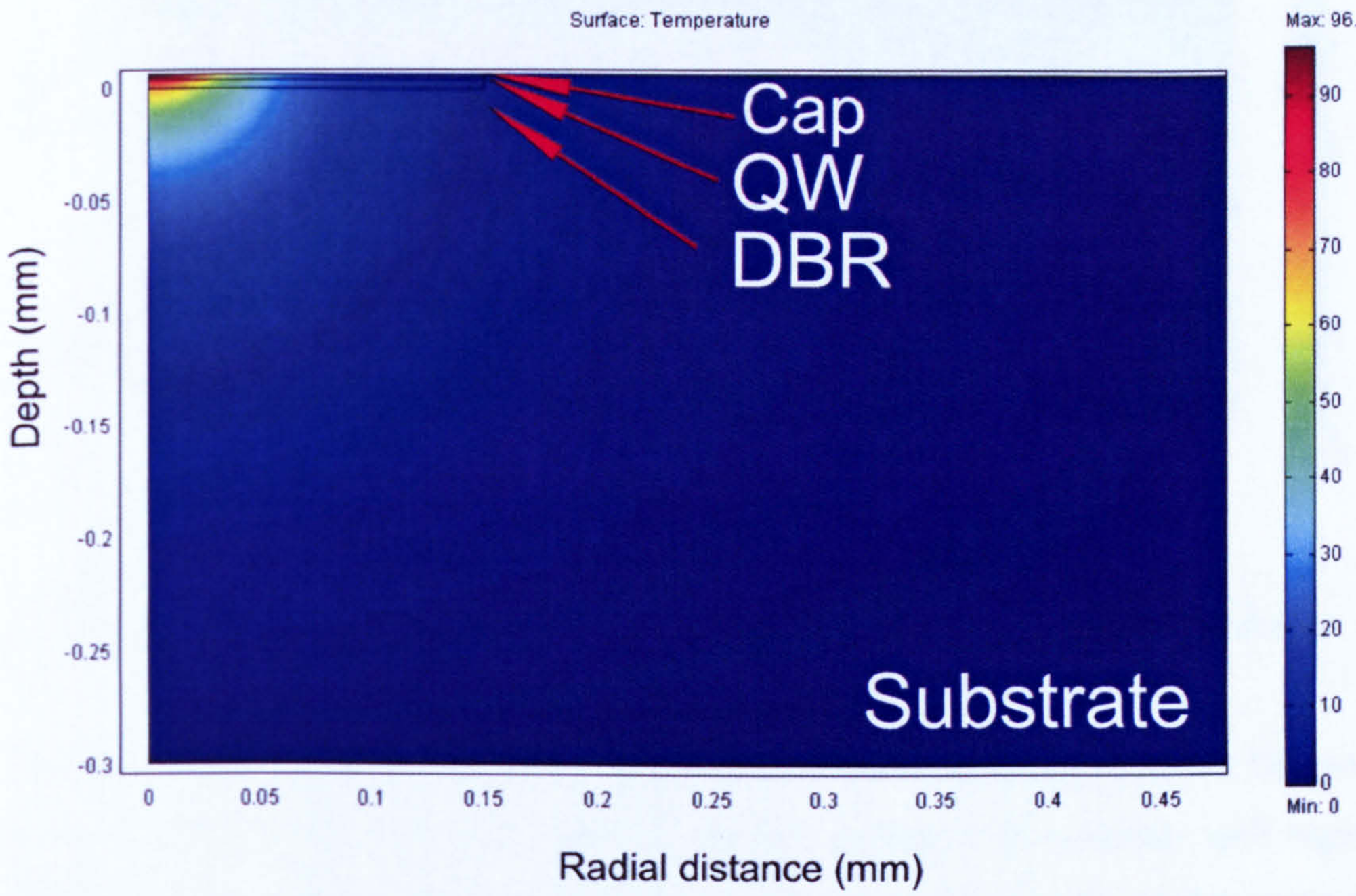

Figure (4.4.2): 300 μ substrate Femlab model

This model shows the VECSEL with no heat-spreader. Cooling is being applied from the rear surface and top right as it would be in a real copper mount. It shows a temperature change of 96^0C. This is a reference to a boundary cooling from the copper heat sink of 0^0C. Heat is absorbed into the gain region and dissipates through the rear surface through the DBR and substrate. A temperature build of 96^0C is well over the designed temperature threshold of around 30^0C, which accounts for thermal expansion, resonant features and thermal rollover. To compare this with a more commonly used type of VECSEL a model was designed, which incorporates a diamond heat spreader.

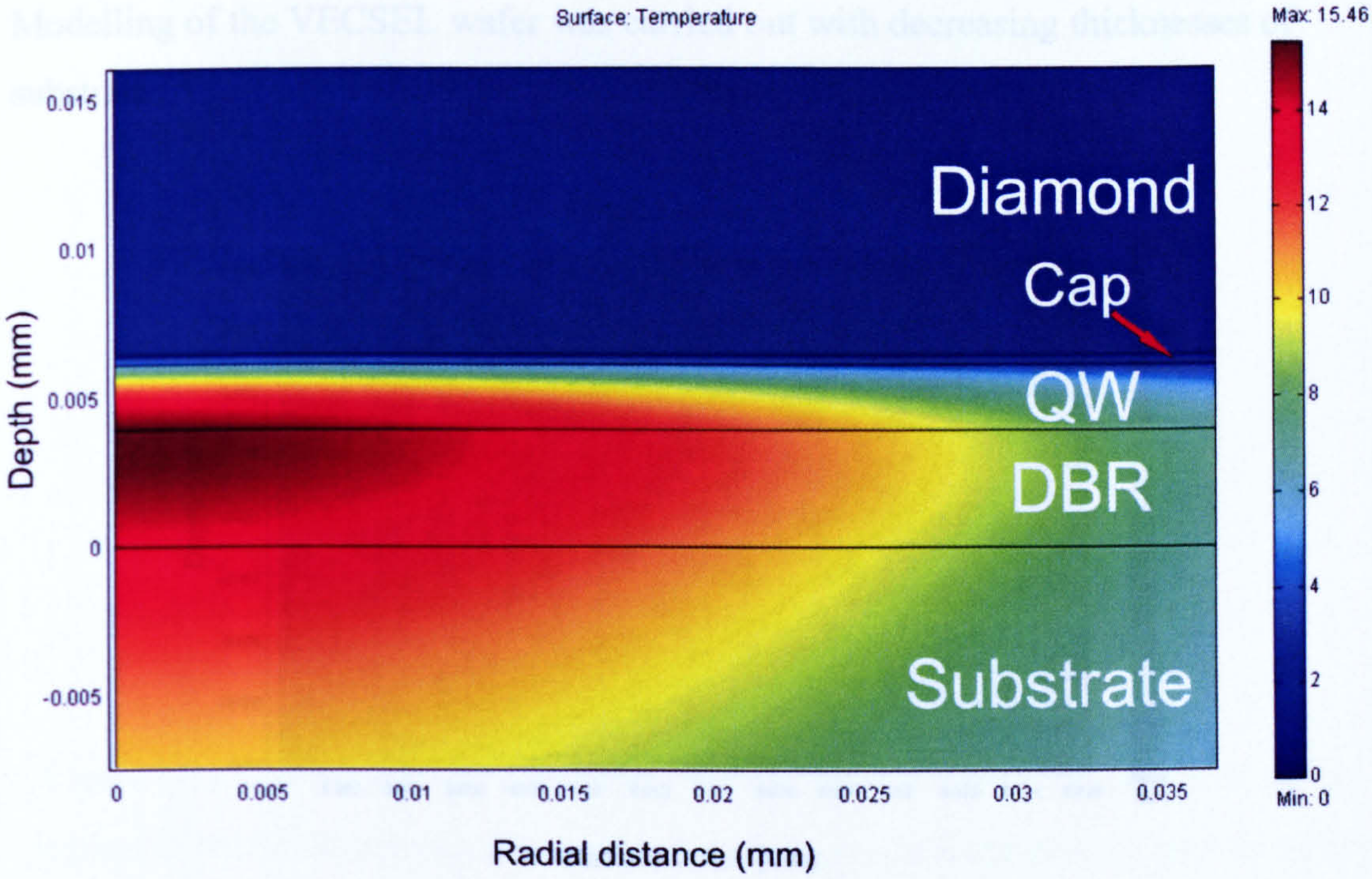

Figure (4.4.3): Diamond heat spreader and VECSEL wafer Femlab simulation

The above figure shows a close up image of the VECSEL/diamond model. Diamond is located on the top layer and followed by the capping layer, quantum well region, DBR and substrate. This figure shows how efficient the diamond is at removing the heat build up in the gain region of the wafer. A max temperature change of 15^0C is predicted for this model, which shows an effective solution to the thermal build-up as seen in figure (4.4.2). Using this model as a reference, further modelling was undertaken to find out how effective substrate removal would be in cooling the VECSEL with no heat spreader.

4.5 Substrate thinning

Modelling of the VECSEL wafer was carried out with decreasing thicknesses of substrate.

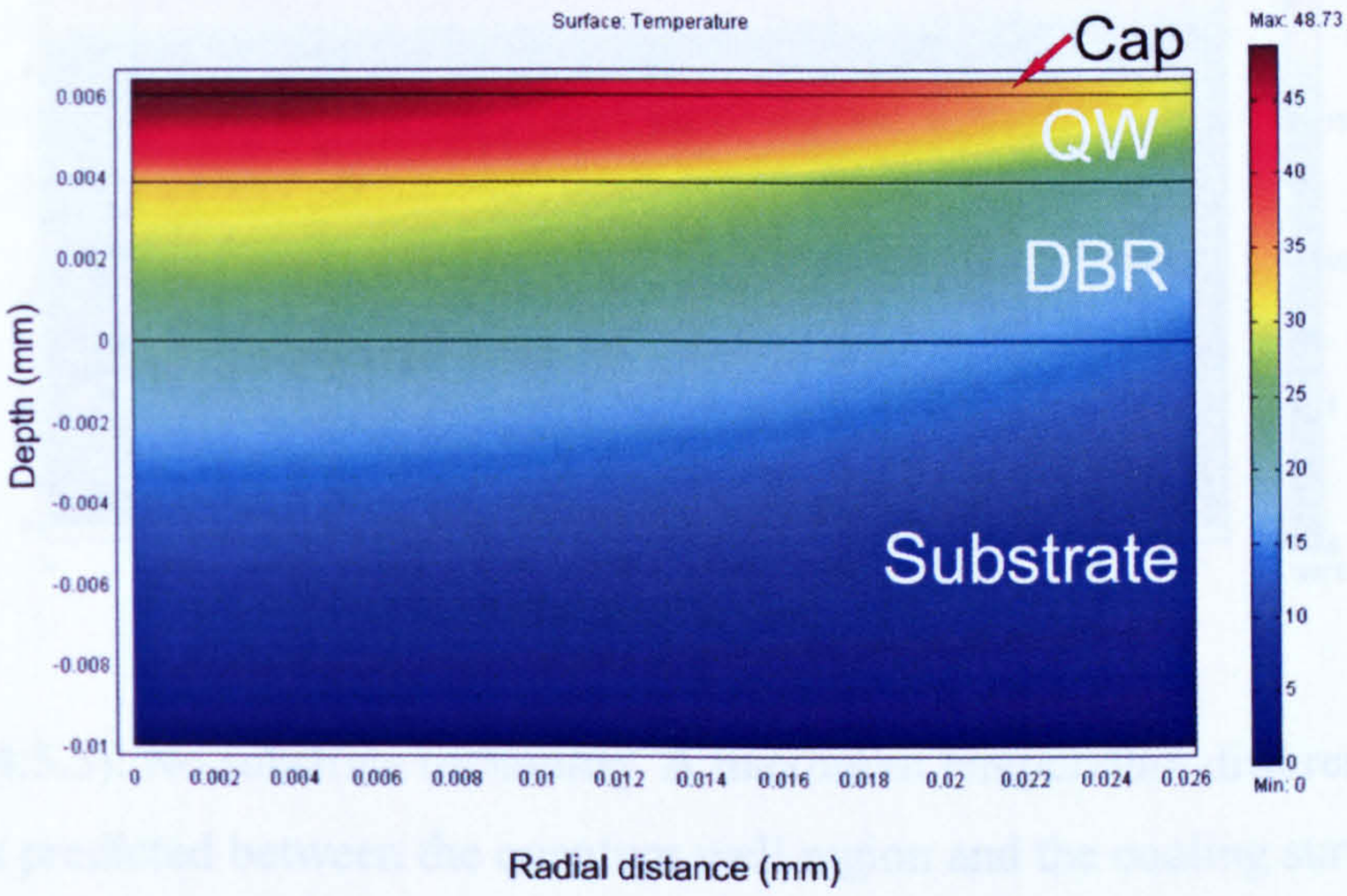

Figure (4.5.1): 100 μm substrate remaining, showing a max temperature difference of 49 degrees between the quantum well region and the cooling surface located at the rear of the substrate.

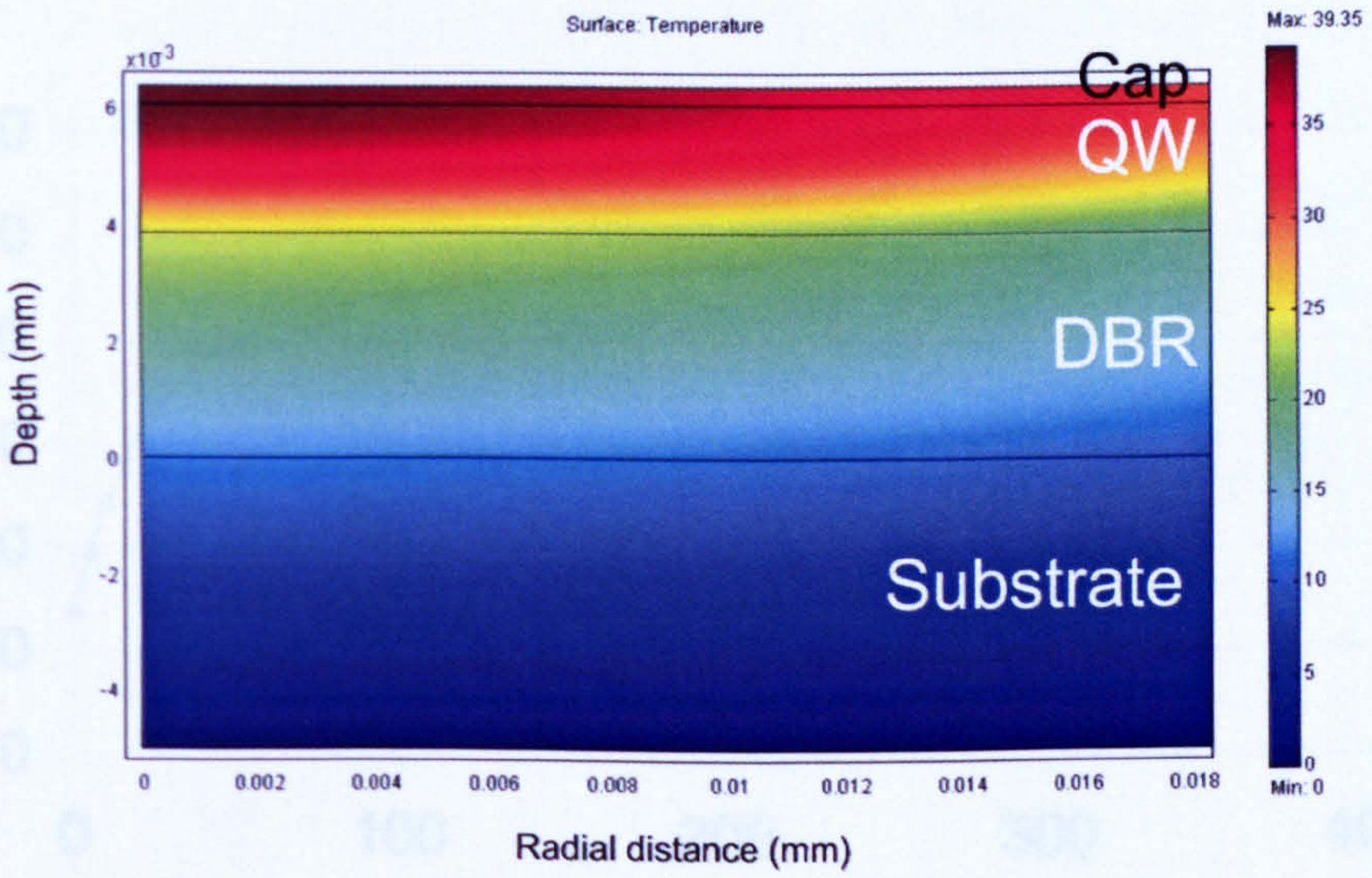

Figure (4.5.2): 10 μm substrate remaining showing a maximum temperature difference of 39 degrees between the quantum well region and the cooling surface located at the rear of the substrate.

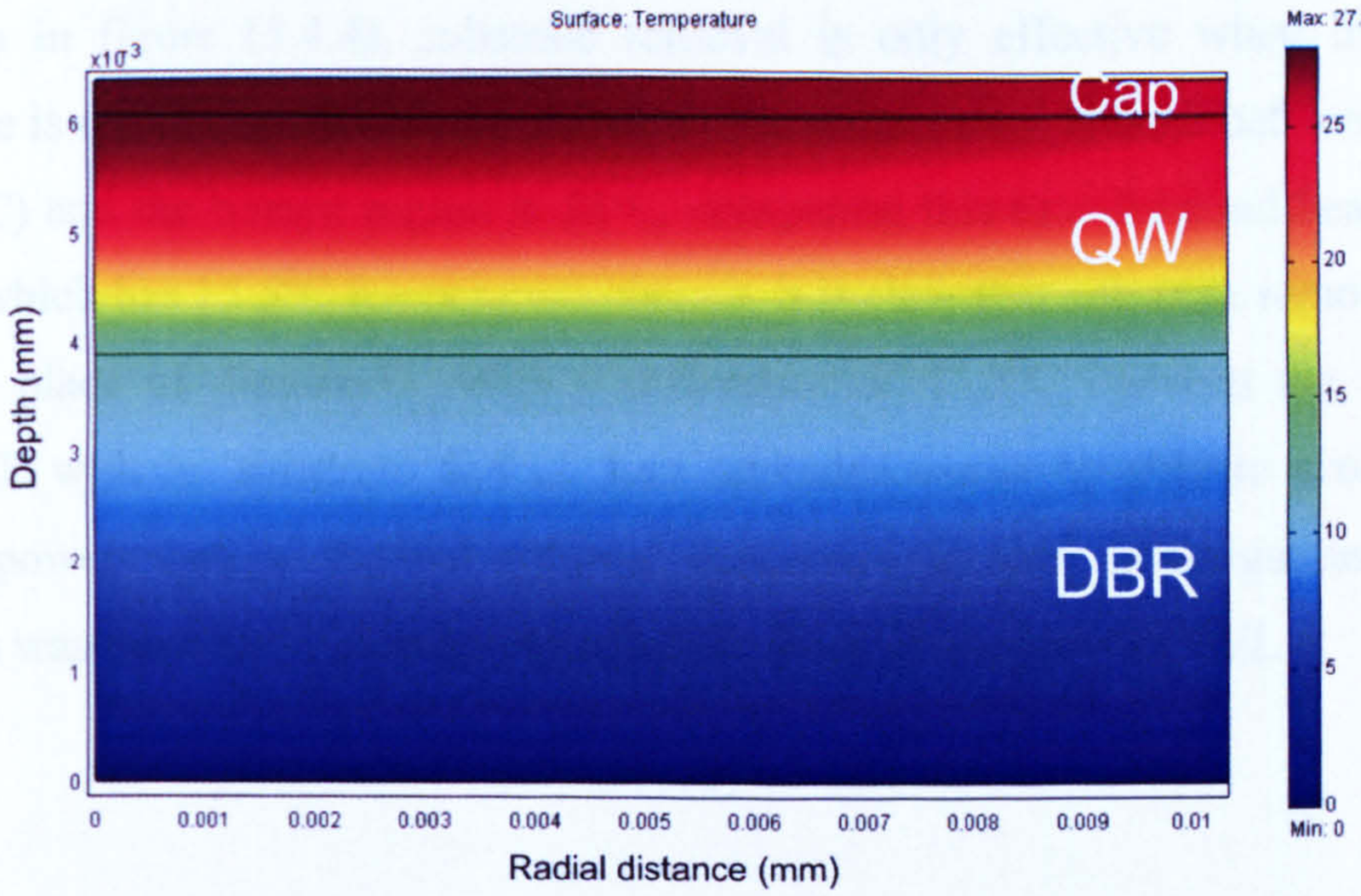

Figure (4.5.3): No substrate remaining. A maximum temperature difference of 28 degrees is predicted between the quantum well region and the cooling surface at the rear of the substrate

The data collected from these plots and more can be seen in figure (5.4.4). This shows the overall maximum temperature change experienced inside the VECSEL wafer.

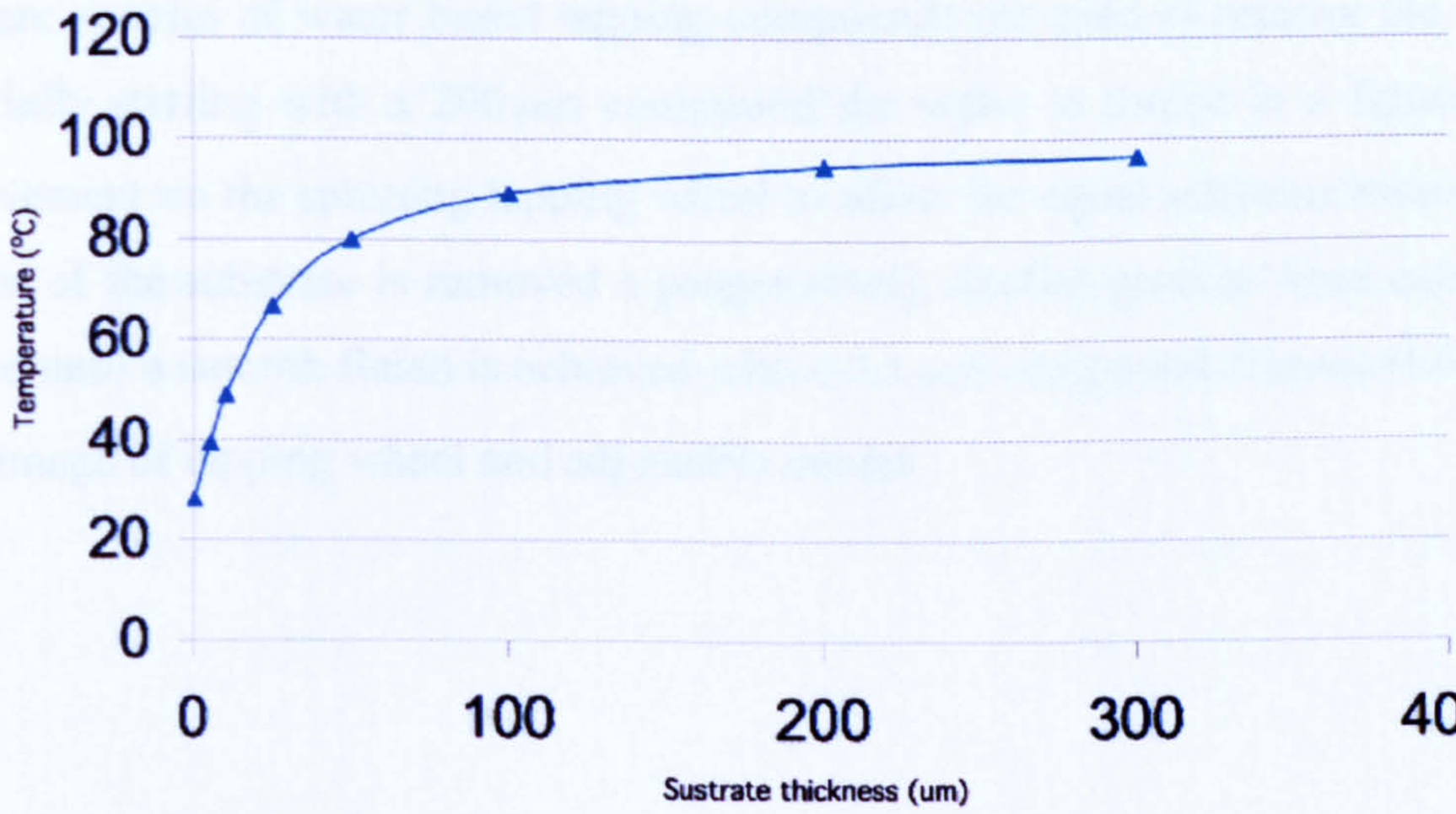

Figure (4.5.4): Substrate removal thermal effects. This shows the decrease of temperature between the quantum well region and the cooling surface as the substrate thickness is reduced.

As seen in figure (5.4.4), substrate removal is only effective when little or no substrate is remaining. With zero substrate the temperature change between the heat sink (0C) and the hottest region is 28^0C, comparing this to a diamond heat spreader model which has 15.5^0C temperature change, it is clear that substrate removal can be used in place of diamond. With a difference of 11.5^0C between the models, a VECSEL with no substrate and no heat spreader would be able to produce high output powers before thermal rollover occurred. Further investigation into this solution was taken by removing the substrate from an 850nm VECSEL.

4.6 Substrate Removal

To remove the GaAs substrate from the rear of the VECSEL wafer two approaches were taken. Firstly an abrasive technique was used which involved lapping. A piece of wafer was stuck to an adjustable brass jig with wax. The jig was specially designed for this procedure, with sapphire pads to limit base removal and micron adjustment to monitor substrate removal. This was then held on a lapping wheel where a series of water based lapping compounds are used to remove the substrate. Initially starting with a 200 μm compound the wafer is forced in a figure of eight movement on the spinning lapping wheel to allow for equal substrate removal. Once most of the substrate is removed a progressively smaller particle sized compound is used until a smooth finish is achieved with a 0.1 μm compound. Figure (4.6.1) shows an image of lapping wheel and adjustable mount.

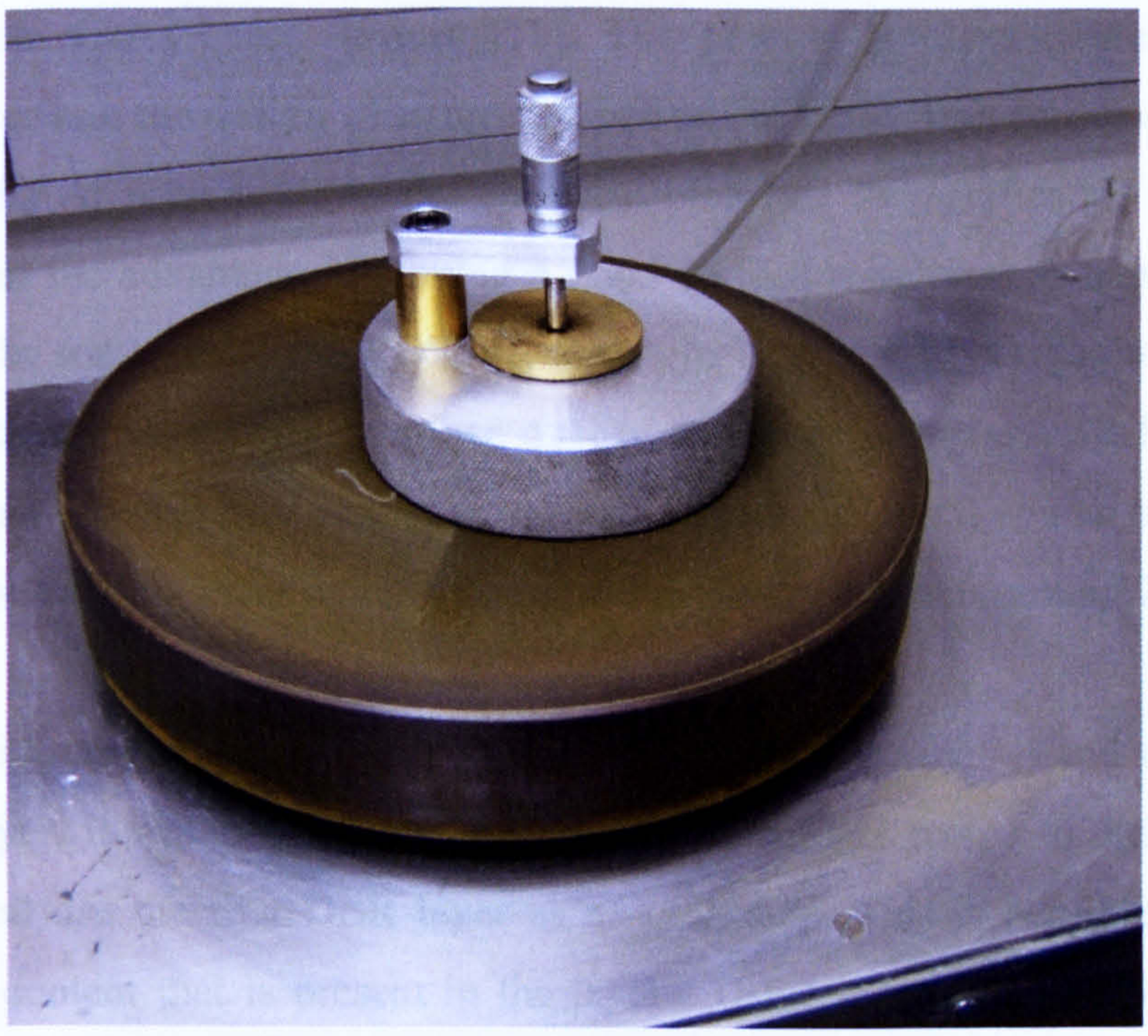

Figure (4.6.1): Lapping wheel and adjustable mount

Initial experiments found that complete substrate removal was unobtainable due to lapping induced stresses. In final stages of lapping the substrate being very thin and brittle was unable to cope with the abrasive compound and this resulted in the wafer breaking up. A lapped wafer with 100 μm of substrate was the best achieved using this method. This wafer was then un-bonded from the mount using heating and mounted on a TEC with copper heat sink for use in a laser cavity. A standard three-mirror cavity was constructed implementing a mode size of 100 μm to match the pump beam diameter. Lasing was achieved with a maximum output power of 0.055mW from the HR output coupler. When comparing this to the Femlab model (figure 4.5.1) it is clear that thermal extraction through the rear surface is inefficient with 100 μm substrate still present. The next substrate removal technique had to be non abrasive and able to remove all the substrate without damaging the remaining structure.

Chemical etching has been performed for many years on semiconductor structures. They are commonly used to create selectively etch detailed structures in all types of semiconductor devices. This method can also be used to etch away unwanted

material from GaAs based devices [11]. The process involves implementing an AlGaAs layer into the design structure just before the DBR. This acts as an etch stop barrier as the Al present slows the chemical etch rate to significantly low levels. This also has the advantage of leaving a good surface roughness as uneven etching can occur. In some cases the VECSEL structure is grown in reverse on the GaAs substrate, this allows a perfect surface quality to remain near the DBR for capillary bonding to an efficient heat sink (e.g. industrial grade diamond) and an etch finished quality to the capping layer which in some cases is more advantageous, [7].

Working with an 850nm anti-resonant VECSEL (grown normally) and with no etch stopping layer, it was possible to find the right chemical recipe to etch the GaAs substrate and use the first DBR layer as an etch stop. This is possible due to the aluminium content that is present in the layers. Using a combination of citric acid ($C_6H_8O_7$) and hydrogen peroxide (H_2O_2) with a ratio of 5:1 respectively, gives a GaAs etch rate of 3140 Å/min. When the chemicals reach the AlGaAs DBR layer the etch rate drops to 27 Å/min [12]. The technique used for chemical etching involves a jet of etching solution being directed at the sample where chemical deterioration of the GaAs takes place. The force of the jet helps remove unwanted etched material from the sample surface giving an equal etch rate across the sample. To mimic this process a magnetic stirrer was used to create a vortex in a beaker of the etching solution. The sample is partially capillary bonded to a piece of glass that is then secured further using wax. This protects the sides of the wafer from being etched and secures the bond to the glass substrate. The glass substrate is then lowered into the solution facing against the vortex-created flow in the beaker. Time is used to measure the etch rate and this is double checked with a 850nm diode which is used to measure the reflectance from the rear of the surface. Due to GaAs having a high absorption at 850nm, a high reflectivity shows the AlGaAs mirror layer has been reached and together with time analysis can provide an accurate measure of substrate removal. Figure (4.6.2) shows a picture of the etching taking place.

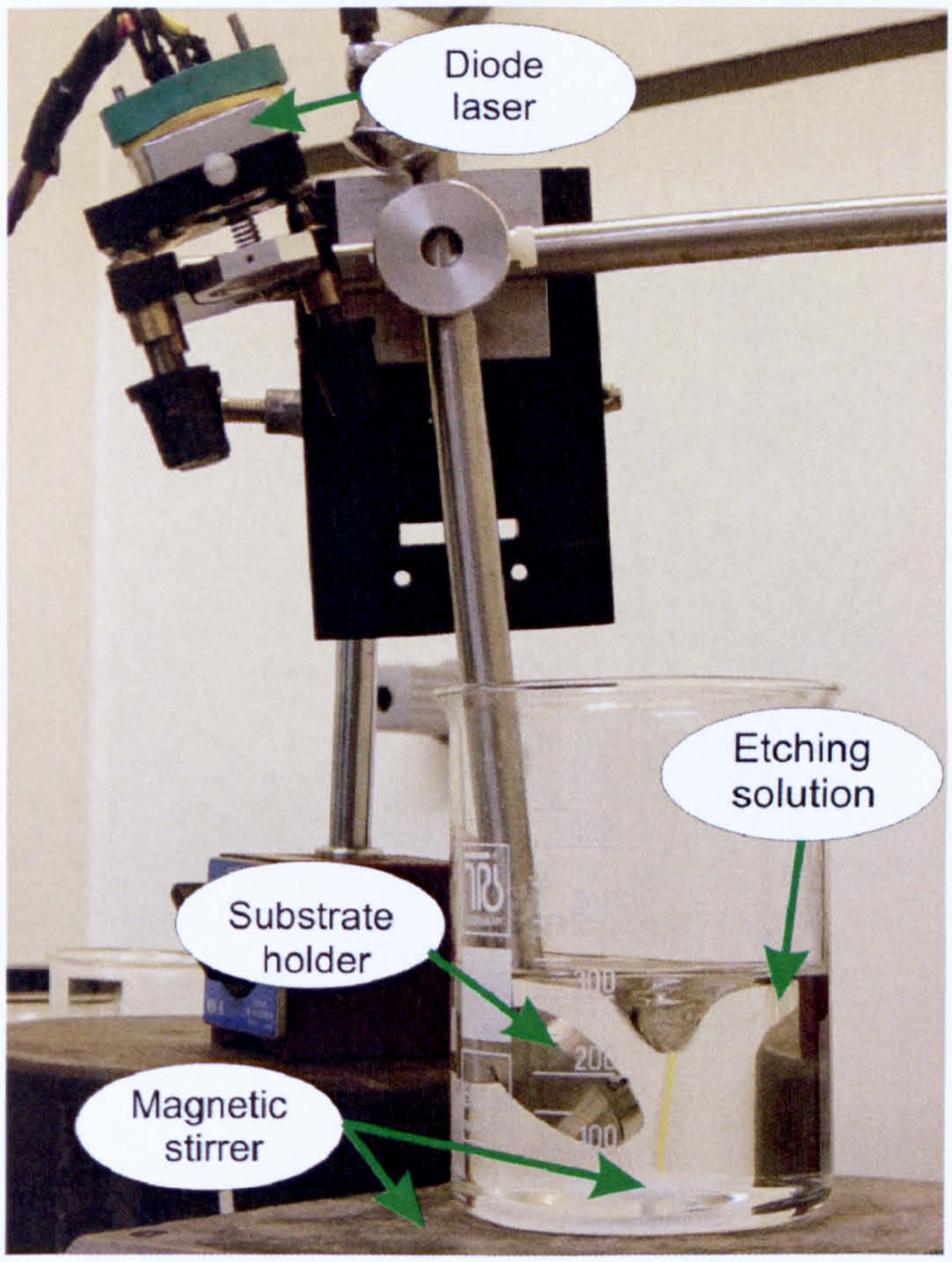

Figure (4.6.2): Etching apparatus

With an etch rate of 3140 Å/min it takes approximately 27 hours to remove 500μm of substrate. Once etching has been complete the sample is extremely thin, ≈ 6.4μm thick. A blueish mirror like finish can be seen on the wafer, indicating the DBR layer. The wafer being very thin and brittle is extremely hard to handle. The sapphire substrate is immersed into a solution of trichloroethylene that dissolves the remaining wax and cleans the wafer. Often in this process the wafer de-bonds and slides off into the beaker. This can be beneficial as the wafer can then be transported in this liquid and poured onto a copper plate. This allows handling of the wafer with the least stress. The wafer needs to be in good thermal contact with the copper heat sink to provide thermal extraction through the DBR. Several methods were used to thermally contact the thinned VECSEL to the copper heat sink including molten indium and solder however this damaged the brittle VECSEL. The solution was to use a conductive paint as an adhesive to thermally connect the wafer to the copper

plate. Once etched and cleaned the wafer was given a thin coat of silver conductive paint, while attached to the sapphire substrate, as seen in figure (4.6.3).

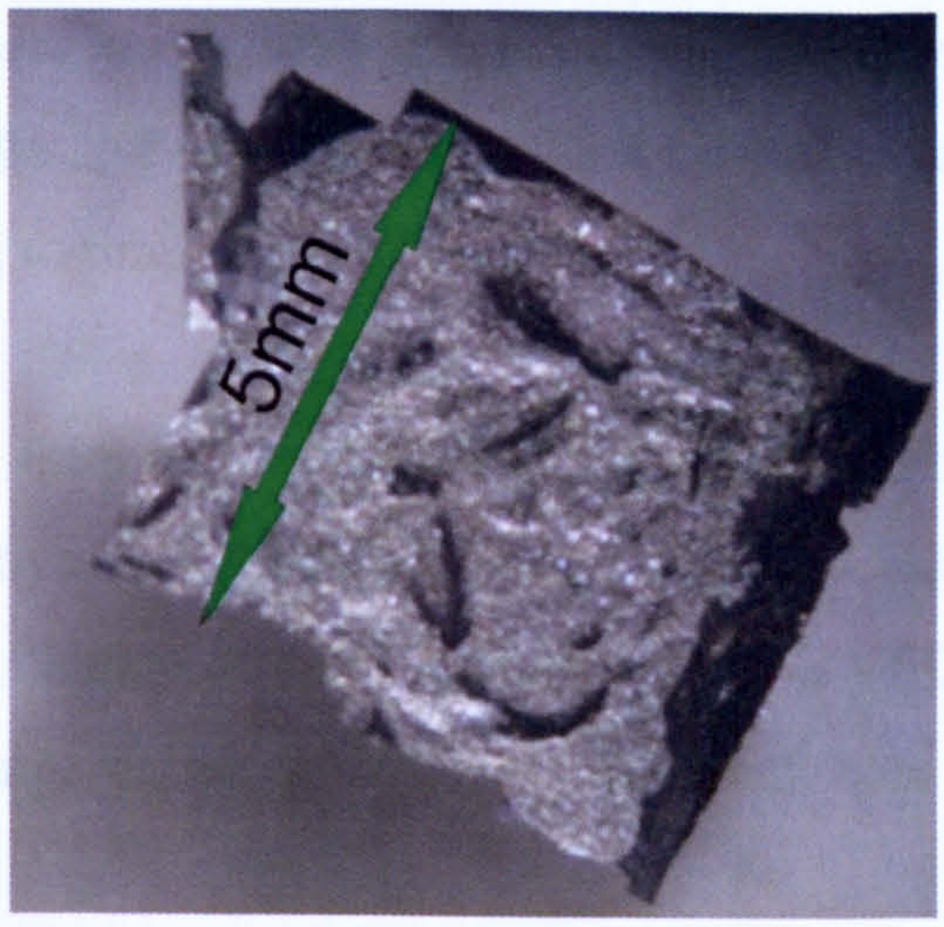

Figure (4.6.3): Microscope image of etched VECSEL with thin coat of silver paint

Once coated the wafer can be handled easier and is placed onto a copper heat sink, where an additional thin coat of silver conductive paint has been applied. This fresh coat bonds the wafer to the copper mount and produces a relatively flat front surface. The VECSEL was placed into a standard 3 mirror cavity and lasing was momentarily achieved with an output power of 0.1mW. On closer inspection of the wafer surface, small micro fractures were found together with some etched areas. This may have been caused during the bonding procedure and etching process respectively. No lasing could be achieved from further samples which all feature these physical defects.

4.7 CONCLUSION

Using a diamond heat spreader is the most efficient and convenient way to reduce the thermal build-up present in the gain region of the VECSEL. Theoretical models predict only a 15.5°C increase in temperature, which gives the laser a high thermal rollover point necessary for high output powers to be achieved. In addition the good optical quality of diamond and the addition of AR coating can provide a low loss

insertion factor. They also reduce the probability of surface damage by effectively removing heat close to the surface and naturally act as a barrier to other damaging elements. However as mentioned before, plane diamond heat spreaders change the spectral output from these lasers due to the addition of surface reflection. This effect can be removed by the use of a wedge diamond heat spreader. This however requires an AR coating to limit surface losses.

In contrast substrate thinning has shown that complete removal of the GaAs substrate allows effective heat transfer through the VECSEL's DBR structure. A maximum temperature change of 28°C is predicted for a VECSEL with no substrate remaining, which compares well with the diamond heat spreader model with substrate remaining.

Thinning of VECSEL wafers involves expensive processes, which require precise and delicate handling of the thinned sample. Although this is an alternative solution to using diamond, the most effective way to remove thermal build-up inside the gain region of a VECSEL is to use a diamond heat spreader.

4.8 References

1. Holm, M. A., Burns, D., Cusumano, P., Ferguson, A. I. and Dawson, M. D., "High-power diode-pumped AlGaAs surface-emitting laser" Applied Optics, **38**, no.27, p 5781, (1999)

2. Electronic Archive: New semiconductor materials, characteristics and properties. Ioffe Physico-Technical institute, St Petersburg, Russia. www.ioffe.ru/sva

3. A. Goldsmith, T. Waterma and H.J. Hirschbaum, "Handbook of thermophysical properties of solid materials", Armour research foundation, (1961).

4. Harris Benson, "University Physics", John Wiley & Sons, p370, (1991).

5. Hastie, J. E., Hopkins, J. M., Calvez, S., Jeon, C. W., Burns, D., Abram, R., Riis, E., Ferguson, A. I., and Dawson, M. D., "0.5-W single transverse-mode operation of an 850-nm diode-pumped surface-emitting semiconductor laser," IEEE Photonics Technology Letters, **15**, no.7, p894, (2003).

6. Bewley, W. W., Felix, C. L., Aifer, E. H., Stokes, D. W., Vurgaftman, I., Olafsen, L. J., Meyer, J. R., Yang, M. J. and Lee, H., "Thermal characterisation of a diamond-pressure-bond heat sink for optically pumped mid-infrared lasers", IEEE Quantum Electronics, **35**, 11, p1597, (1999)

7. L. Fan, M. Fallahi, J. Hader, A. R. Zakharian, J. V. Moloney, J. T. Murray, R. Bedford, W. Stoltz and S. W. Koch. "Multichip vertical external cavity surface emitting laser: a coherent power scaling scheme" Optics Letters, **31**, no.24, (2006)

8. S. J. Mcginily, R. H. Abram, K. S. Gardner, E Riis, A. I. Ferguson and J. S. Roberts, "Novel Gain Meduiim Design for Short-wavelength Vertical-External-cavity Surface-Emitting Laser" IEEE Journal of Quantum Electronics, **43**, no.6, p445, (2007)

9. S. Adachi, "lattice thermal resistivity of III-V compound alloys", Applied Physics, **54**, p1844, (1983)

10. B. M. Paine, A. P. Shah and T. Rust, "the effects of ternary alloys on thermal resistances of HBTs, HEMTs and laser diodes", Microelectronics Reliability, **43**, p853, (2003)

11. R. J. Olson, Jr., M. F. Taylor, T. S. Faska and M. Sundaram, "Alternate backside thinning of GaAs-based devices" International conference on compound semiconductor manufacturing technology, no.15, (1999)

12. G. C. DeSalvo, W. F. Tseng, J. Comas. " Etch rates and selectivities of citric acid/hydroden peroxide on GaAs, AlGaAs, InGaAs, InAlAs and InP". Journal of the Electrochemical Society, **139**, p 831, (1992).

CHAPTER FIVE

RING-CAVITY VECSEL

5.1 INTRODUCTION

Most laser systems use a linear cavity configuration. Due to the linear nature of the cavity, alignment of cavity mirrors and intra-cavity components is relatively simple. The one disadvantage of these cavities however is their susceptibility to feedback. When light is reflected off an external cavity component, for instance a sample holder, it can be directed back into the laser cavity, which can have an undesirable effect on the lasers performance. In single frequency lasers, feedback can cause the loss of single mode operation due to the interference of light experienced from the reflected beam. In these types of applications it is necessary to use a laser that has some tolerance to feedback, thus maintaining the lasers performance.

A ring cavity configuration can create such a laser. Ring cavities are common configurations in laser systems, such as Ti:Sapphire lasers and dye lasers, [1,2] In contrast to a linear cavity where the light oscillates back and forth in the cavity creating a standing wave, the ring cavities geometry allows the light to circulate around the cavity, which generates a travelling wave. A travelling wave is generated in both directions around the cavity, both clockwise and anti-clockwise. The use of intra-cavity elements can suppress one of the propagation directions and create a unidirectional ring laser. This unidirectional beam means intra-cavity elements induce only half the insertion loss to that of an oscillating linear cavity. It also has the benefit of being more insensitive to feedback. The unidirectional travelling wave also eliminates spatial hole burning, as the gain is "swept" by the travelling wave. These features make the ring cavity laser a very desirable tool for many applications. VECSELs experience no spatial hole burning due to the periodic spacing of the gain

region, however they are susceptible to feedback. This chapter details the first reported VECSEL ring cavity configuration.

5.2 Ring-cavity design

Ring cavities have the unique feature of a travelling wave, which propagates around the cavity mirrors forming a ring-like cavity. Although the name suggests a ring-like shape, most ring-cavity lasers are a series of mirrors in a zigzag formation. One common ring-cavity design is the "bow-tie" configuration, this can be seen below in figure (5.2.1).

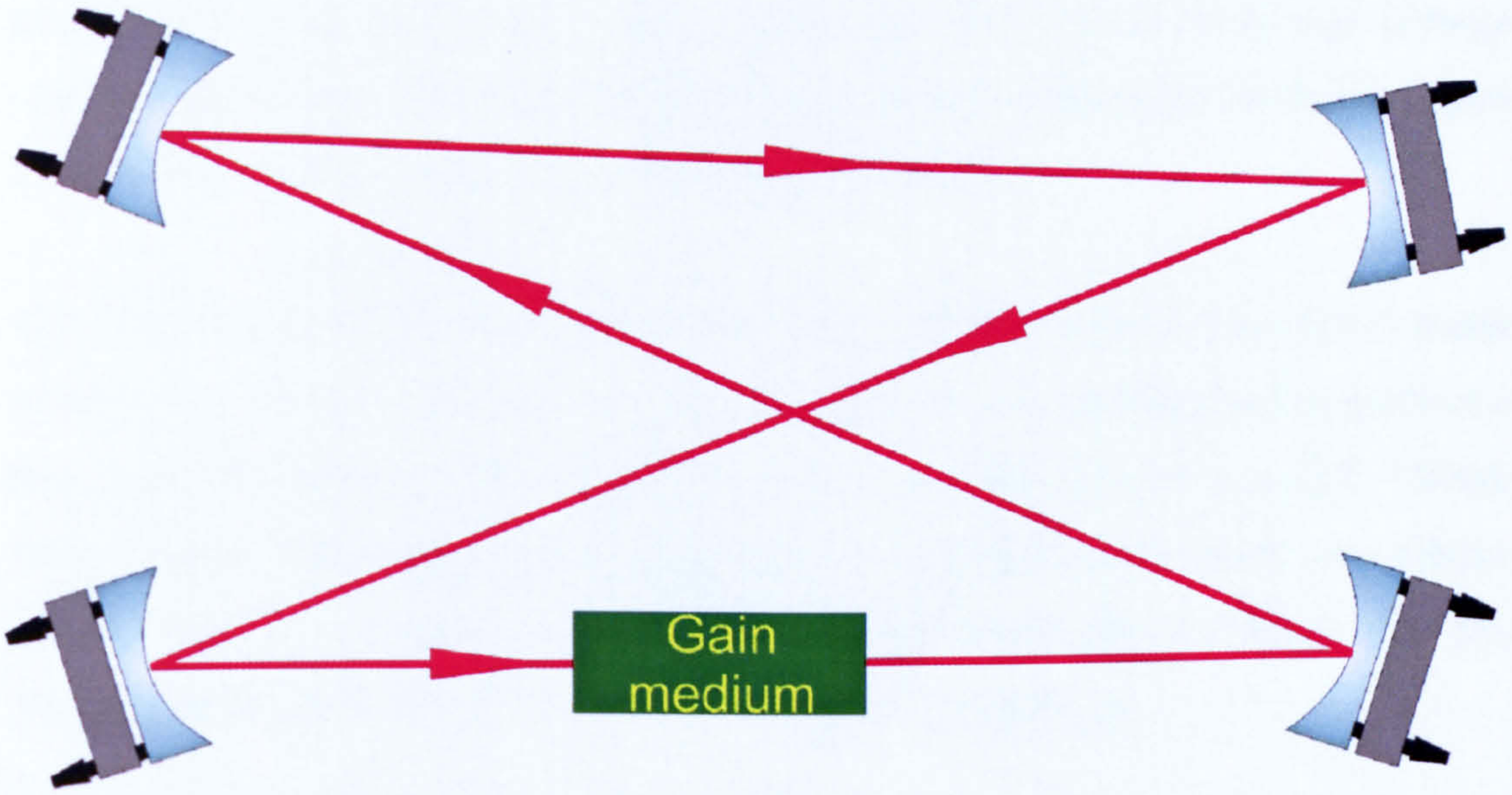

Figure (5.2.1): "bow-tie" ring cavity configuration

The main benefit from this cavity is the two focal points that are generated, which can be used for the gain medium and an intra-cavity element, such as a nonlinear crystal. In addition it also allows space for any other intra-cavity elements that may be required.

In the design of a VECSEL ring-cavity a variety of factors need to be considered. The VECSEL acts as a plane mirror that requires a tight focus of the cavity mode

(100μm), therefore it must be located at a focal point in the cavity. The angle of incidence to the VECSEL must be relatively small to maximise the VECSEL's DBR reflection, as this is angle dependent. Lastly, space for optical pumping optics and intra-cavity elements must be accommodated.

The 980nm VECSEL is designed for linear cavities, with emission at zero incidence, therefore the DBR is centred on 980nm at zero incidence. As the angle of incidence is increased the DBR reflectance band also shifts to higher wavelengths. To check if the wide angles used in a ring-cavity would be suitable for use in this VECSEL a series of reflectance measurements were taken when increasing the angle of incidence on the VECSEL. The results showed that only a reflection deviation of 1% from normal incidence was measured up to a maximum angle of 80°. Large angles can now be used to generate a suitable ring-cavity, however the use of large angles in laser cavities produces astigmatism in the beam, therefore the design angles must be kept as small as possible to minimise this effect.

The other main contributing factor to the design of this cavity is the optical pump system. To reduce the angles in the cavity a pump system was designed to produce a long focal length beam. The laser diode used for this application was a 20W, 980nm fibre coupled Limo module. The Limo laser is a compact unit, which uses micro-optics to couple a single high power laser diode's output into a 100μm fibre [3]. This output can then be focused to provide a bright pump source.

To produce a good pump profile it is essential to use the correct optics to focus the beam. A combination of 2 lenses are used to firstly collimate the output from the fibre then focus the beam to the desired size. Since the laser diode output is emitted from a 100μm fibre, a 1:1 image ratio can be used to produce a 100μm spot size at the focus. The choice of lenses are also very important in this application. To provide a good pump profile lenses which produce low aberrations are used. Figure (5.2.2) show common aberrations produced from a variety of lenses.

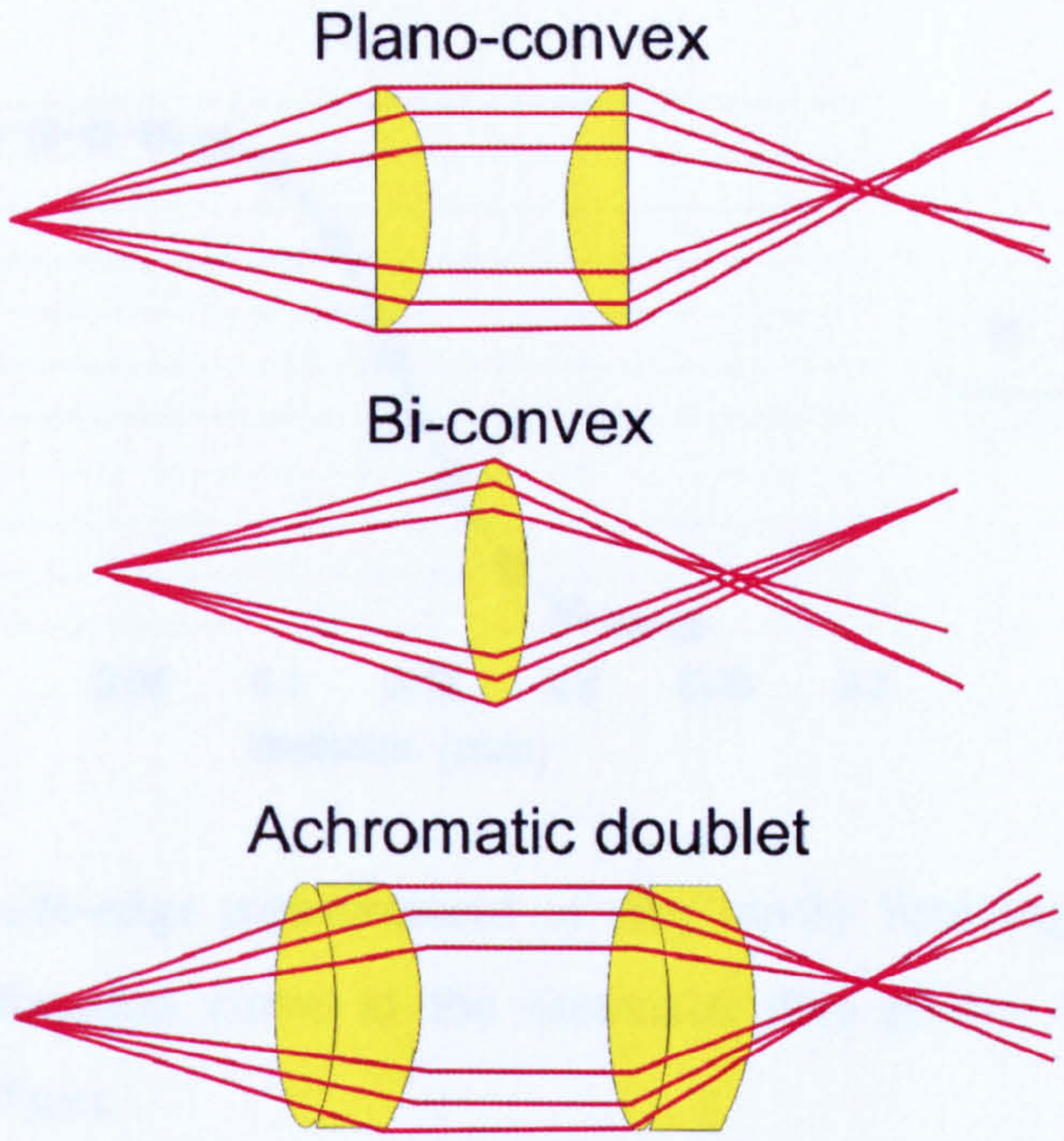

Figure (5.2.2): Lens types showing aberrations

As seen in the above figure (5.2.2), plano-convex and bi-convex lenses produce spherical aberrations that can distort the beam shape near the focus. This can produce several focal points, which is undesirable when designing a pump system. An achromatic doublet lens is constructed from 2 lenses that are cemented together. This type of lens is designed to accommodate for all different ray paths and this reduces the effects of aberrations. One disadvantage to these lenses is the high power limitations. The cement that holds the doublet lens system together deteriorates at high temperatures, which occurs from pump absorption.

A pump system was designed using 2 achromatic doublet lenses of focal length 25mm, to produce a 100μm pump spot. The first lens was placed 25mm from the output end of the fibre, this was used to collimate the beam to 12.5 mm in diameter. The secondary lens was then used to focus the collimated beam, 30mm after the initial lens, to the desired spot size. This gave a 100μm diameter spot 25mm from the final lens. This long focus allows the angles in the ring-cavity to be minimised. Figure (5.2.3) shows the knife-edge measurement of the beam size.

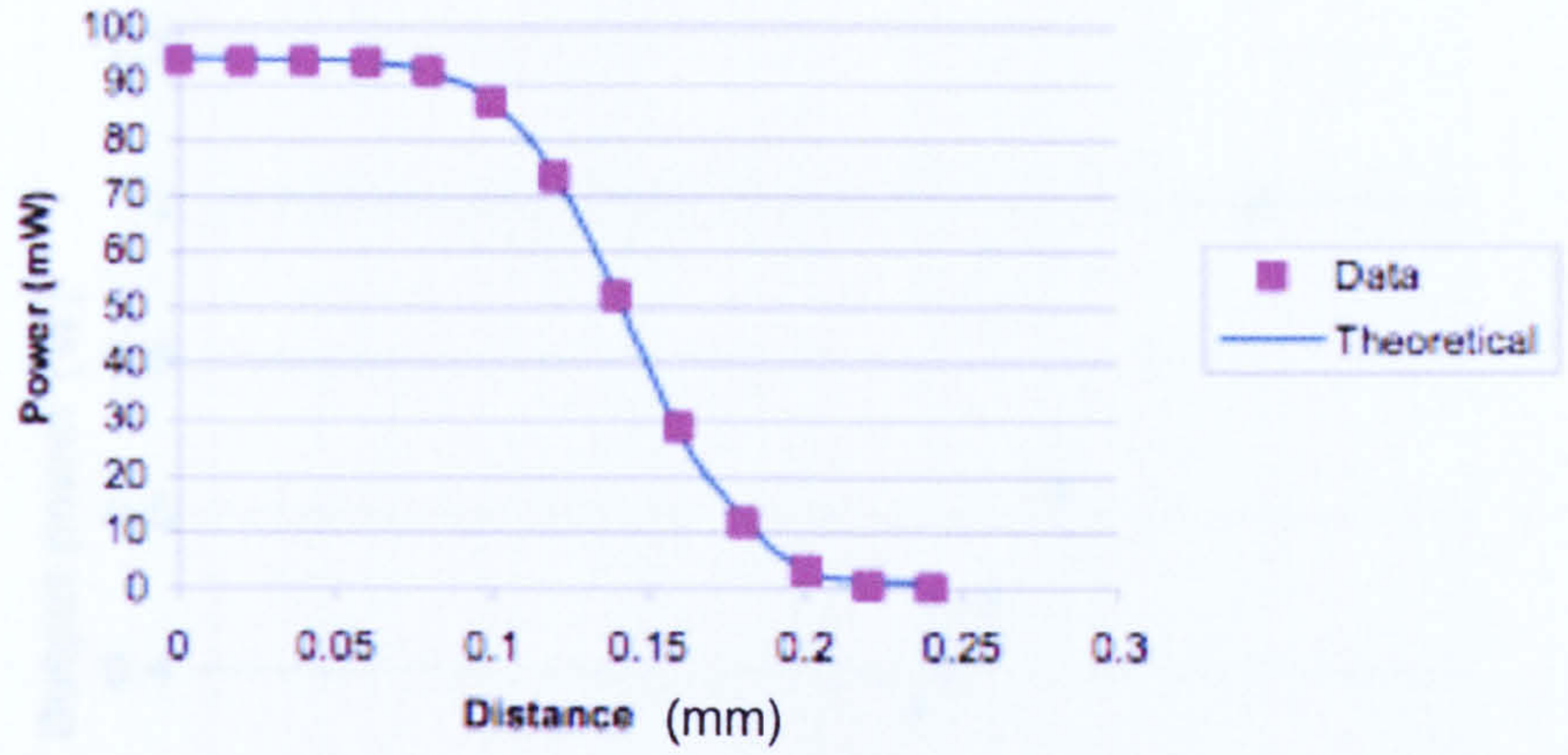

Figure (5.2.3): Knife-edge measurement of ring cavity focusing system. Fitting a theoretical error function curve to the measured data points, the spot size was measured to be 105μm.

Final design of the ring-cavity could now be completed. Using available optics and allowing for intra-cavity elements and minimised angles a stable cavity was designed using a computer-based program called Winlase. Figure (5.2.4) below shows the cavity configuration.

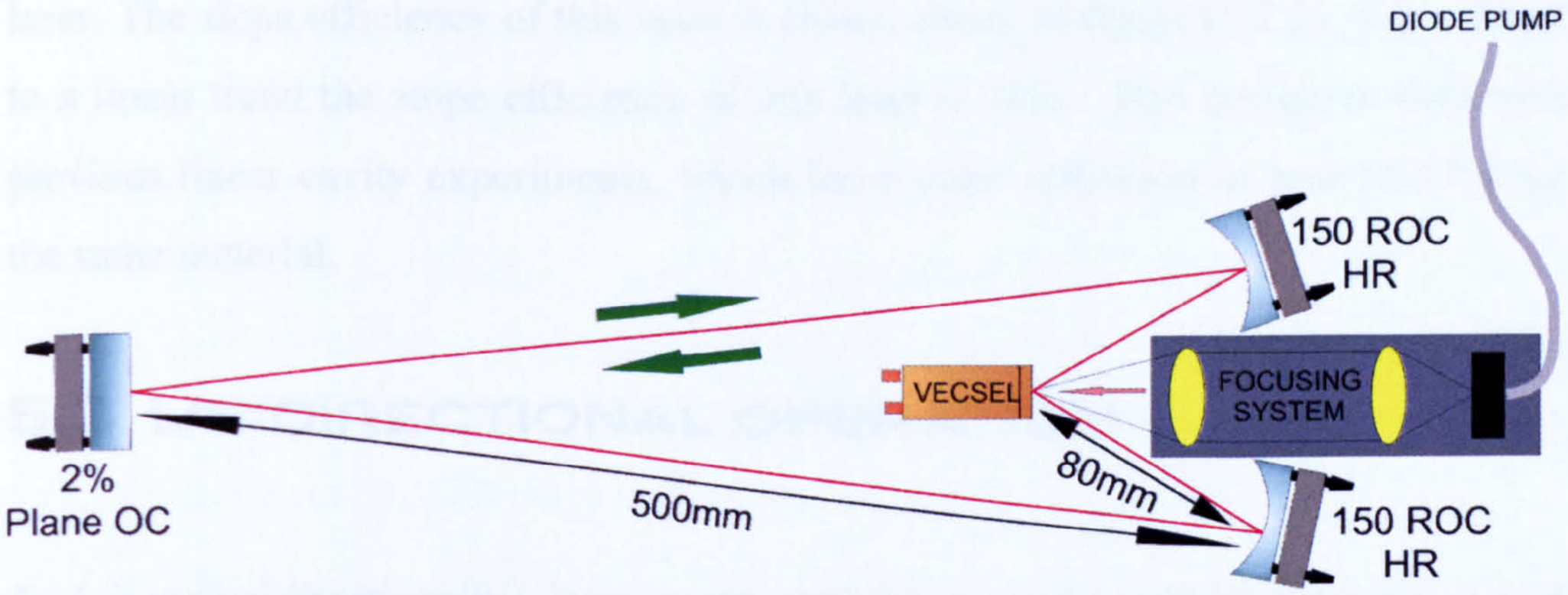

Figure (5.2.4): Ring-cavity configuration

A HeNe laser was injected through the output coupler (OC) to help align the cavity. Lasing was easily achieved with a maximum output power of 1W, from a pump power of 5W. Figure (5.2.5) shows the slope efficiency of the ring-cavity in a bi-directional state.

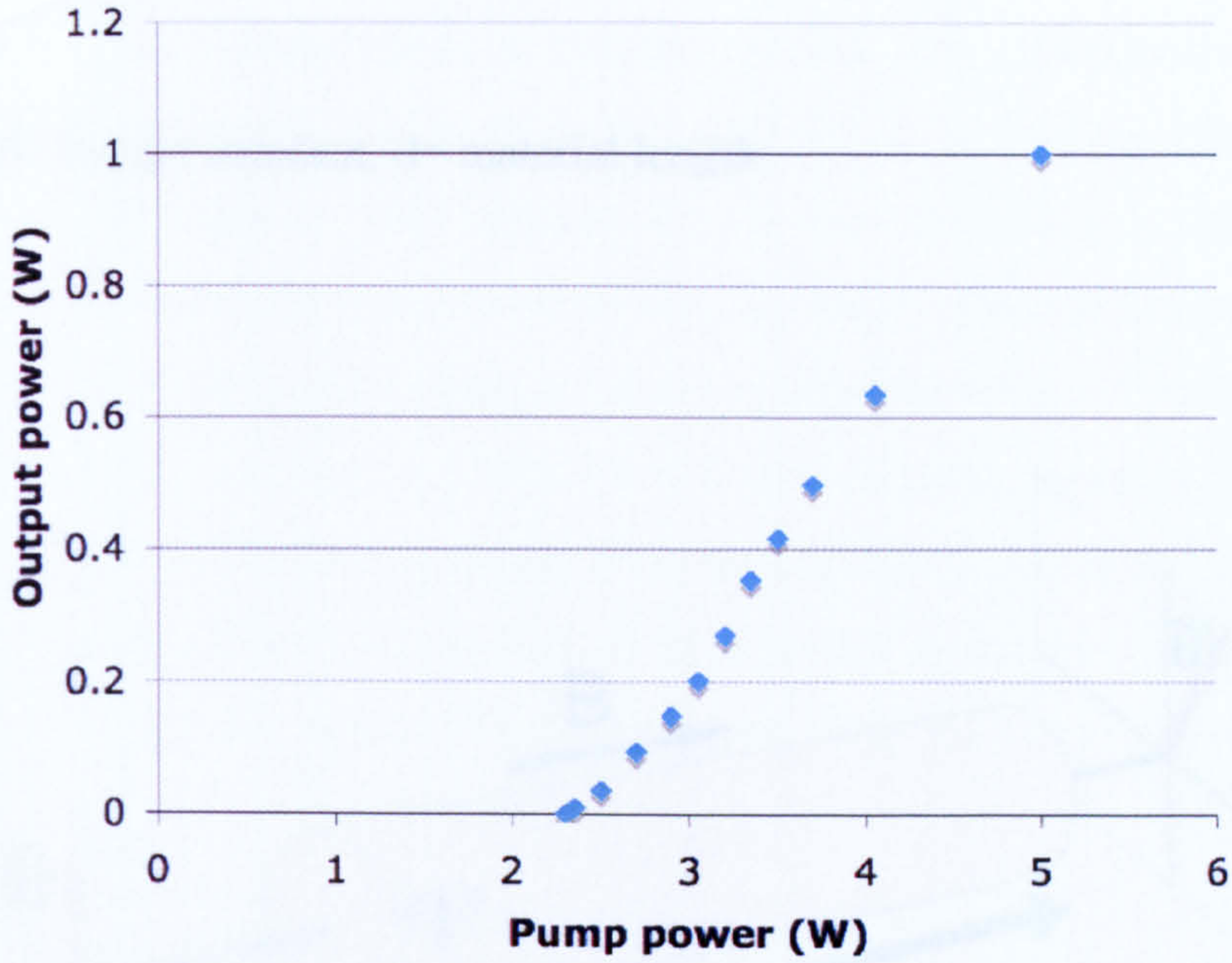

Figure (5.2.5): Slope efficiency of 980nm bi-directional ring-cavity showing a 38% slope efficiency.

The VECSEL ring-cavity, with no intra-cavity elements, operates as bi-directional laser. The slope efficiency of this laser is shown above in figure (5.2.5), When fitted to a linear trend the slope efficiency of this laser is 38%. This compares well with previous linear cavity experiments, which have slope efficiency at best of 37% for the same material.

5.3 Unidirectional operation

To initiate unidirectionality, intra-cavity elements must be used to suppress one of the counter propagating beams. In most common cases this can be achieved with the combined use of a Faraday rotator and compensation plate. A Faraday rotator uses the Faraday effect to rotate the polarisation of the laser beam [4]. A ferromagnetic material is subjected to a magnetic field (B), the strength of this magnetic field determines the angle (θ) by which the polarisation is rotated,

$$\theta = \mathcal{V}\mathrm{Bd} \qquad \text{equ:(5.3.1)}$$

Where, $\mathcal{V}$= Verdet constant, d= material length.

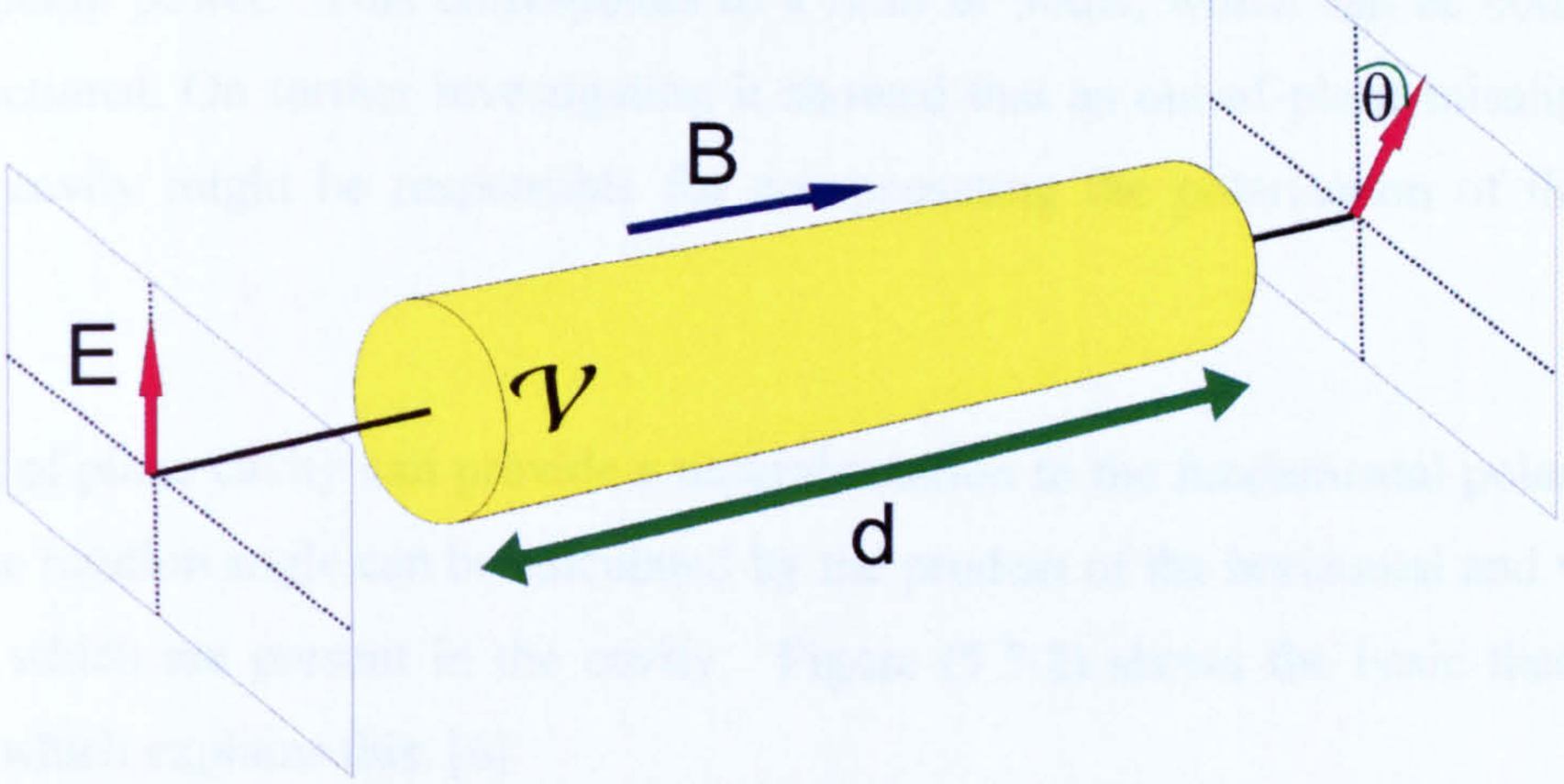

Figure (5.3.1): Theoretical schematic of the Faraday rotator

When an incoming beam travels through the Faraday rotator its polarisation is rotated by θ . A counter-propagating beam will also be rotated by θ but in the opposite direction, relative to propagation. A compensator plate now inserted which "compensates" the polarisation rotation angle experienced by the rotator. Made from a thin plate of birefringent material, it uses birefringence to create a phase delay between the ordinary and extraordinary ray, which creates a rotation in the polarisation of the beam, which is dependent on the materials thickness. As this is not dependent on the directionality of the beam, one circulating beam in the cavity returns to its original polarisation and the other counter-propagating beam is again rotated by θ . This creates a loss mechanism to the beam that experiences a 2θ rotation in polarisation, due to the Brewster surfaces on the Faraday rotator. The other beam continues circulating the cavity with no losses as its polarisation simply get rotated back and forth by the Faraday rotator and compensator plate (optical diode), thus only one direction remains, creating a unidirectional laser.

To create a unidirectional laser a Faraday rotator and compensator plate were inserted into the cavity. Both elements produce a 3 degrees rotation of the fundamental polarisation. The Faraday rotator was inserted into the laser cavity where there was adequate space to allow for alignment. On initial tests the Faraday rotator with no compensation plate, achieved unidirectionality. Output power from the main beam was recorded at 209mW, with the secondary beam only 0.27mW, at 3.4W pump power. This corresponds to a ratio of 30dB, which can be considered unidirectional. On further investigation it showed that an out-of-plane misalignment of the cavity might be responsible for compensating the polarisation of the laser beam.

An out of plane cavity can provide a natural rotation to the fundamental polarisation [5]. The rotation angle can be calculated by the product of the horizontal and vertical angles which are present in the cavity. Figure (5.3.2) shows the basic theoretical model which explains this. [6]

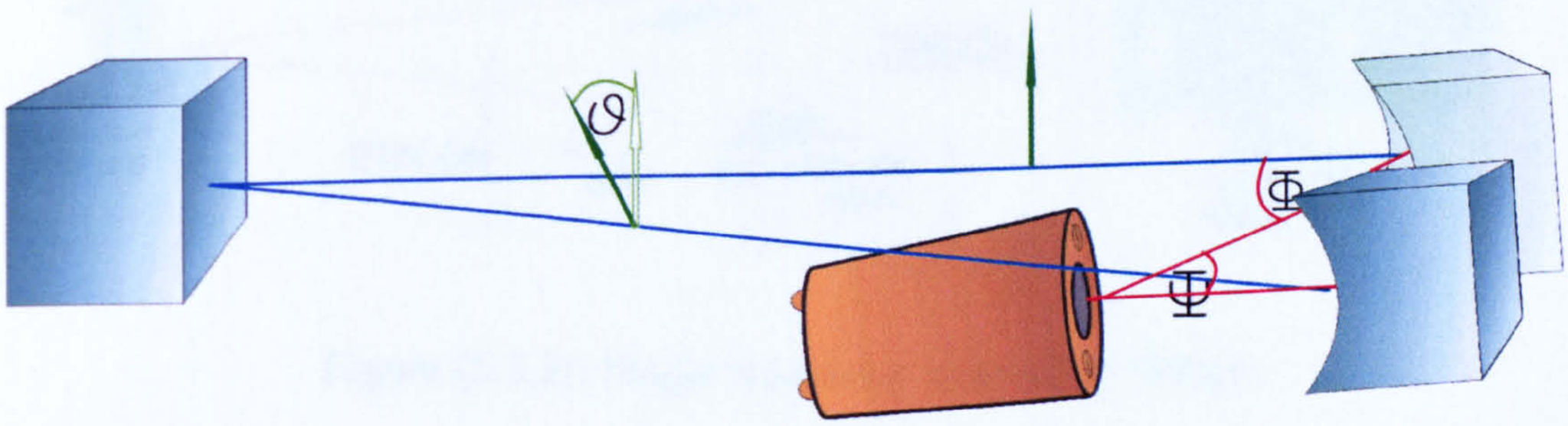

Figure (5.3.2): Out of plane cavity polarization effect. A retardation of ϑ is generated in the polarisation due to the laser cavity being out of plane shown by angles Φ and Ψ.

For small angles approximation ,

$$\vartheta = \Phi.\Psi \quad \text{(radians)} \qquad \text{equ:(5.3.2)}$$

The twist present in the ring-cavity was measured to be,

$$\Phi = 0.012$$

$$\Psi = 0.3665$$

Therefore,

$$\vartheta = 0.0044 = 0.25^{o}$$

The twist in the cavity corresponds to a rotation in the polarisation of 0.25°. This does not match the 3 ° retardation produced by the Faraday rotator, however this small compensation seems to provide enough rotation to favour a single propagation in the cavity.

A BRF and etalon were now added to the cavity to initiate single frequency operation. Figure (5.3.3) shows the cavity design implementing single frequency elements.

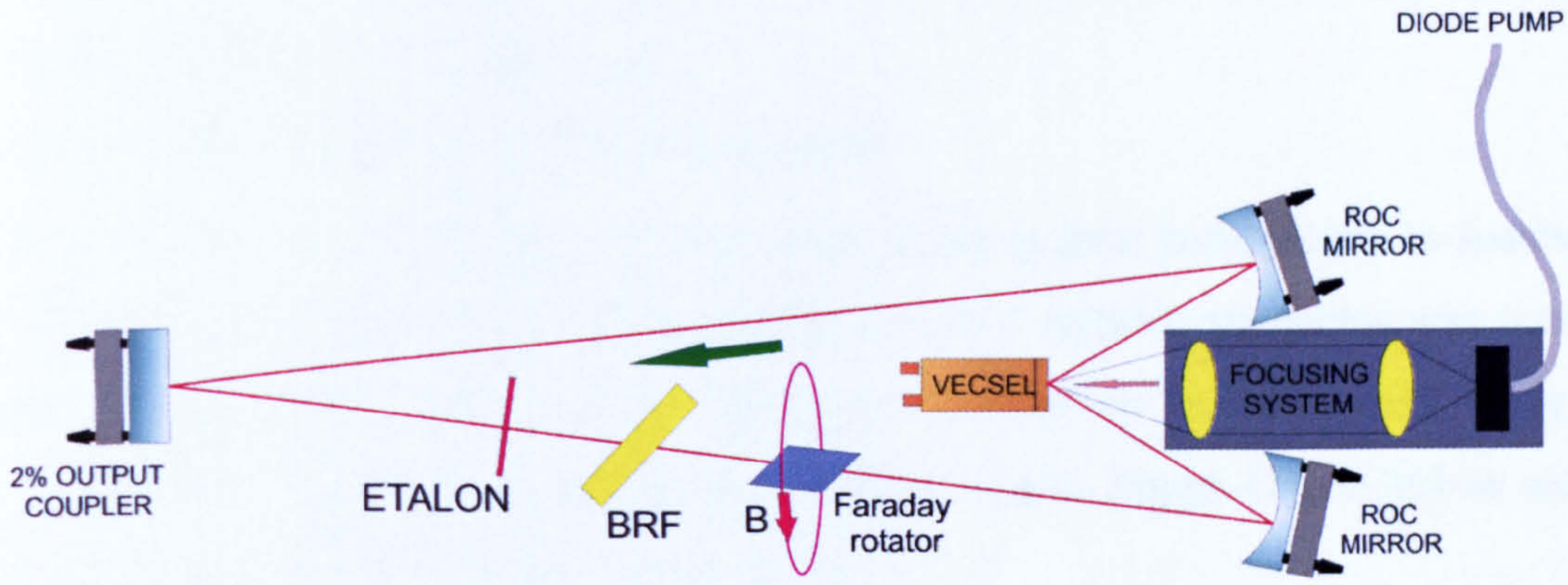

Figure (5.3.3): Single frequency ring-cavity design

Single frequency operation was achieved in the twisted ring-cavity with a 12% reduction in output power due to insertion losses. Single frequency characteristics were checked using a Fabry-Perot reference cavity, 1GHz FSR, finesse ~1000 and a RF spectrum analyser for longitudinal and transverse mode analysis, respectively. Figure (5.3.4) shows the single frequency output generated by the Fabry-Perot cavity.

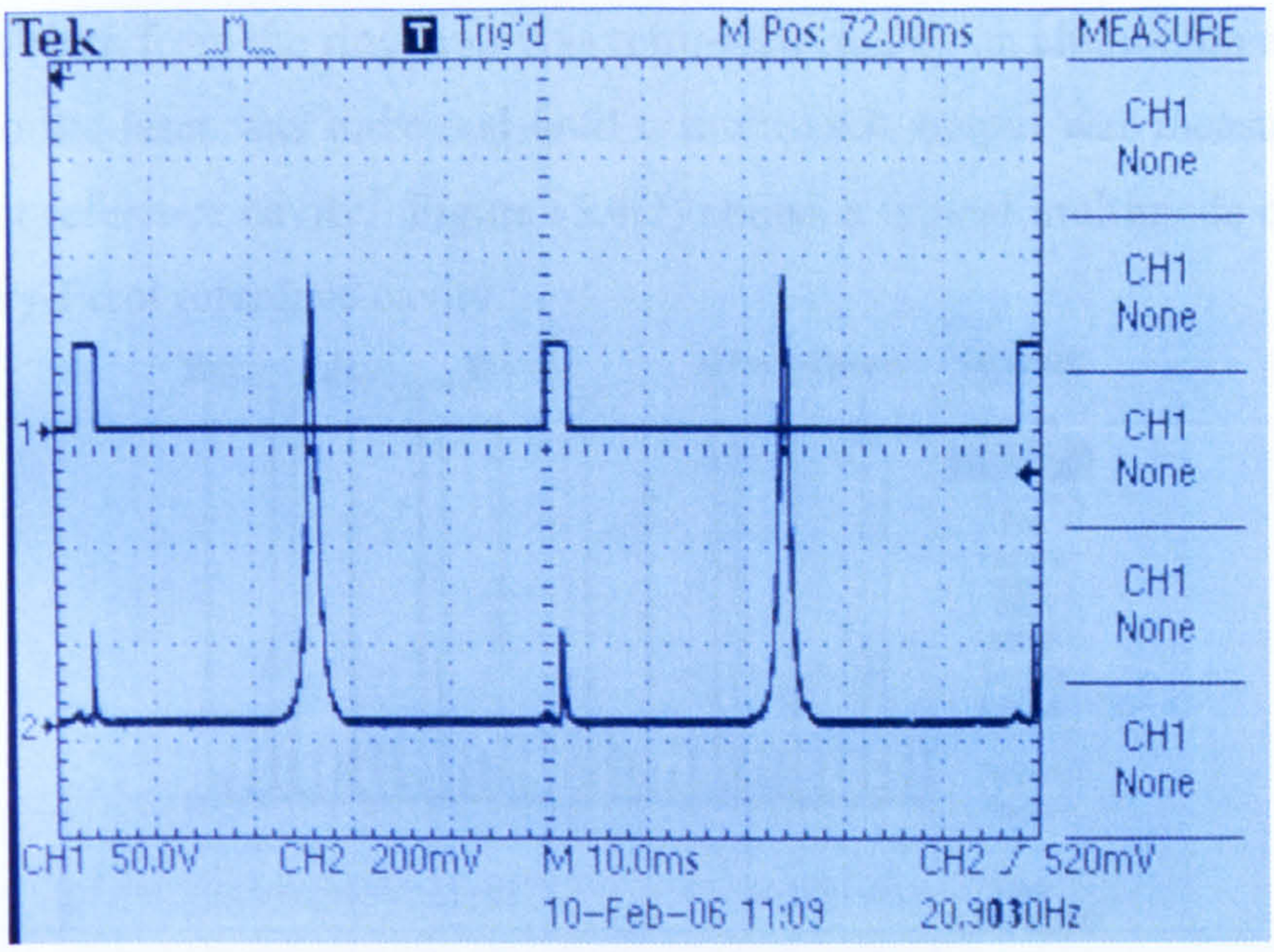

Figure (5.3.4): Single frequency scan of Fabry Perot reference cavity

A single longitudinal mode is shown in the above trace. At the end of the scan a small spike can be seem which occurs due to the mechanical resetting of the reference cavity in-between scans.

5.4 FEEDBACK ANALYSIS

One of the main advantages off ring-cavity lasers is their insensitivity to feedback. To measure the feedback tolerance of this cavity a variable attenuator was used to provide a variable feedback into the laser cavity. This was then monitored using the Fabry-Perot cavity until single mode operation ceased. Figure (5.4.1) below shows the feedback setup used in this experiment.

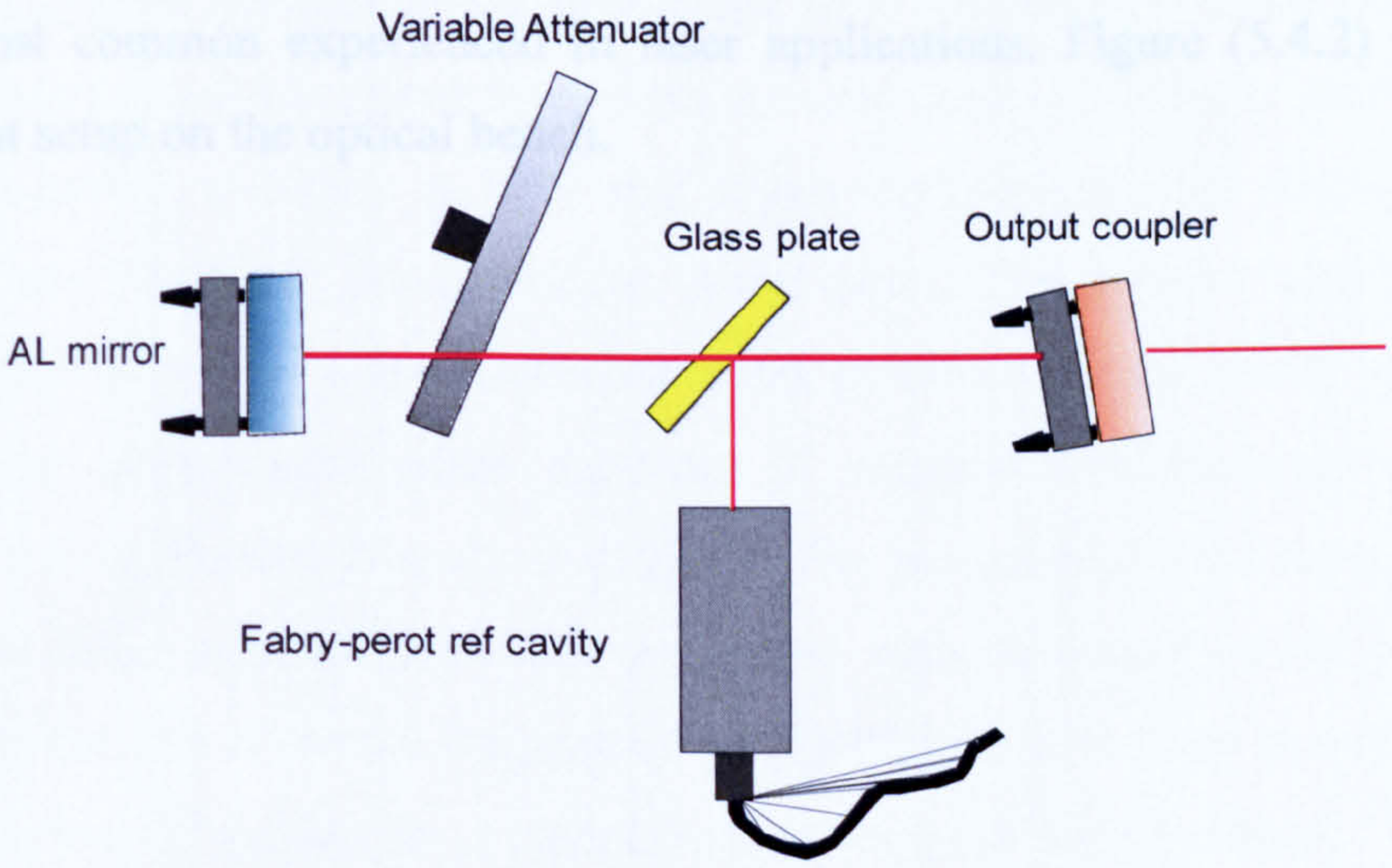

Figure (5.4.1): Feedback analysis setup

The output beam from the ring laser was retro-reflected by an aluminium mirror. The feedback to the laser was increased until a multimode output was measured on the Fabry-Perot reference cavity. Figure (5.4.2) shows a typical multimode output scan on the Fabry-Perot reference cavity.

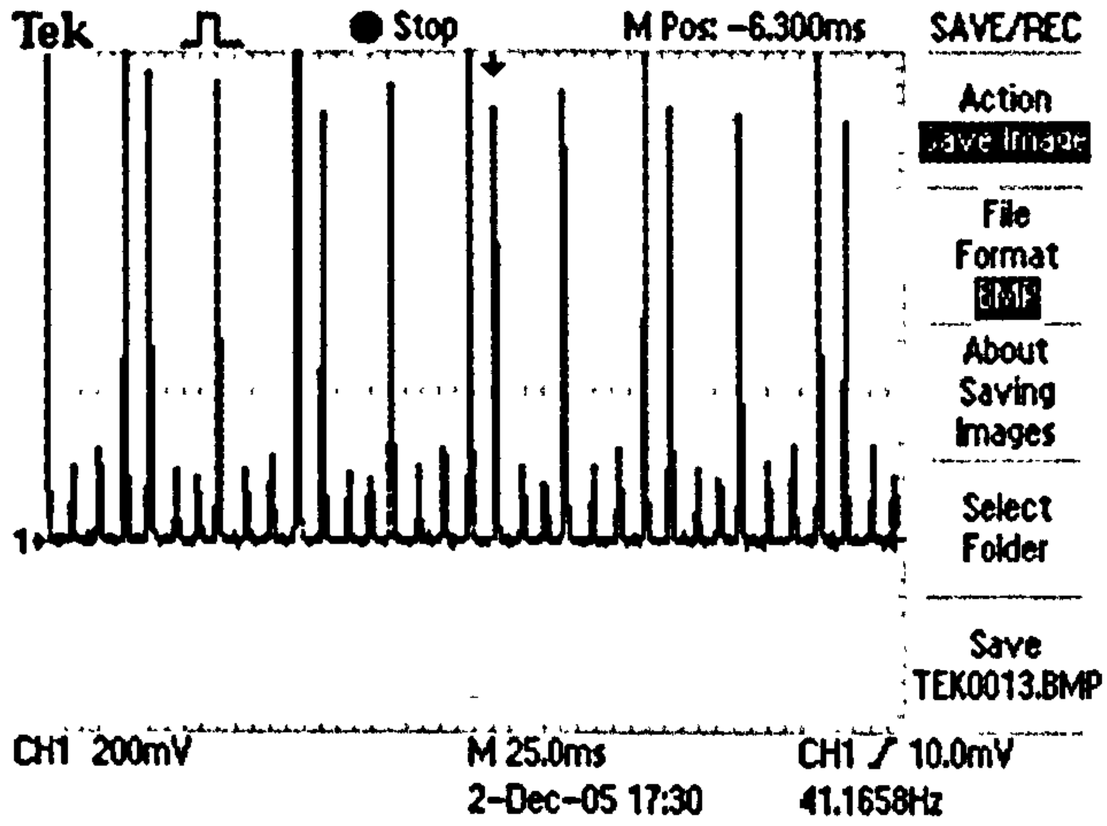

Figure (5.4.2): multimode output from laser due to a high level of feedback (10mW)

This process was repeated several times and an average was taken of the maximum feedback the laser could tolerate. Analysing the losses of each external element and measuring the power at key places in the set-up, the feedback power could be calculated. Using this method it was found that the single frequency ring-cavity featuring a twisted geometry had a tolerance of 2%. This corresponded to the 2.9mW feedback power with an output power of 141mW. The reflected beam was not mode matched to the cavity mode to give a realistic tolerance measurement, which would be the most common experienced in laser applications. Figure (5.4.2) shows the experiment setup on the optical bench.

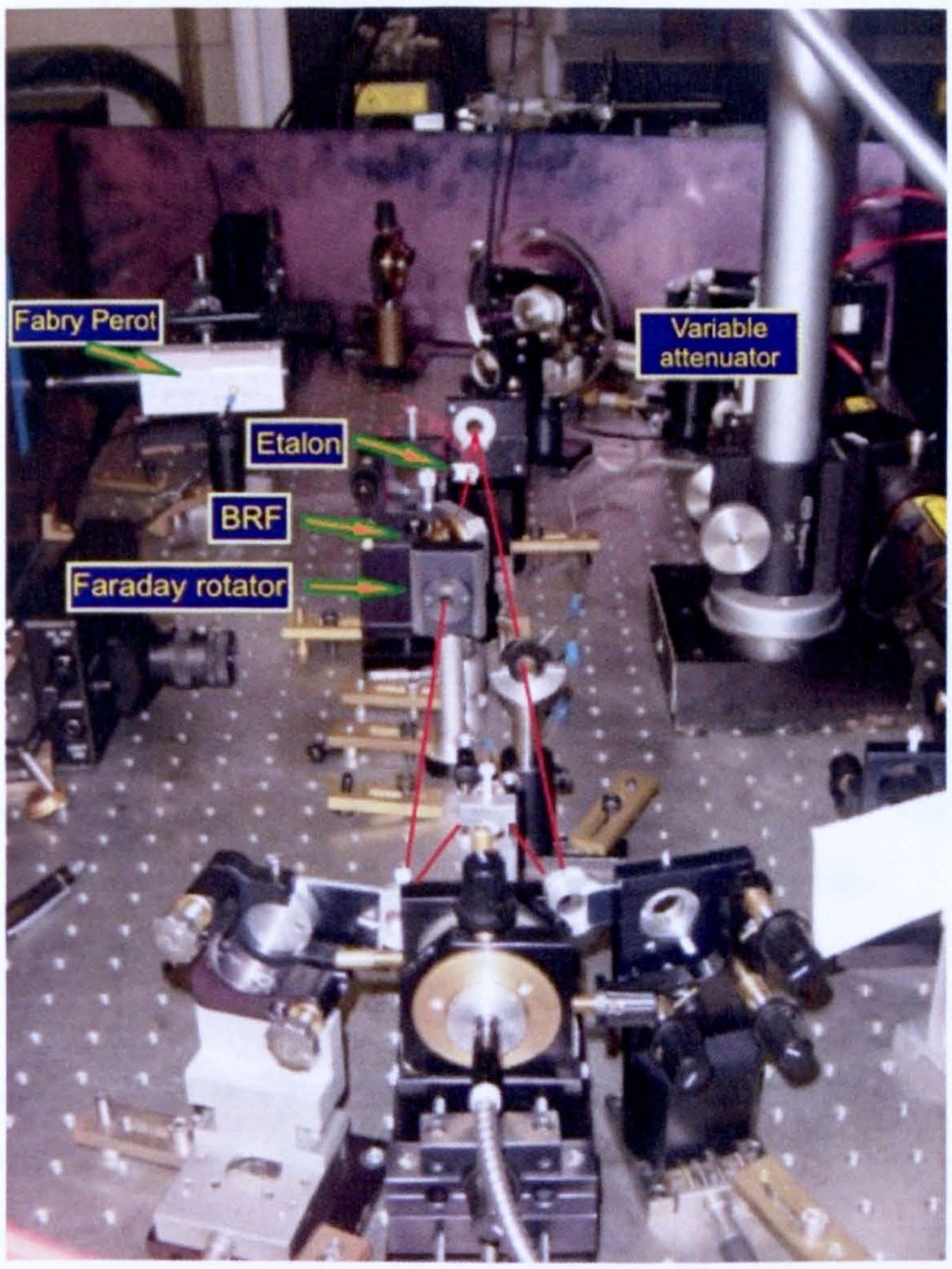

Figure (5.4.2): Experiment photo of ring-cavity laser

To compare this result with a standard cavity featuring a compensation plate, the cavity was aligned parallel to the bench and the compensation plate was inserted. This produced a unidirectional laser with a main beam of 276mW and secondary beam of 0.2mW, (>30dB). A BRF and etalon were inserted for single frequency operation and feedback measurements were taken. The twisted cavity although unidirectional relied on a small compensation produced by the cavity's geometry, however the compensator plate produces 3^{o} rotation and produced a stronger unidirectionality. Feedback analysis of this cavity measured 3.2%, corresponding to the 3.7mW being injected back into the cavity with an output power of 117mW. Comparing the two different ring-cavity configurations it is clear the conventional cavity featuring the compensator plate is more tolerant to laser feedback.

As a comparison, a single frequency linear cavity was constructed to compare feedback measurements. One roundtrip in a ring cavity laser is the distance travelled around all of the cavity mirrors once (L). The corresponding cavity length for a linear configuration will be half the size of the ring configuration (L/2), figure (5.4.3), shows the linear cavity design.

Figure (5.4.3): Single frequency linear cavity design.

Feedback analysis was once again performed using the same method. For an output power of 116mW the maximum feedback tolerance measured before single frequency operation deteriorated was 0.8%, corresponding to a tolerance of 0.96mW. On comparison to the ring-cavity of 3.2%, it is clear that a ring configuration, as in other types of ring lasers, has a higher tolerance for external feedback. This makes it an ideal tool for applications that involve feedback. An additional feature that many applications require is the ability to tune the laser's wavelength. Figure (5.4.4) shows the tuning range of the ring-cavity VECSEL.

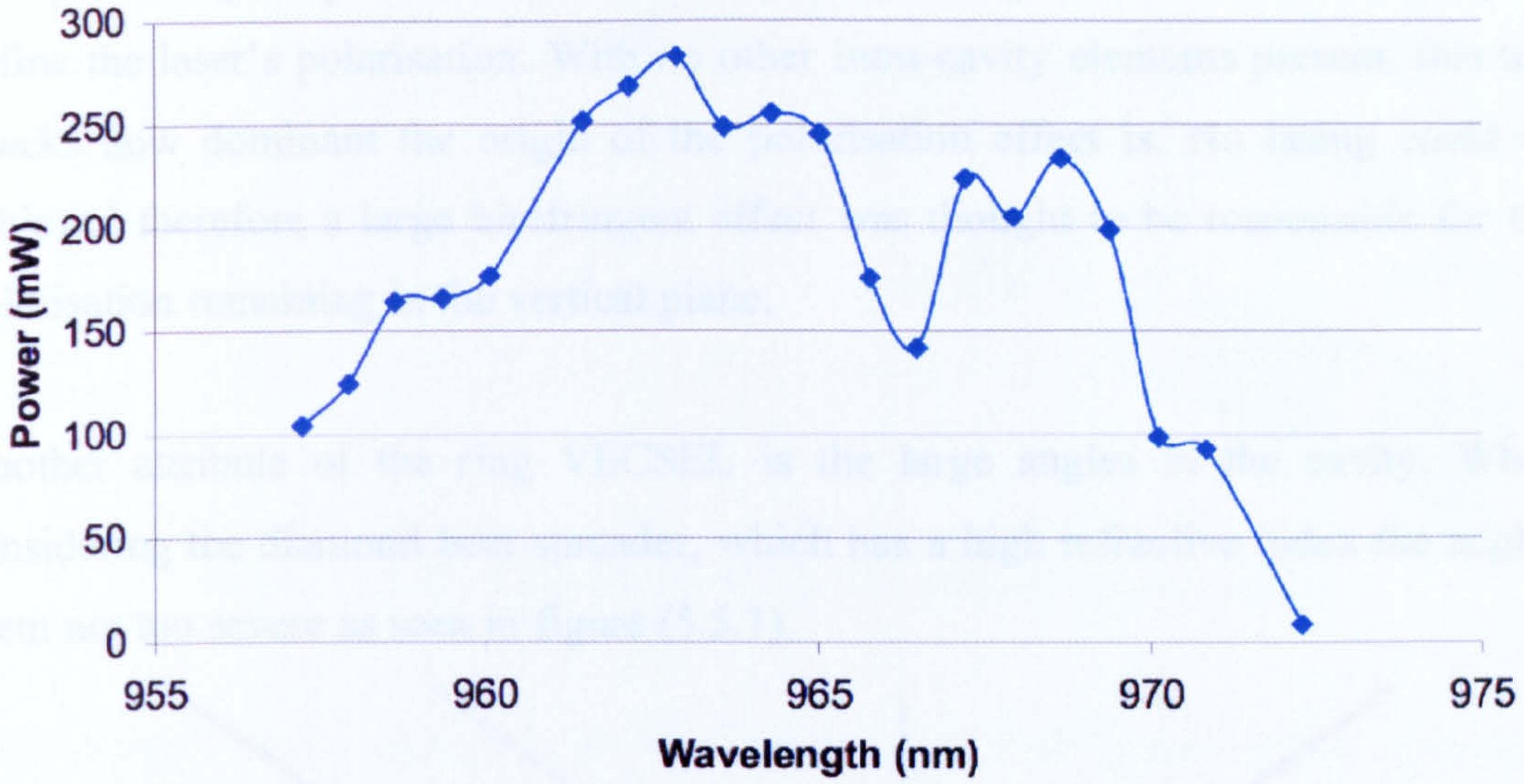

Figure (5.4.4): Single frequency tuning curve of ring-cavity VECSEL as shown in figure (5.3.3). A reduction in output power occurs around 966nm that could be explained by a high level of water absorption at these particular wavelengths[7].

The above figure shows course tuning of the BRF in the ring-cavity VECSEL. This shows 15nm of tuning from 957-972nm at moderate power levels.

5.5 Polarisation analysis

Lasing was only possible in the ring cavity at certain rotation angles of the VECSEL wafer due to large losses in polarisation conflict between the VECSEL wafer and the intra-cavity elements. When introducing Brewster-cut intra-cavity elements to the ring-cavity, the polarisation of the cavity should be matched with the Brewster orientation to limit losses. In this ring cavity a horizontal orientation was used. In normal conditions in a linear cavity it has been demonstrated that the linear polarisation generated in the cavity is directly proportional to the rotation of the VECSEL wafer's axis. The ring-cavity however experienced a linear polarisation, which was independent of the rotation of the wafer. The polarisation remained near vertical, independent of the wafer's rotation, thus another contributing factor was affecting this parameter.

Firstly a thin glass plate was inserted at Brewster's angle in the horizontal plane to define the laser's polarisation. With no other intra-cavity elements present, this test checks how dominant the origin of the polarisation effect is. No lasing could be achieved therefore a large birefringent effect was thought to be responsible for the polarisation remaining in the vertical plane.

Another attribute of the ring VECSEL is the large angles in the cavity. When considering the diamond heat spreader, which has a high refractive index the angles seem not too severe as seen in figure (5.5.1).

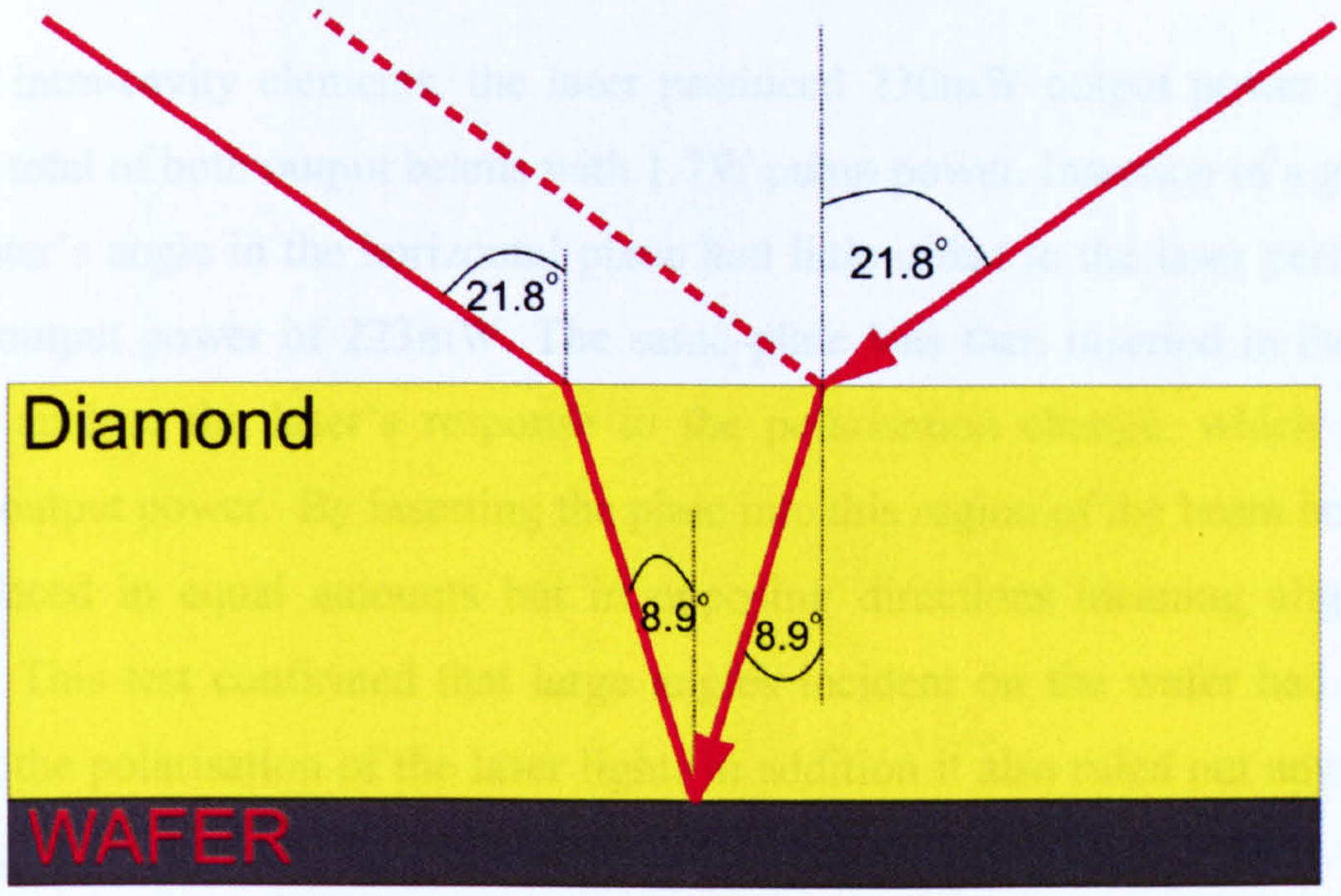

Figure (5.5.1): Incident angles of laser beam on VECSEL wafer

Although the effect of the diamond's high refractive index (n=2.417) lowers the incident angle to 8.9° this angle is still large in comparison to a linear cavity geometry. To experimentally analyse the effect of this angle on the polarisation in the cavity, a ring cavity was constructed with reduced angles. Figure (5.5.2) shows the adapted ring-cavity design.

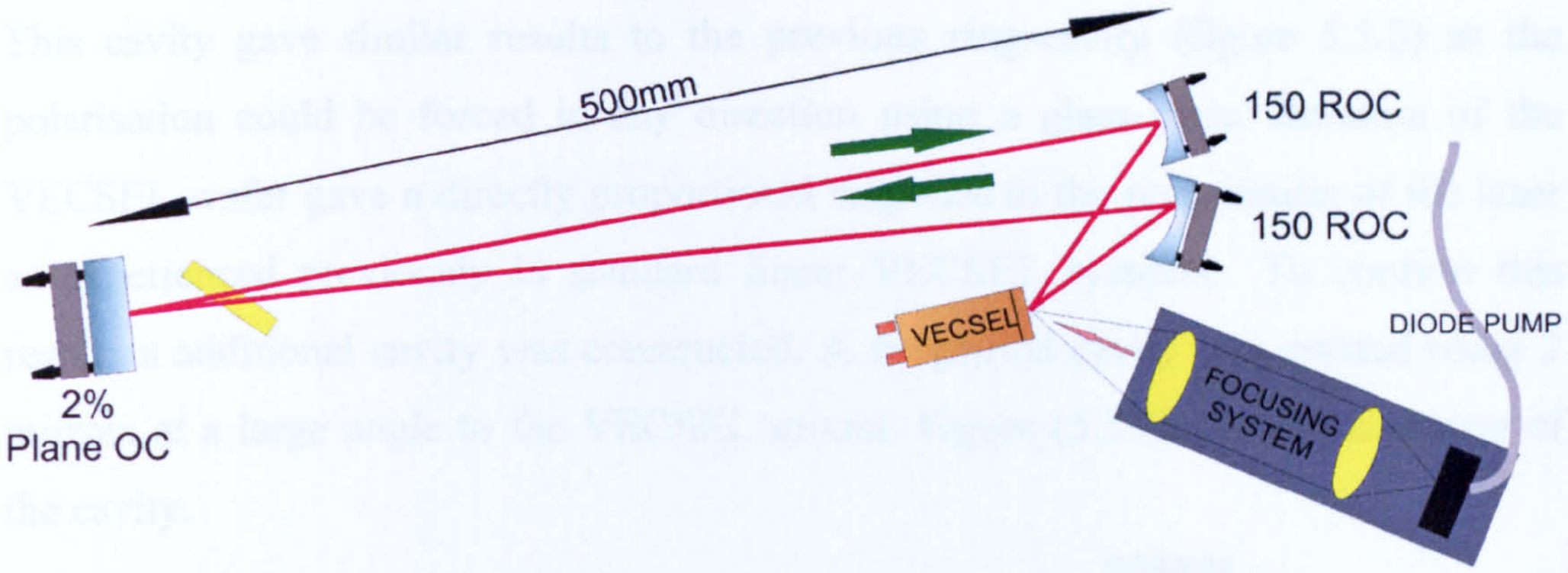

Figure (5.5.2): Ring-cavity VECSEL with minimised angles

With no intra-cavity elements, the laser produced 230mW output power generated from the total of both output beams with 1.7W pump power. Insertion of a glass plate at Brewster's angle in the horizontal plane had little effect to the laser performance, with an output power of 223mW. The same plate was then inserted in the vertical plane to analyse the laser's response to the polarisation change, which produced 200mW output power. By inserting the plate into this region of the beam both beams are displaced in equal amounts but in opposing directions meaning alignment is retained. This test confirmed that large angles incident on the wafer had a role in dictating the polarisation of the laser light. In addition it also ruled out any effects a travelling wave has on the polarisation. To analyse large angle effects a simple adaptation of the first ring cavity was made to form a linear cavity with similar angles. Figure (5.5.3) shows the linear cavity design.

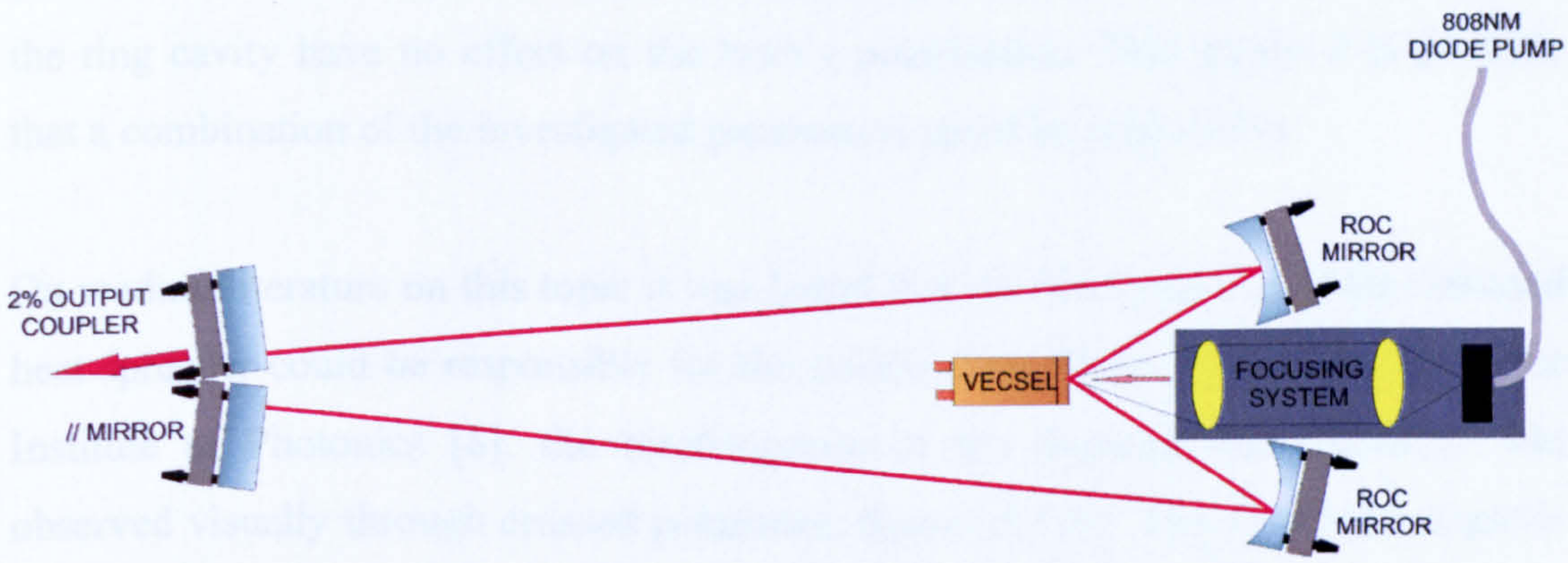

Figure (5.5.3): large angled linear cavity VECSEL

This cavity gave similar results to the previous ring-cavity (figure 5.5.3) as the polarisation could be forced in any direction using a glass plate. Rotation of the VECSEL wafer gave a directly proportional response to the polarisation of the laser as experienced previously in standard linear VECSEL systems. To confirm this result an additional cavity was constructed. A simplified cavity was created using 2 mirrors at a large angle to the VECSEL mount. Figure (5.5.4) shows the design of the cavity.

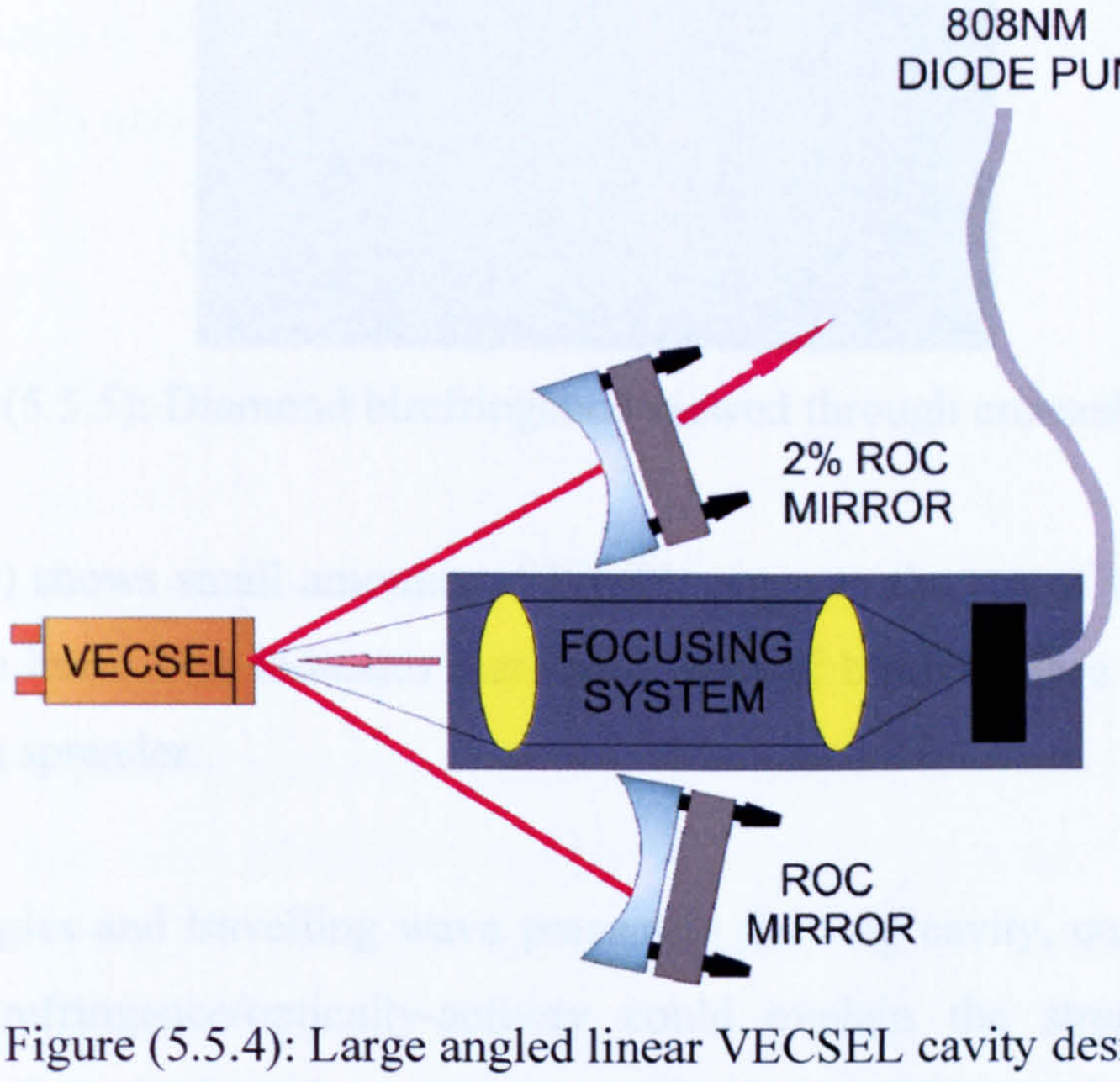

Figure (5.5.4): Large angled linear VECSEL cavity design

This cavity provided identical results to the previous linear cavity shown in figure (5.5.3). These results indicated that the large angles and travelling wave inherent to the ring cavity have no effect on the laser's polarisation. This means it is possible that a combination of the investigated parameters could be responsible.

On reading literature on this topic it was found that the birefringence of the diamond heat spreader could be responsible for the polarisation effect. With reference to the Institute of Photonics [8], the birefringence of the diamond heat spreader was observed visually through crossed polarisers, figure (5.5.5). The diamond sample is placed in-between crossed polarisers, if any birefringent is present the light projected through that area experiences a change in polarisation, which is then transmitted

through the polarizer. This visually indicates if any birefringence is present in the diamond sample.

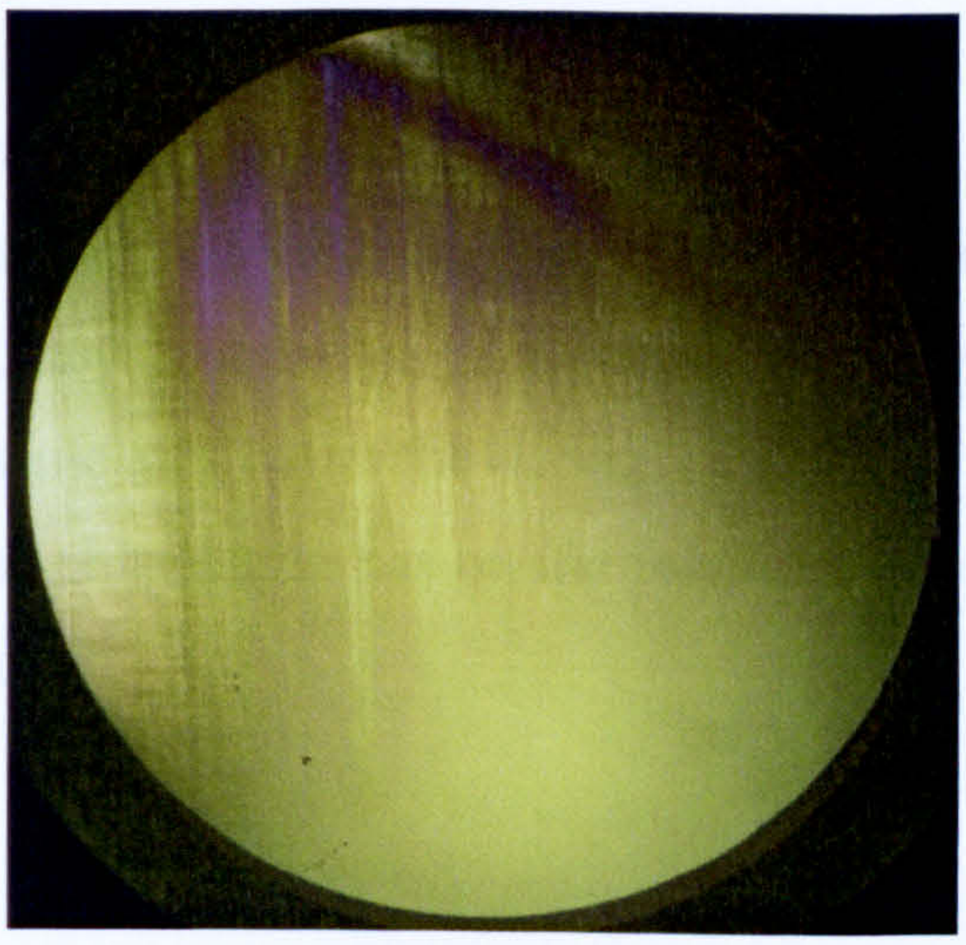

Figure (5.5.5): Diamond birefringence viewed through crossed polarisers

Figure (5.5.5) shows small amounts of birefringence to the top of the image shown by the purple haze. This indicates that some level of birefringence is present in the diamond heat spreader.

The large angles and travelling wave present in the ring cavity, combined with the diamonds birefringence/optically-activity could explain the strange polarisation effects. At a closer look at the geometry near to the VECSEL surface it can be seen that the in-coming and out-going beams do not overlap much within the diamond heat spreader. This is illustrated in figure (5.5.6).

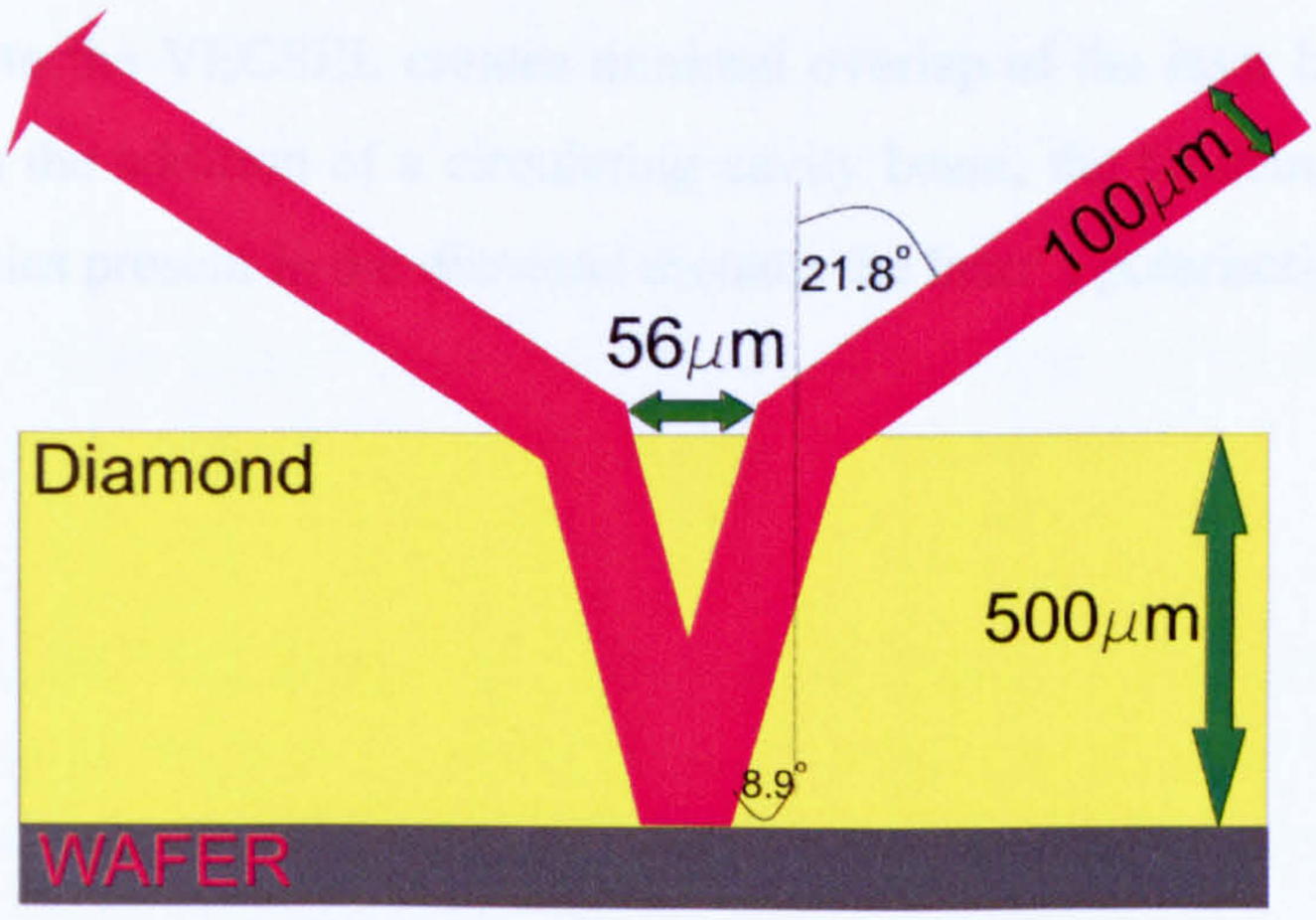

Figure (5.5.6): Beam geometry in diamond heat spreader

If the diamond heat-spreader was optically active this would mean that a beam will experience a level of retardation when passing through the diamond. As the ring cavity produces a travelling wave, which circulates the cavity, it constantly experiences this retardation in the polarisation. In contrast, a linear cavity, the beam is overlapped exactly, any retardation experienced is cancelled out by the beam returning through the same area but in the opposite direction. This could explain the indirect relationship the polarisation has on the rotation of the VECSEL axis, in the ring cavity configuration.

5.6 Conclusion

This chapter has demonstrated the first ever VECSEL ring cavity configuration. A high feedback tolerance of 3.2% can be injected into the cavity until single frequency operation is affected. In comparison to a linear system the ring cavity is more than a factor of 4 times more insensitive to feedback. With a 15 nm tuning range and 280mW maximum power this laser is an ideal tool for many applications including laser spectroscopy.

The polarisation effects experienced in the ring cavity could be primarily caused by the birefringence/optically-active properties of the diamond heat spreader. A large angle incident to the VECSEL creates minimal overlap of the laser beam inside the diamond. With the addition of a circulating cavity beam, the birefringence/optically –active properties present in the diamond dictates the laser's polarisation.

5.7 References

1. W. S. Pelouch, P. E. Powers, and C. L. Tang, "Self-starting mode-locked ring cavity Ti:sapphire laser", Optics Letters, **17**, no.22, (1992).

2. E. R. Carney, D. W. Fahey, and L. D. Scheare."Injection-locked dye laser pumped by a xenon-ion laser", IEEE Journal of Quantum Electronics, **16**, no.1, (1980).

3. www.limo.de

4. W. E. Hord, F. J. Rosenbaum and A. J. Benet, "Theory and Operation of a Reciprocal Faraday-rotation Phase Shifter", IEEE Transactions on Microwave Theory and Techniques, **20**, p112, (1972).

5. T. J. Kane and R. L. Byer, "Monolithic, unidirectional single-mode Nd:YAG ring laser", Optics Letters, **10**, no.2, (1985).

6. F. Biraben. "Efficacite des systemes unidirectionnels utilisables dans les laser en anneau". Optics Communications, **29**, no.3, (1979)

7. C. Zhiping, T. D. Wilkerson and U. N. Singh," Water-vapor absorption line measurements in the 940-nm band by using a Raman-shifted dye laser" Applied Optics, **32**, no.6, p992, (1993).

8. F. van Loon, A. J. Kemp, A. J. Maclean, S. Calvez, John-Mark Hopkins, J. E. Hastie, M. D. Dawson and D. Burns, " Intracavity diamond heatspreaders in lasers: the effects of birefringence" Optics Express, **14**, no.20, (2006).

CHAPTER SIX

MICRO-CAVITY VECSEL

6.1 INTRODUCTION

In the laser industry it is sometimes beneficial to have a small compact laser system for various applications. The most common compact laser source available today is the diode laser. One example of an edge emitting diode uses a small external cavity to initiate single longitudinal mode operation and with electrical pumping, the overall size of these lasers can be very small [1]. Another compact laser, which has evolved in recent years, is the fibre laser. The laser cavity is created from doped fibres that can be tightly compacted. The use of photonics crystal fibres and Bragg gratings allow single frequency generation and polarisation-maintaining operation [2,3]. In solid-state lasers a very small cavity geometry can be confined to the laser crystal itself allowing single frequency selection to occur naturally [4]. The VECSEL is a unique combination of both diode and solid-state lasers. The external cavity length is flexible with possible cavity sizes from microns to meters [5,6]. With optical pumping high multi-watt output powers can be generated and with intra-cavity elements single frequency operation can be achieved. This makes the VECSEL an ideal source for small cavity applications. This chapter demonstrates a single frequency VECSEL with 6mm cavity length, which incorporates a novel air etalon.

6.2 THEORETICAL DESIGN

A small laser cavity length inherently benefits single mode selection. The small cavity length increases the longitudinal mode spacing, which means fewer modes exist in the cavity. As in previous experiments where a combination of a BRF and an etalon are used to select a single mode, a small cavity length can assist the mode selection of the laser and only a single element is needed to initiate single mode operation. To form a small VECSEL cavity a single concave mirror could be used at normal incidence. The focal length of this mirror can be chosen to provide a desirable cavity mode size on the VECSEL surface and adequate room for an intra-cavity etalon. However as mentioned in chapter 3, tilting an etalon with respect to a small cavity mode size can produce significant losses that limit the laser tunability.

A small VECSEL cavity can be formed using a convex mirror in reverse. This creates a cavity formed from the substrate of the mirror. Leaving a small space between the mirror rear surface and the VECSEL wafer creates a variable air-gap that can be utilised as an etalon. The laser can then be tuned be altering the air gap, which eliminates the walk off experienced by a normal solid etalon. Figure (6.2.1) shows this cavity design.

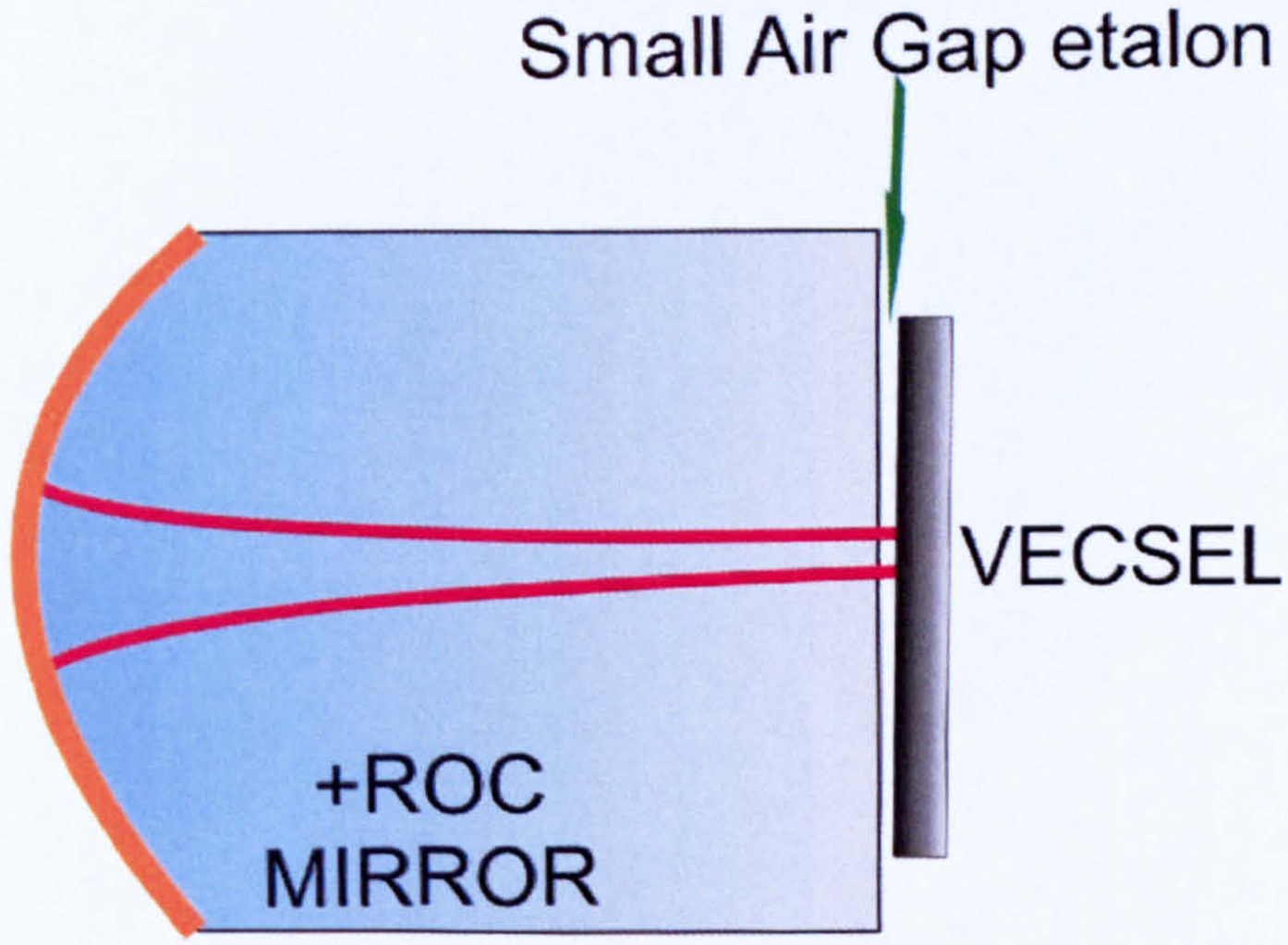

Figure (6.2.1): Micro-cavity VECSEL design

The air gap can be increased or decreased to change the FSR of the etalon respectively, to allow different modes to be selected from the laser cavity. A Brewster cut can be made in the mirror substrate, which allows for finite changes in cavity length, allowing finer tuning of the available modes. This can be seen in figure (6.2.2).

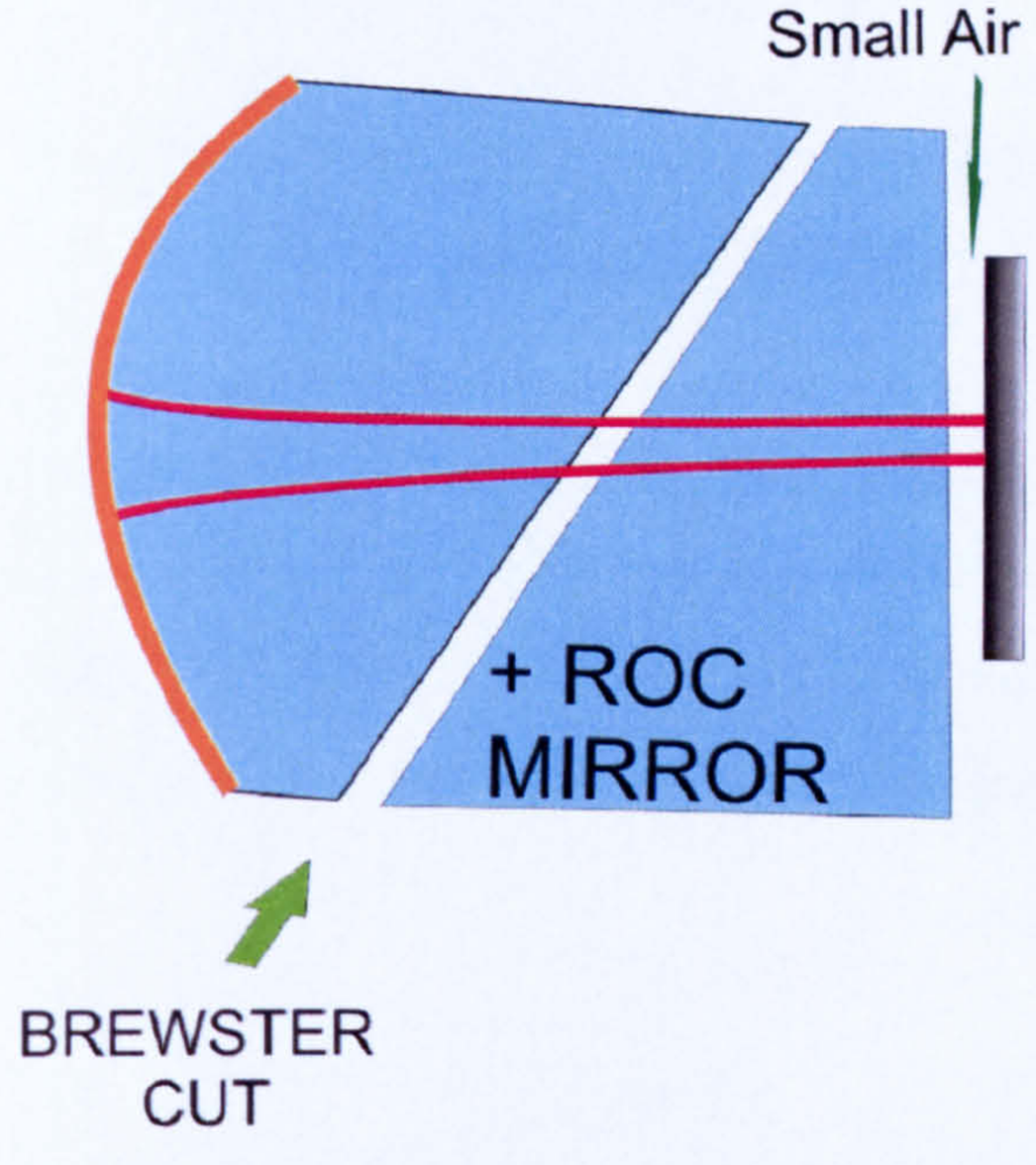

Figure (6.2.2): Fine tuning micro-cavity design

The Brewster cut space additionally provides a strong linear polarisation of the laser output. To confirm this hypothesis, mathematical simulations were run to analyse the mode selection present in a passive cavity. At each interface in the cavity Fresnel equations can be used to represent the reflections that occur at all interfaces. Figure (6.2.3) shows the relevant reflections at each of the key interfaces.

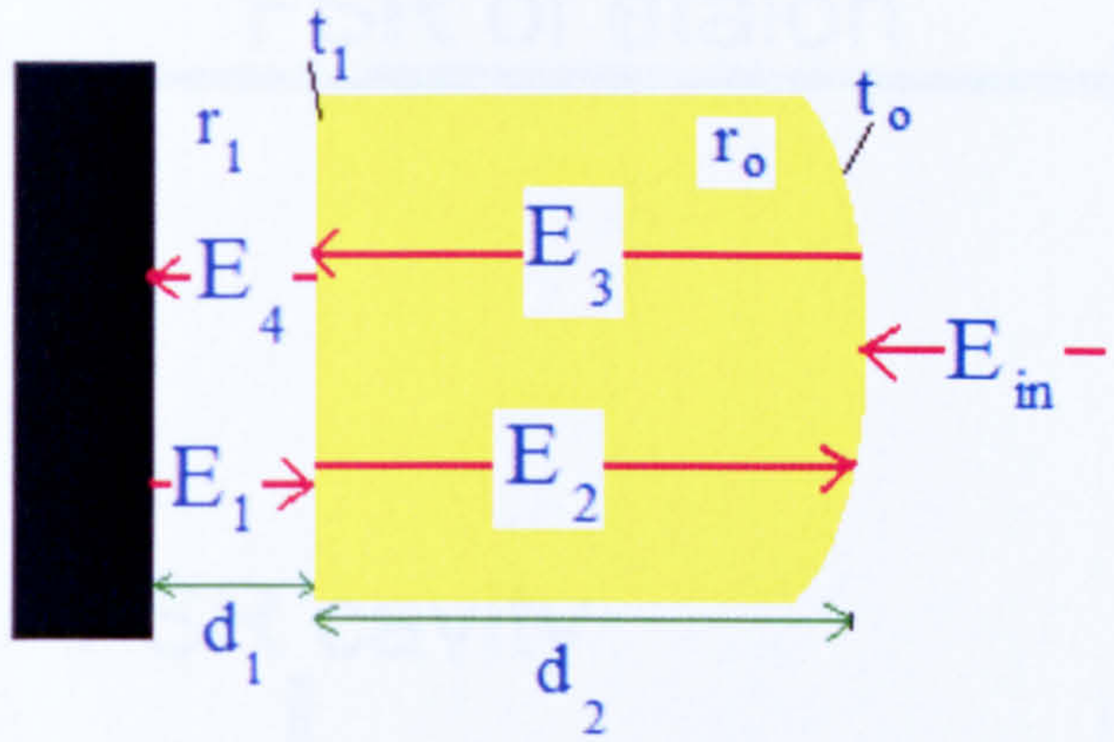

Figure (6.2.3): Theoretical model of micro-cavity (figure 6.2.2) showing dominant Fresnel reflections.

As seen in figure (6.2.3), an electric field E_{in} is injected into the cavity where it experiences losses due to the transmission (t_0) at the mirrors interface. The electric field can be represented at any point in the cavity by the relevant sum of the Fresnel reflection and transmissions. The four equations produced from these reflections are shown below.

$$E_1 = E_4\, e^{ikd_1} \qquad \text{equ:(6.2.1)}$$

$$E_2 = tE_1e^{ikd_1} - rE_3e^{ikd_2} \qquad \text{equ:(6.2.2)}$$

$$E_3 = -r_oE_2e^{ikd_2} + t_oE_{in} \qquad \text{equ:(6.2.3)}$$

$$E_4 = tE_3e^{ikd_2} + rE_1e^{ikd_1} \qquad \text{equ:(6.2.4)}$$

Solving these 4 equations for E_1-E_4, produces the following results which can be plotted out to show the allowed laser cavity modes.

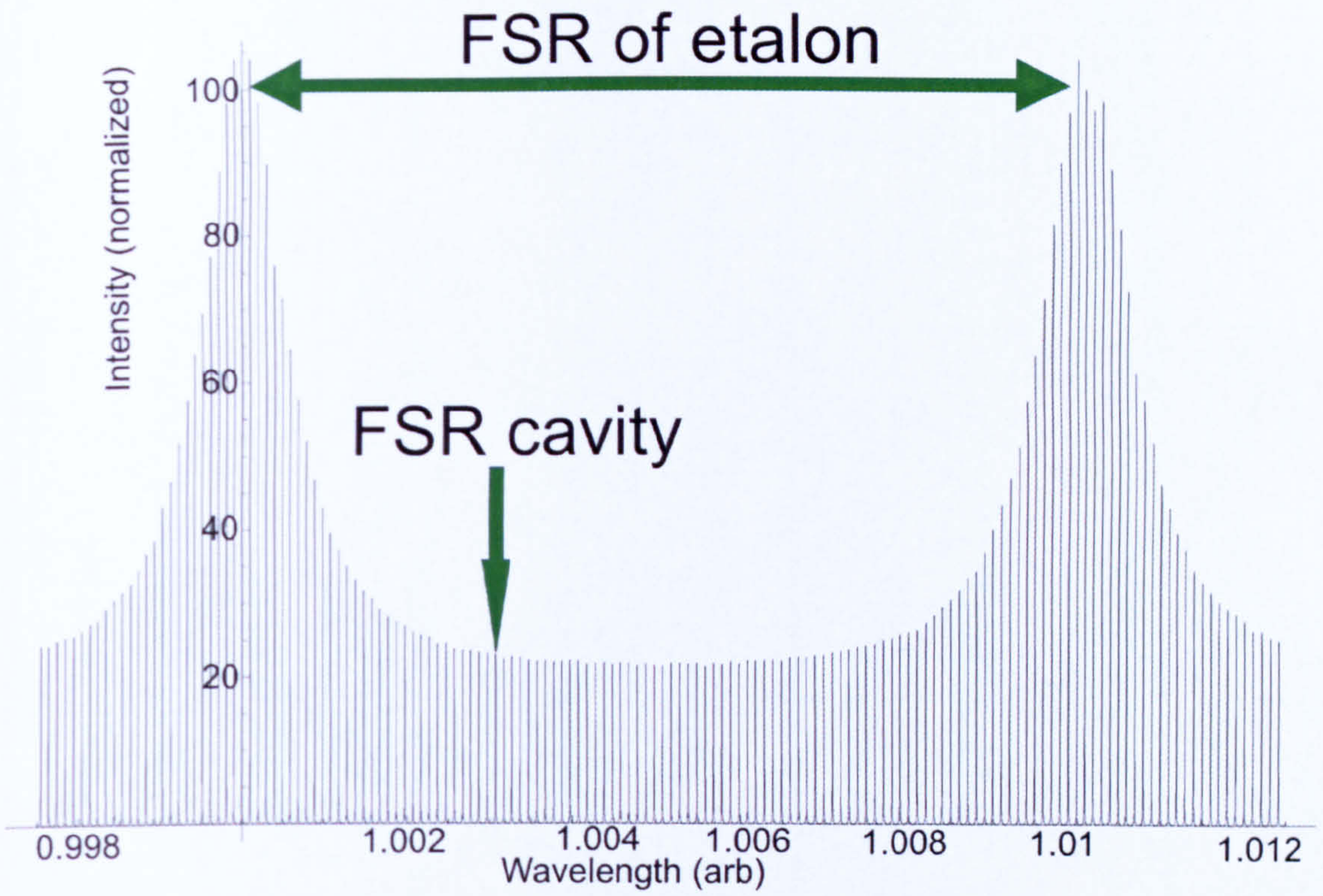

Figure (6.2.4): Mathematical modelling of micro-cavity laser modes

The figure (6.2.4) shows the allowed cavity modes within one free spectral range of the air-gap etalon. The small lines within this show the cavity modes that can be selected by altering the finite air-gap, which increases the overall length of the laser cavity. This can be seen in more detail in figure (6.2.5).

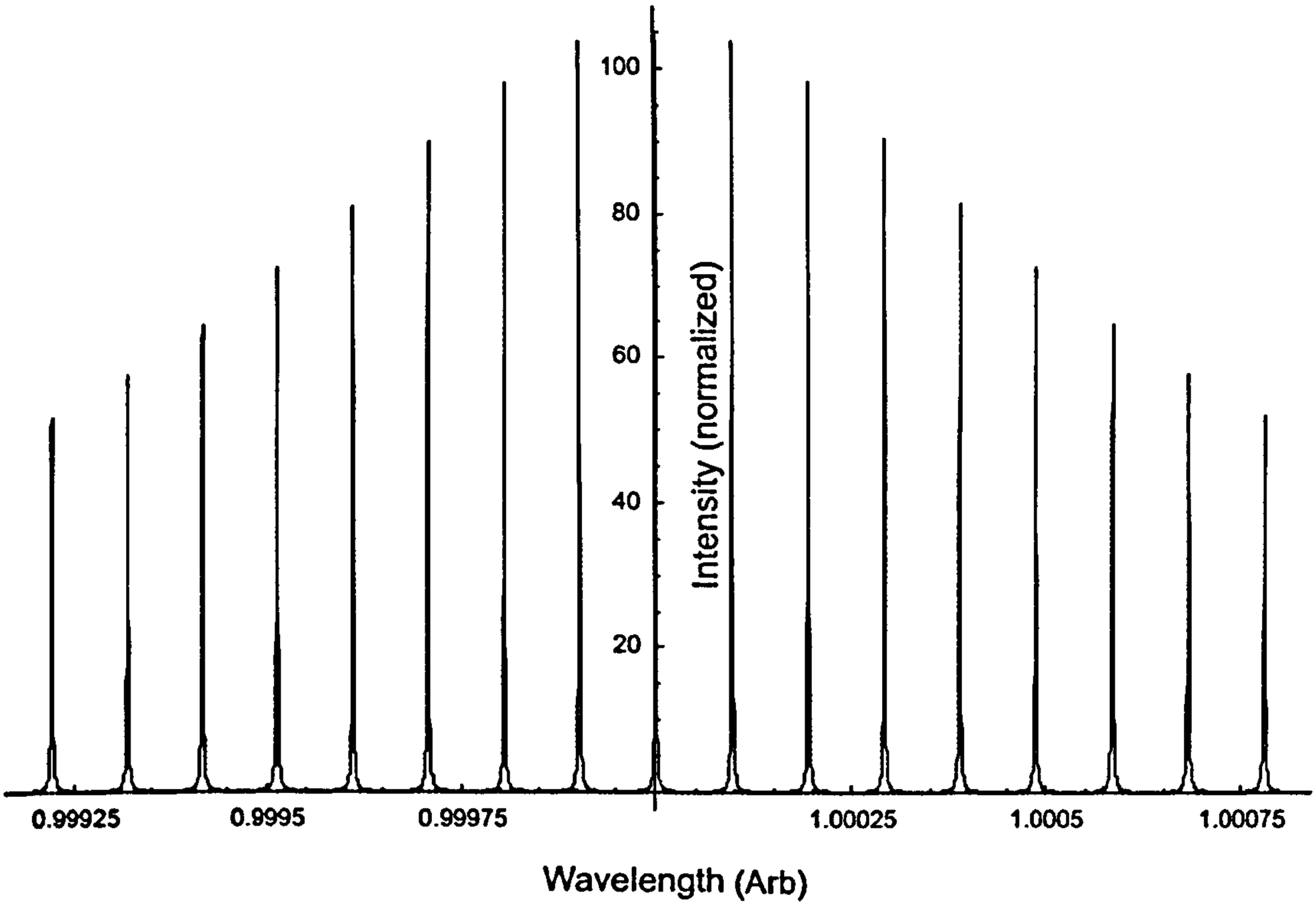

Figure (6.2.5): Zoomed in view of laser cavity modes of micro-cavity

From the above image it is clear to see the available cavity modes that will be generated in the micro-cavity. This confirmed the intuitive model of using the air gap as an etalon for smooth tuning of the laser frequency.

6.3 CAVITY AND PUMP DESIGN

The cavity design involved a 12.5mm positive radius of curvature mirror with 98% reflectivity coating at 970nm and AR coating at 808nm. Used in reverse this formed a cavity with length 6.25mm, using the glass substrate of the mirror for the bulk of the cavity medium. A small air gap was then left to act as the etalon.

The cavity design relies on the air-gap between the wafer and mirror surfaces. As in a standard VECSEL cavity where a diamond heat spreader would be used to control thermal effects, the micro cavity must rely on cooling from the rear surface of the

VECSEL. The use of diamond heat spreader in the cavity would hinder the tuning capability of the laser as it forms its own sub-cavity. This sub-cavity formed within the diamond interferes with the selecting mechanism of the air gap etalon, effectively creating a thick etalon with a small ineffective FSR. In replacement of the diamond heat spreader a TEC is used to cool the VECSEL wafer to a low temperature. This, although not as efficient as the diamond heat spreader, provides adequate thermal management for low power operation. Figure (6.3.1) shows the theoretical design.

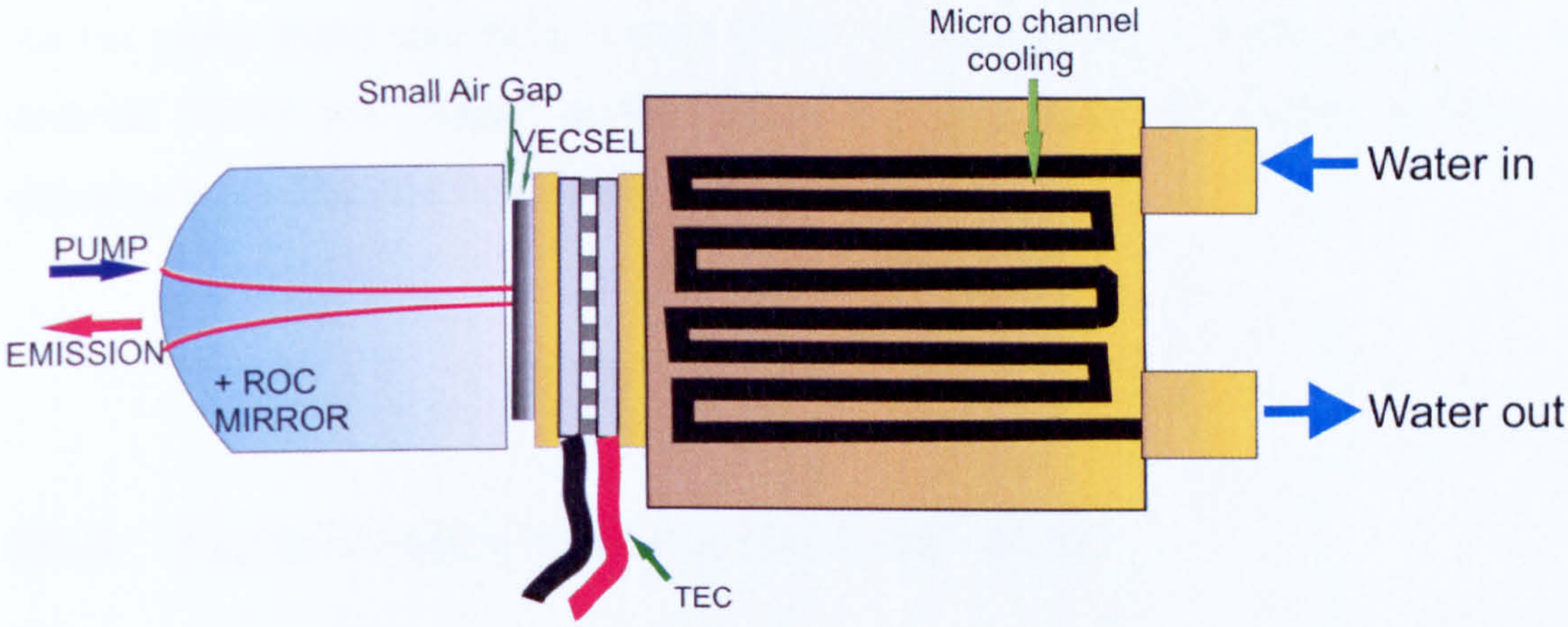

Figure (6.3.1): Micro cavity laser with TEC cooling

A specially designed pump system was required for this laser. A long focus is required to propagate through the cavity mirror to reach the VESCEL. As this curved mirror would alter the focusing of the pump beam calculations were made incorporating the cavity mirror into the pump system to generate an 80μm spot diameter at the wafer's surface. Figure (6.3.2) shows the pump geometry.

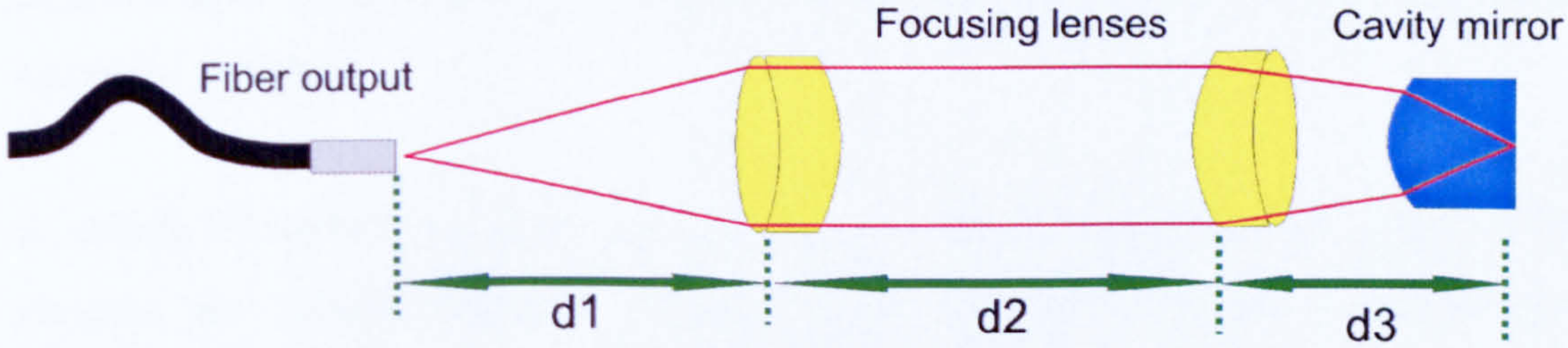

Figure (6.3.2): Optical pump system incorporating cavity mirror

Using mathematical software [7], matrix calculations were made to determine the necessary distances required between optics to produce an 80μm diameter spot at the focal point. Two 25mm focal length achromatic doublet lenses were used to produce a high quality focused beam, as seen in the previous chapter, figure (5.2.2). The corresponding calculated distances are shown below.

$$d_1 = 26.75\text{mm}, \; d_2 = 40\text{mm}, \; d_3 = 18\text{mm}$$

As the pump beam and laser output from the micro-cavity overlap each other a dichroic mirror was placed at 45° inside the pump optics to direct the 980nm emission away from the laser to monitor the laser output.

6.4 ALIGNMENT AND MOUNTING

Initial alignment of the laser cavity proved to be very difficult. Due to the laser's size only minor adjustments could be made to the cavity to induce lasing. Due to no optical heat spreader being used, the thermal rollover point of the laser was particularly low. This limits the pump power thus the fluorescence levels are low. This made it difficult to see any photo luminescent enhancement of the laser cavity. Another contributing factor to difficult alignment was the size of the laser cavity itself. Being a very small cavity (6mm) and made of glass it was impossible to use standard intra-cavity techniques to align the cavity. Therefore an external approach had to be designed.

A variety of techniques were used to try and align the laser cavity, using CCD cameras and various alignment lasers. These methods produced no significant enhancement of the laser cavity. The solution was to wind the cavity out till sufficient space was acquired to optically pump the VECSEL from a side angle. This produced an increase in sensitivity as there was no reflection from additional optics in the pump system. Once lasing was achieved the pump systems were

swapped back to normal incident pumping. By scanning the new pump system across the VECSEL surface, cavity enhancement could now be detected when approaching the original pump spot and lasing could easily be achieved. The cavity could now be shortened while maintaining lasing to reach the desired length. Figure (6.4.1) shows a photo of the experimental laser setup in operation.

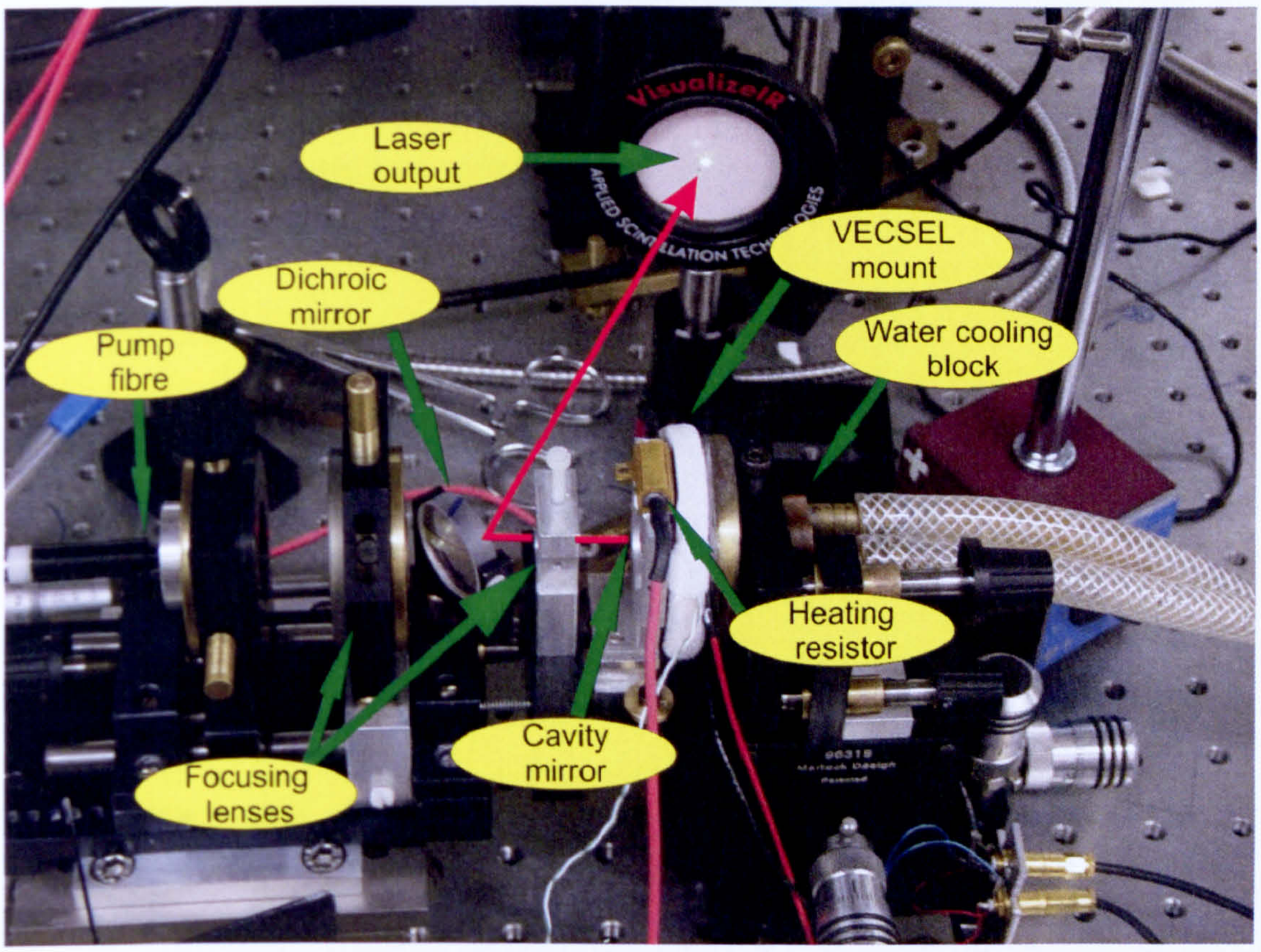

Figure (6.4.1): Photo of micro-cavity laser setup showing ice build up on VECSEL heat sink

The VECSEL was mounted on a brass plate using silver conductive paint. This was thermally contacted to a TEC using a heat sink compound, which in turn was then chilled by a water-cooling copper mount. The TEC provided effective cooling to -20°C. Ice crystals formed on the brass plate as a result of the low temperature. For fine adjustment the cavity mirror and VECSEL were mounted onto an adapted fibre alignment mount. This mount was adapted to provide 3-dimensional movements with sub micron adjustment with the aid of piezo-electric tubes imbedded inside the mount. This gave fine control of the air gap etalon to allow for minor adjustments

and tuning. Due to the micron sized air gap between the optics, condensation on the cavity mirror was prevented using a 100Ω thermal resistor to provide heating.

6.5 Experimental results

Lasing was achieved with a maximum output of 19.4mW single frequency at 965nm. Using the piezo-electric mount the air gap was increased to tune the cavity. These results can be seen in figure (6.5.1) below.

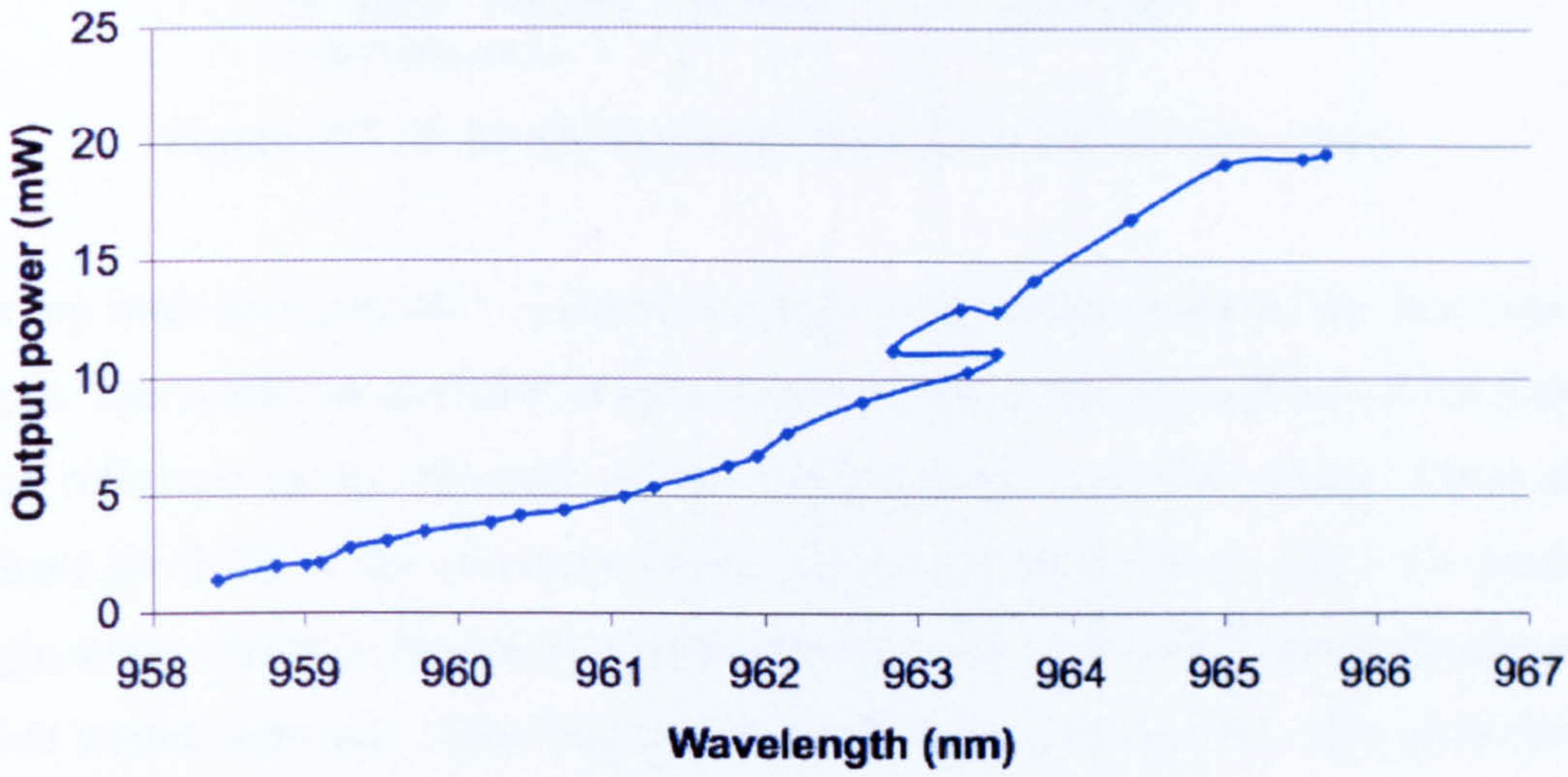

Figure (6.5.1): Tuning of single frequency micro cavity

As seen in figure (6.5.1), the tuning range extends for 7nm. The sudden drop off at the end of the tuning range is where the laser frequency returns to previous frequencies, indicating the end of the tuning range. The spectral deviation around 963nm was an unexpected yet repeatable result that may have been caused by vibrational effects from the water-cooling mount or a mechanical error when tuning the cavity length.

The output was analysed using a Fabry Perot reference cavity to check the spectral characteristics. Figure (6.5.2) shows the output obtained.

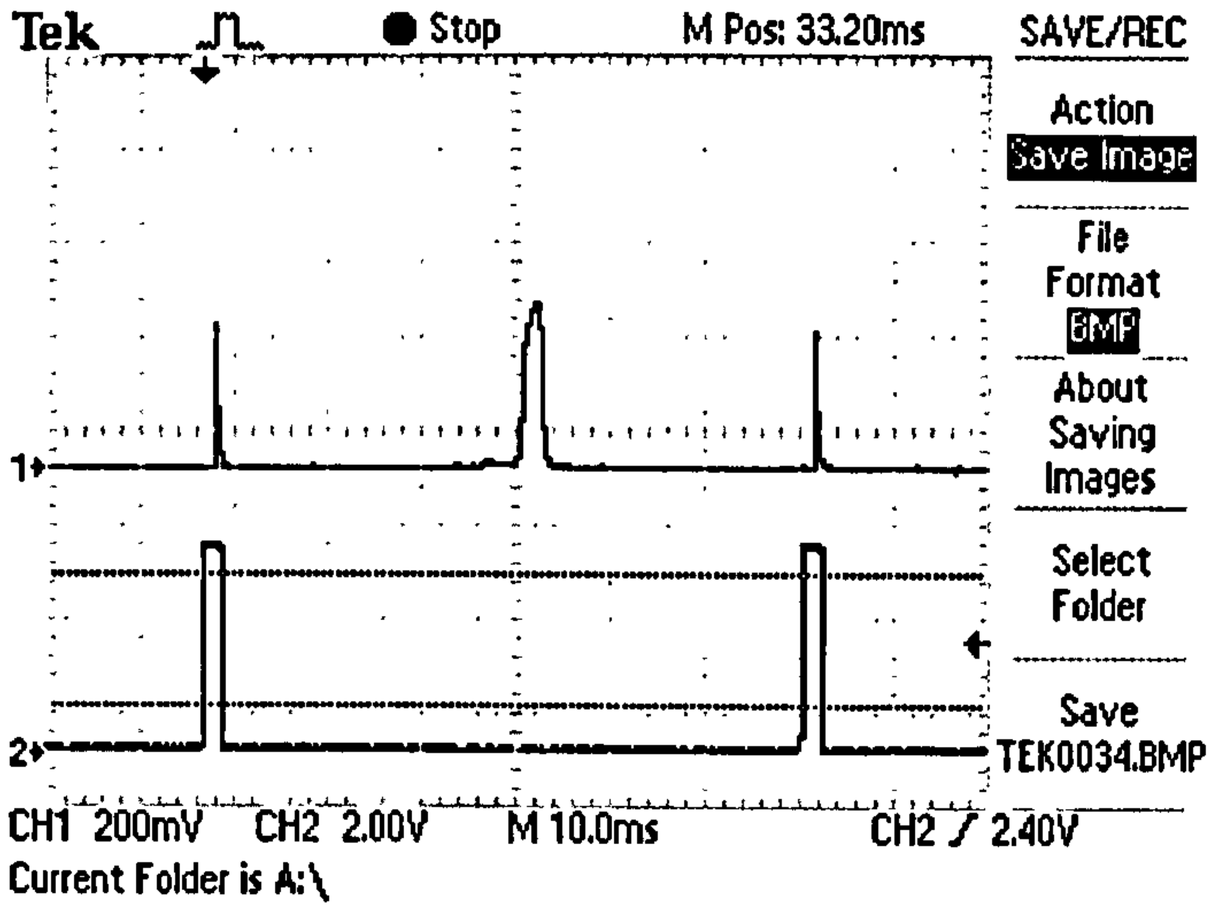

Figure (6.5.2): Single frequency trace from Fabry Perot cavity

The top trace in figure (6.5.2) shows a single longitudinal mode of the laser cavity output. The smaller peaks with steeper slopes represent the fluctuations of the Fabry-perot reference cavity fly-back as the piezo-electric controller scans. These also indicate the FSR of the reference cavity as seen in the bottom trace. To confirm single mode operation the cavity output was analysed with an RF spectrum analyser, which would show any transverse modes oscillating in the cavity. The presence of no additional transverse modes detected confirmed this result.

A standard solid etalon uses identical surface reflectivites to provide strong interference filtering of the available modes in a laser. In the micro-cavity the flat surface of the cavity mirror and capping layer incorporated in the VECSEL wafer are used to re-create this effect. Due to unequal reflectivites, the etalon effect is less dominant and therefore single mode operation was unsustainable for a long period of time. With a surface reflectivity of around 4%, the flat surface of the cavity mirror was primarily responsible. In further experimentation on this laser an appropriate reflective coating could be applied to this surface to match the slightly higher reflectivity of the capping layer. This would produce a stronger filtering effect and produce a more stable output.

To simulate an equal reflectance, a glass plate was added inside the air gap. This having equal reflectance as the flat surface of the cavity mirror due to being comprised of the same material. The insertion of this glass plate adds a further sub-cavity into the laser, this can be seen below in figure (6.5.3).

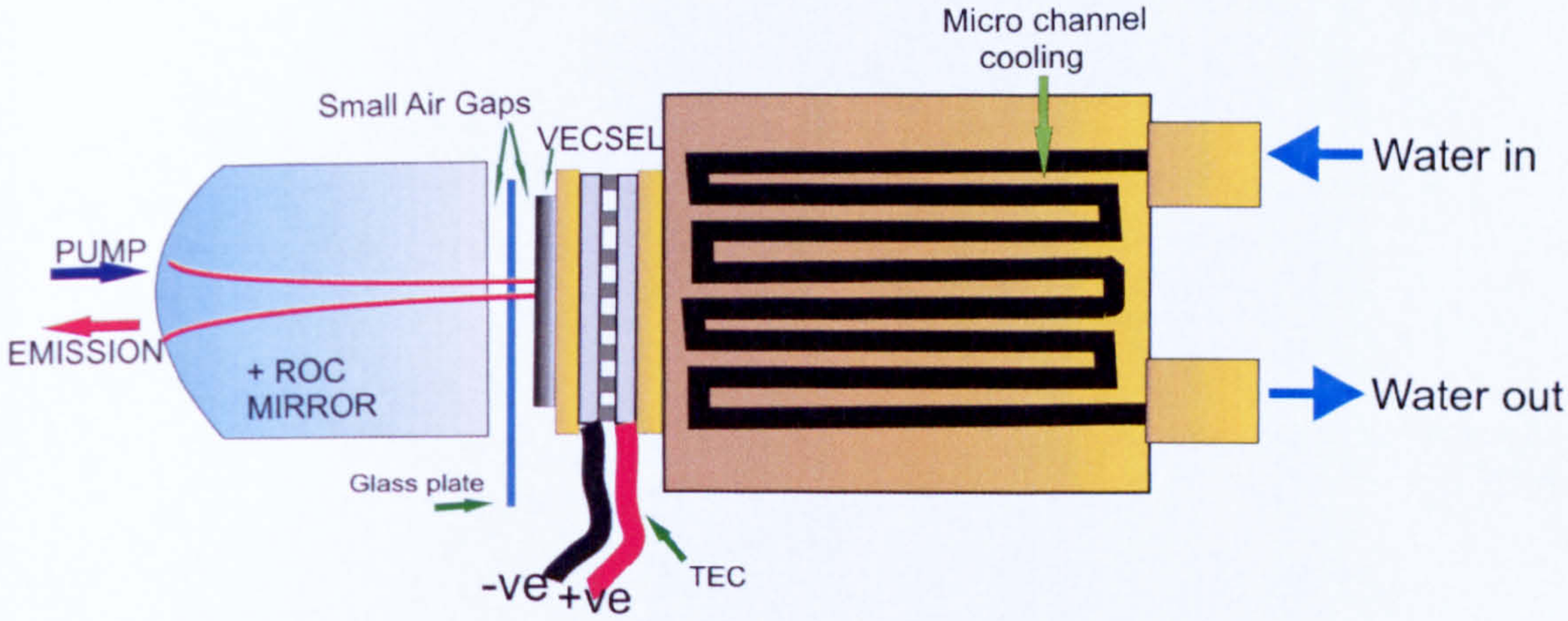

Figure (6.5.3): Micro cavity including glass plate

To analyse the mode selection of this laser with the new sub-cavities, further mathematical modelling was undertaken. Using the Fresnel reflection for each surface interaction as in the previous section 6.2. Several scenarios of air gaps can be modelled, one of which is shown in figure (6.5.4).

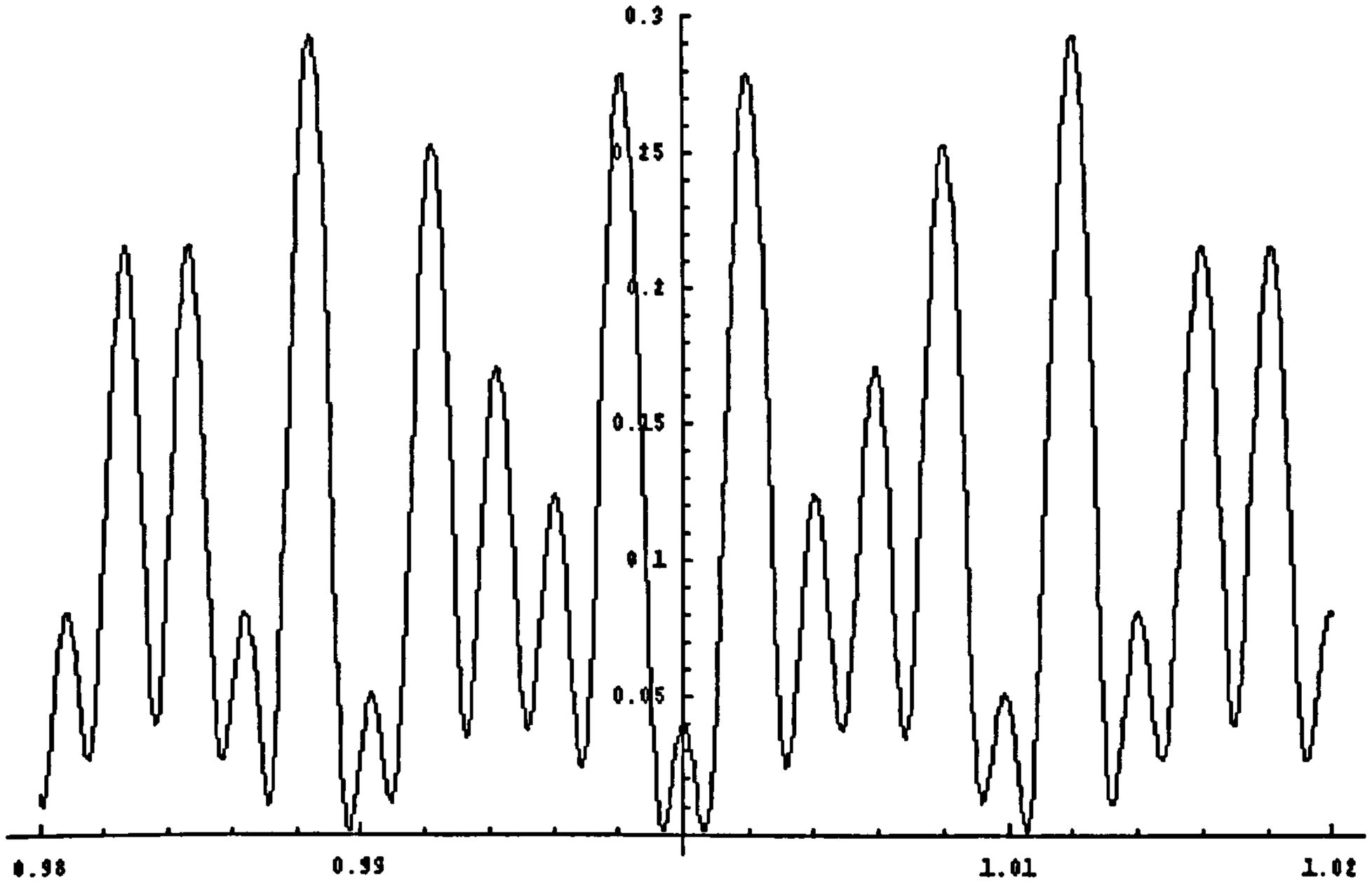

Figure (6.5.4): Mode selectivity from glass plate micro-cavity

The figure shows 2 modes, which will occur simultaneously. This can be seen at the (1,0) coordinates of figure (6.5.4). This indicates that the 3 sub-cavities will produce multimode action from the laser. To confirm this experimentally a glass plate was inserted on a piezo-electric controlled mount as seen in figure (6.5.3).

Lasing was achieved and multimode action was confirmed using a Fabry Perot reference cavity. Single mode operation was achieved with slight adjustments to the cavity although this was very unstable. Figure (6.5.5) shows the tuning results.

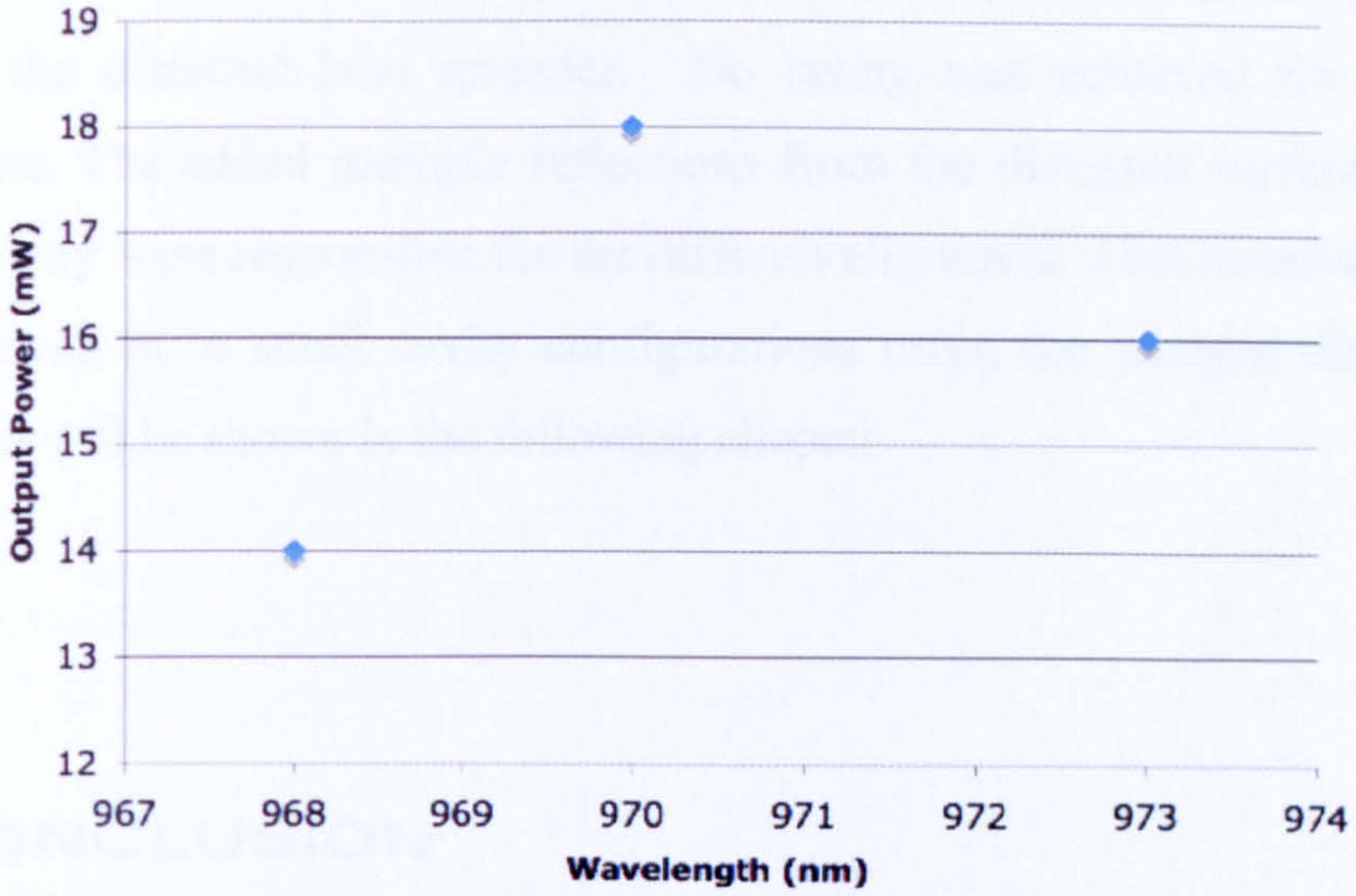

Figure (6.5.5): Tuning curve from glass plate micro-cavity

As seen in the above figure only 3 tuning points could be obtained from this cavity. The 3nm jumps correspond to the FSR of the glass plate.

To further this investigation and to increase the output power of this small cavity geometry, Wedged diamond was used as an optical heat spreader. The wedged diamond uses a 2^{o} wedge to eliminate the etalon effect created from the diamond sub-cavity [8]. Figure (6.5.6) shows the experimental setup.

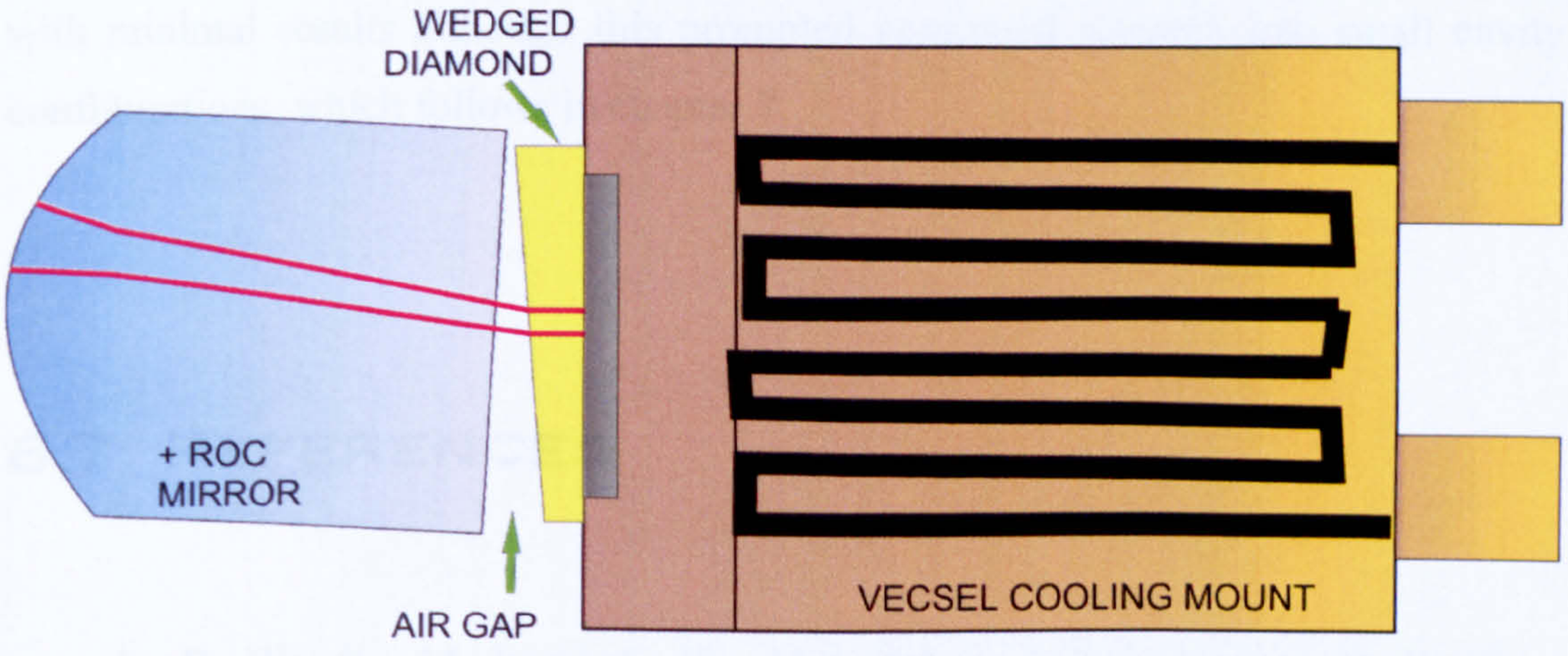

Figure (6.5.6): Wedged diamond micro-cavity VECSEL

An intra-cavity etalon is created between the flat surface of the mirror and the rear surface of the diamond heat spreader. No lasing was achieved for this cavity configuration. The added multiple reflections from the diamond surfaces and tight cavity geometry were responsible for the difficult alignment. This however prompted further research in to small cavity configurations using the wedged diamond heat spreader that will be shown in the following chapter

6.6 Conclusion

Single frequency operation of the micro-cavity was shown over a 7nm tuning range with a maximum output power of 19.4mW obtained. This was limited due to thermal rollover of the VECSEL wafer.

The addition of a glass plate inside the air-gap to promote a stronger etalon response produced a less tunable and unstable micro-cavity VECSEL. Only 3 single frequency mode could be selected from this cavity due to the large FSR of the glass plate hindering the tuning characteristics of the VECSEL.

Further investigation into utilising a wedged diamond heat spreader was undertaken with minimal results although this prompted continued research into small cavity configurations, which follows in chapter 7.

6.7 References

1. D. Wandt , M. Laschek, F. Alvensleben, A Tunnermann, H. Welling. "Continuously tunable 0.5W single frequency diode laser source". Optics Comm. **148**, 4, 261, (1998).

2. A. Schülzgen, L. Li, V. L. Temyanko, S. Suzuki, J. V. Moloney, and N. Peyghambarian. "Single-frequency fiber oscillator with watt-level output power using photonic crystal phosphate glass fiber". Optics Express, **14**, 16, (2006).

3. F. McNeillie and E. Riis. "Highly polarized photonic crystal fiber laser". Optics Express, **12**, 17, (2004).

4. T. J. Kane and R. L. Byer, "Monolithic, unidirectional single-mode Nd:YAG ring laser", Optics Letters, **10**, 2, (1985).

5. J. E. Hastie, L. G. Morton, S. Calvez, and M. D. Dawson, "Red microchip VECSEL array" Optics Express, **13**, 18, (2005).

6. W. Zhang, T. Ackemann, M. Schmid, N. Langford, A. I. Ferguson, " Femtosecond synchronously mode-locked vertical-external cavity surface-emitting laser", Optics Express, **14**, 5, (2006).

7. Mathmatica version 4.1

8. R.H. Abram, K.S. Gardner, E. Riis, and A.I. Ferguson, "Narrow linewidth of a tunable optically pumped semiconductor laser", Optics Express, **12**, p5434, (2004).

CHAPTER SEVEN

SMALL-CAVITY VECSEL

7.1 INTRODUCTION

Compact lasers are desirable tools for many applications but the smaller you make a laser the more intricate the design and optics become. This can be costly and very difficult to manufacture. This chapter explores the use of small cavity geometry in a single frequency VECSEL laser. The cavity design is made just large enough to insert standard intra-cavity components for single frequency operation. The use of a wedge diamond heat spreader allows high power operation with no effects to intra-cavity elements allowing single frequency operation to be implemented [1].

7.2 LASER DESIGN

The laser cavity was designed to be as small as possible but to allow the insertion of a BRF and a solid etalon. For adequate space for these elements a 50mm cavity was constructed from a previous laser mono-block. A laser mono-block, being made from a single machined block of aluminium, has the advantage of providing a very stable cavity as the mechanical drift and vibration of the mounts are minimised. Figure (7.2.1) shows a schematic representation of this block.

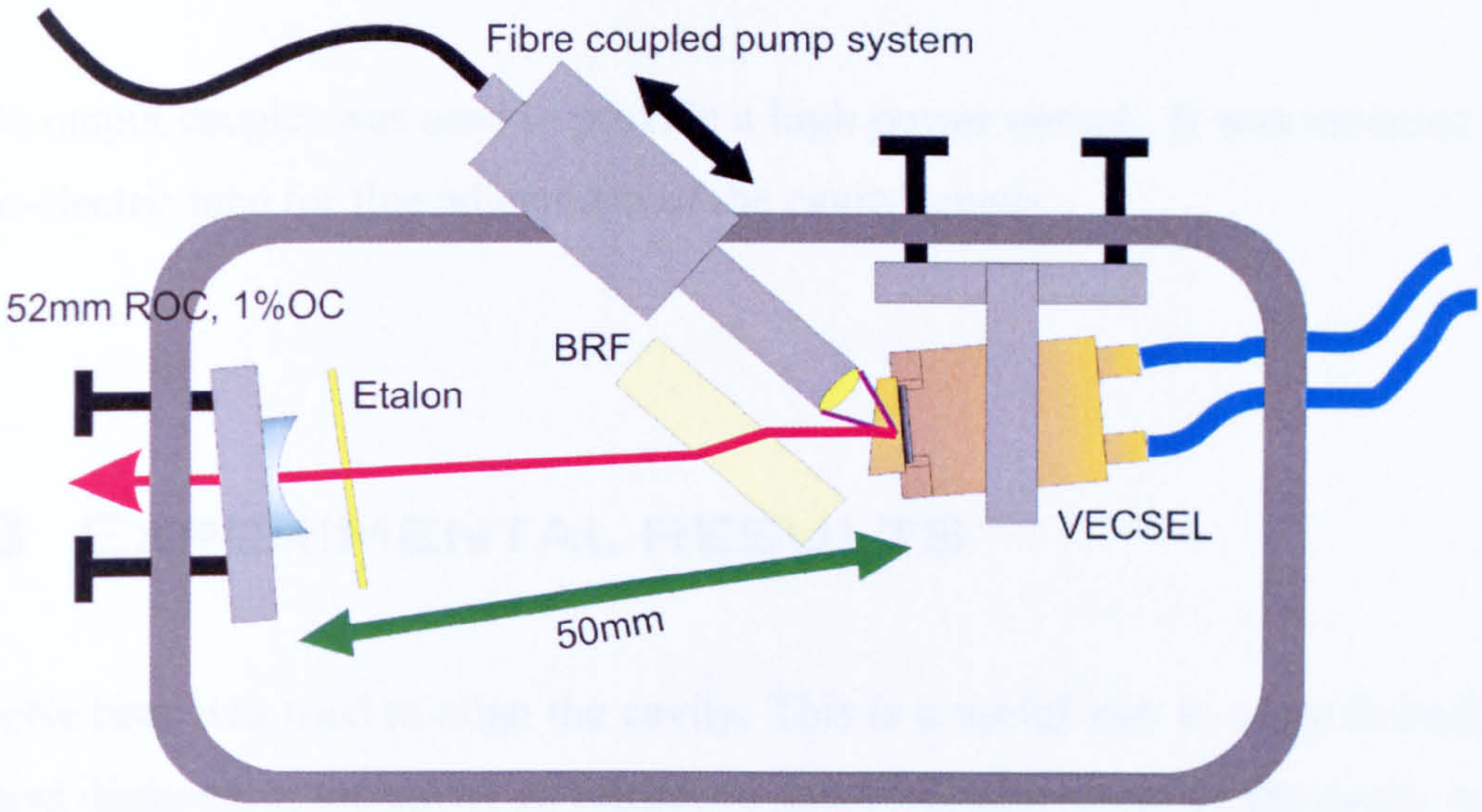

Figure (7.2.1): laser mono-block schematic

Using this mono-block intra cavity elements could then be inserted from the top of the block where they could be securely fixed. Adapted mounts were constructed to minimise their space and provide delicate tuning of the intra-cavity elements. Figure (7.2.2) shows an image of the finished laser cavity mono-block.

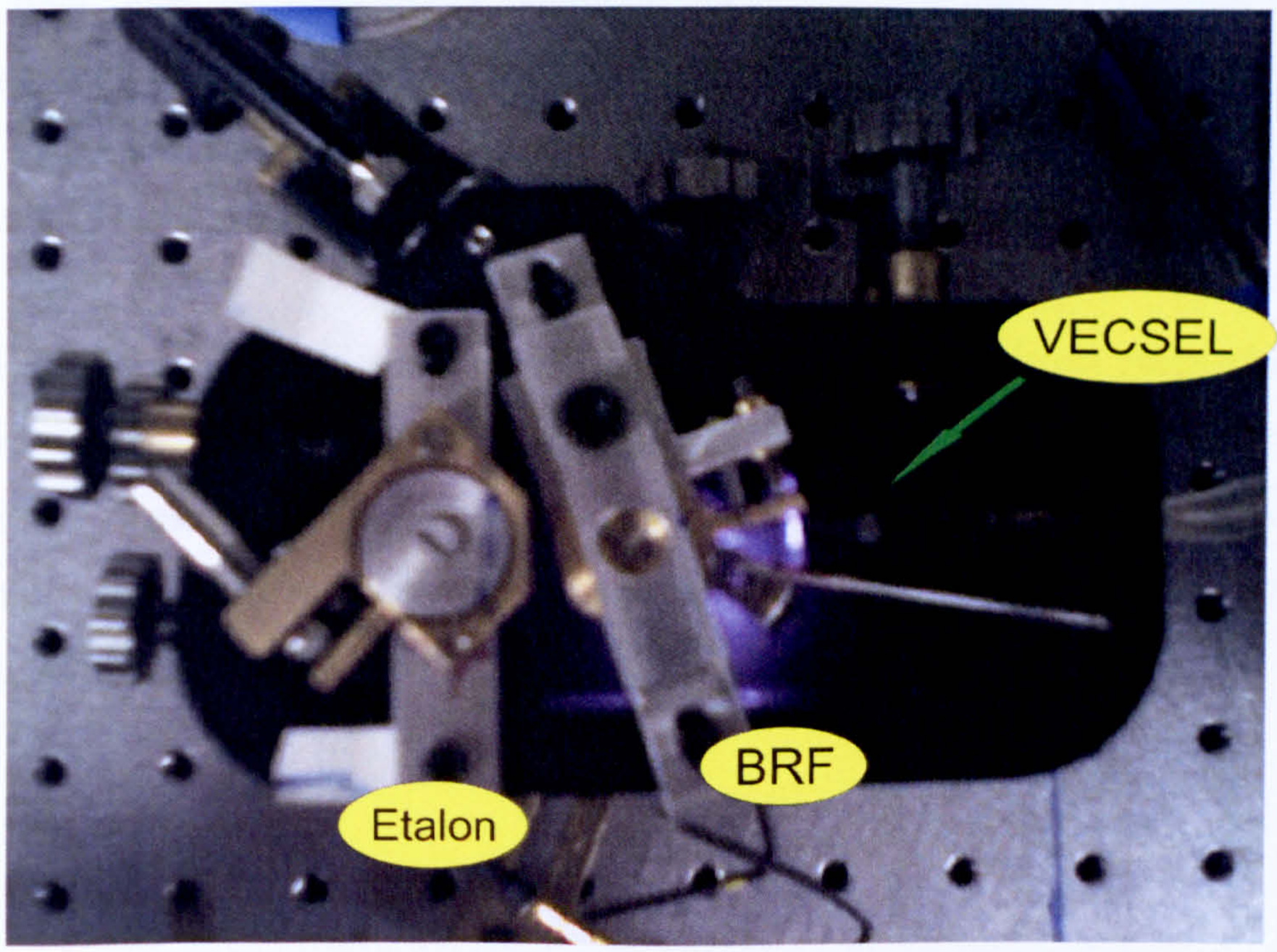

Figure (7.2.2): laser mono-block

A 2% output coupler was used to provide a high power output. It was mounted on a piezo-electric tube for fine adjustment of the cavity length.

7.3 Experimental results

A HeNe laser was used to align the cavity. This is a useful way to align through the wedged diamond in the cavity as refraction causes displacement of the cavity beam. Lasing was achieved with a maximum output power of 1.1W at 3.2W pump power, before thermal rollover occurred. The insertion of the BRF reduced the output power to a maximum of 700mW. Similarly the insertion of the etalon also reduced this maximum power to 400mW. This corresponds to a total power loss of 64%. In a standard "dog leg" (figure 5.4.3) VECSEL cavity intra-cavity elements are inserted into the long arm of the laser cavity. In this area of the cavity the wave-front of the laser beam are almost flat making insertion easy and low loss. Typically a 25% loss is experienced with the insertion of a BRF and similarly with a solid etalon giving a 48% total loss of intra-cavity elements [1]. In the small 2-mirror cavity configuration the insertion of intra-cavity elements is much harder, due to the curved wave fronts and refraction from the Brewster angled BRF. This corresponds to a greater loss from inserting components as seen by the 64% power loss.

Analysis of the output beam was achieved using a scanning Fabry-Perot reference cavity. Consisting of a confocal arrangement the reference cavity has a FSR of 1GHz and finesse of 1000. The output beam is focused into the reference cavity, which on scanning revealed that single frequency operation had been achieved. This can be seen in figure (7.3.1).

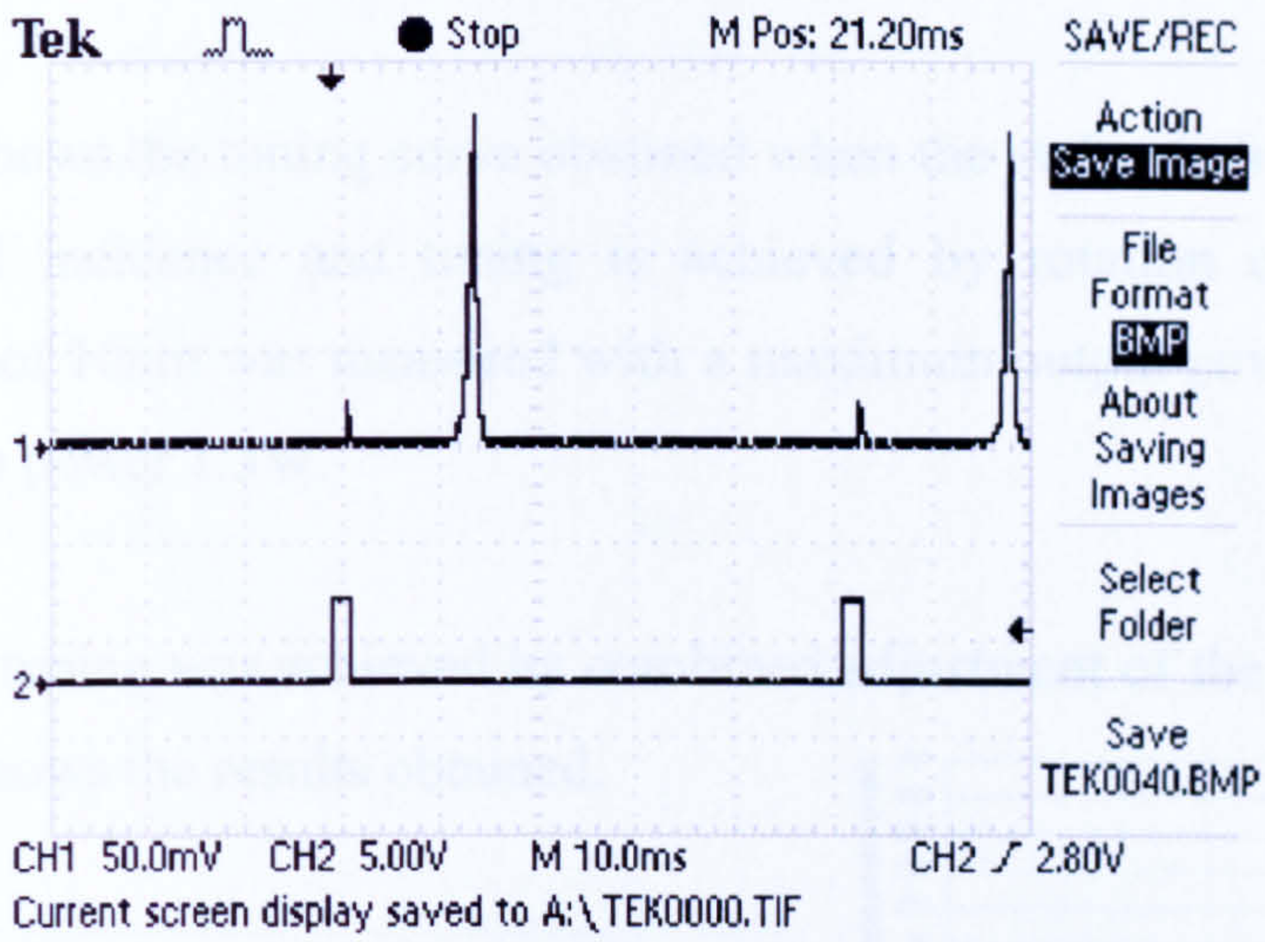

Figure (7.3.1): Single frequency signal from Fabry-Perot reference cavity set for close inspection with a 50MHz scan length.

A close up scan of 50MHz of the single longitudinal mode shows that there are no other modes present, which can be seen in figure (7.3.1). To confirm this, the scan rate was further increased until two subsequent repeating modes were obtained from one scan of the reference cavity. As no other smaller modes are seen between these two progressive modes, the output from the laser is determined to be single mode.

The cavity was now tuned using the BRF to measure the available spectrum. This can be seen in figure (7.3.2).

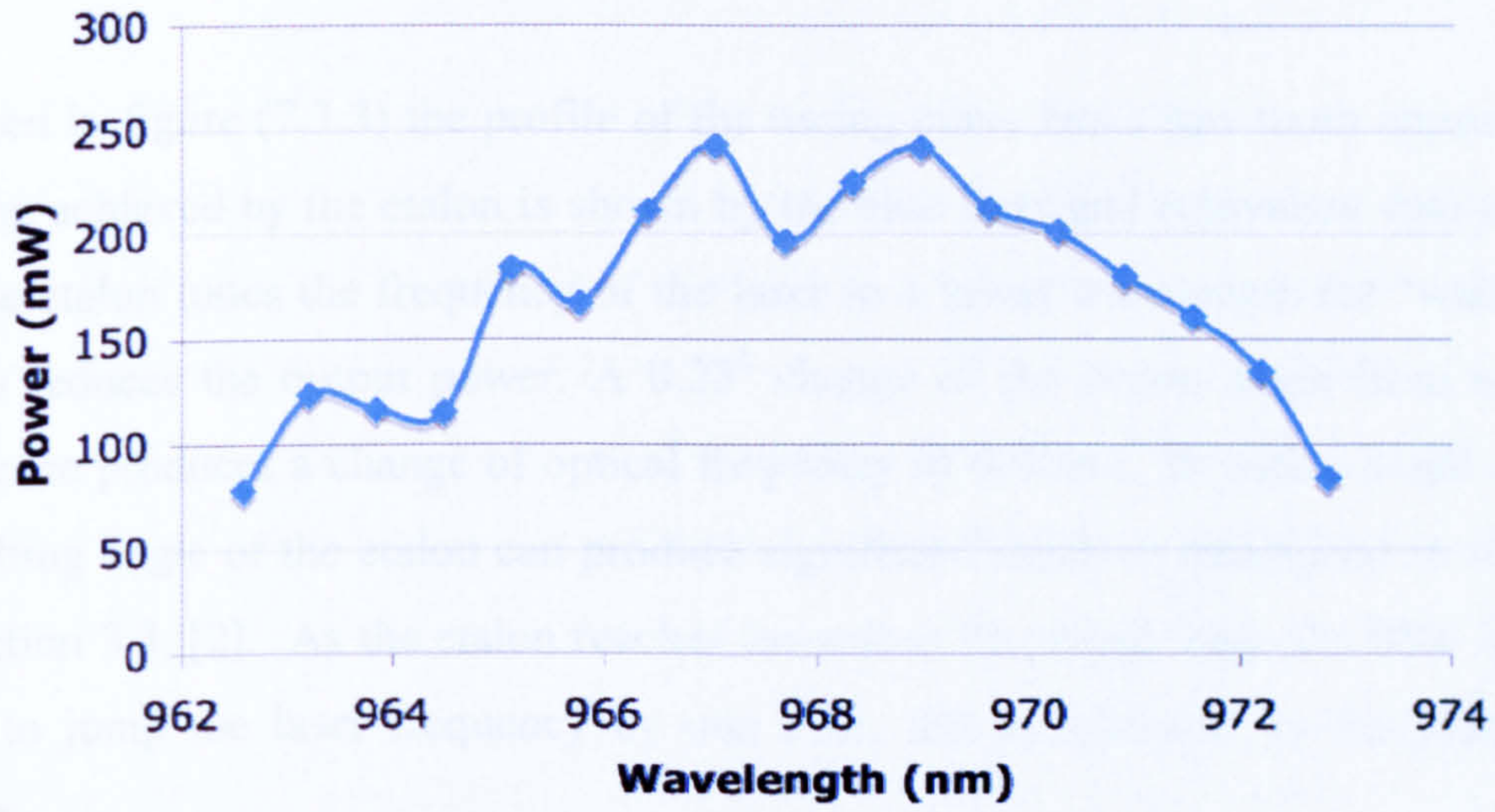

Figure (7.3.2): BRF tuning of small cavity VECSEL

Figure (7.3.2) shows the tuning curve obtained when the etalon is in a fixed position just off normal incidence and tuning is achieved by rotation of the BRF. A maximum span of 10nm was measured with a maximum output power of 242mW at a constant pump power 1.3W.

Additional fine-tuning was achieved by combined adjustment of the etalon and BRF. Figure (7.3.3) shows the results obtained.

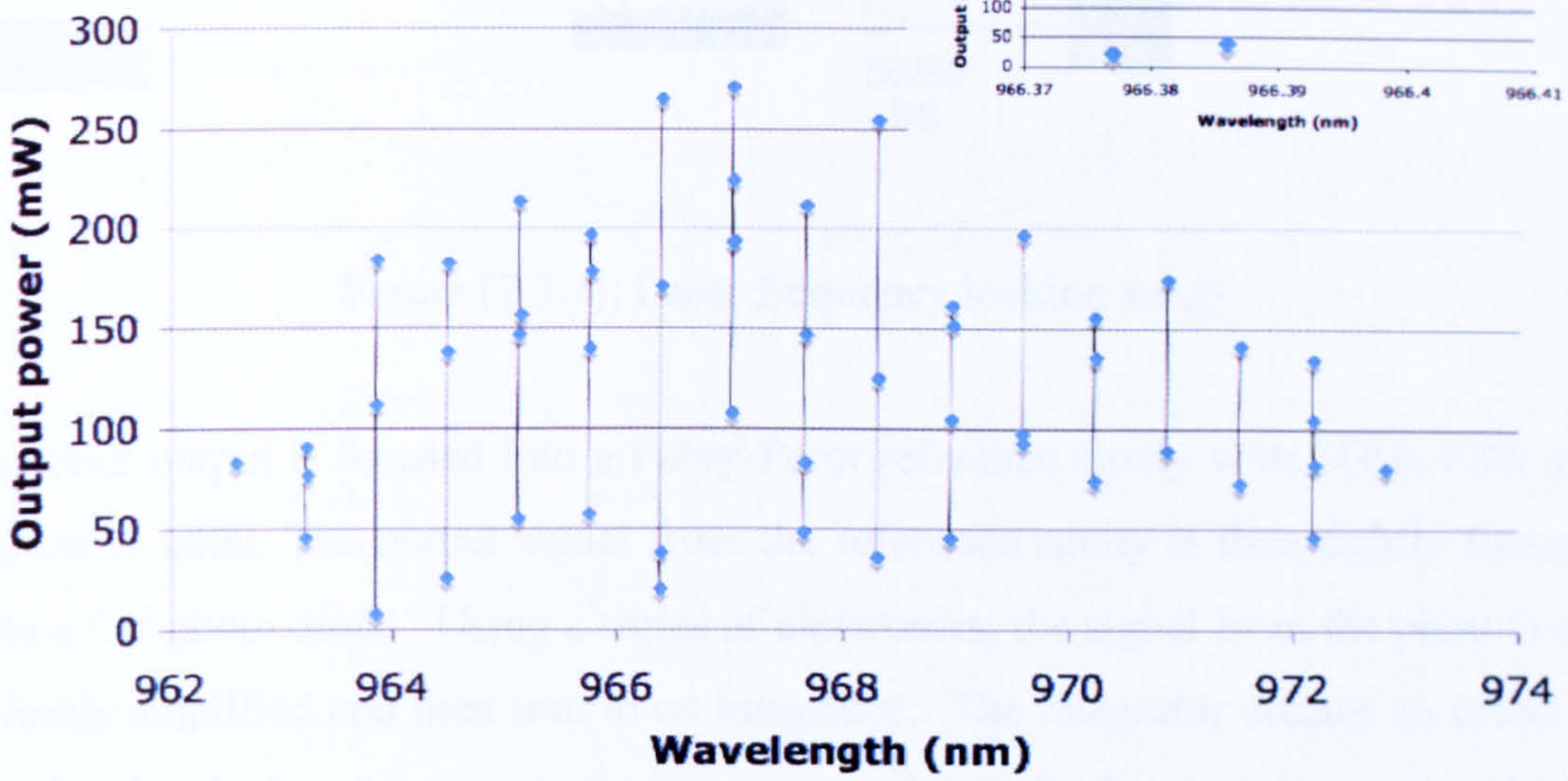

Figure (7.3.3): Tuning of small cavity VECSEL with zoomed in view showing fine-tuning around 966nm.

As seen in figure (7.3.3) the profile of the tuning curve has a saw tooth appearance. Tuning achieved by the etalon is shown by the blue lines and equivalent data points. As the etalon tunes the frequency of the laser to a lower wavelength the "walk off" losses reduces the output power. A 0.23^0 change of the etalon angle from normal incidence produces a change of optical frequency of 0.01nm. In such a small cavity the tilting angle of the etalon can produce significant losses as mentioned in chapter 3, section 3.3, [2]. As the etalon reaches the end of its tuning range the BRF is then used to jump the laser frequency by one FSR, this is indicated by the pink data points.

The laser cavity's resonant frequency was now locked using feedback electronics to the piezo-electric mount on the cavity output coupler. Figure (7.3.4) shows the external cavity setup.

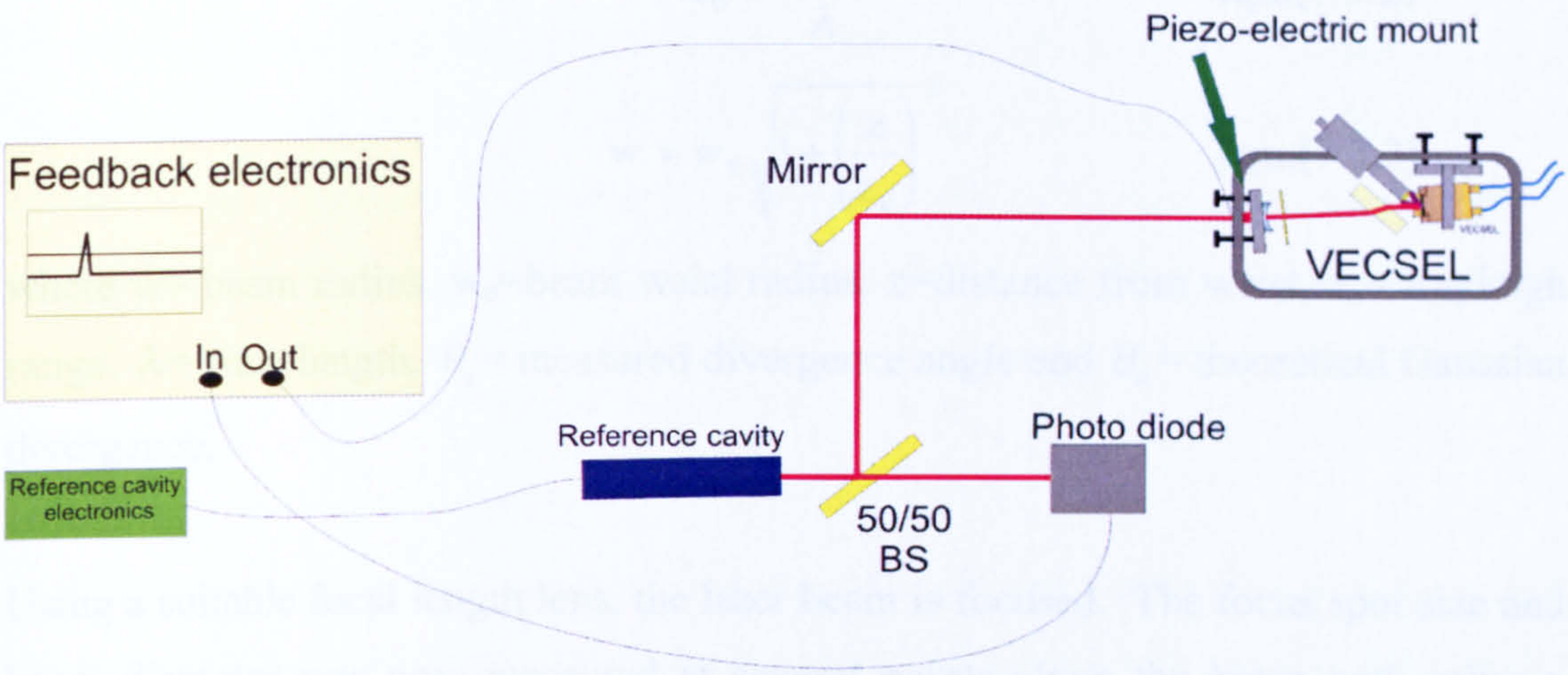

Figure (7.3.4): Laser frequency locking setup

The laser output is focused into a Fabry-Perot reference cavity with 1GHz FSR and finesse of 1000. The output signal from the reference cavity is then tightly focused onto a fast photo diode. Using a series of electronics, the signal from the photodiode is firstly amplified and then sent to an integrator. The integrator creates an offset in the signal, which can be used as a reference point to feedback an error signal to a piezo-electric mount on the output coupler. If the signal deviates from this set point the corresponding error signal is sent to the piezo-electric control, which adjusts the cavity length to compensate, thus the cavity is locked at a single frequency. The error signal was then used to measure the laser's linewidth of 180kHz. Further testing showed that the line width of the laser was limited to this value. It is essential to lock the lasers frequency with rapid movement of the cavity mirror, the faster the response of this mirror the more gain can be applied to the signal, which ultimately provides a stable response to the fluctuations in the laser frequency. As the mirror used in this laser cavity was large and heavy, its response time is slow and limited the linewidth of the laser to 180kHz.

The M^2 of the laser was now measured to determine the mode quality of the beam. The M^2 of the laser is the ratio of the actual beams divergence to that of the theoretical diffraction limited Gaussian fit [3],[4].

$$M^2 = \frac{\theta_e}{\theta_d} \qquad \text{equ:(7.3.1)}$$

$$z_0 = \frac{\pi w_0^2}{\lambda} \qquad \text{equ:(7.3.2)}$$

$$w = w_0 \sqrt{1 + \left(\frac{z}{z_0}\right)^2} \qquad \text{equ:(7.3.3)}$$

where w= beam radius, w_0=beam waist radius, z=distance from waist, z_0= Rayleigh range, λ= wavelength, θ_e= measured divergence angle and θ_d= theoretical Gaussian divergence.

Using a suitable focal length lens, the laser beam is focused. The focus spot size and beam diameter was now measured at several points along the beam path using a Coherent Lasercam 3D. A comparison can now be made between the measured diameters at a set distance from the focal point and the theoretical diameters using equations (7.3.2) and (7.3.3). The difference between these values corresponds to the M^2 of the laser. Using this technique the M^2 of the laser is found to be 1.1. As an ideal TEM_{00} mode is represented by an M^2=1, the laser's M^2 of 1.1 suggests it has a relatively good quality beam. However the difference of 0.1 indicates the possible presence of additional transverse modes in the cavity. This can occur if the pump beam is not correctly matched to the lasers cavity mode.

7.4 PUMP PROFILE ANALYSIS

As a VECSEL is optically pumped, the size and profile of the pump beam can be a crucial factor in the laser's performance. If this beam is too large, it supplies sufficient optical energy to the extremes of the cavity mode, which can allow additional transverse modes to oscillate in the cavity. This hinders the single frequency operation of the laser and generates a large undesirable M^2 value. In contrast, if the pump beam is two small, insufficient optical gain is influenced and lasing will not occur. In past experiments the profile of this pump beam has never been analysed in great detail. A typical VECSEL laser uses a pump spot size that matches the cavity mode size of the laser at the VECSEL surface.

To analyse the pump beam in more detail a Coherent Lasercam 3 beam analyser was modified. A 10-times microscope objective lens was fitted to the Lasercam at a distance of 12cm from the CCD chip. This created a 10-times magnification of the focal point directly on the CCD chip, allowing small beam diameters to be measured at an extended distance. The calibration of this modified focusing lens was achieved by imaging a series of pinholes that were illuminated using the laser output. As the pinhole diameters are of known size a direct calibration of the imaging system could be achieved.

In previous experiments a "top-hat" pump profile is used, where the pump beam has the same intensity throughout its area. Figure (7.4.1) & (7.4.2) show a 2D and 3D profile image acquired from the beam analyser, respectively.

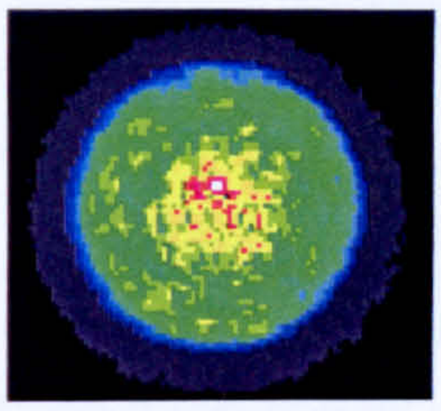

Figure (7.4.1): 2D image of the pump laser's 100μm diameter beam at focus

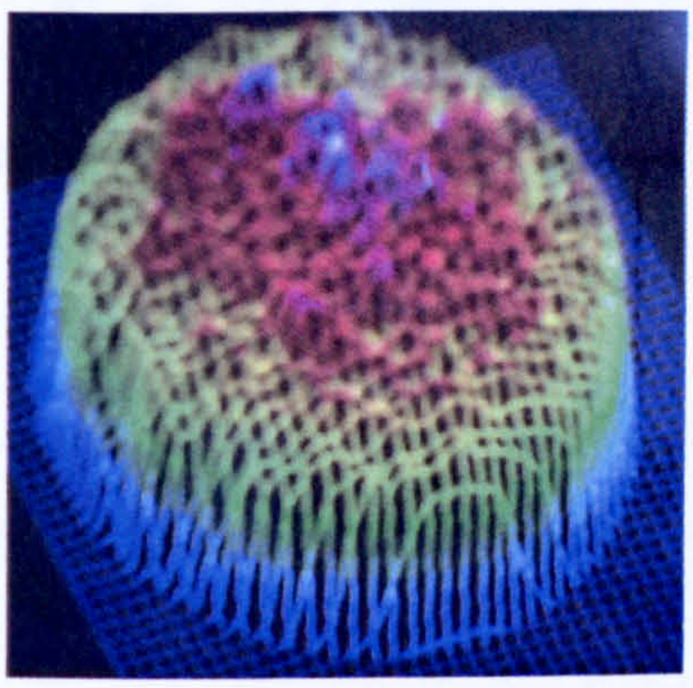

Figure (7.4.2): 3D image of "top-hat" pump characteristics, showing steep sides and uniform intensity levels.

The intensity levels are shown by a spectrum of colours, from low power (dark blue), to high power (white). Figure (7.4.1) and figure (7.4.2) show an almost homogeneous power lever throughout the pump area, however the intensity level is slightly higher in the centre of the beam.

At any point in a laser cavity the beam can be described to have a Gaussian profile. This is true also at the VECSEL surface where the pump beam is absorbed into the barrier regions and the quantum wells. To fit the Gaussian mode profile the optical pump system should also exhibit a similar intensity profile. This provides an exact match of relative area intensities of the two beams. To relate this to the pump system used on the small cavity, a series of measurements were taken to indicate the beam's profile near to the focus. Figure (7.4.3) shows these results.

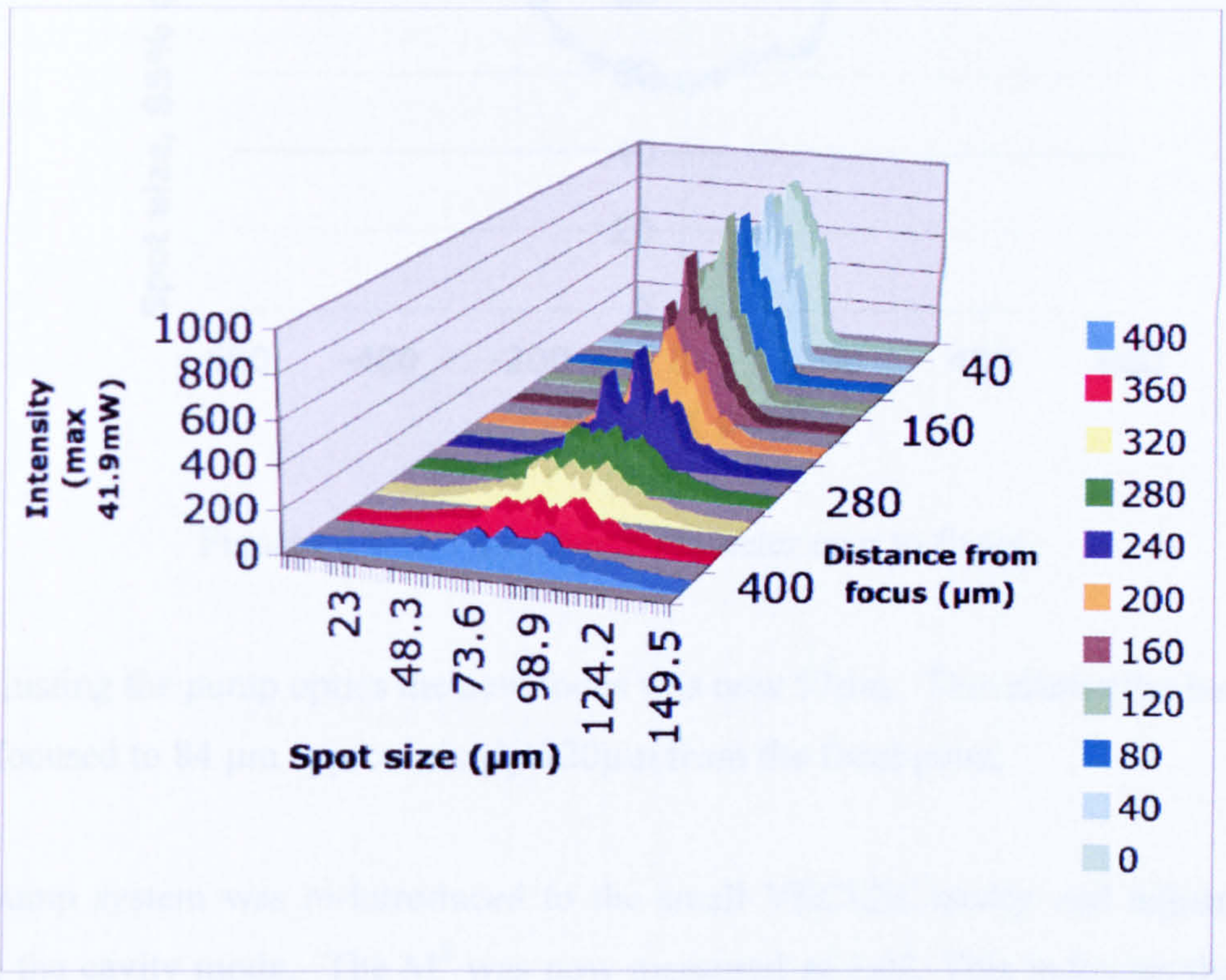

Figure (7.4.3): Pump beam profile near to the focus

Figure (7.4.3) shows the "top hat" style beam's profile located at the focus, indicated by its vertical sides. As you increase the distance from the focus the beam expands and takes on a smoother shaped profile, as seen 200µm from the focus. However at 200µm from the focus the beam diameter increases to over 100µm, which is greater than the cavity mode of approximately 84µm. To compensate for this, adjustments were made to the focusing lenses of the pump optics to reduce the size of the focused beam. This allows for de-focusing of the pump beam to match the cavity mode of

84μm and have a bell-shaped profile. Figure (7.4.4) shows the adjusted focusing system spot sizes as your scan across its focal region.

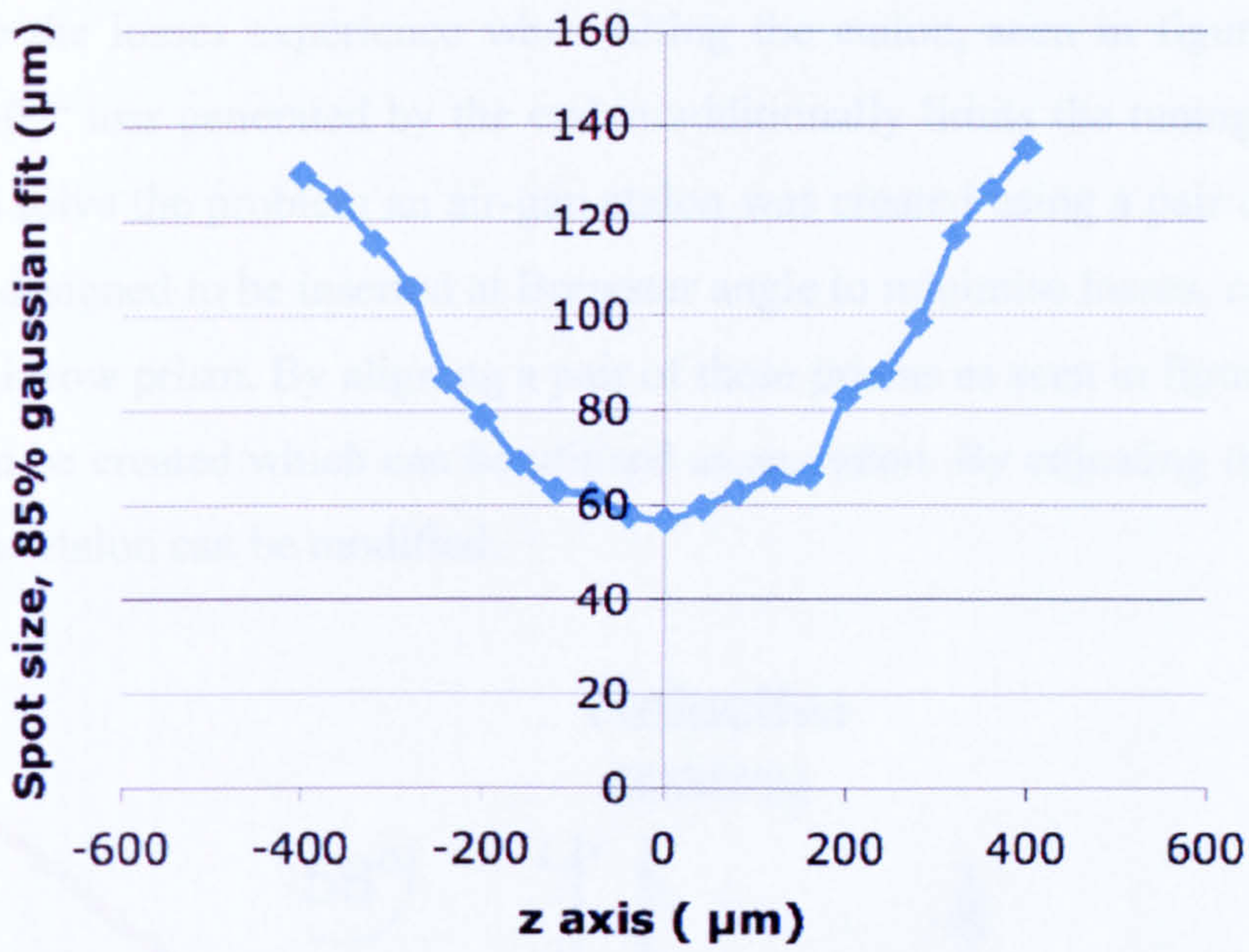

Figure (7.4.4): Pump beam diameter near to focus

By adjusting the pump optics the new focus was now 57μm. This allows the beam to be defocused to 84 μm approximately 220μm from the focal point.

The pump system was re-introduced to the small VECSEL cavity and adjusted to match the cavity mode. The M^2 was now measured at 1.02. This indicates that the adjustment of the pump profile has benefited the lasers output beam by providing a more effective intensity matched profile to the pump beam.

7.5 AIR-SPACED ETALON

The fine tuning of the VECSEL laser was performed by a combination of BRF and solid etalon adjustments. This produced an undesirable saw tooth effect to the output power due to the losses experience when tilting the etalon, seen in figure (7.3.3). This "walk off " loss generated by the etalon additionally limits the tuning range of the laser. To solve the problem an air-gap etalon was created using a pair of prisms. The prism is designed to be inserted at Brewster angle to minimise losses, commonly known as a Littrow prism. By aligning a pair of these prisms as seen in figure (7.5.1), an air gap can be created which can be utilised as an etalon. By adjusting the air gap the FSR of the etalon can be modified.

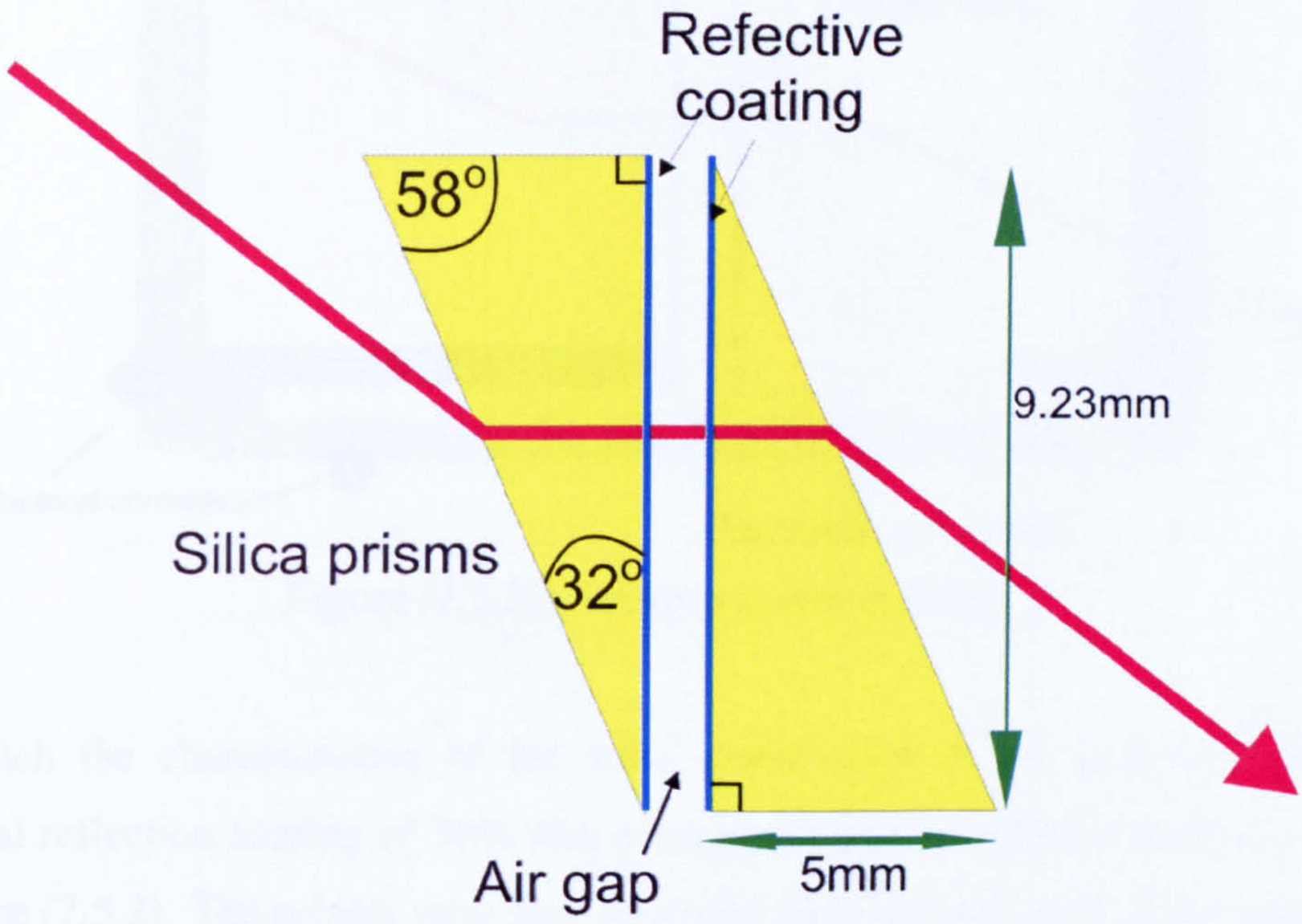

Figure (7.5.1): Littrow prisms forming an air etalon

The laser is then tuned by increasing or decreasing the air-gap and provides no "walk off" losses.

Air-gap etalons are commercially available using this very method, however they are too large to insert into the small VECSEL cavity and very expensive (>$1000). By

building an air etalon, it is possible to make a compact unit, which can be modified to suit the cavity conditions.

To provide movement fine adjustment to the air gap a piezo-electric tube was used. Designing the prisms to fit exactly inside this tube and fixing them at both ends of the tube meant that an increase in 1 volt applied to the piezo-electric tube would provide 1.75 nm adjustment of the air gap. Figure (7.5.2) shows the design parameters.

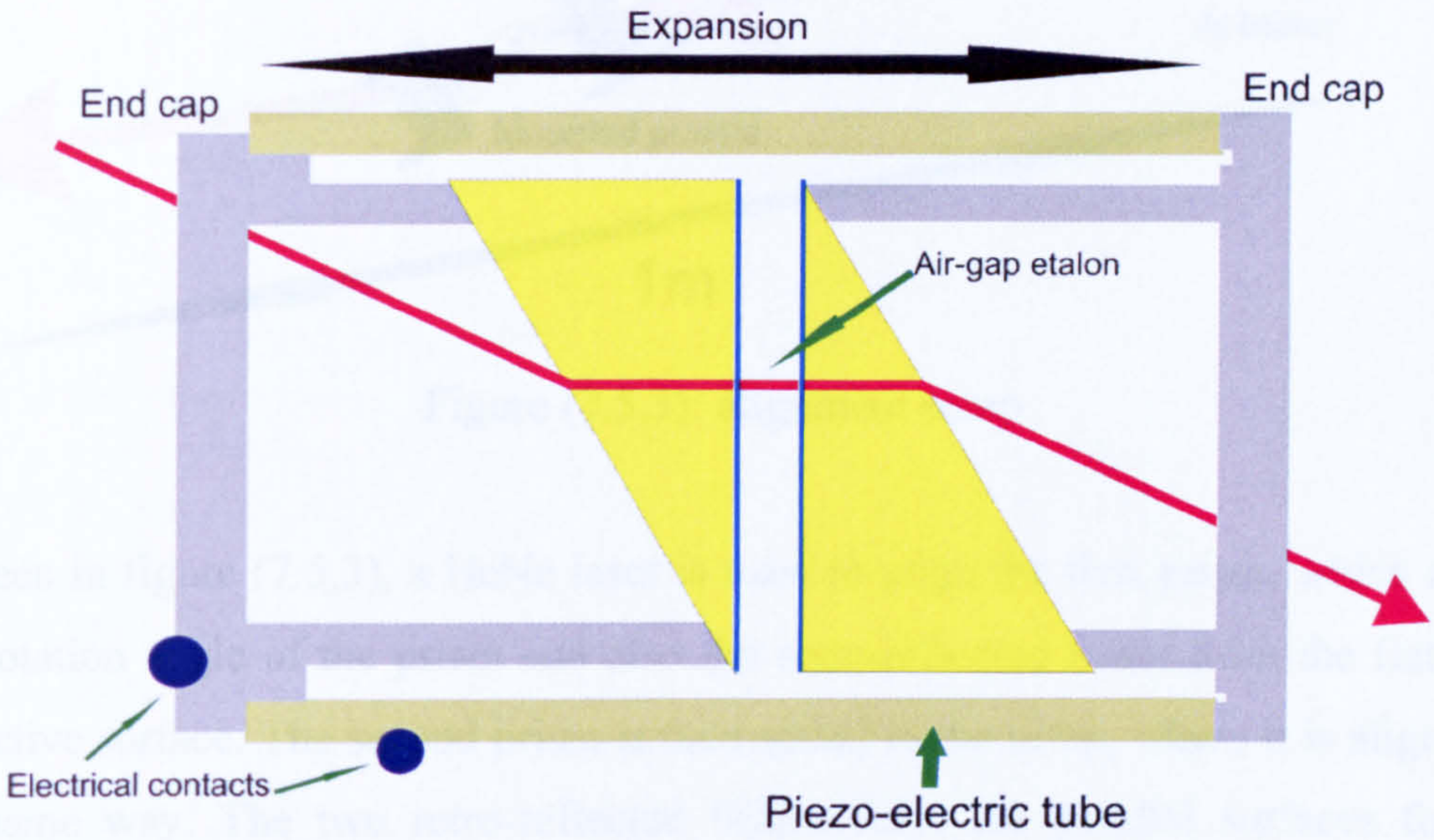

Figure (7.5.2): Air-spaced etalon design

To match the characteristics of the solid etalon used in the previous setup, an identical reflection coating of 30% was used on the prisms parallel surfaces, as seen in figure (7.5.2). The prisms were first mounted onto the end caps of the unit, using ultraviolet curing glue for a rapid setting time. One prism is then stuck firmly in place inside the piezo-electric tube using Torr Seal epoxy. This hard insulating epoxy proved to be an excellent adhesive for the mounting as it exhibits low levels of curing stress. The remaining prism was then mounted into an alignment setup, which can be seen in figure (7.5.3).

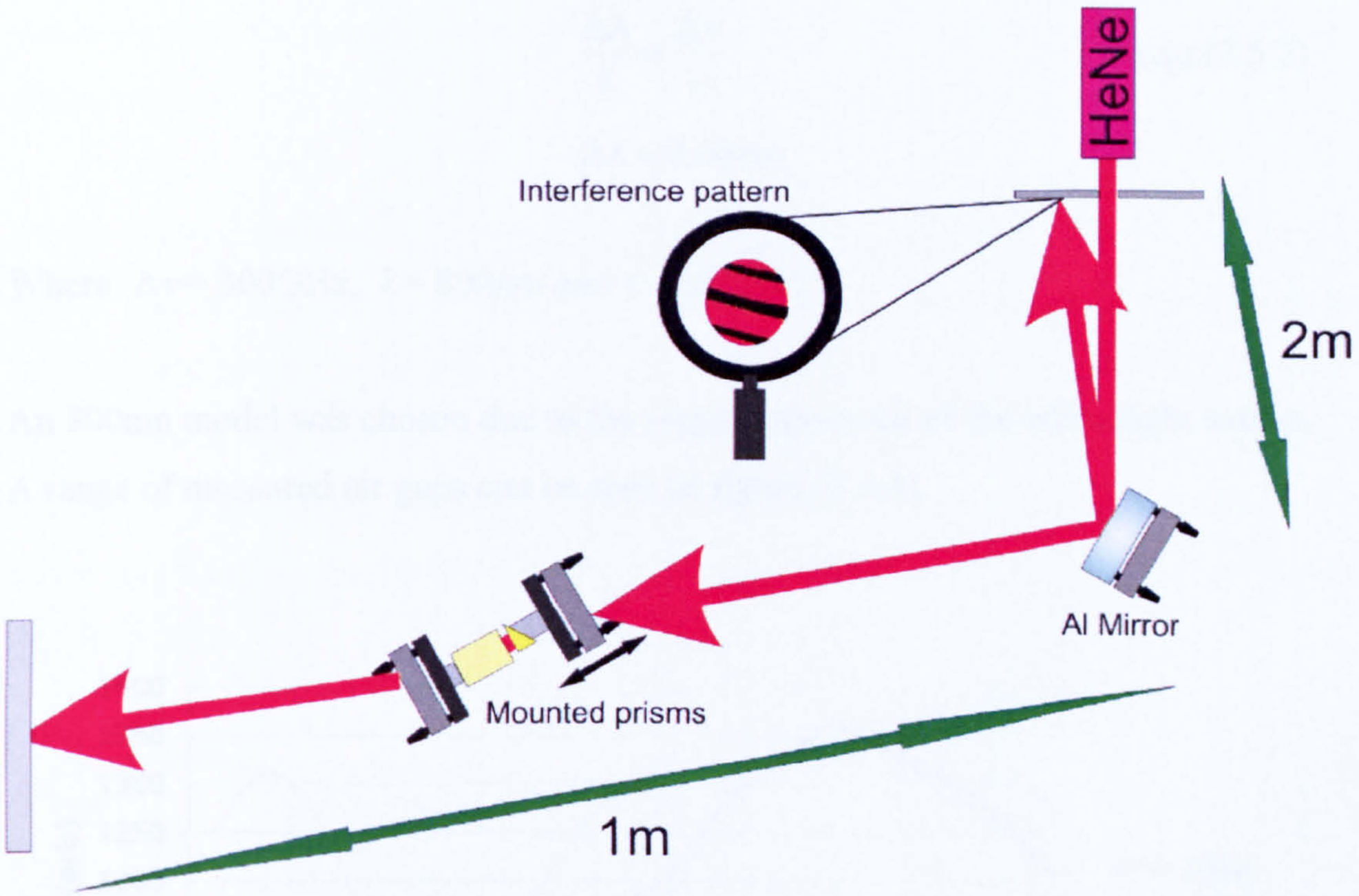

Figure (7.5.3): alignment setup

As seen in figure (7.5.3), a HeNe laser is used to align the first prism, which aligns the rotation angle of the prism and also the retro-reflected beam from the flat 30% reflective surface. The second prism is then added to the setup, where it is aligned in the same way. The two retro-reflected beams from the parallel surfaces form a interference pattern on the distant white card, where they can be aligned with good precision.

A tungsten/halogen light is now used to emit a collimated white light beam through the prism pair to measure the air gap. The interference fringes produced from the parallel surfaces can be measured using a spectrometer. Fine adjustment can be made to the air gap using the optical mounts until the desired air gap has been established. To match the solid etalon used in the cavity with a free spectral range (FSR) of 300GHz, an air gap of 0.5mm must be created.

In relation to the interference pattern produced by the white light source an air gap of 0.5mm corresponds to an interference pattern of 0.68nm. This can be seen in the following equation.

$$\frac{\Delta\lambda}{\lambda} = \frac{\Delta\nu}{\nu} \qquad \text{equ:(7.5.2)}$$

$$\Delta\lambda = 0.68nm$$

Where $\Delta\nu$= 300GHz, λ= 800nm and ν=353THz

An 800nm model was chosen due to the output spectrum of the white light source. A range of measured air gaps can be seen in figure (7.5.4).

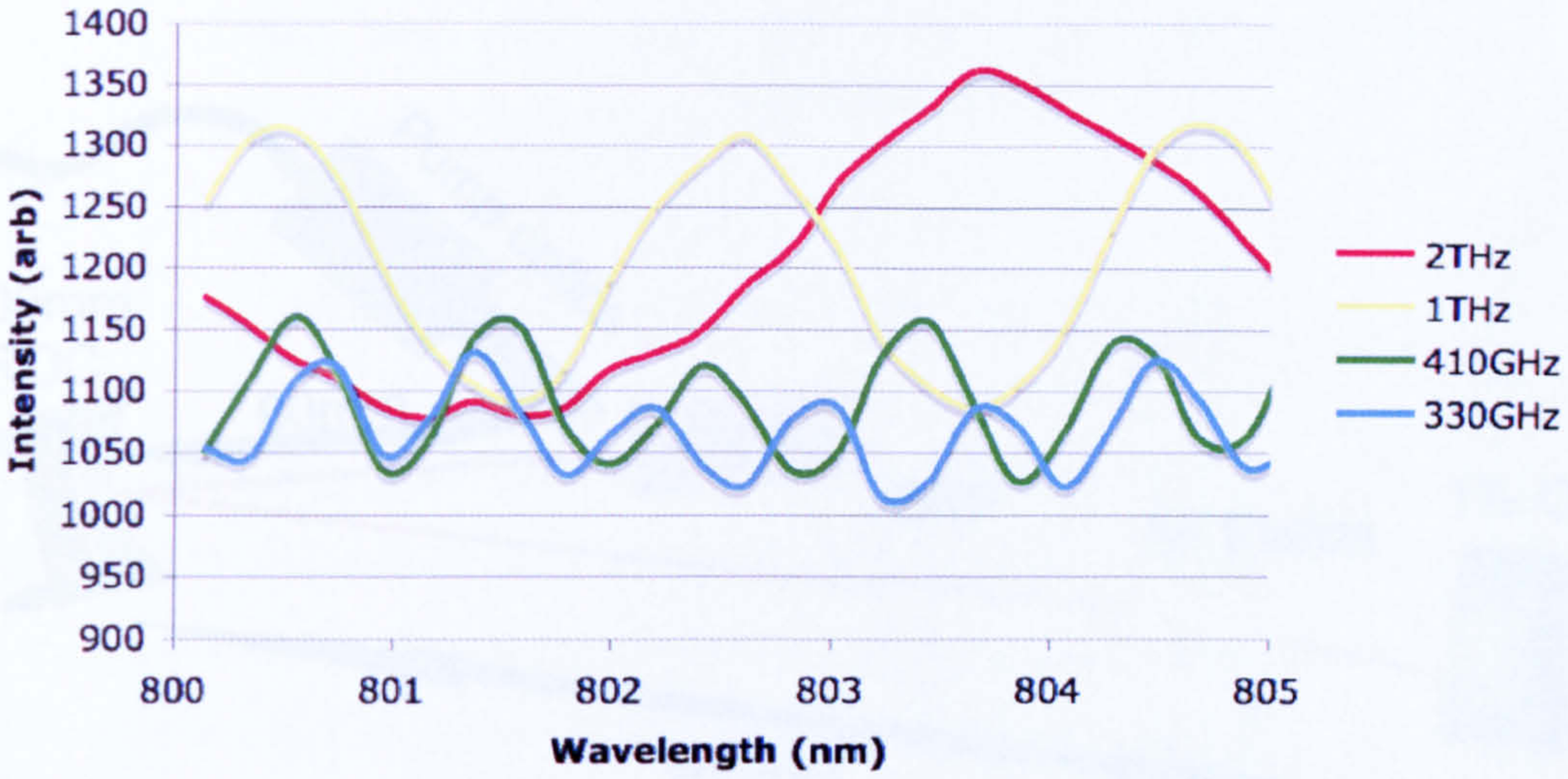

Figure (7.5.4): Interference fringes shown by spectrometer, used to measure air gap

Figure (7.5.4) shows a range of interference fringes produced by the air gap. A small air gap of 75 μm gives the interference pattern shown in red, corresponding to a FRS of 2THz, as the air gap is increased to 450 μm the interference fringes decrease, shown by the blue trace of 330GHz.

Using this method a prism pair was aligned with a FSR of 300GHz and bonded with Torr Seal. Once the epoxy was set an additional check of the interference fringes was carried out. This would show any mechanical drift or bonding stresses that occurred while the epoxy set over the course of 24hrs. Electrical contacts were added by

soldering onto the outside of the piezo-electric tube and one of the end caps of the prism mount.

As the prism creates a large displacement in the laser cavity path, insertion of the air etalon was very difficult, as precise alignment was needed. After several attempts lasing could not be achieved, so another cavity design was used to test the etalon. The air etalon was inserted into a longer "dog leg" cavity where alignment is easier due to the plane output coupler and flat wave fronts. An intra-cavity iris and HeNe beam was used to precisely align the air etalon. This cavity setup can be seen in figure (7.5.5).

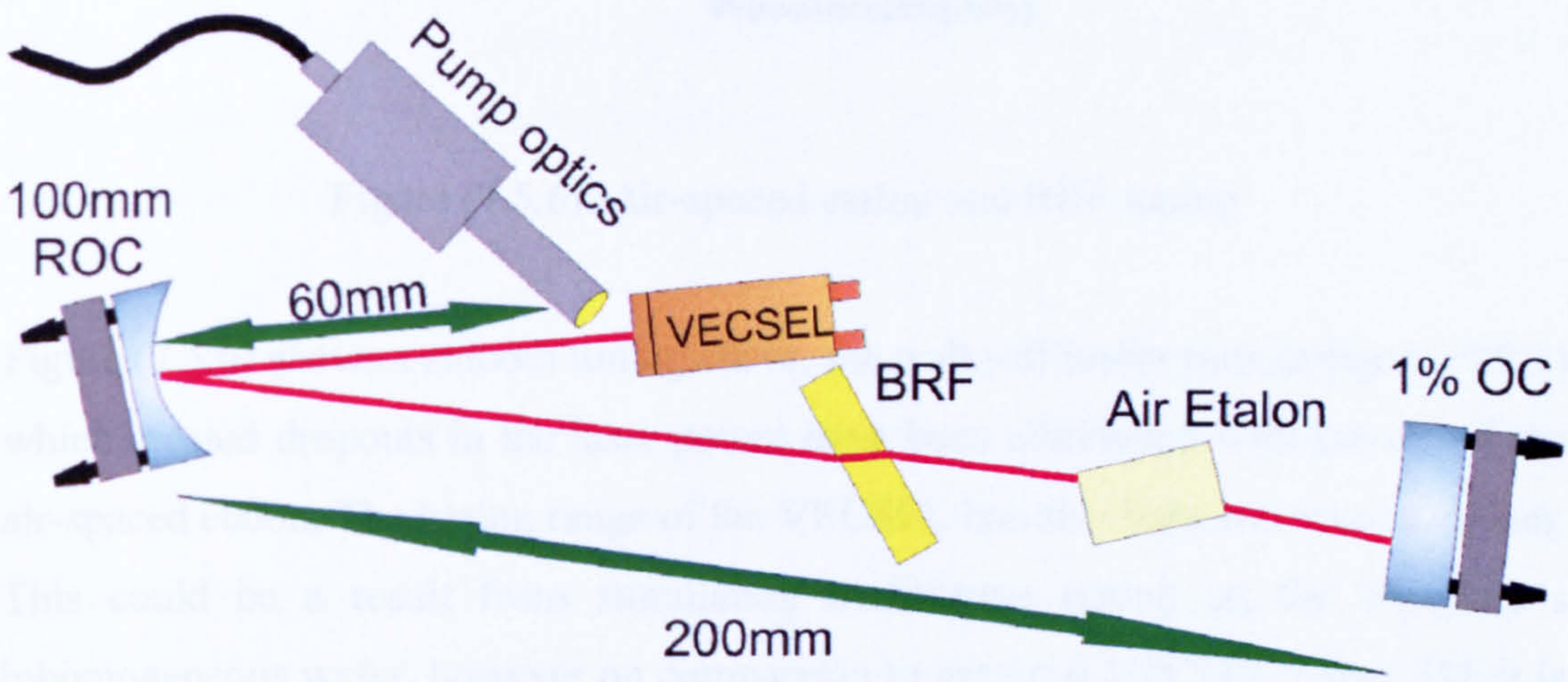

Figure (7.5.5): "dog leg" cavity incorporating air etalon

Lasing was achieved with a maximum output power of 88mW,with a pump power of 4.7W. The insertion power loss of the air etalon was 61%. This large loss was due to the relatively poor optical quality of the prisms.

The laser was then tuned using a combination of the BRF and 300GHz air-spaced etalon to provide smooth tuning over the available wavelengths, this can be seen in figure (7.5.6).

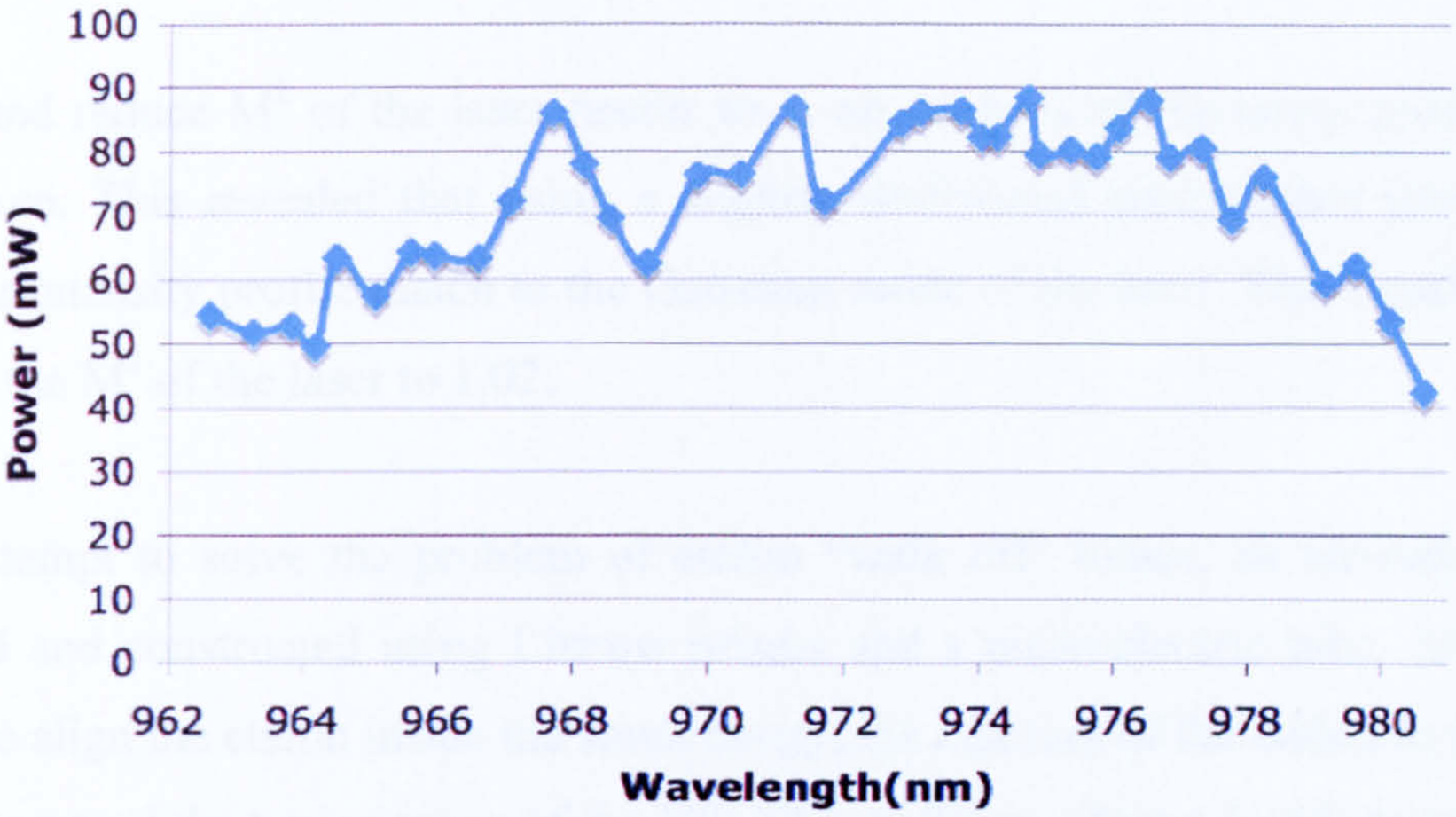

Figure (7.5.6): Air-spaced etalon and BRF tuning

Figure (7.5.6) shows a smooth tuning curve, the walk-off losses seen in figure (7.3.3) which created dropouts in the laser power have been eliminated with the use of the air-spaced etalon. The tuning range of the VECSEL has also been increased to 20nm. This could be a result from stimulating a different region on the VECSEL's inhomogeneous wafer, however on comparison to previous VECSEL lasers, [1], it is clear that the air-spaced etalon has increase the tuning range.

7.6 Conclusion

To create a compact single frequency VECSEL, a 50mm cavity was constructed. With solid etalon and BFR, single mode was achieved and produced a 10nm tuning range with a maximum power of 271mW. Fluctuations in power levels occurred due to large losses from the solid etalon tilt angles (walk off). The laser frequency was locked using a reference cavity and the line width was measured to be 180kHz. This

could not be reduced further due to large optics inhibiting the response time of the cavity mirror. The M^2 of the laser was measured at 1.1.

To try and reduce M^2 of the laser nearer to 1, an analysis of the pump profile was undertaken. This revealed that using a slightly de-focused pump beam provides a excellent intensity profile match to the Gaussian mode of the laser. This significantly reduced the M^2 of the laser to 1.02.

In an attempt to solve the problem of etalon "walk off" losses, an air-etalon was designed and constructed using Littrow prisms and a piezo-electric tube. Although unable to align the etalon inside the small cavity, the addition of the etalon to a larger cavity increased the tuning range of the VECSEL to 20nm, almost double to previous experiments. This also removed the uneven "saw-tooth-like" power levels when tuning the solid etalon, as seen in figure (7.5.6).

Further work was carried out in constructing a prism pair with a larger air gap, which was equivalent to the BRF's FSR. This would allow the lasers frequency to be tuned "hands free" using electronics. However the losses experienced by the two air tuning devices were too large to initiate lasing in the VECSEL.

7.7 References

1. R.H. Abram, K.S. Gardner, E. Riis, and A.I. Ferguson, "Narrow linewidth of a tunable optically pumped semiconductor laser", Optics Express, **12**, 5434, (2004).

2. J.C. Cotteverte, F. Bretenaker, A. Le Floch. " Jones matrices of a tilted plate for Gaussian beams", Applied Optics, **30**, 3, (1991).

3. A. E. Siegman, "A cononical formulation for analyzing multielement unstable resonators", IEEE journal of Quantum Electronics, **12, 1, p35,** (1976)

4. A. E. Siegman, "Lasers", Oxford University Press, p665 (1896).

Chapter eight

Frequency doubled VECSEL

8.1 Introduction

A laser can be used in a variety of applications, harnessing its attributes of a directional coherent beam of light. Since the invention of the laser by Theodore Maiman in 1960 [1], laser scientists have endeavoured to create lasers over the whole wavelength spectrum. Harnessing the properties of key elements doped into crystal hosts, it was possible to create suitable laser gain media, which emit radiation when optically pumped. However the range of optical pumping wavelengths and available gain media is limited by a natural selection of elements and host crystals, most of which emit in the infrared region. In 1961 a new method of achieving new wavelengths was discovered by Franken [2]. Using a ruby laser with a wavelength of 694nm, frequency conversion was achieved using a quartz crystal, which doubled the lasers frequency, producing laser light at 347nm. This pioneered the development of frequency doubling laser light, making a whole range of previously unobtainable wavelengths achievable.

In modern times frequency doubling is still an effective means to generate short wavelength light sources. In recent years a significant motivation of low wavelength laser has been the optical storage industry. The invention of optical storage devices like the CD and DVD rely on lasers to read information from the surface of these media. The smaller the wavelength of light used the more information can be stored. The recent development of the blue laser diode by Nakamura and colleagues in 1997 [3] has again increased the capacity of these media with the introduction of Blu-ray discs. In addition to optical storage, short wavelength lasers can be used in several

applications including bio-medical, high-resolution spectroscopy and visual display systems.

Many of these applications require good laser beam quality, with narrow line widths and TEM_{00} mode. Frequency doubled light naturally inherits the properties of the fundamental source like pulse duration and beam quality. The VECSEL is an ideal laser to frequency double due to its spectral and spatial qualities. It has low line width operation, TEM_{00} mode capability, high output powers and can be designed to operate at a variety of wavelengths. This chapter demonstrates an 850nm VECSEL frequency doubled to 425nm with the use of $KNbO_3$.

8.2 FREQUENCY DOUBLING THEORY

Second harmonic generation is a non-linear optical effect. High intensities generated in the doubling crystal result in non-linear response. When a small electric field is applied to a material its electrons are manipulated into a state of polarisation. This has a linear response and can be expressed by the following equation,

$$P = \varepsilon\chi^{(1)}E \qquad \text{equ(8.2.1)}$$

where P is the polarisation vector, ε is the permittivity of the medium, $\chi^{(1)}$ is the linear polarisation susceptibility and E is the electric field vector. When the same medium is subjected to a large electric field, like that of a laser beam, the material responds in a non-linear fashion. A series of ordered effects and can therefore be expressed as,

$$P = \varepsilon(\chi^{(1)} + \chi^{(2)}E + \chi^{(3)}E^2 + ...)E \qquad \text{equ(8.2.2)}$$

where $\chi^{(2)}$ and $\chi^{(3)}$ are the second and third order nonlinear susceptibilities of the medium involved. These higher orders of optical responses are the properties that are exploited in the host medium to generate a new frequency of light. In second harmonic generation the second order nonlinear susceptibility $\chi^{(2)}$ doubles the initial

electrics field frequency (ω), generating a field of 2ω. The same nonlinear effect also produces sum-frequency mixing ($\omega=\omega_1+\omega_2$), difference-frequency mixing ($\omega_3=\omega_1-\omega_2$) and the Pockels effect ($\omega=\omega_1$).

The corresponding electro-magnetic wave equations for these new frequencies can be derived from Maxwell's equations, by considering an insulating, non-magnetic material [2].

$$\frac{\partial E_{(2w)}}{\partial z} = -\frac{iw_2}{2}\sqrt{\frac{\mu}{\varepsilon_2}}d_{eff}E_3E_1\exp\left[-i(k_3-k_2-k_1)z\right] \qquad \text{equ:(8.2.3)}$$

where μ is the magnetic permeability of the medium, d_{eff} is the effective nonlinear coefficient and $k_{(i=1,2,3)}$ are the wave vectors for the relative wave frequencies. This equation describes the second harmonic wave amplitude as a function of the wave amplitudes of the other two frequencies present when propagating through the medium. In terms of optical intensity,

$$I_{(2w)} = \frac{2w^2{d_{eff}}^2l^2}{n_{(2w)}{n_{(w)}}^2c^3\varepsilon}\left(\frac{\sin(\Delta kl/2)}{\Delta kl/2}\right)^2 I^2_{(w)} \qquad \text{equ:(8.2.4)}$$

Frequency conversion efficiency can be increased by minimising the wave vector mismatch $\Delta k = k_3 - k_2 - k_1$. Phase matching occurs when $\Delta k = 0$.

Phase matching is a vital parameter of a frequency doubling crystal. If phase matching is not achieved correctly then the result is a poor frequency conversion of the fundamental wave. There are two types of phase matching, type I phase matching occurs when both fundamental waves interact with identical polarisation states. Type II phase matching occurs when the two polarisation directions are perpendicular to each other.

Phase matching in bulk media can be achieved using two methods, Angle tuning and temperature tuning. Angle tuning is optimised by changing the direction of the fundamental beam to the crystal axis. In a uniaxial crystal this corresponds to

changing the angle between the wave vector k and the crystals optic axis, known as critical phase matching. As both the fundamental and second harmonic beam experience different refractive indices (ordinary and extra ordinary) to each other due the crystal cut and angle dependence, phase matching can be achieved. This however is sometimes undesirable as the frequencies generated do not propagate collinearly with each other, which can cause angular walk off of the fundamental beam and limit the efficiency of the frequency conversion. Temperature tuning is a much-preferred method as this it obviates the need for angular dependence. Altering the crystals temperature changes its birefringence for both ordinary and extraordinary propagation directions. When a certain temperature is reached where the two waves match, phase matching has been achieved. This is known as non-critical phase matching and is the preferred method for a temperature tunable crystal, if temperatures are within reasonable limits.

When choosing a frequency doubling crystal two main parameters have to be considered. Firstly and most importantly an appropriate medium must be chosen which interacts with the desired pump wavelength, making frequency doubling achievable while being optically transparent to the wavelengths involved. Secondly the phase matching type must be determined for optimum yield. Other characteristics, which should also be considered, are the birefringence of the material, effective non-linear coefficient (maximum conversion), dispersion, optical power levels for damage control, chemical durability (hygroscopic) and price.

8.3 ANALYSIS OF CONVERSION EFFICIENCY

To generate efficient frequency doubled light, consideration of the intra-cavity losses must first be taken into account. The optimum output coupling (T_{opt}) is related to internal losses (δ_0), unsaturated gain (g_o) and the unsaturated gain (g_o) by the following equation [4].

$$T_{opt} = -\delta_0 + \sqrt{g_o \delta_0} \qquad \text{equ:(8.3.1)}$$

As intra-cavity frequency doubling acts as a loss inside the cavity this can be directly related to this optimum output coupling (T_{opt}) thus maximising second harmonic generation. For further investigation the second harmonic conversion efficiency must be considered.

The theoretical conversion efficiency for the 10mm long $KNbO_3$ used in this experiment can be obtained as follows [6]. Second harmonic power generated, P(2w), can be expressed as,

$$P(2\mathrm{w}) = \Gamma \cdot L \cdot P^2(\mathrm{w}) \cdot h(\sigma\zeta) \qquad \text{equ:(8.3.2)}$$

where L is the crystal length, P(w) is the fundamental power. The factor $h(\sigma\zeta)$, containing the Boyd-Kleinman factor, represents the focusing parameters and has an optimum value of 1.068.

Γ is the crystalline material properties given by,

$$\Gamma = \frac{2\mathrm{w}_1{}^3 d_{eff}{}^2}{\pi n_1 n_2 c_0{}^4 \varepsilon_0} = \frac{16\pi^2 d_{eff}{}^2}{\lambda^3 n_1 n_2 c_0 \varepsilon_0} \qquad \text{equ:(8.3.3)}$$

for $KNbO_3$ crystal in the VECSEL cavity,

d_{eff}= 13.973pm/V, n_1=n_2=2.25, λ=850nm, ε_0=8.85x10^{-12}F/m, c_0=3x10^8ms^{-1}, [7]

Substituting values gives, Γ= 3.74

Using equ:(8.3.2) the theoretical frequency conversion is,

$$\frac{P(2w)}{P(w)} = \Gamma \cdot L \cdot h(\sigma\zeta)$$

For a crystal length of 10mm, $h(\sigma\zeta)$=1.068 and Γ= 3.74, thus the theoretical conversion efficiency is 3.99%/W.

Thus an intra-cavity power of 1W will produce ~40mW of second harmonic radiation. As the conversion process acts as a loss in the VECSEL cavity, the

available gain must be analysed to maximise frequency conversion without hindering the laser's performance.

The optimum output coupling of the 850nm VECSEL in question has been shown to be approximately 4% which can be seen in the following plot, figure (8.3.1),

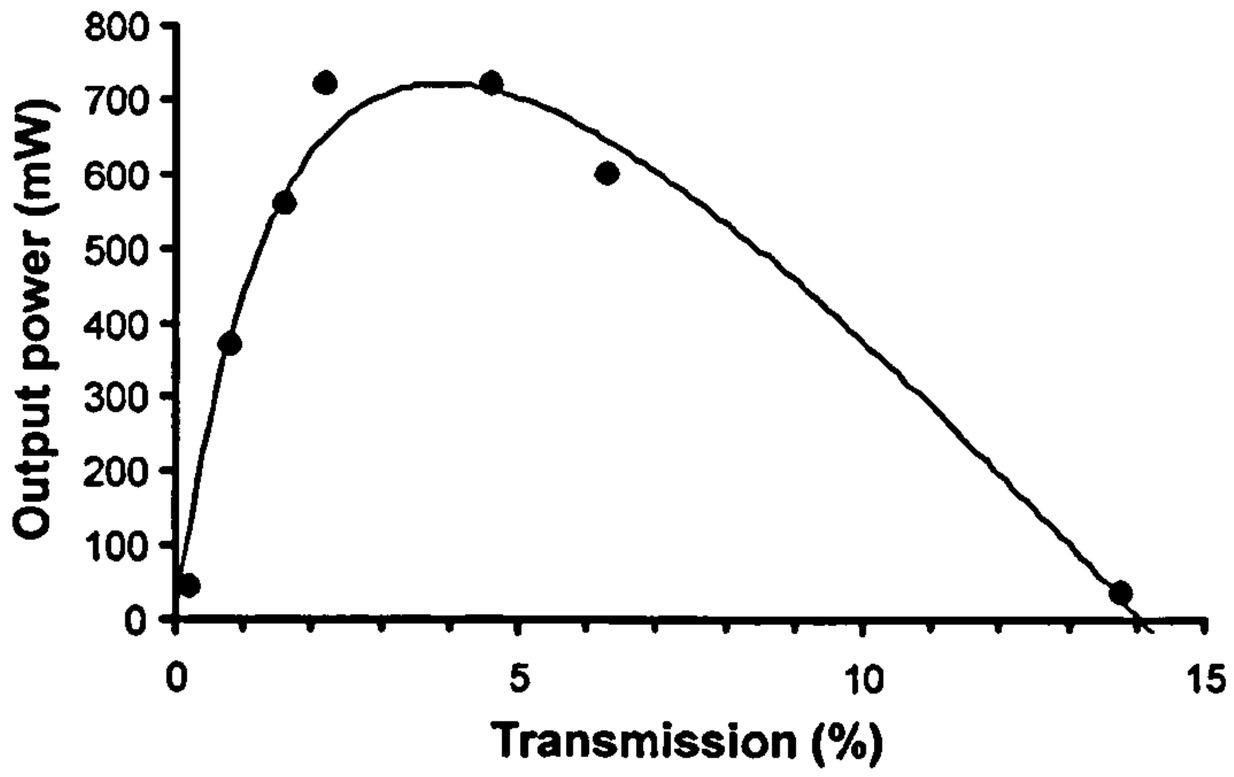

Figure (8.3.1): Output power from the VECSEL as a function of output coupler transmission, 2.4W pump power. A theoretical curve (line) has been fitted to the experimental data points (dots) [5].

Matching the frequency conversion efficiency to a maximum output coupling of 4% would yield the most frequency-converted light. In the case of $KNbO_3$ crystal with an optimum conversion efficiency of 4%/W, an intra-cavity power of 1W would obtain optimal performance, producing 40mW of frequency doubled light.

The gain threshold of a laser can be given by the following expression [8],

$$g_{th} = \delta_0 + \ln\frac{1}{R_1 R_2} = \frac{g_0}{1+{2P_c}/{P_{sat}}} \quad \text{equ:(8.3.4)}$$

Where δ_o represents the internal losses, R_1 and R_2 are the mirror reflectivities, g_0 is the unsaturated gain factor and P_c, P_{sat} are the intra-cavity power and saturation power respectively. When the threshold condition is reached the laser's gain is reduced to that of the threshold value by the factor $(1+{2P_c}/{P_{sat}})$ seen in equation (8.3.4). The effective output coupling of the laser is given by the term

($\delta_e = \ln\frac{1}{R_1 R_2}$), which incorporated the mirror reflectivities. By replacing the laser's output coupling with the conversion efficiency of the $KNbO_3$ crystal the optimum second harmonic conversions conditions can be calculated.

The total output power of a given laser cavity configuration can be calculated from the following expression [8],

$$P_{out} = \delta_e \left[\frac{g_0}{\delta_o + \delta_e}\right]\frac{P_{sat}}{2} \qquad \text{equ:(8.3.5)}$$

The data shown in figure (8.3.1) indicates that for a pump power of 2.4W the unsaturated gain equals 16.2% with a optimum output coupling of 5% and internal losses of 2%. Using this data and equation:(8.3.5) the saturation power was calculated to be approximately 22W.

The analysis of the second harmonic conversion is based on these experimental results. The logarithmic unsaturated gain versus pump power of the semiconductor shown in figure (8.3.2) may correspond for a more complicated saturation effect like that of a pump power dependent saturation power. The following analysis is not intended to predict any variation of the second harmonic output away from these operating conditions.

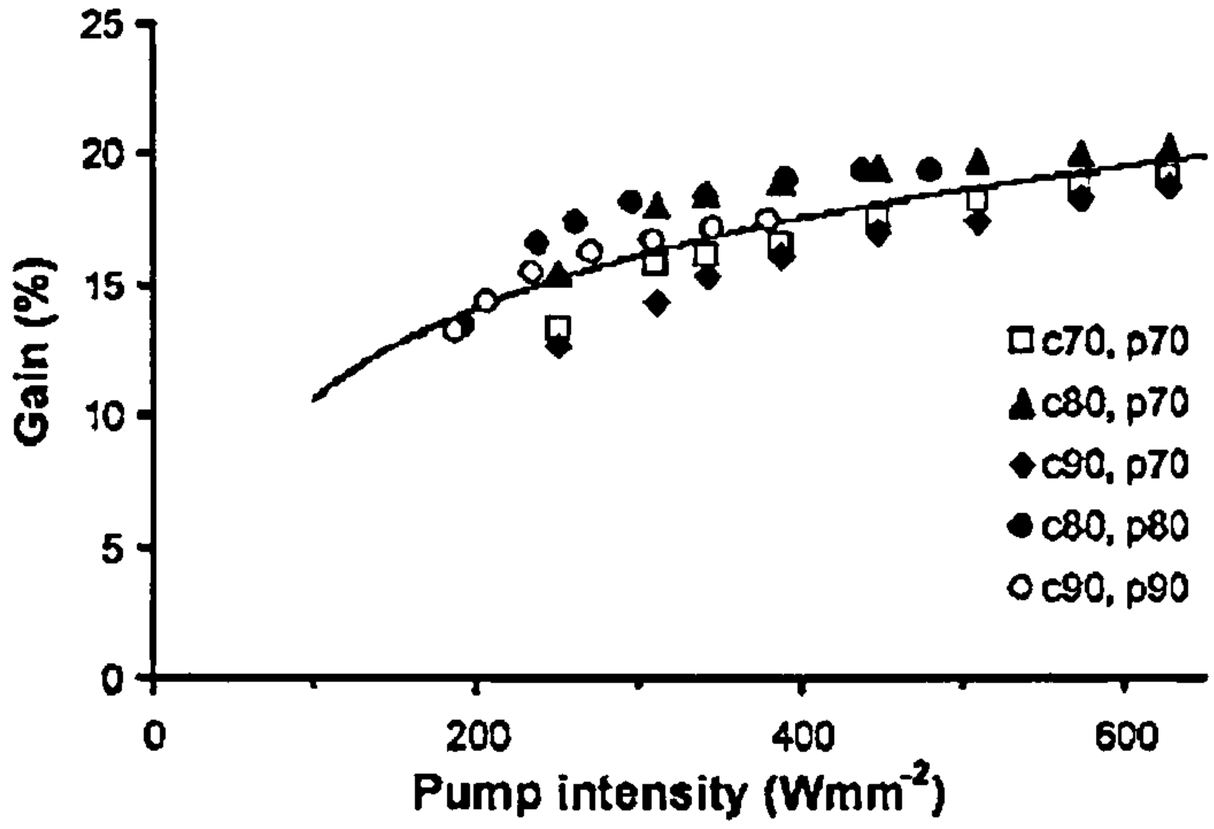

Figure (8.3.2): Experimental data showing the logarithmic dependence of the unsaturated gain and pump intensity [5]. The data points indicate various combinations of cavity mode size (c--) and pump spot size (p--).

As frequency doubling acts effectively as a loss inside the laser cavity, simple substitution of the output coupling losses (δ_e) can be made for the frequency conversion efficiency of the doubling crystal (η) with relation to the circulating power, $\delta_e = \eta P_c$. The unsaturated gain of the laser can then be related to the circulating power by the following equation [8],

$$g_0 = (1 + 2P_c / P_{sat})(\delta_o + \eta P_c) \qquad \text{equ:(8.3.5)}$$

Solving the quadratic equation gives a positive term of,

$$P_c = \frac{-(2\delta_0 + 2\eta P_{sat}) + \sqrt{(2\delta_0 - \eta P_{sat})^2 - 8\eta P_{sat}(\delta_0 - g_0)}}{4\eta} \qquad \text{equ:(8.3.6)}$$

The simple laser model, which forms the basis for equation (8.3.6) [8], assumes that the saturation of the laser gain can be described by a single universal parameter, P_{sat}. However, for a semiconductor material it is not clear that a pump power independent P_{sat} is a good approximation. Combined with the logarithmic dependence of the unsaturated gain on the pump intensity (figure (8.3.2), [5]) it would lead to a non-linear output vs pump power characteristics in contradiction with the observations as

seen below in figure (8.3.3). Hence equation (8.3.6) will only be used as a model for the saturation of the gain at a particular set of operating conditions with the purpose of determining the optimum non-linear conversion efficiency for intra-cavity second harmonic generation in $KNbO_3$.

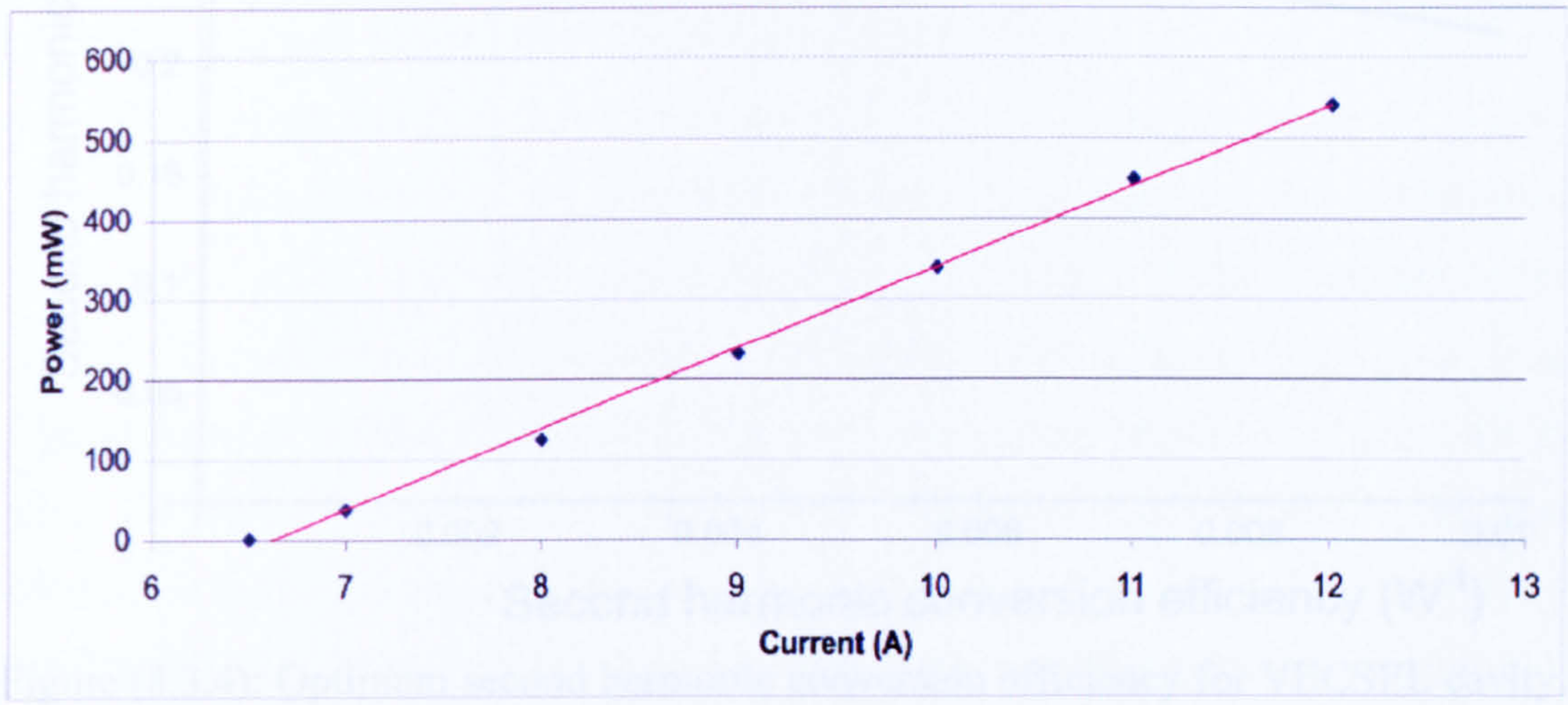

Figure (8.3.3): Output characteristics from the VECSEL ring cavity showing typical linear output power response to input current. Data points are shown with a red linear trend line.

Using equation (8.3.6) a maximum intra-cavity power of 2.7W can be achieved with the 850nm VECSEL material with a threshold value of ~800mW.

A total of 8%/W loss is generated from the $KNbO_3$ as 4% is generated from each pass through the crystal. Only half of this value can be effectively coupled out of the cavity due to cavity configuration thus this acts as an additional loss for the intra-cavity power. This can be eliminated by the use of a ring cavity configuration, which under unidirectional operation would only have a single second harmonic output from the crystal. In this linear cavity, a smaller conversion efficiency would yield a larger intra-cavity intensity which ultimately increases the second harmonic power. Analysis of the doubling crystal's conversion efficiency and second harmonic power is shown in figure (8.3.4).

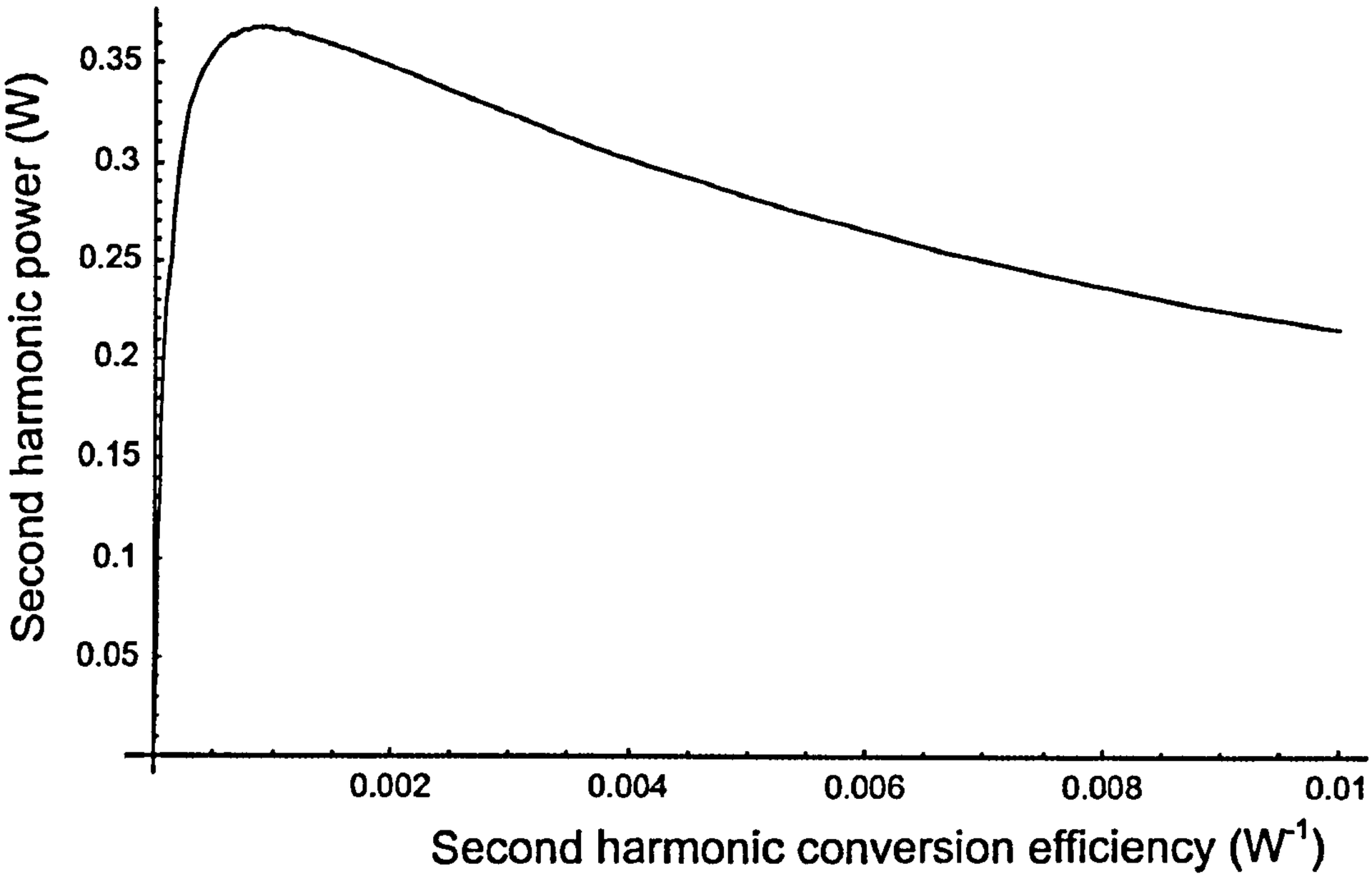

Figure (8.3.4): Optimum second harmonic conversion efficiency for VECSEL cavity. The second harmonic power is a plot of the product of the square of the circulating power and conversion efficiency ($\eta P_c(\eta)^2$) vs. η.

Figure (8.3.4) shows that a maximum second harmonic power of 370mW is achievable with an optimum conversion efficiency of ~0.1%/W. $KNbO_3$ has a conversion efficiency of 4%/W. Defocusing of the cavity mode at the crystal centre will reduce this value resulting in an increase in second harmonic generation, this can also be achieved by changing the temperature of the crystal. This indicates that the optimum focal spot size in the Boyd-Kleinman criteria is not always desirable.

8.4 Cavity Design

To design any form of laser cavity for effective frequency doubling, the crystal's parameters must first be considered. In this experiment the effective means of frequency doubling an 850nm VECSEL was using potassium niobate ($KNbO_3$). This crystal is a commonly used material for the generation of blue light therefore its properties are well known and documented [9],[10],[11]. This was set for type I non-critical phase matching at a temperature of 12^0C. This means the crystal is non-critical to the alignment of the propagating beam. Phase matching is accomplished by the use of a TEC and water-cooled block to provide controlled temperature of the crystal. The addition of AR coating on the crystal faces reduced its insertion loss. The addition of a BRF is needed to reduce the laser line width to around 1nm to allow for the crystals acceptance bandwidth. The main aspect of this crystal that determines the cavity design is the focusing parameter. As theoretically described by Boyd and Kleinman [6], the focusing parameter for second harmonic generation was established to be 2.84. This focusing parameter (ξ) is related to the length of the crystal (l) and the confocal parameter (b) by the following equation,

$$\xi = \frac{l}{b} \qquad \text{equ(8.4.1)}$$

This can then be related to the spot size of the laser w_0 by substitution,

$$b = 2z_0 = \frac{2\pi n_w w_0^{\,2}}{\lambda_w} \qquad \text{equ(8.4.2)}$$

$$w_0 = \frac{l\lambda_w}{2.84(2\pi n_w)} \qquad \text{equ(8.4.3)}$$

where l is the crystal length with refractive index n_w and laser wavelength of λ_w.

For the crystal in question of 10mm length with refractive index of 2.25 at 850nm it was calculated that the optimum spot size was $22\,\mu m$.

A suitable cavity design was then created incorporating the tight focusing parameter of the $KNbO_3$ crystal. Figure (8.4.1) shows the cavity design.

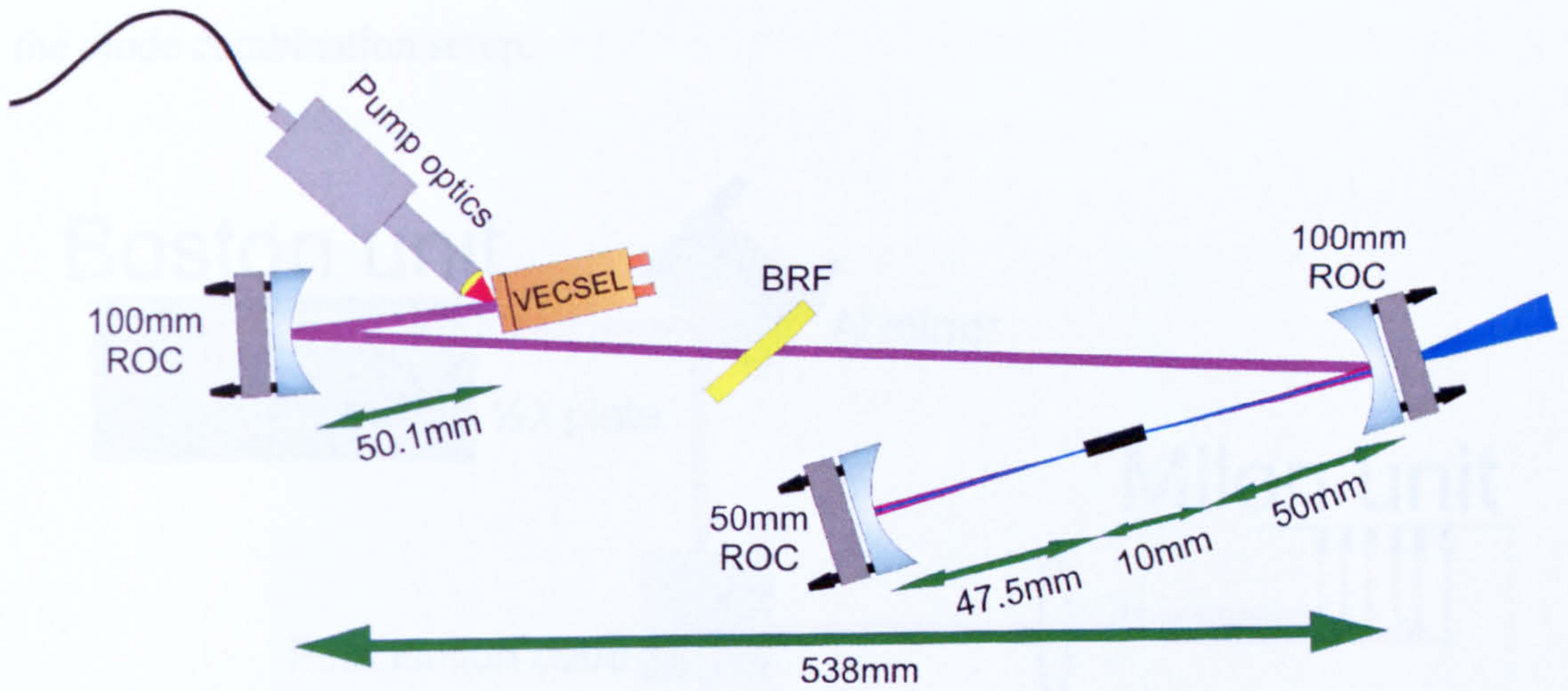

Figure (8.4.1): Intra-cavity frequency doubling VECSEL cavity designed to suit the focusing parameter of $22\,\mu m$.

The far right curved mirror with a radius of curvature of 100mm was specially coated to transmit 425nm radiation, thus optimising the frequency-converted output. This also generates a $65\,\mu m$ focus of the cavity mode on the VECSEL surface, which will be matched by the pump optics.

The 850nm VECSEL used in this cavity is a unique design incorporating indium in the quantum well region, which increases the lifetime and over all efficiency by pinning defects from propagating into the active region. This new material composition has shown signs of high power single spatial mode operation [5] and is ideal for frequency doubling. The VECSEL wafer was capillary bonded to a silicon carbide optical heat spreader for thermal management.

To create a high intra-cavity power for effective frequency doubling a bright optical pump source is needed. To increase the power available for pumping, polarisation combination of two 670nm diode arrays was undertaken. Both commercially available units from Boston Lasers and Milon Laser Group are sources that use micro-optics to combine 6 high power laser diodes into an optical fibre. Removal of the optical fibre produces a square laser output, directly from the individual laser diodes, using suitable focusing lenses and a polarisation dependent beam splitter,

both laser diode units were focused into a 100 μm optical fibre. Figure (8.4.2) shows the diode combination setup.

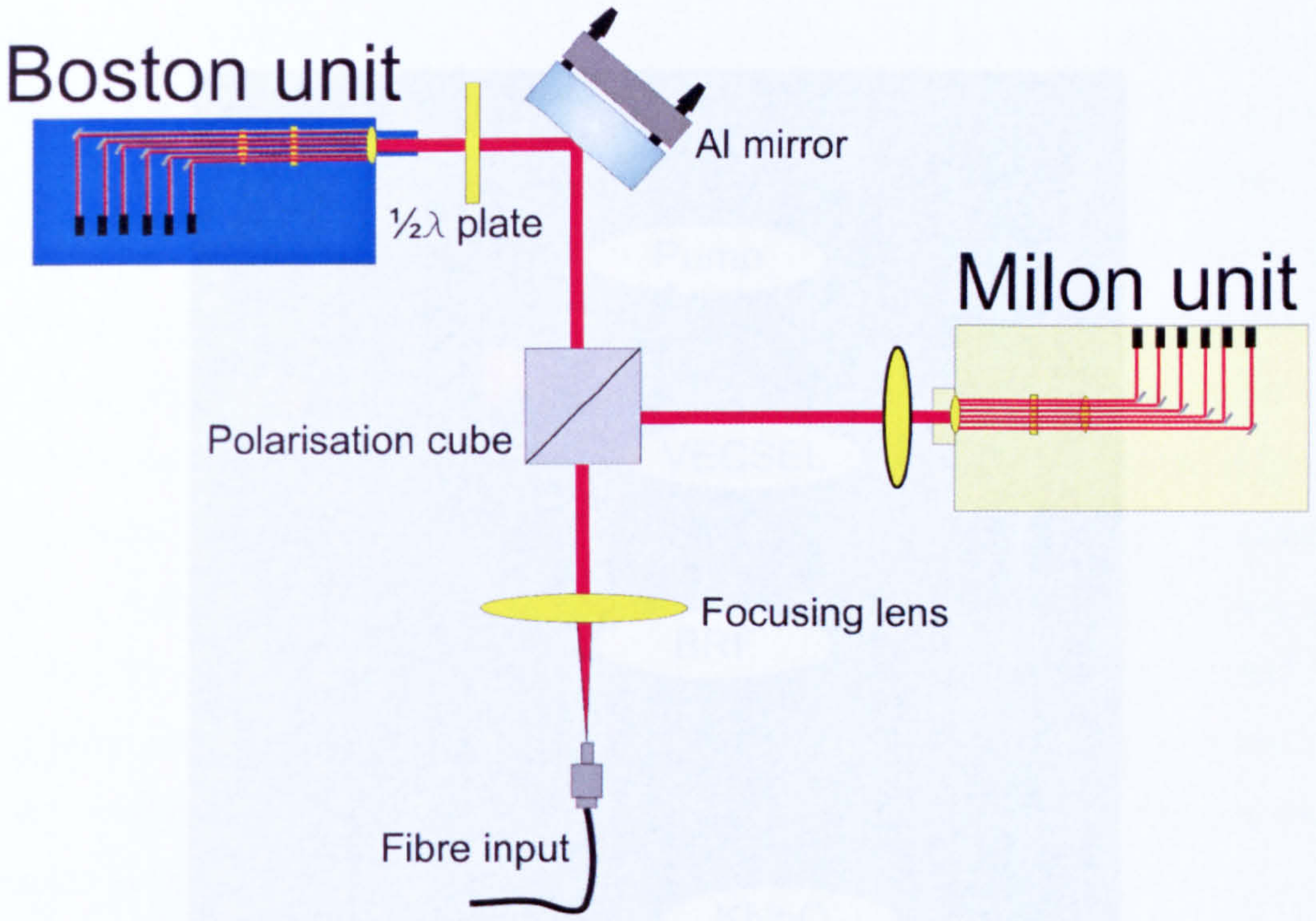

Figure (8.4.2): Combination of 2 diode arrays for high power optical pumping

As both unit's polarisation was in the horizontal plane, a $\lambda/2$ plate was used to rotate one unit's polarisation where they could be efficiently combined using a polarisation depended beam splitting cube. After combining, a total of 2.8W of 670nm laser radiation was available from the 100 μm fibre, with a total combination and coupling efficiency of 84%.

8.5 Experimental results

To measure the intra-cavity power of the laser once operational the corresponding output coupler transmission was measured. With a transmission of 0.2%, intra-cavity power could now be monitored at anytime using this measurement.

Initial lasing was achieved with a bare cavity and insertion of the BRF followed. The crystal was then inserted and aligned into the focusing region of the cavity as seen in

figure (8.3.2). Crystal alignment and temperature were altered until a maximum output of frequency doubled light was achieved. Figure (8.5.1) shows an image of the cavity generating blue light.

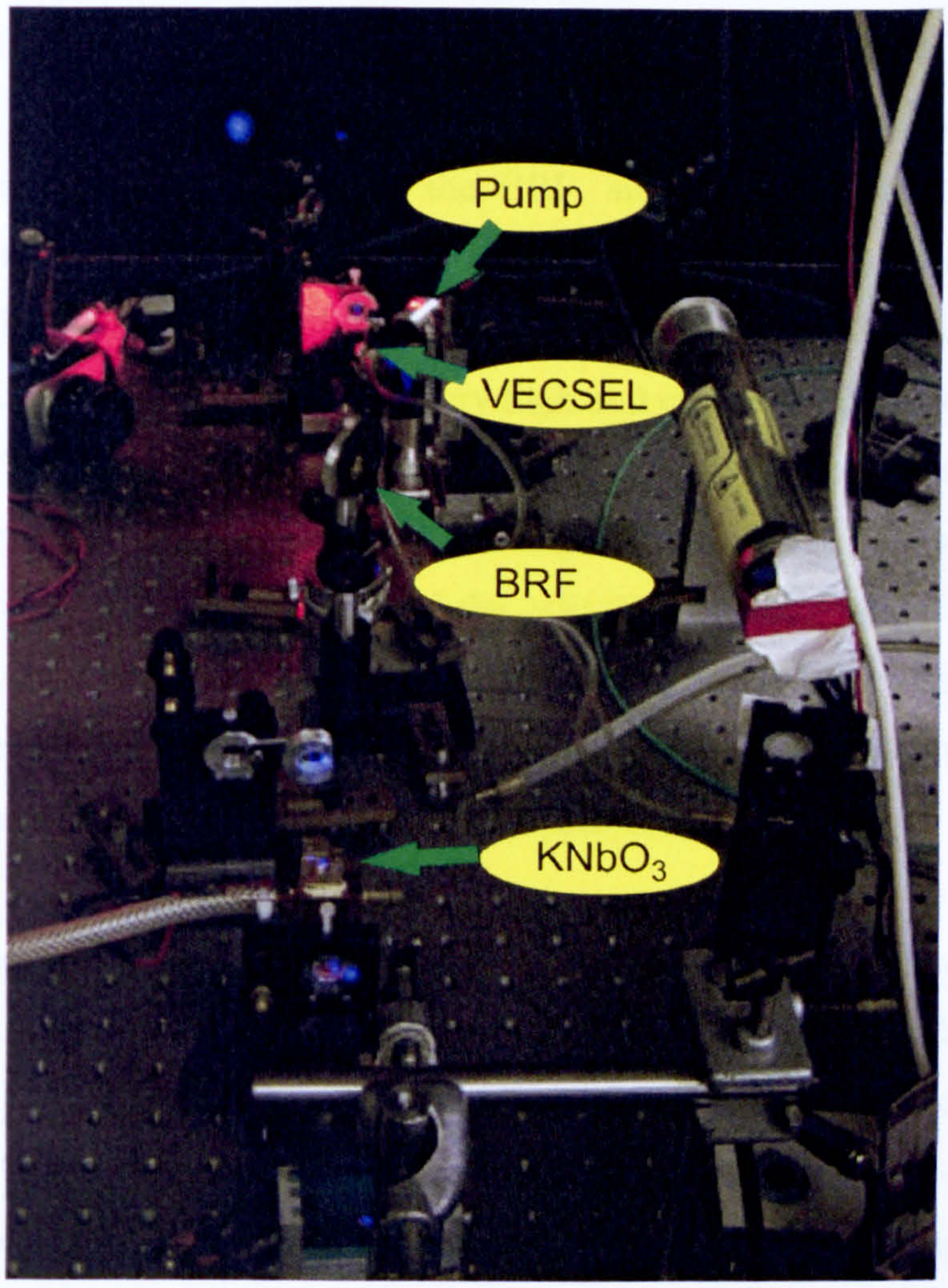

Figure (8.5.1): Intra-cavity blue light generation

A blue transmission filter was used to distinguish the 425nm beam from that of the fundamental 850nm output. A maximum output of 1.8mW at 425nm was achieved from an intra cavity power of 237mW. This corresponds to a frequency doubled efficiency of 3.2%/W.

Using equation (8.4.1) an intra-cavity power of 237mW corresponds to an expected output of 2.25mW at 425nm. This compares well with the experimental output of 1.8mW.

8.6 Conclusion

A good conversion efficiency of 3.2%/W was achieved with intra-cavity frequency doubling on a 850nm VECSEL with $KNbO_3$ compared to the theoretical maximum of 4%/W. This yielded a maximum output power of 1.8mW at 425nm. The low intra-cavity power, which hindered the second harmonic generation can be explained by the polarisation interactions between the BRF, silicon carbide heat spreader and doubling crystal. As silicon carbide is birefringent this produces a natural rotation of the lasers polarisation. When inserting the BRF at Brewster's angle, suited for horizontal polarisation the losses were very high and created an undesirable elliptical polarisation. This loss together with inherent intra-cavity losses and frequency doubling conversion losses contributed to a high total intra-cavity loss, which was too high for the corresponding gain of the VECSEL. This ultimately limited the laser intra-cavity power, thus a poor second harmonic power level was achieved. As no diamond heat-spreaders were available at this point in time no adjustment could be made to the VECSEL cavity to resolve this problem.

As seen in section 8.4, to maximise the intra-cavity power, a lower conversion efficiency crystal is required. An appropriate crystal could for this application would be periodically poled potassium titanyl phosphate (ppKTP), which has a conversion efficiency of 1%/W. This would produce significantly smaller losses to the VECSEL cavity and yield a higher intra-cavity power, which in turn would generate more frequency-doubled light. With the addition of a diamond heat spreader an optimum intra-cavity power of 4W could be easily achieved with ppKTP, which would yield 160mW. This is a considerable increase in frequency-doubled power compared with 40mW from the $KNbO_3$ crystal. Additionally the use of a defocused beam could further drop the conversion efficiency of the crystal lower that 1%/W and further increase the second harmonic power.

8.7 REFERENCES

1. T.H Maiman, "Stimulated Optical Radiation in Ruby". Nature, **187**, 4736, p 493, (1960).

2. P. A Franken, A. E Hill, C.W Peters and G. Weinreich, "Generation of Optical Harmonics", Physics Review Letters, **7**, p 118 (1961)

3. Shuji Nakamura, Masayuki Senoh, Shin-ichi Nagahama, Naruhito Iwasa, Takao Yamada, Toshio Matsushita, Yasunobu Sugimoto, and Hiroyuki Kiyoku, "Room-temperature continuous-wave operation of InGaN multi-quantum-well structure laser diodes with a lifetime of 27 hours" Applied Physics Letters, **70**, 11, pp1417, (1997).

4. S. Lutgen, T. Albrecht, P.Brick, W. Reill, J. Luft and W. Spath, " 8W high-efficiency countinuous-wave semiconductor disk laser at 1000nm" Applied Physics Letters, **82**, p3620, (2003).

5. Stephen J. McGinily, Richard H. Abram, Kyle S. Gardner, Erling Riis, *Member, IEEE*, Allister I. Ferguson, *Fellow, IEEE*, and John S. Roberts, "Novel gain medium design for short-wavlength vertical-external-cavity surface-emitting laser", Optics Express, **43**, no.6, (2007)

6. G. D. Boyd, D. A. Kleinman, "Parametric interactions of focused Gaussian light beams", Applied Physics, **39**, p3597, (1968).

7. Photox Optical Systems Ltd, http://www.photox.co.uk

8. A. E. Siegman, "Lasers", Oxford University Press, p475, (1986).

9. E. S. Polzik and H. J. Kimble, "Frequency doubling with $KNbO_3$ in an external cavity", Optics Letters, **16**,no.18, (1991)

10. P. Günter, “Near-infrared noncritically phase-matched second-harmonic generation in $KNbO_3$”, Applied Physics Letters, **34**, 10, p650, (1979)

11. C. Baumert, J. Hoffnagle, and P. Gunter, "High-efficiency intracavity frequency doubling of a styryl-9 dye laser with KNbO3 crystals", Applied Optics. **24**, 1299, (1985)

CHAPTER NINE

OVERALL CONCLUSION

9.1 VECSEL APPLICATIONS

VECSELs have the unique properties of both a semiconductor diode laser and solid-state laser rolled into one. They provide high power laser sources of high quality beams over a wide range of ever expanding wavelengths, which can be used for a number of applications. As its performance is equal to that of the Ti:Sapphire laser and with current wavelength emissions at 391nm,670nm, 850nm, 960-1030nm, 1300nm, 1500nm, 2300nm and many under development, the VECSEL laser is becoming the new source for many laser applications. This chapter summarises the work presented in the previous chapters and discusses the relevant details.

9.2 CHAPTER ONE – INTRODUCTION AND BACKGROUND

In the first chapter of this thesis an introduction to VECSELs was given with detailed analysis of the characteristic layers of the VECSEL's composition.

9.3 CHAPTER 2 - WAFER ANALYSIS

In this chapter a general overview was given to correctly analyse a VECSEL wafer before utilising in a laser cavity. A detailed description of capillary bonding was given to produce a perfect bond between the VECSEL and diamond, which is critical to the laser's performance. In addition to this, instructions on how to correctly cleave

a wafer using a series of specially designed jigs were also given, enabling a good surface quality finish for capillary bonding. Once bonded the VECSEL/diamond package is mounted in a water-cooled copper block to provide a heat sink for the diamond heat spreader.

9.4 CHAPTER 3-SINGLE FREQUENCY LASERS

This chapter gives a general comparison of single frequency laser types currently available. In addition it also describes the physics of the intra-cavity elements (BRF, etalon) that are used to induce single frequency operation.

9.5 CHAPTER 4-THERMAL MANAGEMENT

In this chapter, detailed analysis of the thermal management of the VECSEL was investigated. With computer modelling it was found that an effective solution to using a heat-spreader is to remove some or all of the GaAs substrate from the rear of the wafer structure. The temperature build up inside the quantum well region was predicted to be 28^0C with no substrate remaining, compared with that for a diamond heat spreader of 15.5^0C. This shows that removal of the substrate provides efficient extraction of the heat build-up in the quantum well region. Chemical etching was undertaken to remove this substrate, and was done successfully. However an experimental comparison could not be achieved due to handling aspects of the thinned wafer. To achieve a suitable chemically etched wafer, a VECSEL grown in reverse with etch stop built into the wafer design would produce the best results. This allows the wafer to be bonded to a diamond heat sink prior to etching to minimise handling difficulties. When analysing the thermal and practical comparisons between diamond heat sinks and wafer removal it is clear that the use of a diamond heat sink is more beneficial. The only drawback in using diamond is the etalon effect, which is created by the sub cavity that affects the spectral output of the laser. This however can be removed using a wedged diamond.

9.6 Chapter Five- Ring cavity VECSEL

This chapter outlined the design of the first ever-reported VECSEL in ring-cavity configuration. Although many solid state lasers have been designed like that of the dye laser and Ti:Sapphire, the VECSEL being a semiconductor based laser with several differences to the gain medium had not been explored. The ring cavity VECSEL produced a maximum of 1W output power with no intra-cavity elements. This compares well with other VECSEL based laser systems previously designed. It also can be forced into unidirectional operation with the use of a Faraday rotator. It was shown that a twist in the laser's plane introduced a natural rotation of the laser polarisation which compensated the Faraday rotator enough to enable uni-directionality to a level of >30dB. It was also shown that the insertion of a BRF and solid etalon into the cavity initiated single frequency operation. A 15nm tuning range was established with a maximum output power of 300mW. As in all ring cavity configured lasers, this layer exhibits a natural insensitivity to feedback. This was tested on the ring cavity VECSEL and confirmed with a maximum tolerance of 3.2%, 4 times that of a standard single frequency linear cavity VECSEL. These results indicate that the VECSEL would be a very useful source for applications involving a laser with feedback tolerance and tunablity, like that in spectroscopy and bio-medical applications. In addition this cavity is ideal for intra-cavity frequency doubling due to the low insertion loss and unidirectional beam that provides only one frequency doubled beam, thus maximising the frequency doubled output.

The ring cavity's polarisation was investigated since unlike in a linear cavity, the polarisation is not dictated by the rotation of the VECSEL axis. At several rotational position of the VECSEL, the polarisation assumed a near vertical orientation, which produced significant losses when inserting horizontal components such as the BRF. After numerous experimental procedures it was considered that the large angle incident to the diamond heat spreaders surface and the birefringence/optically activity of the diamond could be responsible for the polarisation effect experienced. A small area where the beams do not overlap in the diamond heat spreader and a circulating beam the propagating laser beam experiences a retardation determined by the birefringence/optical activity of the diamond heat spreader.

9.7 Chapter six- Micro-cavity VECSEL

In this chapter a novel technique was demonstrated to utilise an air gap as a cavity etalon, creating a small tunable laser source. Using a positive curvature mirror in reverse as the main bulk of the laser cavity it was shown that a small air-gap between the mirror's plane surface and VECSEL surface could create an effective etalon which can tune the laser wavelength. A tuning range of 7nm of single frequency laser emission was demonstrated with a maximum output power of 19.4mW. This was limited in power scalability, as the cavity required no heat spreader to be present which greatly reduces the thermal rollover point. Additional experimentation were carried out using wedged diamond, however, due to difficulties with the cavity alignment and low levels of photoluminescence detectable, lasing was never established. This however prompted the design of a slightly larger cavity, which featured in the following chapter.

9.8 Chapter seven- Small cavity VECSEL

As a progression from the previous chapter, a small cavity VECSEL was created to produce single frequency tunable emission. A small cavity of 50mm was constructed and single frequency operation was achieved with the insertion of a BRF and solid etalon. A 10nm tuning range was obtained with a maximum output power of 271mW. The frequency was locked using electronic feedback and the piezo-mounted output coupler. A linewidth of 180kHz was measured, however, this was the lowest achieved due to the large and heavy cavity mirror, which inhibited the bandwidth of the piezo-electric response.

A detailed investigation was carried out on the pump system of the laser. By analysing the profile of the pump it was determined that a defocused beam provides a more accurate intensity match to the cavity mode. This close match of relative intensities limits the power available to unwanted additional transverse modes. This

ultimately produces a good quality output beam with a better M^2 value. It was shown experimentally that after pump alterations the M^2 of the laser was reduced from 1.1 to 1.02.

The laser experienced significant losses from the solid etalon walk off. This is a common occurrence in a small laser with a solid etalon, which limits the available tuning of the laser as well as producing variations in the laser output power. The creation of an air-spaced etalon was then achieved using a pair of Littrow prisms and a piezo-electric tube creating a novel compact tunable etalon. This produced no walk off losses and a tuning range of 20nm was achieved. This single frequency tuning range is the largest ever recorded in our experience of the 980nm material, which indicated the benefits to using an air-etalon. Additional construction of a larger air-space between the prisms was achieved to act as an equivalent BRF, however the insertion losses of the two components were too large for laser action to be established. It should also be possible to construct a small cavity with a single air based tuning element with a FSR larger than that of an etalon which would produce single frequency operation due to a small cavity naturally needing a lesser mode selection process.

9.9 Chapter eight- Frequency doubled VECSEL

Detailed numerical analysis of the relationship between gain and intra-cavity frequency doubling was given. This indicated that a small conversion efficiency crystal would yield the most second harmonic power. Using a $KNbO_3$ crystal an appropriate VECSEL cavity was designed for intra-cavity frequency doubling. A maximum of 1.3mW was achieved corresponding to a 3.2%/W conversion efficiency. This compares well with the theoretical prediction of 3.99%/W. A specially adapted pump system was implemented using the polarisation coupling of two separate diode arrays into a 100μm optical fibre. This delivered 3W pump power at 670nm. The use of a silicon carbide optical heat spreader limited the laser intra-cavity power due to birefringent interaction with the BRF and doubling crystal. This caused high intra-cavity losses that could not be eliminated. A diamond heat

spreader would be an advantageous addition to this cavity as it would increase the laser power and limit the birefringence effects. However at the present time of experimentation no suitable diamond was available. In future work on the generation of frequency doubled light an additional crystal to implement in the cavity would be periodically poled potassium titanyl phosphate (ppKTP), this crystal is an acceptable replacement for $KNbO_3$ in the laser cavity and should yield a higher second harmonic power as its conversion efficiency is lower.